Synthesis & Development of Symmetric and Asymmetric Silicon Phthalocyanines Functionalized for Click-Chemistry

TIGIST TILAHUN

Thesis submitted to the University of Ottawa
In partial Fulfillment of the requirements for the
Master of Science Chemistry

Department of Chemistry and Biomolecular Sciences
Faculty of Sciences
University of Ottawa

Abstract

Although organic field-effect transistors (OFETs) are still advancing flexible and affordable electronics, their wider application is still constrained by their instability, processing difficulties, and ideal charge transfer properties, among other challenges. Because of their environmental stability, customizable optoelectronic characteristics, and two axial coordination sites that allow structural manipulation without affecting the phthalocyanine core, silicon phthalocyanines (SiPcs) present a viable platform to overcome these constraints. The design, synthesis, and characterisation of several axially substituted SiPc compounds intended to improve solution processability, provide clickable functionality, and modify solid-state organization for OFET applications are presented in this thesis. Optimized techniques were used to create symmetrical and asymmetrical SiPcs with benzyloxy-alkyne or thienyl-alkyne axial ligands, with a focus on regulating axial substitution patterns. The effects of axial ligand identity on solubility, aggregation behavior, frontier orbital energies, and redox stability were assessed through extensive structural, optical, and electrochemical characterization, including NMR spectroscopy, mass spectrometry, UV-vis absorption, and cyclic voltammetry.

Copper(I)-catalyzed azide-alkyne cycloaddition (CuAAC) reactions were carried out on one of the SiPc derivatives isolated to demonstrate the functional utility of the designed ligands. This established a basis for future polymer-SiPc covalent hybrid systems achieved via click-chemistry and supports their compatibility with post-synthetic modification. The promise of these materials as *n*-type semiconductors is demonstrated by preliminary OFET device integration, where axial asymmetry and alkyne-based substituents provide chemical diversification. All in all, this work develops a modular design approach for SiPc-based organic semiconductors, offering fresh perspectives on how axial functionalization controls structure-

property relationships and facilitating the creation of covalently linked polymer-SiPc architectures for stable, high-performance OFETs in the future.

Newly synthesized axially substituted silicon phthalocyanines:

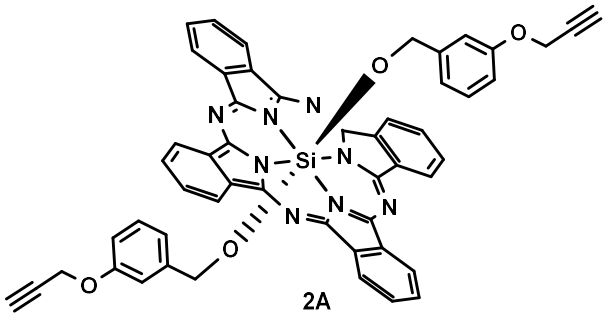

2A

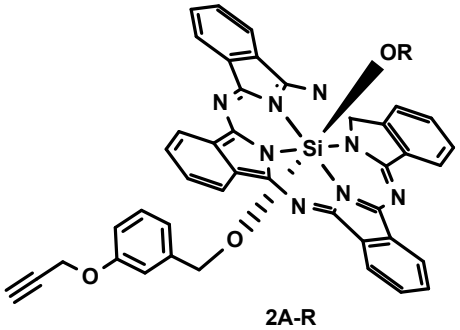

2A-R

R =

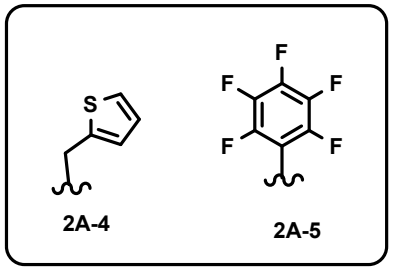

2A-4 2A-5

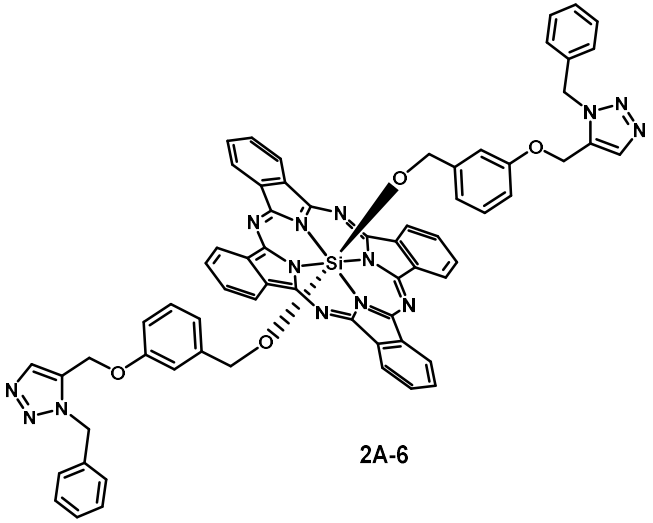

2A-6

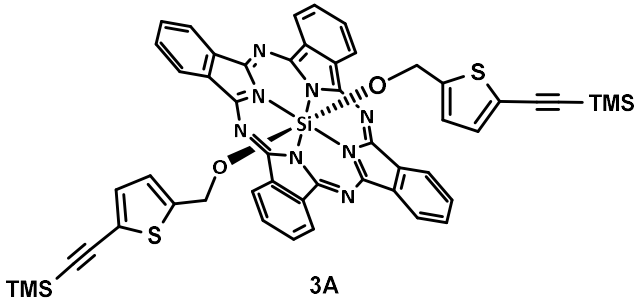

3A

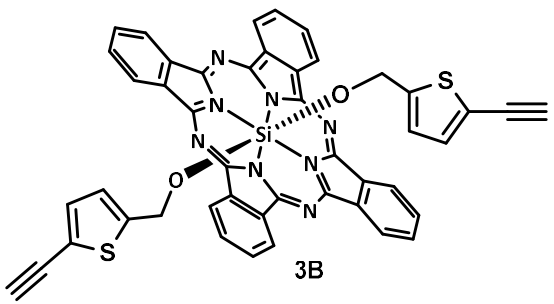
3B

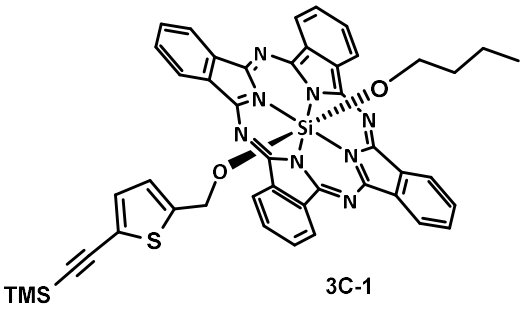
TMS
3C-1

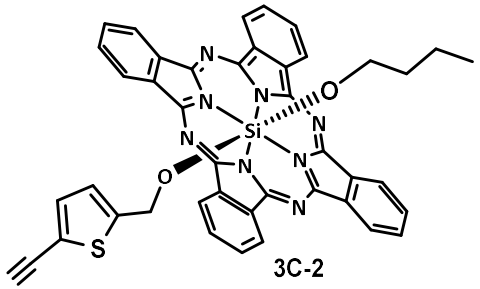
3C-2

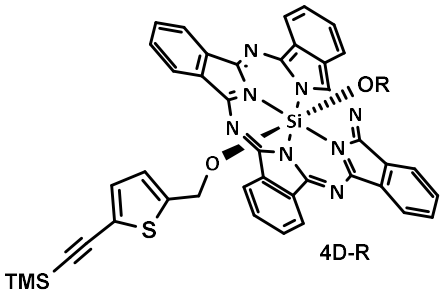
TMS
4D-R

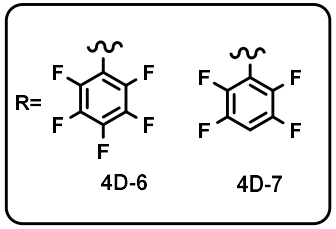
R=
4D-6
4D-7

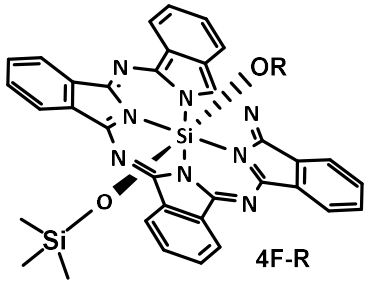
4F-R

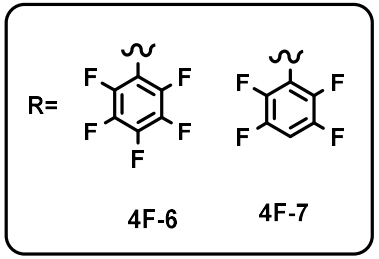
R=
4F-6
4F-7

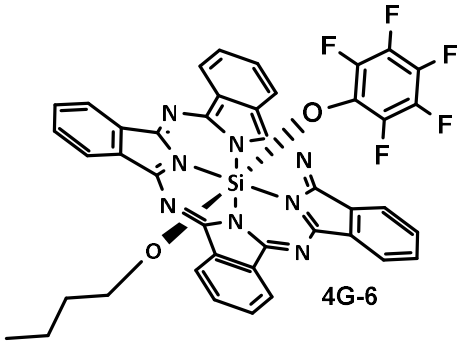
4G-6

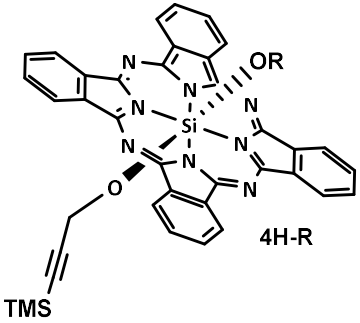
TMS
4H-R

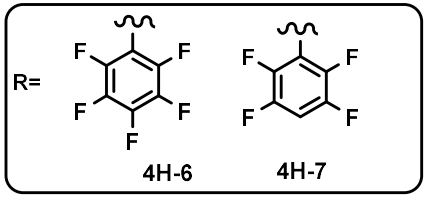
R=
4H-6
4H-7

Acknowledgments

I would like to express my sincere gratitude to my supervisor, Dr. Jaclyn Brusso, for her guidance, support, and mentorship throughout the course of this research. Dr. Brusso's scientific insight, critical feedback, and encouragement were instrumental in shaping both this thesis and my development as an independent researcher. Coming from an analytical chemistry background with little prior experience in materials science, I am especially grateful for her patience and support as I learned new techniques and shifted research directions. I also appreciate the freedom she provided to explore challenging ideas, as well as her understanding during periods of experimental difficulty.

I would like to thank my supervisory committee members, Dr. Benoit Lessard and Dr. Darrin Richeson, for their valuable discussions and thoughtful suggestions, which significantly strengthened this work. Their expertise and perspectives were greatly appreciated.

I am thankful to the members of the Brusso research group, both past and present. In particular, I would like to thank Dr. Sonia Lin, Michael Triglav, and Mélanie Cyr for welcoming me into the group, showing me around the lab, and providing early support. I would also like to acknowledge the current group members, Dr. Nicolas Ledos, Mélanie Cyr, and Adam Renco, for helpful discussions, technical assistance, shared troubleshooting, and camaraderie throughout my graduate studies. I am also grateful to members of the Lessard group, especially May Ourabi and Dr. Hyungjun Cho, for their assistance and helpfulness. I would like to thank the NMR facility managers and staff for their technical support.

Finally, I would like to thank my family and friends for their constant support, patience, and encouragement throughout this journey. This work would not have been possible without their continued understanding and support.

TABLE OF CONTENTS

List of Figures

Supporting Figures:

List of Tables

List of Schemes

Supporting Schemes:

CHAPTER 1: INTRODUCTION

Field effect transistors (FETs) are essential in modern electronics, enabling management of electrical current through the application of an electric field. FETs have made a large contribution to today's electronics, from the development of metal-oxide FETs (MOSFETs) in the 1960s to modern-day flexible electronics.[1,2] FETs are core components in integrated circuits, microprocessors, memory devices, displays, and sensors;[3–7] operating through a three-terminal on/off switch system.[8–10] The on/off is controlled by the gate voltage applied at the gate electrode, which will then control the channel's current path from the source to the drain, and the other two electrodes (see **Figure 1.1**).[10] The flow of current between the source and the drain is dependent on the voltage gate applied, as well as the electronic properties of the semiconductor material used.[5,9,11] FETs are classified into four types: MOSFET, junction (JFET), high electron mobility transistors (HEMT) with inorganic semiconductors, and organic field-effect transistors (OFET) using organic materials.[8]

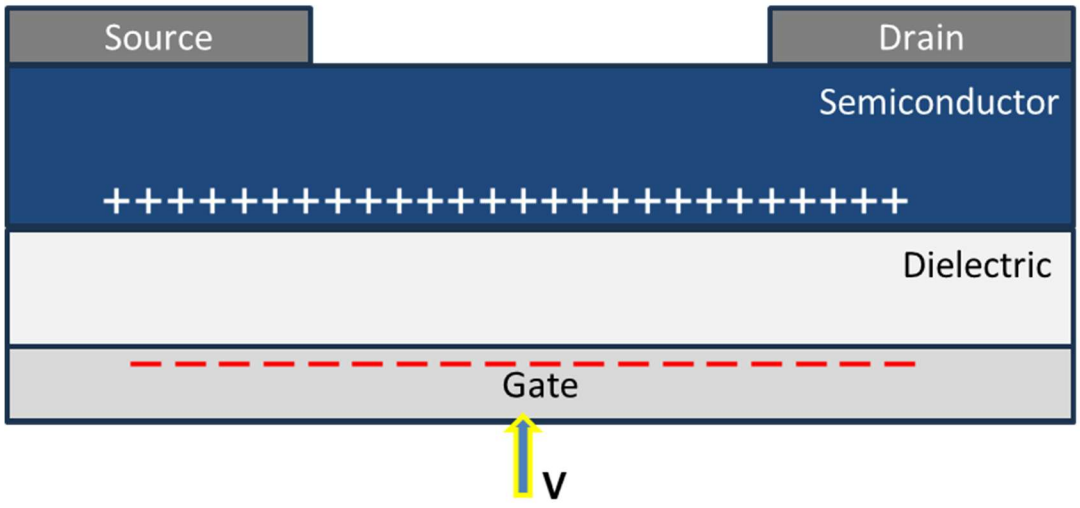

Figure 0.1: Schematic representation of a *p*-type semiconductor in a bottom-gate top-contact FET device architecture in its on state.

1.1 ELECTRICAL CHARACTERIZATION

Electrical characterization of field-effect transistors (FETs) provides valuable insights into charge transport, device stability, and overall functionality. The charge-carrier mobility (μ) reflects how quickly carriers move through the semiconductor under an applied electric field; higher μ indicates more efficient transport and is generally desirable for high-performance devices.[12] The threshold voltage (V_T) represents the gate voltage required to form a conductive channel; a lower V_T is preferred for low-power operation, provided it remains stable and well-defined.[13,14] The on/off current ratio (I_{ON}/I_{OFF}) quantifies the device's ability to switch between conducting and insulating states, with higher ratios indicating better switching performance and reduced leakage. Finally, hysteresis, the difference between forward and reverse gate sweeps-serves as an indicator of charge trapping and interfacial defects; minimal hysteresis is desirable for stable and reproducible operation.[13,14] **Figure 1.2** outlines the key electrical measurements utilized in this characterization. The output characteristics show how the source-drain current (I_{SD}) varies with the applied source-drain voltage (V_{SD}) at fixed gate voltages (V_{GS}).[13,14] As depicted in **Figure 1.2a**, there are two primary transport regimes: 1) **Linear Regime** (Ohmic Region), at low V_{SD}, the channel is uniformly accumulated, making the device act like a voltage-controlled resistor; here, I_{SD} increases linearly with V_{SD}, with a slope that rises alongside V_{GS}.[15] 2) **Saturation Regime**, at sufficiently high V_{SD}, the channel near the drain gets pinched off, leading to saturation of the current; this regime is essential for determining charge-carrier mobility (μ) and threshold voltage (V_T) from the transfer characteristics. The transfer curves track I_{SD} as a function of V_{GS} at a constant V_{SD}, typically within the saturation regime.[14,16] **Figure 1.2b** presents both forward and reverse sweeps, which help assess hysteresis and charge trapping. The minimal gap between these curves

suggests low trap density and stable device operation. Within the saturation regime, the square-root relationship between I_{SD} and V_{GS} enables linear fitting to extract μ and V_T.[13,14]

Figure 1.2c illustrates the typical plot of SQRT(I_{SD}) against V_{GS}. Together, these metrics provide a comprehensive view of the performance and reliability of the FET devices investigated in this study.

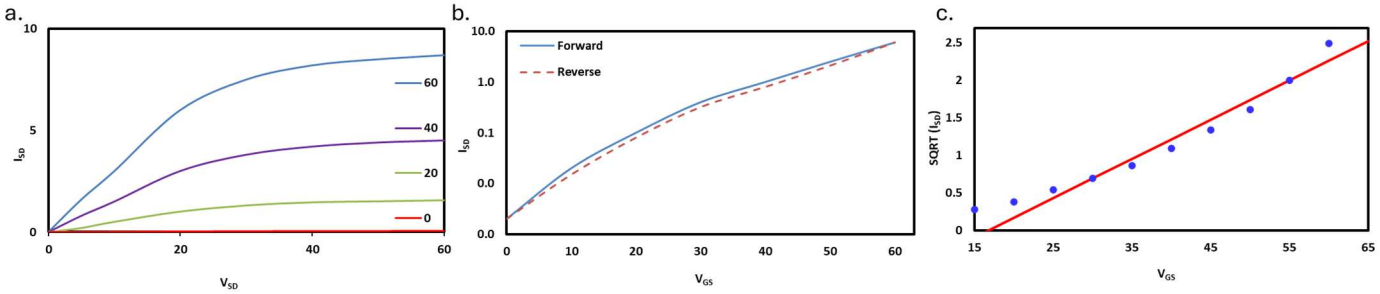

Figure 0.2: An exemplary electrical characteristic derivation of a FET device. a). Output curve, with various bias V_{SD} applied, b). forward and reverse transfer curves, and c). plot of SQRT(I_{SD}) versus V_{GS} with dashed line representing the tangent that may be used to calculate μ and V_T for an *n*-type devices.

1.2 ORGANIC THIN-FILM TRANSISTORS

OFETs, or often referred to as organic thin-film transistors (OTFTs), have drawn a lot of interest because of their potential for low-cost production, mechanical adaptability, and compatibility with large-area processing.[17–20] The mechanically adaptable nature of OTFTs, in contrast to the brittle inorganic semiconductors, allows them to be integrated from flexible, bendable displays to wearable biomedical devices.[21–26] OTFTs can be categorized into three different subgroups, *p*-type, *n*-type, and ambipolar, depending on the charge carrier nature of the semiconductors.[27] *P*-type is characterized as materials that permit holes to migrate through the layer, while *n*-type permits electrons to migrate, whereas ambipolar materials allow for holes and electrons to effectively transport through the active layer.[28] While *p*-type organic

semiconductors (OSCs) have been extensively explored and credited for efficient device performance and thus adopted, the broader adoption of *n*-type and ambipolar *OSCs* is limited by environmental instability, injection barriers, and transport variability.[29–31] Due to these properties, the selection of the active-layer material is a critical determinant of the OTFT's performance.

Important device properties, including charge carrier mobility, threshold voltage, and on/off current ratio, are determined by the molecular structure, packing, and morphology of the active organic semiconductor layer.[32] The electrical characteristics of the OSC are fundamentally affected by the nature of charge transport, which takes place in materials that are mainly bonded by weak van der Waals forces.[19,33] In contrast, the inorganic semiconductors tend to form extensive crystalline lattices characterized by substantial intermolecular bonds that facilitate band-like charge transport.[8] Owing to these fundamental differences, OSC molecular design and the subsequent solid-state interactions are essential parameters for developing high-performing organic electronics.[27,34–36]

Another critical set of factors influencing organic semiconductor performance arises from thin-film processing conditions, including deposition method, solvent selection, and thermal treatment, which collectively govern film morphology, molecular orientation, and grain structure and thereby exert a direct impact on charge-transport characteristics.[37–40] Consequently, charge transport in OSCs is strongly influenced by molecular structure, including degree of π-conjugation, molecular planarity, intermolecular packing, and aggregation behavior, making the OSC design an important factor.[27,38,41] Shorter intermolecular distances and well-organized molecular packing facilitate more efficient charge transfer, while proper energy-level alignment with the electrodes is required for effective charge injection.[27,42]

Conjugated polymers and macromolecular semiconductors represent the most common classes of OSCs employed in OTFTs due to their ease of availability, low cost, and chemical tunability, both relying on π-conjugated frameworks that support charge transport through delocalized electronic systems.[18,43] As seen in **Figure 1.2**, polymeric semiconductors such as polythiophene,[44] poly(3-hexylthiophene),[45] or polyfluorenes[46] have been employed in transistors; similarly, small molecules like pentacene,[34] rubrene,[47] and phthalocyanines[48] are also commonly utilized in OSCs due to their reproducible charge-transport, vacuum and solution processability, control of structure-properties and more.[49–52]

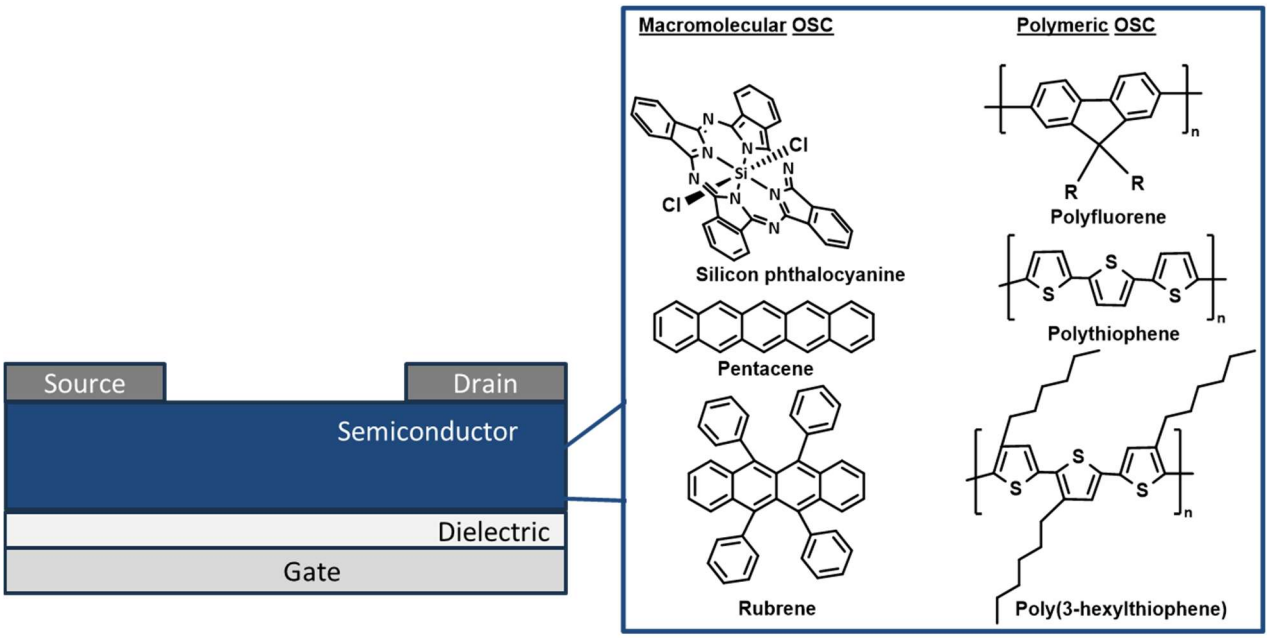

Figure 0.3: Chemical structures of some polymers and small molecules employed as organic semiconductors.

1.3 PHTHALOCYANINES: SILICON PHTHALOCYANINE

Of particular importance to this thesis, phthalocyanines (Pcs) are a class of planar, conjugated macrocyclic compounds consisting of an 18-electron system.[53] The extensive π-conjugation inherent to the phthalocyanine macrocycle results in highly delocalized frontier

molecular orbitals, which are responsible for the characteristic redox behavior, electronic conductivity, and distinctive optical absorption of these materials.[54,55] Historically, Pcs have been used in a variety of applications since their first discovery in the early 20th century as pigments and dyes due to their intense green/blue colors.[56] Beyond pigmentation, the robust thermal, chemical and environmental stability of phthalocyanines and their tunable electronic properties have enabled their integration into a broad range of electronic devices; these include OTFTs,[57–59] organic photovoltaics (OPVs),[60,61] organic light-emitting devices (OLEDs),[62,63] photodynamic therapy agents,[64,65] catalysts[66,67] and more.[68–70] Strong light absorption, electron transfer abilities, and structural modularity are some of the advantageous components of these macromolecules. These versatile macrocyclic compounds are often associated with great optoelectronic properties, such as absorption in the visible-near-infrared (NIR) region and tunable electrochemical characteristics, making them ideal materials for OSCs.[8,48]

These macromolecules can exist with or without a central element. The core metal/metalloid can also be varied to alter the electronic, optical, and chemical tunable properties.[71,72] Chemical tailoring of these macrocycles can be done along the periphery positions (see **Figure 1.3**), either extending the π-system, planarity or enhancing the solubility by disrupting the aggregation or through polar interaction.[59] The phthalocyanine core's electrical and effective conjugation are mainly affected by functionalization at the peripheral (α or β) regions of the macrocycle.[73–78] Through inductive and resonance effects, electron-donating substituents like alkoxy or alkylthio groups and electron-withdrawing substituents like fluorinated or cyano-containing moieties modulate HOMO and LUMO energy levels, allowing for the methodical tuning of redox potentials and charge-injection barriers.[59,72,78–81] Phenyl

and other aromatic units are examples of conjugated peripheral groups that can enhance intermolecular electronic coupling, extend the delocalized π-system outside the phthalocyanine ring, and expand optical absorption into the visible-NIR region.[73–76] While conjugation extension is often beneficial for charge transport and light harvesting, it also might enhance molecular planarity, which might increase π–π stacking interactions, promote excessive aggregation, and thus limit the solubility.[77,80,82–84]

Inherently, phthalocyanines tend to be insoluble; therefore, the conformational flexibility of the substituents (peripheral or axial) might control aggregation behavior and solubility.[85–88] Long alkoxy substituents, nonplanar functional groups, and bulky or branched alkyl chains create steric hindrance that prevents close face-to-face π-stacking, preventing aggregation and greatly increasing its chances of solubility,[86,89–91] a crucial prerequisite for solution-based processing and thin-film fabrication.[59] Small, rigid, and planar substituents, on the other hand, promote increased crystallinity and dense molecular packing.[86] The intrinsic trade-off between electrical performance and morphological control is highlighted by the fact that while enhanced crystallinity can improve charge transport in the solid state, it typically reduces solubility and processability.[90]

Additionally, depending on the valency of the metal or metalloid selected, the core element can be further functionalized for property modulation through axial substitution as well.[59,71,72,96] Aluminum phthalocyanines usually support a single axial ligand,[97] while group 14 elements like silicon and tin can support two axial ligands, allowing for more structural freedom and symmetry control.[98,99]

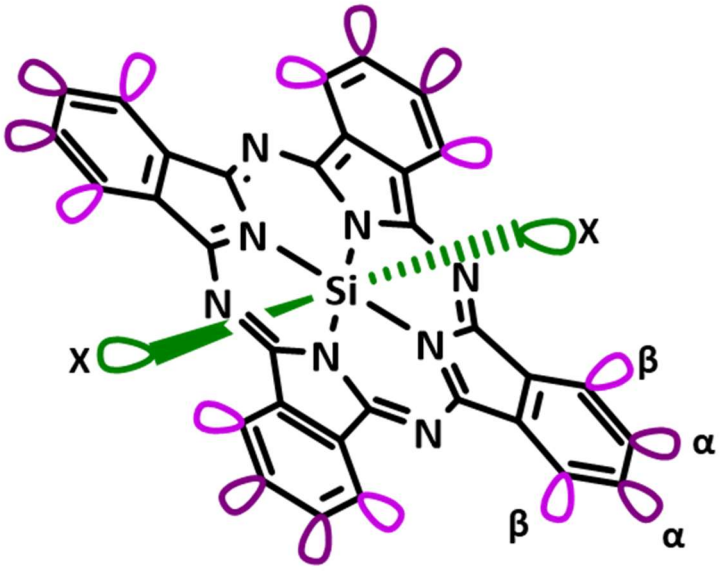

Figure 0.4: Chemical structure of silicon phthalocyanine displaying possible functionalization at the peripheral positions (α & β) and axial positions (X).

Because of these properties and their stability, silicon phthalocyanines (SiPcs) have been modulated for specific applications. Specifically, the presence of two axial coordination sites often enables control over intermolecular packing, π–π interactions, and thin-film morphology without a large impact on the optoelectronic integrity of the phthalocyanine core;[59] since the axial substituents lie out of the π-conjugated plane and have minimal orbital overlap with the delocalized π-system that governs the energy levels and optical absorption.[100] Depending on their steric bulk and conformational flexibility, axial substituents can significantly enhance solubility and solution processability by disrupting excessive π–π aggregation[101–103] and facilitating a low-cost, large-area fabrication technique while maintaining reproducible film quality.[37,104] For example, axially pegylated SiPcs are found to have greater solubility,[105] while rigid perfluorinated phenyl axial groups tend to have poor solubility.[101] In addition to the tunable properties of SiPcs, the axial substituent can act as a reactive site, further broadening their applications. For example, by methodically designing the axial ligand, chemical

functionalization such as electropolymerization can be induced on the axial substituent.[106–108] In doing so, new properties may be added to the SiPc molecules, which can either enhance the overall performance or add more functionality, and therefore potentially expand their applications. For instance, electropolymerization of dimethylamino-derived SiPcs for electrochemical applications demonstrated the formation of polymeric SiPc films through oxidative coupling.[109] Likewise, inclusion of a variety of functional groups, such as terminal alkynes on the axial positions, may permit the OSC materials to be used in homocoupling or click reactions. The axial moiety and planar SiPc core structural separation often enables axial ligands to operate as chemically orthogonal handles, allowing for post-synthetic modifications without interfering with the SiPc backbone's primary optoelectronic activity.[101,110,111] Recent research on axially substituted silicon phthalocyanines shows that large aromatic axial substituents, such as pyrenebutoxy and anthrylmethylamino groups, have a significant impact on solubility, intermolecular interactions, and act as a tether to fix the molecule onto the inorganic surface (TiO_2 nanoparticles).[98] The ability of axial groups to mediate surface attachment and interfacial interactions highlights their utility for surface grafting or polymer-small molecule interface engineering in transistor architectures.

SiPcs pose as promising materials for OTFT, due to their unique *n*-type charge carrier properties, unlike most OSCs classified as *p*-type.[101] Due to this, optimizing SiPcs and fabricating a stable and high-performing OTFT is important. The tetra valency of the SiPc macromolecules can further be manipulated to induce chemical diversity by introducing asymmetry via the axial position (X_1 and X_2). The two distinct axial moieties on the silicon phthalocyanine, as demonstrated in the Cranston *et al.* OTFT study with one siloxane and a fluorine atom, and the Martín-Gomis *et al.*'s triad with distinct perylenediimide and

fulleropyrrolidine (C_{60}) ligands, demonstrated selective reactivity by tuning steric hindrance, electronic coupling, and spatial proximity to favor directional electron transfer or charge transport over competing pathways.[112,113] More in-depth, Martín-Gomis *et al.* initially synthesized their asymmetrical SiPc (where X_1 = aldehyde, X_2 = terminal alkyne), followed by subjecting one axial group to a dipolar cycloaddition, while the other was subjected to click chemistry reactions, respectively,[113] demonstrating axially substituted SiPcs' potential for chemical tuning at two different sites.

1.4 CLICK CHEMISTRY REACTIONS

Although it's possible to create a strong covalent bond through other means, click chemistry reactions proceeding under mild conditions allow for the quick and dependable synthesis of complex compounds from easily accessible building blocks since they are effective, selective, and operationally straightforward.[114,115] This process is known to produce compounds in quantifiable levels with simpler purification procedures and fewer byproducts.[114] Sharpless and co. first defined the idea of "click chemistry," outlining specific criteria for reactions to be classified as "click" processes, such as high thermodynamic driving force, ease of operation, and the production of few byproducts that can be eliminated without chromatography.[116] Click chemistry can be useful since it allows modular side-chain engineering and post-functionalization without interfering with delicate π-conjugated cores.[104,117,118] This makes it ideal for retaining synthetic reproducibility while adjusting solubility and intermolecular interactions in organic semiconductors, such as polymer-small molecule systems. Moreover, click chemistry is especially valuable in the realm of materials science and organic electronics. Marrocchi *et al.* reviewed click-based methods for the synthesis and modification of π-conjugated polymers used in organic field-effect transistors, organic

photovoltaics, and related optoelectronic devices, providing a thorough basis for the application of click chemistry in organic electronics. Because of its remarkable regioselectivity, high yields, and compatibility with a wide range of conjugated backbones, this study emphasizes the copper(I)-catalyzed azide–alkyne cycloaddition (CuAAC) as the most extensively used click reaction. Crucially, the review highlights how click chemistry permits modular side-chain engineering and late-stage functionalization without interfering with backbone conjugation, enabling systematic adjustment of solubility, shape, and intermolecular interaction.[119,120] These attributes make click reactions particularly attractive for polymer–small molecule systems and organic electronic architectures, where reproducibility and structural precision are essential. This characteristic is essential for maintaining synthetic reproducibility, a key factor when developing materials with consistent performance characteristics. Knoll *et al*. demonstrated the practical resilience of click chemistry in organic electronic device engineering through a click-mediated covalent modification of poly(3,4-ethylenedioxythiophene) (PEDOT) materials, which shows that post-fabrication functionalization may be accomplished without impairing core device performance.[121] Additionally, their follow-up work using the PEDOT as an OSC for biosensing demonstrated interface engineering post-deposition enabled through click chemistry.[122] Without sacrificing the electrical performance of conducting polymer films, these techniques allow for precise interface engineering and functional diversification. Furthermore, related research in bio-organic electronics and sensing shows that click chemistry enables the integration of biomolecular functionalities and redox probes with electronically active substrates, underscoring the versatility and adaptability of click-based functionalization techniques.[119] Collectively, these investigations demonstrate click chemistry as a scalable, dependable, and expandable tool for developing organic electronic materials, especially for

applications that need interfacial control, post-synthetic functionalization, and electronic structure preservation.

1.5 ENHANCING THE PERFORMANCE OF ORGANIC SEMICONDUCTORS

The overall device performance of OTFTs can be enhanced by strategic semiconductor design, as well as by the inclusion of polymer additives in a manner of polymer/small molecule blend (as illustrated in **Figure 1.4)**, which has aided in improving the charge mobility, processability, and overall thin-film morphology of these type of devices, as demonstrated by the following blends: (thienoacenes and polystyrene) or (2,8-difluoro-5,11-bis(triethylsilylethynyl) anthradithiophene and poly(α-methylstyrene)) or (6,13-bis(triisopropylsilylethynyl)-pentacene) and poly(α-methylstyrene).[123–127] For instance, hole mobility was enhanced by up to an order of magnitude when thieno[3,2b]thiophene-based thienoacenes were blended with polystyrene (1:1 wt/wt), where one blend system had a maximum mobility of 9.2×10^{-3} $cm^2 V^{-1} s^{-1}$ and demonstrated >1000% mobility enhancement in comparison to neat thienoacene films, combined with much lower device-to-device variability and more reliable airborne operation.[123] Similarly, in contrast to neat films, which showed mobilities scattered by more than an order of magnitude and frequent device failure, 2,8-difluoro-5,11-bis(triethylsilylethynyl) anthradithiophene/poly(a-methylstyrene) blend OTFTs exhibit significantly improved uniformity and stability, as shown by narrowing the saturation mobility distribution window to around 10^{-2} $cm^2 V^{-1} s^{-1}$. While neat semiconductor devices demonstrated a considerable decline, improved operational stability in the blended devices was maintained under continuous bias in air.[124] The blend systems combine the outstanding film-forming ability, mechanical adaptability, and processability of polymers with the advantageous charge-transport features of the conjugated

semiconductors. In addition to lowering defects, grain boundaries, and trap densities, the polymer matrix controls semiconductor crystallization and phase separation, allowing continuous percolation channels for charge transfer.[128,129] It should be noted that most of these systems are obtained using a simple blend (i.e. without forming any covalent bonds between the blended species).

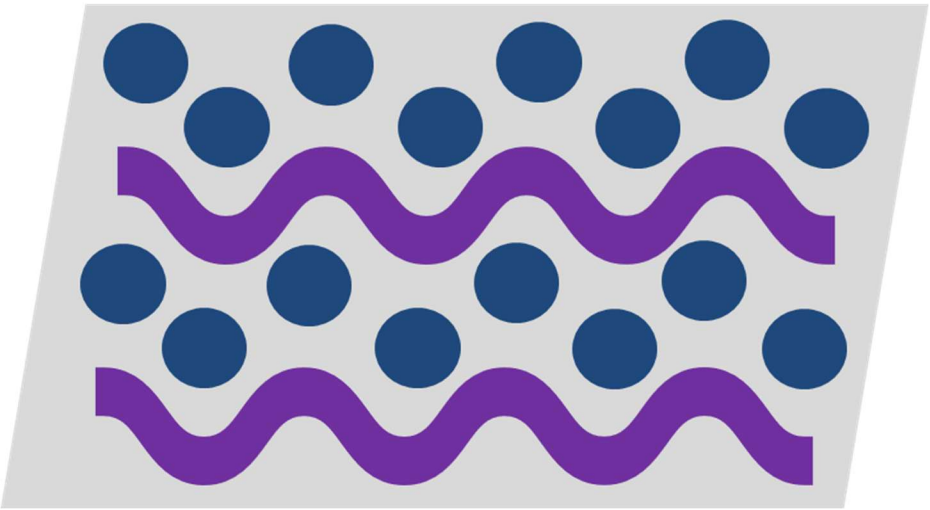

Figure 0.5: Representative morphology of polymer-small-molecule OSC, showing a conjugated polymer matrix (purple) with dispersed small-molecule semiconductors (blue).

Although blended systems have demonstrated enhanced device performance, challenges regarding film morphology and phase segregation are associated with this technique as well.[130–132] The blends' solvent evaporation rate, viscosity, and solvent-solute interactions are some of the few parameters contributing to these observations.[127] However, unlike the simple blend, in organic solar cells, a polymer backbone and a pendant have been covalently attached to act as a single active layer, instead of the conventional two-component donor/acceptor bilayers,[133–135] which is suggested to enhance the stability of the active layer in the long run.[134]

Current OFET materials have several enduring drawbacks that prevent their mainstream acceptance, despite significant advancements. Charge mobility and reproducibility are limited by energy disorder and trap states resulting from weak intermolecular interactions, while environmental instability, particularly for *n*-type and ambipolar semiconductors, leads to performance degradation under ambient conditions.[39,136,137] These problems arise due to *n*-type organic semiconductors being intrinsically unstable under ambient conditions because of insufficient LUMO stabilization (typically > -4.0 eV), enabling oxygen and moisture to act as electron traps and chemical oxidants, leading to superoxide formation, unintentional *p*-doping, and progressive degradation of charge transport and device stability.[138–141] Often, there is a trade-off between electrical performance and scalable manufacturing since efforts to improve crystallinity and π–π stacking frequently impair solubility and processability, among other drawbacks.[50,142–144] The need for new material platforms that combine ideal optoelectronic characteristics, regulated solid-state organization, and strong operational stability is highlighted by issues such as ineffective charge injection, morphological instability under operation, and limited mechanical durability.[27,39,145]

The optoelectronic and morphological characteristics of conjugated polymers may be changed by covalently linked side chains. Sommer *et al.'s* report demonstrates a P3HT polymer with pendant fullerene (C_{60} or Phenyl-C_{61}-butyric acid methyl ester (PCBM)) side chains as a single-component active layers, achieving a power conversion efficiency (PCEs) up to 1.8% (vs. 3-4% for P3HT: PCBM blends), with ideal phase separation (~10 nm Donnor-Acceptor domains) from pendant fullerenes acting as electron acceptors along the donor backbone.[146] Controlling miscibility and phase separation between conjugated backbones and covalently attached electron-acceptor side units is also reported to affect exciton separation and charge transport in

double-cable conjugated polymers intended for single-component organic solar cells, allowing a record PCE of more than 8% within a single-material system.[133] More significantly, Peters and Tovar reported pendant photochromic conjugated polymers with thieno[3,4-b]thiophene units as stimulus-responsive side chains, showing that covalently appended functional pendants can modify optoelectronic properties without interfering with backbone conjugation.[147] This design approach is similar to the use of chemically reactive handles on axial ligands and small molecules in semiconductor systems.

While typical polymer or small-molecule semiconductors are often investigated in OTFTs, strategies that covalently incorporate discrete semiconducting units into a polymer framework are comparatively underreported in this device class. An intriguing example is a poly(rod-coil) polymer that covalently joins conjugated diketopyrrolopyrrole-based cores with flexible butylene units to create an OTFT active layer with improved film formation and repeatable charge transport comparable to the original small molecule.[148] This work demonstrates that covalent bonding of small semiconductor chromophores into a macromolecular backbone can address morphological constraints without compromising mobility and sets a design precedent for polymer-small-molecule architectures, such as clickable polymer pendants in future OTFT materials.

1.6 THESIS OBJECTIVE

Expanding the polymer-pendant system into OTFTs using SiPcs, an approach would be through a specific axial ligation that would covalently attach the SiPc framework to a polymer surface as a pendant or graft them at the surface of a polymer through the formation of a triazole ring via click chemistry; an area of research that has not been explored much, but is the

motivation behind the current research/dissertation. Through the covalent bond, OTFT fabrication challenges associated with material stability, phase separation, and mechanical robustness may be addressed. The click chemistry and formation of the triazole ring pave the way for a strong bond between the polymer and SiPc, and thus may extend to improved interfacial properties, lower surface roughness, improved crystallinity, and control over the orientation and spacing, leading to better device performance by potentially enhancing the charge transport and lower operating voltage. Challenges associated with the weaker interfacial interaction between the two blended materials and their susceptibility to environmental stress might be addressed by the formation of triazole rings. Overall, this exploration is anticipated to advance knowledge in organic semiconductors, specifically *n*-type small molecules (SiPc), as a potential for low-cost, flexible electronics with controlled/compatible interfaces.

To do the above, designing SiPc frameworks with suitable axial moieties for click chemistry is crucial. That being improved solubility, suitable electronic performance, and most importantly, an axial unit with an available reactive site. As mentioned before, the tetra valency of the Si core in SiPcs allows for two axial substitutions, and in most cases, the axial moieties are identical. To produce a functional polymer-SiPc system, cross-linking of the system should be minimized. The cross-linking would potentially take place if the polymer folds over and the click reaction happens at both axial positions of the SiPc (see **Figure 1.5**). With that in mind, the objective of the thesis was to i) design and synthesize novel silicon phthalocyanines with clickable functionality, ii) characterize their structural, optical, and electronic properties, and iii) evaluate their performance as active layers in OFET devices. In this thesis, designing axial ligation with a reactive terminal alkyne group for click chemistry, demonstrating click chemistry on the axial unit post SiPc synthesis (as an illustration to future polymer coupling), exploring

SiPcs' solubility induced through the axial moieties, and lastly designing axially asymmetrical SiPcs for chemical diversity are explored.

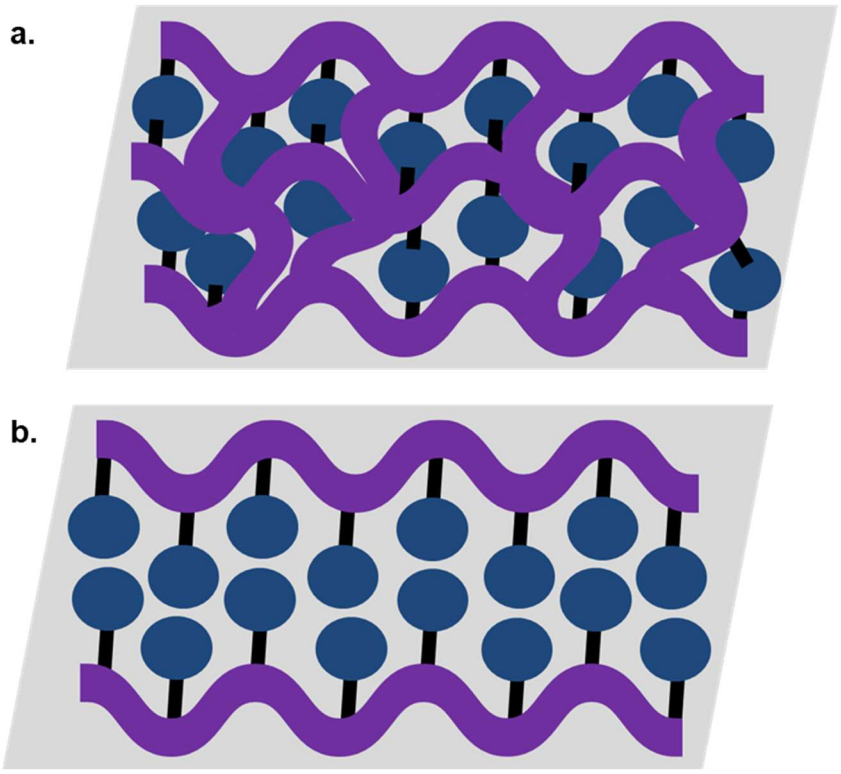

Figure 0.6: Polymer-small molecule based OSCs design; a). schematic representation of polymer crosslinking with a symmetrically substituted SiPc to create a covalent bond; b). proposed polymer-SiPc coupling through a singular axial unit of the SiPc.

1.7 SCOPE OF THESIS

This thesis focuses on the development and advancement of axially substituted silicon phthalocyanine OSC for OTFTs, to better understand the structure–property relationships and electric properties. **Chapter 2** presents the methodical development of clickable silicon phthalocyanine platforms for flexible semiconductor functionalization. Alkyne-functionalized benzyloxy-substituted symmetrical and asymmetrical silicon phthalocyanines are designed, synthesized, and integrated into OTFTs. Additionally, as a demonstration for future polymer-SiPc

systems, copper (I)-catalyzed azide–alkyne cycloaddition (CuAAC) click chemistry is highlighted as a versatile technique for coupling the SiPc derivatives to a polymer. This chapter highlights the advantages of axial asymmetry and modular functionalization for optimizing silicon phthalocyanines for organic electronic applications, particularly OTFTs.

Akin to **Chapter 2**, **Chapter 3** focuses on the chemical design and synthetic methodologies of alkyne-thienyl-based axially functionalized silicon phthalocyanines. The optical and electrochemical features are investigated, while attention is given to assessing how axial ligand identity influences solubility and stability, as these properties are critical for downstream processing and functional diversification.

In-depth experimental synthesis, characterization, and analysis of silicon phthalocyanine derivatives are provided in **Chapter 4**. The preparation of asymmetrical axially substituted silicon phthalocyanines from various starting materials is the primary focus, along with an evaluation of synthetic approaches, reaction optimization, and difficulties in attaining controlled axial substitution. To verify molecule identification and purity, a thorough structural characterization is provided utilizing spectroscopic and electrochemical methods. The optical and electrochemical features of the produced compounds are also systematically investigated in this chapter, with a focus on how molecular symmetry and axial substitution patterns affect frontier orbital energies, absorption behavior, and redox characteristics.

The key findings from each study are presented in **Chapter 5**, along with suggestions for further research on the use of the newly synthesized OSCs in OTFTs, click reaction with an appropriate polymer, and further implementation of the asymmetrical synthesis methodology for the synthesis of other functional silicon phthalocyanine.

1.6 REFERENCES

1. Sun M, Wang S, Liang Y, Wang C, Zhang Y, Liu H, Zhang Y and Han L. *Nano-Micro Lett.* 2024; **17**: 34.

2. Yuan JS and Liou JJ. In Yuan JS, Liou JJ, eds Semiconductor Device Physics and Simulation. Boston, MA: Springer US, 1998; 127-161.

3. Sheraw CD, Zhou L, Huang JR, Gundlach DJ, Jackson TN, Kane MG, Hill IG, Hammond MS, Campi J, Greening BK, Francl J and West J. *Appl. Phys. Lett.* 2002; **80**: 1088-1090.

4. Physics of Semiconductor Devices. Boston: Kluwer Academic Publishers; 2002.

5. Ohring M. In Reliability and Failure of Electronic Materials and Devices. Elsevier, 1998; 37-104.

6. Panahi A and Ghafar-Zadeh E. *Bioengineering (Basel)* 2023; **10**: 793.

7. Ahmad W, Gong Y, Abbas G, Khan K, Khan M, Ali G, Shuja A, Tareen AK, Khan Q and Li D. *Nanoscale* 2021; **13**: 5162-5186.

8. Sun Y, Liu Y and Zhu D. *J. Mater. Chem.* 2005; **15**: 53-65.

9. Anzi L, Tuktamyshev A, Fedorov A, Zurutuza A, Sanguinetti S and Sordan R. *npj 2D Mater Appl* 2022; **6**: 28.

10. Kim H. *Electron. Mater. Lett.* 2025; **21**: 650-666.

11. Narula MS and Pandey A. In 2022 8th International Conference on Signal Processing and Communication (ICSC). , 2022; 554-559.

12. Katz HE and Bao Z. *J. Phys. Chem. B* 2000; **104**: 671-678.

13. DOI:10.1016/B978-012533084-8/50015-X.

14. Zaumseil J and Sirringhaus H. *Chem. Rev.* 2007; **107**: 1296-1323.

15. Un H, Wang J and Pei J. *Adv Sci (Weinh)* 2019; **6**: 1900375.

16. Chatzigiannakis G, Soultati A, Palilis LC, Polydorou E, Davazoglou K, Filippatos P-P, Perumallapelli GR, Bukke RN, Yusoff AbdR bin M, Ryu I, Gao P, Chroneos A, Nazeeruddin MK and Vasilopoulou M. *Advanced Electronic Materials* 2026; **12**: e00568.

17. Lee JM, Jung J-Y and Baeg K-J. *J. Korean Phys. Soc.* 2023; **83**: 350-357.

18. Luo L, Huang W, Yang C, Zhang J and Zhang Q. *Front. Phys.* 2021; **16**: 33500.

19. Dimitrakopoulos C d. and Malenfant P r. l. *Advanced Materials* 2002; **14**: 99-117.

20. Li Y-F, Guo Y-L and Liu Y-Q. *Chin J Polym Sci* 2023; **41**: 652-670.

21. Wang C, Hwang D, Yu Z, Takei K, Park J, Chen T, Ma B and Javey A. *Nature Mater* 2013; **12**: 899-904.

22. Oh JY and Bao Z. *Advanced Science* 2019; **6**: 1900186.

23. Yang JC, Mun J, Kwon SY, Park S, Bao Z and Park S. *Advanced Materials* 2019; **31**: 1904765.

24. Wang S, Xu J, Wang W, Wang G-JN, Rastak R, Molina-Lopez F, Chung JW, Niu S, Feig VR, Lopez J, Lei T, Kwon S-K, Kim Y, Foudeh AM, Ehrlich A, Gasperini A, Yun Y, Murmann B, Tok JB-H and Bao Z. *Nature* 2018; **555**: 83-88.

25. Son D, Kang J, Vardoulis O, Kim Y, Matsuhisa N, Oh JY, To JW, Mun J, Katsumata T, Liu Y, McGuire AF, Krason M, Molina-Lopez F, Ham J, Kraft U, Lee Y, Yun Y, Tok JB-H and Bao Z. *Nature Nanotech* 2018; **13**: 1057-1065.

26. Niu S, Matsuhisa N, Beker L, Li J, Wang S, Wang J, Jiang Y, Yan X, Yun Y, Burnett W, Poon ASY, Tok JB-H, Chen X and Bao Z. *Nat Electron* 2019; **2**: 361-368.

27. Zhou Y, Zhang K, Chen Z, Zhang H, Zhou Y, Zhang K, Chen Z and Zhang H. *Materials* 2023; **16**.

28. Wu X, Jia R, Pan J, Zhang X and Jie J. *Nanoscale Horizons* 2020; **5**: 454-472.

29. Zaumseil J and Sirringhaus H. *Chem. Rev.* 2007; **107**: 1296-1323.

30. Zhang Y, Wang Y, Gao C, Ni Z, Zhang X, Hu W and Dong H. *Chem. Soc. Rev.* 2023; **52**: 1331-1381.

31. Mei J, Diao Y, Appleton AL, Fang L and Bao Z. *J. Am. Chem. Soc.* 2013; **135**: 6724-6746.

32. Chen X, Guo J, Peng L, Wang Q, Jiang S and Li Y. *Materials Today Electronics* 2023; **6**: 100077.

33. Kagan CR, Mitzi DB and Dimitrakopoulos CD. *Science* 1999; **286**: 945-947.

34. Zhang L, Zhao Y, Li J, Fu Y, Peng B, Yang J, Lu X and Miao Q. *J. Am. Chem. Soc.* 2025; **147**: 3459-3467.

35. Brédas J-L, Beljonne D, Coropceanu V and Cornil J. *Chem. Rev.* 2004; **104**: 4971-5004.

36. Miao C, Liang D, Gu L, Li C, Liu M, Li J, Vivo P and Zhang H. *Dyes and Pigments* 2023; **209**: 110855.

37. Sirringhaus H. *Advanced Materials* 2005; **17**: 2411-2425.

38. Brinkmann M and Rannou P. *Advanced Functional Materials* 2007; **17**: 101-108.

39. Noriega R, Rivnay J, Vandewal K, Koch FPV, Stingelin N, Smith P, Toney MF and Salleo A. *Nature Materials* 2013; **12**: 1038-1044.

40. Kline RJ, McGehee MD, Kadnikova EN, Liu J, Fréchet JMJ and Toney MF. *Macromolecules* 2005; **38**: 3312-3319.

41. Schwartz BJ. *Annual Review of Physical Chemistry* 2003; **54**: 141-172.

42. Li R, Dai Z, Zheng M, Wang C, Deng Z, Zhuang T, Feng K, Yang W, Yang K and Zhang H. *Macromolecular Rapid Communications* 2021; **42**: 2000703.

43. Li J, Ji Z, He A and Zhang H. *Front. Chem.* 2023; **11**.

44. Thanasamy D, Jesuraj D, Konda Kannan SK and Avadhanam V. *Polymer* 2019; **175**: 32-40.

45. Sirringhaus H, Brown PJ, Friend RH, Nielsen MM, Bechgaard K, Langeveld-Voss BMW, Spiering AJH, Janssen RAJ, Meijer EW, Herwig P and De Leeuw DM. *Nature* 1999; **401**: 685-688.

46. Scherf U and List E j. w. *Advanced Materials* 2002; **14**: 477-487.

47. McGarry KA, Xie W, Sutton C, Risko C, Wu Y, Young VGJr, Brédas J-L, Frisbie CD and Douglas CJ. *Chem. Mater.* 2013; **25**: 2254-2263.

48. Bao Z, Lovinger AJ and Dodabalapur A. *Appl. Phys. Lett.* 1996; **69**: 3066-3068.

49. Mishra A and Bäuerle P. *Angewandte Chemie International Edition* 2012; **51**: 2020-2067.

50. Amna B and Ozturk T. *Journal of Materials Chemistry C* 2025; **13**: 8354-8424.

51. Song X, Gasparini N, Nahid MM, Chen H, Macphee SM, Zhang W, Norman V, Zhu C, Bryant D, Ade H, McCulloch I and Baran D. *Advanced Functional Materials* 2018; **28**: 1802895.

52. Chen J, Zhang W, Wang L and Yu G. *Advanced Materials* 2023; **35**: 2210772.

53. Evangelisti M. In Encyclopedia of Supramolecular Chemistry - Two-Volume Set (Print). CRC Press, 2004.

54. Mitra K and T. Hartman MC. *Organic & Biomolecular Chemistry* 2021; **19**: 1168-1190.

55. Wong EWY, Walsby CJ, Storr T and Leznoff DB. *Inorg. Chem.* 2010; **49**: 3343-3350.

56. Linstead RP. *J. Chem. Soc.* 1934: 1016-1017.

57. Boileau NT, Cranston R, Mirka B, Melville OA and Lessard BH. *RSC Adv.* 2019; **9**: 21478-21485.

58. Li L, Tang Q, Li H, Hu W, Yang X, Shuai Z, Liu Y and Zhu D. *Pure and Applied Chemistry* 2008; **80**: 2231-2240.

59. Zhou W, J. Yutronkie N, H. Lessard B and L. Brusso J. *Materials Advances* 2021; **2**: 165-185.

60. de la Torre G, Bottari G and Torres T. *Advanced Energy Materials* 2017; **7**: 1601700.

61. Torre G de la, Claessens CG and Torres T. *Chem. Commun.* 2007: 2000-2015.

62. Flora WH, Hall HK and Armstrong NR. *J. Phys. Chem. B* 2003; **107**: 1142-1150.

63. Pearson AJ, Plint T, Jones STE, Lessard BH, Credgington D, Bender TP and Greenham NC. *J. Mater. Chem. C* 2017; **5**: 12688-12698.

64. Boileau NT, Melville OA, Mirka B, Cranston R and Lessard BH. *RSC Adv.* 2019; **9**: 2133-2142.

65. Gil-Martínez A, Hernández A, Galiana-Roselló C, López-Molina S, Ortiz J, Sastre-Santos Á, García-España E and González-García J. *J Biol Inorg Chem* 2023; **28**: 495-507.

66. Feng Y-C, Wang X and Wang D. *Mater. Chem. Front.* 2023; **8**: 228-247.

67. Cao R, Thapa R, Kim H, Xu X, Gyu Kim M, Li Q, Park N, Liu M and Cho J. *Nat Commun* 2013; **4**: 2076.

68. Urdaniz C, Taherpour S, Yu J, Reina-Galvez J and Wolf C. *J. Phys. Chem. A* 2025; **129**: 2173-2181.

69. Wong EWY, Walsby CJ, Storr T and Leznoff DB. *Inorg. Chem.* 2010; **49**: 3343-3350.

70. GÜNSEL A, USLUOĞLU A, BİLGİÇLİ AT, Büşra T, ARABACI G and YARAŞIR MN. *Turk J Chem* 2020; **44**: 923-931.

71. Lawrence DS and Whitten DG. *Photochemistry and Photobiology* 1996; **64**: 923-935.

72. R. Cranston R and H. Lessard B. *RSC Advances* 2021; **11**: 21716-21737.

73. B. Kc C, N. Lim G and D'Souza F. *Nanoscale* 2015; **7**: 6813-6826.

74. Matsushita O, Derkacheva VM, Muranaka A, Shimizu S, Uchiyama M, Luk'yanets EA and Kobayashi N. *J. Am. Chem. Soc.* 2012; **134**: 3411-3418.

75. Dubinina TV, Tomilova LG and Zefirov NS. *Russ. Chem. Rev.* 2013; **82**: 865-895.

76. Heuplick LJ, Fan Q, Astvatsaturov DA, Dubinina TV and Gottfried JM. *Commun Chem* 2024; **7**: 292.

77. Mack J and Kobayashi N. *Chem. Rev.* 2011; **111**: 281-321.

78. Furuyama T, Satoh K, Kushiya T and Kobayashi N. *J. Am. Chem. Soc.* 2014; **136**: 765-776.

79. Li R, Zhang X, Zhu P, Ng DKP, Kobayashi N and Jiang J. *Inorg. Chem.* 2006; **45**: 2327-2334.

80. Iida N, Tanaka K, Tokunaga E, Mori S, Saito N and Shibata N. *ChemistryOpen* 2015; **4**: 698-702.

81. Bench BA, Brennessel WW, Lee H-J and Gorun SM. *Angewandte Chemie International Edition* 2002; **41**: 750-754.

82. Li H, Jensen TJ, Fronczek FR and Vicente MGH. *J. Med. Chem.* 2008; **51**: 502-511.

83. de la Torre G, Vázquez P, Agulló-López F and Torres T. *Chem. Rev.* 2004; **104**: 3723-3750.

84. Hofman J-W, van Zeeland F, Turker S, Talsma H, Lambrechts SAG, Sakharov DV, Hennink WE and van Nostrum CF. *J. Med. Chem.* 2007; **50**: 1485-1494.

85. Rawling T, Xiao H, Lee S-T, Colbran SB and McDonagh AM. *Inorg. Chem.* 2007; **46**: 2805-2813.

86. Mitra K and Hartman MCT. *Org. Biomol. Chem.* 2021; **19**: 1168-1190.

87. Liao M-S, Kar T, Gorun SM and Scheiner S. *Inorg. Chem.* 2004; **43**: 7151-7161.

88. Chernonosov AA, Ermilov EA, Röder B, Solovyova LI and Fedorova OS. *Bioinorg Chem Appl* 2014; **2014**: 952632.

89. Li S, Qi Y, Wang J, Niu W, Ma W, Tang B and Zhang S. *ACS Omega* 2024; **9**: 50774-50785.

90. Dridi S, Khiari JE, Magna G, Stefanelli M, Lvova L, Mandoj F, Khezami K, Durmuş M, Natale CD and Paolesse R. *Molecules* 2023; **28**.

91. Saka ET, Çakır D, Bıyıklıoğlu Z and Kantekin H. *Dyes and Pigments* 2013; **98**: 255-262.

92. Bıyıklıoğlu Z. *Dyes and Pigments* 2013; **99**: 59-66.

93. Nyokong T. *Coordination Chemistry Reviews* 2007; **251**: 1707-1722.

94. Anthony JE. *Chem. Rev.* 2006; **106**: 5028-5048.

95. Kobak RZU, Arı MU, Tekin A and Gül A. *Chemical Physics* 2015; **448**: 91-97.

96. Potlog T, Lungu I, Airinei A and Tigoianu R. *ChemPhotoChem* 2025; **9**: e202400385.

97. Lamontagne HR, Cranston RR, Comeau ZJ, Harris CS, Shuhendler AJ and Lessard BH. *Adv Sci (Weinh)* 2024; **11**: 2305515.

98. Fazlı H, Akkol Ç, Kesmez Ö, Saka ET and Biyiklioglu Z. *Journal of Organometallic Chemistry* 2024; **1022**: 123408.

99. Grant TM, Rice NA, Muccioli L, Castet F and Lessard BH. *ACS Appl. Electron. Mater.* 2019; **1**: 494-504.

100. Pal AK, Varghese S, Cordes DB, Slawin AMZ, Samuel IDW and Zysman-Colman E. *Sci Rep* 2017; **7**: 12282.

101. Lessard BH. *ACS Appl. Mater. Interfaces* 2021; **13**: 31321-31330.

102. Wang M, Funabiki K and Matsui M. *Dyes and Pigments* 2004; **62**: 115-119.

103. Vebber MC, King B, French C, Tousignant M, Ronnasi B, Dindault C, Wantz G, Hirsch L, Brusso J and Lessard BH. *The Canadian Journal of Chemical Engineering* 2023; **101**: 3019-3031.

104. Facchetti A. *Chem. Mater.* 2011; **23**: 733-758.

105. Ourabi M, C. Vebber M, Cyr M, Weintrager FS-D, Ledos N, R. Lamontagne H, Nyayachavadi A, L. Brusso J and H. Lessard B. *Journal of Materials Chemistry C* 2025; **13**: 18167-18175.

106. Biyiklioglu Z and Alp H. *Dyes and Pigments* 2016; **132**: 213-222.

107. Biyiklioglu Z and Alp H. *Dalton Trans.* 2015; **44**: 18993-18999.

108. Biyiklioglu Z, Bas H and Alp H. *Dalton Trans.* 2015; **44**: 14054-14062.

109. Biyiklioglu Z and Alp H. *Dyes and Pigments* 2016; **132**: 213-222.

110. Cai X, Zhang Y, Qi D and Jiang J. *J. Phys. Chem. A* 2009; **113**: 2500-2506.

111. Ömeroğlu İ, Kaya EN, Göksel M, Kussovski V, Mantareva V and Durmuş M. *Bioorganic & Medicinal Chemistry* 2017; **25**: 5415-5422.

112. Cranston RR, Vebber MC, Faleiro Berbigier J, Brusso J, Kelly TL and Lessard BH. *Advanced Electronic Materials* 2022; **8**: 2200696.

113. Martín-Gomis L, Peralta-Ruiz F, Thomas MB, Fernández-Lázaro F, D'Souza F and Sastre-Santos Á. *Chemistry – A European Journal* 2017; **23**: 3863-3874.

114. Kolb HC, Finn MG and Sharpless KB. *Angewandte Chemie International Edition* 2001; **40**: 2004-2021.

115. Hein JE and Fokin VV. *Chem. Soc. Rev.* 2010; **39**: 1302-1315.

116. Kolb HC, Finn MG and Sharpless KB. *Angewandte Chemie International Edition* 2001; **40**: 2004-2021.

117. Juríček M, Kouwer PHJ, Rehák J, Sly J and Rowan AE. *J. Org. Chem.* 2009; **74**: 21-25.

118. Binder WH and Sachsenhofer R. *Macromolecular Rapid Communications* 2008; **29**: 952-981.

119. Degirmenci A, Yeter Bas G, Sanyal R and Sanyal A. *Bioconjugate Chem.* 2022; **33**: 1672-1684.

120. Marrocchi A, Facchetti A, Lanari D, Santoro S and Vaccaro L. *Chemical Science* 2016; **7**: 6298-6308.

121. Fenoy GE, Hasler R, Quartinello F, Marmisollé WA, Lorenz C, Azzaroni O, Bäuerle P and Knoll W. *JACS Au* 2022; **2**: 2778-2790.

122. Fenoy GE, Hasler R, Lorenz C, Movilli J, Marmisollé WA, Azzaroni O, Huskens J, Bäuerle P and Knoll W. *ACS Appl. Mater. Interfaces* 2023; **15**: 10885-10896.

123. Rice NA, Magnan F, Melville OA, Brusso JL, Lessard BH, Rice NA, Magnan F, Melville OA, Brusso JL and Lessard BH. *Materials* 2017; **11**.

124. Kim Y-H, Anthony JE and Park SK. *Organic Electronics* 2012; **13**: 1152-1157.

125. Niazi MR, Li R, Qiang Li E, Kirmani AR, Abdelsamie M, Wang Q, Pan W, Payne MM, Anthony JE, Smilgies D-M, Thoroddsen ST, Giannelis EP and Amassian A. *Nature Communications* 2015; **6**: 8598.

126. Park B, Jeon HG, Choi J, Kim YK, Lim J, Jung J, Cho SY and Lee C. *J. Mater. Chem.* 2012; **22**: 5641-5646.

127. Smith J, Hamilton R, McCulloch I, Stingelin-Stutzmann N, Heeney M, Bradley DDC and Anthopoulos TD. *J. Mater. Chem.* 2010; **20**: 2562-2574.

128. Kim Y-H, Anthony JE and Park SK. *Organic Electronics* 2012; **13**: 1152-1157.

129. Chung YS, Shin N, Kang J, Jo Y, Prabhu VM, Satija SK, Kline RJ, DeLongchamp DM, Toney MF, Loth MA, Purushothaman B, Anthony JE and Yoon DY. *J. Am. Chem. Soc.* 2011; **133**: 412-415.

130. Higgins AM, Martin SJ, Thompson RL, Chappell J, Voigt M, Lidzey DG, Jones RAL and Geoghegan M. *J. Phys.: Condens. Matter* 2005; **17**: 1319.

131. Ton-That C, Shard AG, Teare DOH and Bradley RH. *Polymer* 2001; **42**: 1121-1129.

132. Kim J-S, Ho PKH, Murphy CE and Friend RH. *Macromolecules* 2004; **37**: 2861-2871.

133. Jiang X, Yang J, Karuthedath S, Li J, Lai W, Li C, Xiao C, Ye L, Ma Z, Tang Z, Laquai F and Li W. *Angewandte Chemie International Edition* 2020; **59**: 21683-21692.

134. Liang S, Jiang X, Xiao C, Li C, Chen Q and Li W. *Acc. Chem. Res.* 2021; **54**: 2227-2237.

135. Lai W, Li C, Zhang J, Yang F, Colberts FJM, Guo B, Wang QM, Li M, Zhang A, Janssen RAJ, Zhang M and Li W. *Chem. Mater.* 2017; **29**: 7073-7077.

136. Kim S, Yoo H, Choi J, Kim S, Yoo H and Choi J. *Sensors* 2023; **23**.

137. Bobbert PA, Sharma A, Mathijssen SGJ, Kemerink M and De Leeuw DM. *Advanced Materials* 2012; **24**: 1146-1158.

138. de Leeuw DM, Simenon MMJ, Brown AR and Einerhand REF. *Synthetic Metals* 1997; **87**: 53-59.

139. Sun H, Gerasimov J, Berggren M and Fabiano S. *Journal of Materials Chemistry C* 2018; **6**: 11778-11784.

140. Di Pietro R, Fazzi D, Kehoe TB and Sirringhaus H. *J. Am. Chem. Soc.* 2012; **134**: 14877-14889.

141. Jones BA, Facchetti A, Wasielewski MR and Marks TJ. *J. Am. Chem. Soc.* 2007; **129**: 15259-15278.

142. Bersselaar BWL van den, W. Cattenstart EH, Ella Elangovan K, Yen-Chi C, Waal BFM de, Tol J van der, Diao Y, W. Meijer E and Vantomme G. *Journal of Materials Chemistry C* 2024; **12**: 6637-6644.

143. Hwang T, Kim Y, Tsogbayar D, Seo J, Park J, Oh S and Lee HS. *ACS Appl. Mater. Interfaces* 2025; **17**: 62370-62378.

144. Iino H and Hanna J. *Polym J* 2017; **49**: 23-30.

145. Chen X, Wang Z, Qi J, Hu Y, Huang Y, Sun S, Sun Y, Gong W, Luo L, Zhang L, Du H, Hu X, Han C, Li J, Ji D, Li L and Hu W. *Nature Communications* 2022; **13**: 1480.

146. Gholamkhass B, Peckham TJ and Holdcroft S. *Polym. Chem.* 2010; **1**: 708-719.

147. Peters GM and Tovar JD. *J. Am. Chem. Soc.* 2019; **141**: 3146-3152.

148. Xiao W-J, Wang J, Li H-J, Liang L, Xiang X, Chen X-Q, Li J, Lu Z and Li W-S. *RSC Advances* 2018; **8**: 23546-23554.

CHAPTER 2: DEVELOPMENT OF NOVEL SYMMETRICAL AND ASYMMETRICAL ALKYNE-FUNCTIONALIZED SILICON PHTHALOCYANINES, A POTENTIAL FUNCTIONALITY CONTROL FOR ORGANIC SEMICONDUCTORS.

This chapter is adapted from: Tigist Tilahun, Mélanie Cyr, May Ourabi, Benoît H. Lessard, and Jaclyn L. Brusso. Development of novel symmetrical and asymmetrical alkyne-functionalized silicon phthalocyanines, a potential functionality control for organic semiconductors. ***Tilahun*** *T. et al; J. Porphyrins Phthalocyanines 2026;* ***30****: 134–136*

Context

As the primary goal of my thesis was to develop functional SiPcs that can be linked to a polymer via its axial handle, one of the molecules of interest was bis((3-(prop-2-yn-1-yloxy)benzyloxy) silicon phthalocyanine (**2A**). The axial ligand 3-(prop-2-yn-1-yloxy)benzyloxy was designed to enable click chemistry with an azide-functionalized polymer. Ahead of the click reactions, the SiPcs' electrical characteristics were explored in organic thin-film transistors (OTFTs). However, the symmetrical derivative exhibited modest device performance and raised concerns regarding potential crosslinking during polymer attachment because of the two readily available terminal alkyne units, which could lead to poor processability in future applications. To address these limitations, asymmetry was introduced at the axial positions to simultaneously modulate electronic properties and reduce the likelihood of uncontrolled crosslinking.

Within this context, this chapter demonstrates how axial asymmetry enhances OTFT performance and chemical versatility through the development of asymmetrical alkyne-functionalized SiPcs. Importantly, it demonstrates that the incorporation of terminal alkynes provides a reactive handle for click chemistry, suggesting SiPcs as chemically flexible platforms

for integration into polymers, thereby positioning axial ligand engineering as a key strategy for advancing chemically tunable SiPc-based semiconductors.

Contribution

This work was completed through the contributions of all authors. I synthesized and, characterized all SiPc derivatives presented, conducted data analysis and wrote the first draft of the manuscript. M.C. assisted in the writing and editing of the manuscript as well as data analysis. M.O. fabricated and characterized the OTFTs and wrote **Section 2.2.5**. B.H.L. and J.L.B. provided supervision for the project.

Abstract

Metal or metalloid phthalocyanines offer a wide variety of chemical modifications that can be exploited to tailor the material properties to target different applications. This work demonstrates the electrochemical and optical finetuning of silicon phthalocyanine (SiPc) derivatives through the introduction of asymmetry at the axial position. When integrated in organic thin film transistors (OTFTs) as organic semiconductors, the studied asymmetric derivatives demonstrate modest *p*-type performance compared to the symmetrical equivalent. The highest performing derivative, an asymmetrical fluorinated SiPc, also demonstrated ambipolarity with performance similar to its fluorinated symmetrical counterpart. Owing to the presence of terminal alkynes on the axial handles, further chemical modifications were executed through click chemistry reactions to highlight the possibility of chemical tuning post-SiPc synthesis. The success of the click reaction suggests that these derivatives can be applied in the future to, for example, be attached to polymers, used to surface graft OTFTs, among other possibilities.

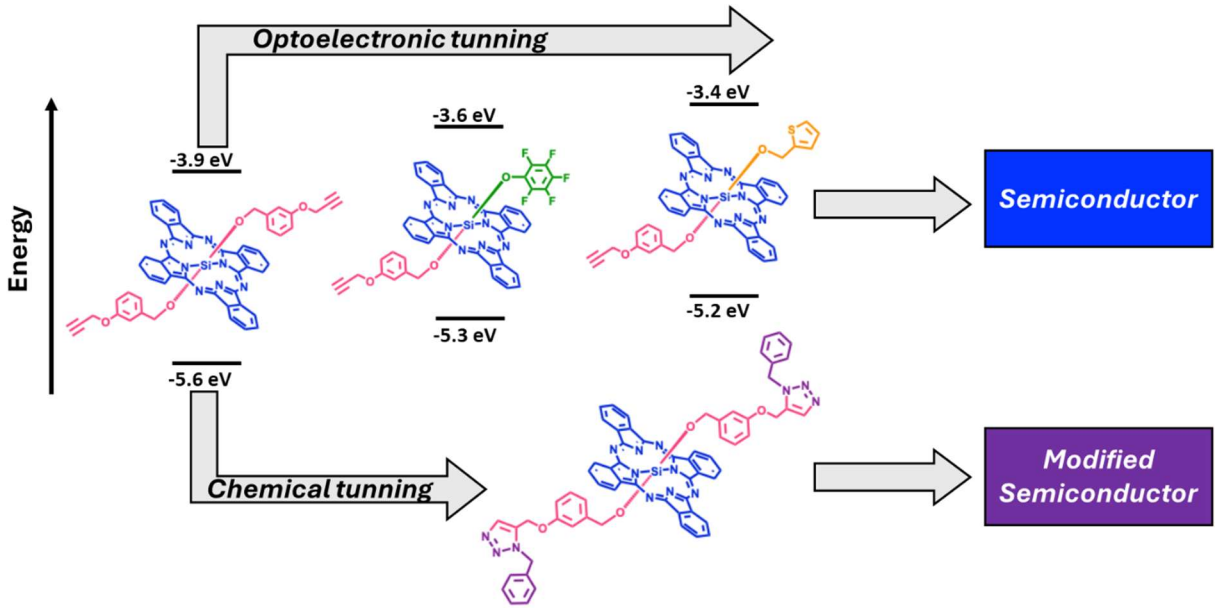

2.1 INTRODUCTION

Metal and main group phthalocyanines (MPcs) are considered a highly versatile class of materials with a broad range of applications in fields varying from biotechnology,[1,2] electrochromics,[3] catalysis,[4,5] and more.[6–8] In particular, their unique physical and chemical properties paired alongside their strong chemical and thermal stability make them ideal candidates for organic electronic applications.[1,9,10] With potential structural tunability at the core, periphery and axial positions, MPcs stand out as a versatile class of organic semiconductors with an inherent ability to undergo finetuning of their optical and electronic properties.[11] Having a central element provides a gateway to obtaining different valencies and axial ligations depending on oxidation state. This includes divalent planar MPcs, such as copper phthalocyanine (CuPc) or zinc phthalocyanine (ZnPc),[6,12] trivalent MPcs like aluminium phthalocyanine (R-AlPc),[13] which possess a lone axial ligand, and tetravalent MPcs such as silicon or tin phthalocyanine with double ligation (R_2-SiPc or R_2-SnPc, respectively).[14,15]

For tetravalent MPcs such as SiPc, studies have shown that specific axial substitution can significantly influence the bulk properties, such as solubility,[16] molecular packing and electrical conductivity of the resulting material.[11,17,18] Owing to their facile synthesis and scalability, SiPcs are often used as semiconducting materials in organic electronic devices, such as organic light emitting diodes (OLEDs),[11,19,20] organic photovoltaics (OPVs),[11,20] organic electrochemical transistors (OECTs)[21] and organic thin-film transistors (OTFTs).[11,22–25] Notably in OTFTs, SiPcs have been explored using a variety of silanes and aryl substituents at the axial positions to alter the solid-state packing with various surface treatments,[14] which in turn affects charge mobility and threshold voltage.[11,26–28] It has also been demonstrated that the addition of perfluorinated phenoxy groups at the axial positions of R_2-SiPcs stabilizes the highest occupied molecular orbital (HOMO) and the lowest unoccupied molecular orbital (LUMO) energy levels due to their strong electron withdrawing nature, affording materials that act as *n*-type organic semiconductors.[29,30] Aside from modifying the bulk properties of the SiPc, axial ligation can also be exploited as a means to facilitate other chemical changes such as photocatalysis,[31] electropolymerization,[32,33] or click chemistry.[34] For example, Grant *et al.* employed a cross-linkable azido axial ligand, bis(6-azidohexanoate)silicon phthalocyanine ($(HxN_3)_2$-SiPc) as a multifunctional derivative as a mean to lock-in the morphology of the active layer, which in turn optimized the optical properties and overall OPV device performance.[35] This demonstrates that strategic ligand design of the axial components can serve as active sites for surface grafting of SiPcs. In the instance of ligands bearing a terminal alkyne, the alkyne can serve as a reactive site for post functionalization through click chemistry.[34] To that end, axial click reactions of SiPcs can be exploited in a variety of different ways such as expansion of the molecule with additional functional groups,

anchoring of the SiPc to a surface, or attachment of the SiPc as a pendant to polymeric materials. Overall, the axial group plays a pivotal role in SiPc modification and its potential applications.

SiPcs have also been explored in terms of their symmetry, with differences in axial substituents (e.g., R_2-SiPc versus RR'-SiPc)[36,37] leading to marked variances in properties. Furthermore, an asymmetrical RR'-SiPc can provide a higher level of control over post-synthetic modulations. For example, symmetric SiPcs (R_2-SiPc), where the axial positions bear two identical groups, have been explored in various applications including OTFTs.[11,17,21,25,38,39] Whereas asymmetrical SiPcs (RR'-SiPc) bearing two different axial ligands[40] have been implemented in some biological applications;[41–45] however, they remain somewhat underexplored, especially for OTFT applications,[46,47] despite their potential to be further manipulated for chemical versatility. Common challenges with the asymmetrical SiPc synthesis are lower yields and double replacement of the axial units.[36,41,45,48] Asymmetrical axial substitution can serve as a mean for selective functionalization, enhanced packing, and tailored electronic behavior; all important characteristics to obtain high performing organic electronics. For instance, Martín-Gomis *et al.* designed asymmetrical SiPc with one alkenyl axial substituent, which was employed in a click reaction post the SiPc synthesis, while the other axial substituent was subjected to a 1,3-dipolar cycloaddition, leaving the SiPc to bear two electron-acceptors ligands.[46]

The work presented herein explores the synthesis and characterization of three axially functionalized SiPcs with symmetric and asymmetric substituents to investigate their varying optical and electrical properties. In particular, a symmetrical SiPc with 3-(prop-2-yn-1-yloxy) benzyloxy substituents, bis((3-(prop-2-yn-1-yloxy)benzyloxy) silicon phthalocyanine (**2A**) is reported, from which the terminal alkyne groups can be used for subsequent click chemistry

reactions. As well, asymmetrical SiPcs were realized using **2A** as a precursor. In doing so, the asymmetrical SiPcs consisted of 3-(prop-2-yn-1-yloxy)benzyloxy on one side of the SiPc plane, while the other side had either a thienyl methoxy or pentafluorophenoxy group as axial substituents. Following successful isolation, the electrochemical and optoelectronic properties of the three SiPc derivatives were characterized *via* cyclic voltammetry and UV-vis-NIR spectroscopy, revealing the influence of the axial modifications on their redox behavior and HOMO/LUMO energy levels. The results presented herein demonstrate that the symmetrical alkyne-derived R_2-SiPc had an overall greater stabilization of the HOMO/LUMO levels compared to its asymmetrical counterparts. The alkyne containing R_2-SiPc was further modified using a copper-catalyzed alkyne-azide click reaction with benzyl azide, showing no disturbances to its optical properties, demonstrating a platform for further finetuning of the semiconductor at the axial position. Based on our results, axial functionalization can be utilized to modify the photo/electrochemical behavior of SiPc derivatives, create a chemically flexible platform (such as a clickable site), and optimize semiconductor performances.

2.2 RESULTS AND DISCUSSION

2.2.1 Synthesis of Symmetrically Functionalized SiPc

Synthesis of bis((3-(prop-2-yn-1-yloxy)benzyloxy) silicon phthalocyanine (**2A**) was achieved by adapting previously reported methods by Lessard *et al.*, as outlined in **Scheme 2.1**.[49] Prior to axial functionalization of the SiPc, the substituent was prepared by reacting 3-hydroxybenzaldehyde with bromo-propargyl, affording 3-(prop-2-yn-1-yloxy) benzaldehyde (**2-1**) as a faint yellow oil with a 90% yield. Subsequent reduction of the aldehyde on **2-1** to afford 3-(prop-2-yn-1-yloxy)phenyl methanol (**2-2**), was achieved via nucleophilic addition using

sodium borohydride. Upon successful isolation of **2-2**, its reaction with silicone phthalocyanine dichloride (**2-0**) to afford **2A** was carried out in the presence of triethylamine, which acts to neutralize any HCl present that could potentially attack the readily available alkyne proton present on **2-2**. As well, toluene was selected as the solvent, leading to a 30% increase in the overall yield compared to chlorobenzene, which is the commonly employed solvent for SiPc axial functionalization. The crude product, which appeared to have a deep blue color, was precipitated out in isopropanol and purified *via* recrystallization in a dichloromethane (DCM): hexanes mixture, yielding a purple semicrystalline powder. Both **2-2** and **2A** were characterized by ^{1}H NMR, Fourier Transform Infrared (FT-IR), and HRMS (see supporting information). High Performance Liquid Chromatography (HPLC), UV-vis-NIR spectroscopy and Cyclic Voltammetry (CV) analyses were also performed for compound **2A**.

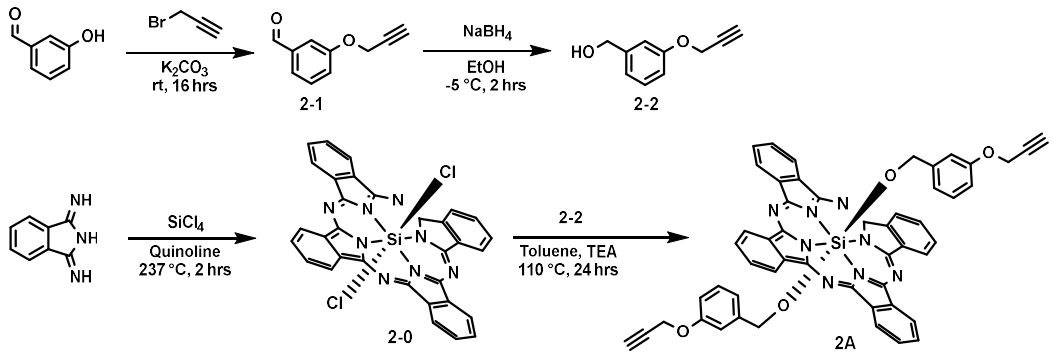

Scheme 2.1: General synthetic route to axially substituted symmetrical SiPc with clickable functionality.

2.2.2 Synthesis of Asymmetrically Functionalized SiPcs

A report by Lo *et al.* describes the use of 1,3-bis(dimethylamino)-2-propanoxyl substituents at both axial positions of an SiPc (**2B**) to enable replacement of a lone axial component (**Scheme 2.2a**),[36] thus making it an efficient pathway to obtain asymmetrically derived SiPcs. Inspired by this work, we sought to employ a similar approach involving a two-

step reaction where Cl_2-SiPc was functionalized with 1,3-bis(dimethylamino)-2-propanoxyl groups, followed by a singular axial substitution. To that end, compound **2B** was synthesized according to literature precedent,[36] and subsequently used as the starting material to produce an asymmetrical SiPc containing 3-(prop-2-yn-1-yloxy)benzyloxy and 1,3-bis(dimethylamino)-2-propanoxy as the axial substituents (**2B-2**, **Scheme 2.2b**). Unfortunately, following this route, the asymmetric SiPc **2B-2** remained elusive regardless of variations to reaction conditions listed in **Scheme 2.2b**. Given these challenges, a different approach was explored using the symmetric SiPc **2A** as the starting material and introducing one equivalent of a non-alkyne functionalized aromatic substituent (i.e., thienyl methoxy or pentafluorophenoxy; **Scheme 2.2c**). This alternate synthetic route was caried out under similar reaction conditions as that used to obtain **2A** and ^{1}H NMR was employed to monitor the reaction progress towards conversion to the asymmetric derivatives **2A-4** (RR'-SiPc; where R = 3-(prop-2-yn-1-yloxy)benzyloxy and R' = thienyl methoxy) and **2A-5** (RR'-SiPc; where R = 3-(prop-2-yn-1-yloxy)benzyloxy and R' = pentafluorophenoxy). The new products were precipitated from toluene in methanol with minimal impurities and were purified through a series of solvent washes to yield a blue fine powder of 75% and 65% for **2A-4** and **2A-5**, respectively. Final purity was confirmed *via* HPLC (**Section 2.5**). The asymmetric products **2A-4** and **2A-5** were fully characterized, akin to **2A,** by ^{1}H NMR, FT-IR, HRMS, and HPLC analysis (see **Section 2.5**). And lastly, CV and UV-vis-NIR were also performed to evaluate their optical and electrochemical properties.

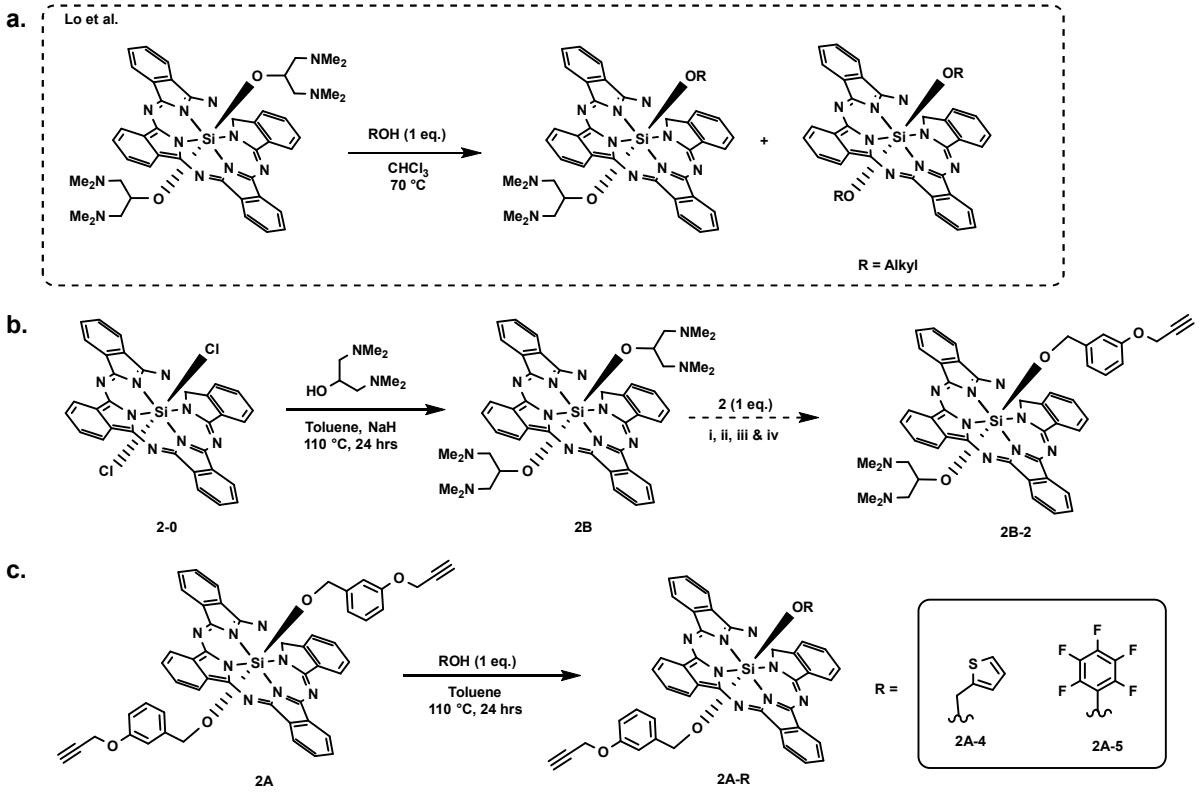

Scheme 2.2: Synthetic pathway to obtain asymmetrically substituted SiPcs. a). General pathway of previous approaches described by Lo *et al.*[36] b). Initial approach to isolate new asymmetrical alkyne functionalized SiPc under various conditions: i) $CHCl_3$, reflux for 24 hrs. ii) $CHCl_3$, reflux for 72 hrs. iii) Toluene, reflux for 24 hrs. iv) TEA, Toluene, reflux for 24 hrs and c). modified synthetic route employed in this work; compound **2A-4** required the addition of a base for the reaction, while **2A-5** was collected under the outlined conditions above.

2.2.3 Electrochemical Analysis

The redox behaviour of the newly synthesized symmetrical and asymmetrical SiPcs **2A**, **2A-4** and **2A-5** were probed by cyclic voltammetry (CV). The measurements were collected in anhydrous DCM with 0.1 M Tetrabutylammonium hexafluorophosphate (NBu_4PF_6) as the supporting electrolyte and Pt wires as the working, counter, and reference electrodes. All three derivatives demonstrate quasi-reversible redox processes for both oxidation and reduction, with **2A** and **2A-5** also exhibiting a second reduction process (see **Figure 2.1a)**. For compound **2A**, the half potential for oxidation was found to be 0.80 V, while the two reduction processes had

half potentials of -0.97 and -1.40 V. For compound **2A-4**, the half potentials are located at 0.38 and -1.34 V for its oxidation and reduction, respectively. In comparison to its symmetrical counterpart, both processes are shifted towards a lower voltage, which could be due to the replacement of one of the axial-substituted phenyl propargyl groups with a thienyl substituent. Unlike **2A**, only one reduction process is observed for **2A-4**; however, it is probable that the lack of a secondary reduction process could be a limitation of the solvent window, as a noticeable drop in current is observed near -1.70 V. The electron-donating nature of the thienyl moiety can also play a role in the shift in oxidation onset in comparison to **2A** (0.69 V vs. 0.32 V). Similar differences in the first reduction onset are also noticed, with -0.90 V for **2A** and -1.26 V for **2A-4**. As for compound **2A-5**, the redox potentials sit between those of **2A** and **2A-4**. We credit the electron-withdrawing pentafluorophenoxy group for the higher oxidation onset compared to its thienyl counterpart, although it is still lower than the symmetrical analogue **2A**. According to previously reported electron-withdrawing and electron-donating SiPcs, the anodic shift observed in compounds **2A** and **2A-5** seems to be within trend, compared to the cathodic shift observed in **2A-4**.[50] With **2A** and **2A-5** both containing electron-withdrawing functional groups, the introduction of asymmetry can be used to further see their dissimilarities. Whereas compound **2A** contains two phenyl methoxy bonds onto the silicon centre, **2A-5** bears a phenyl methoxy and a fluorinated phenoxy bond on either side of the silicon centre. Differences in axial bond connectivity (Si–O–CH_2–aryl vs. Si–O–aryl) could likely impact the electrochemical properties of each complex. Note that the symmetrical bis(pentafluorophenoxy) SiPc (F_{10}SiPc), bearing two perfluorinated phenoxy axial substituents, has been reported to have an oxidative half potential of 1.22 V and reductive half potentials of -0.46 and -0.91 V.[30] When comparing F_{10}SiPc to

compound **2A-5**, a lower potential is observed, translating to lower reductive and oxidative onsets.

Using the half peak potentials of the oxidation and first reduction processes, the HOMO/LUMO energy levels of all three derivatives can be calculated (**Table 2.1**). The HOMO/LUMO levels for compound **2A** are lower in energy compared to **2A-5**. Although both materials contain electron withdrawing groups at both axial positions, the loss of symmetry could explain the destabilization of the HOMO/LUMO levels for **2A-5**. In comparison to other symmetrically functionalized Si-O-aryl derivatives such as bis(phenoxy) SiPc (PhOSiPc), bis-(3,4,5-trifluorophenoxy) SiPc (345FSiPc), bis(pentafluorophenoxy) SiPc (F_{10}SiPc), the HOMO levels are somewhat comparable (energy values from DFT); however, the LUMO levels in comparison to compound **2A** (-3.9 eV) and **2A-5** (-3.60 eV) are more destabilized (-2.92, -3.21, and -3.13 eV, respectively).[51] Through the asymmetry, a more stabilized LUMO level for compound **2A-5** is observed in comparison to symmetric fluorinated SiPcs (F_{10}SiPc), but less destabilised than the symmetrical analogue **2A**. Alternatively, PhOSiPc is reported to have higher HOMO/LUMO levels,[51] which can be attributed to its electron-rich characteristics similar to those of compound **2A-4.** Moreover, further destabilization of the HOMO/LUMO levels is seen for **2A-4**, where not only is the symmetry absent, but there is also a gain of electron-donating properties provided by the thienyl moiety. When comparing these groups to bis(3-pentadecylphenoxy) SiPc ($(PDP)_2$SiPc), which has HOMO/LUMO levels of -5.25 and -3.62 eV, respectively,[30] $(PDP)_2$SiPc has the most similarity with compound **2A-5**; a result of the Si-O-aryl bond pattern observed for both groups. These observations suggest that the inherent symmetry and added electron-withdrawing properties play a key factor in the stabilization of the HOMO/LUMO levels of these materials.

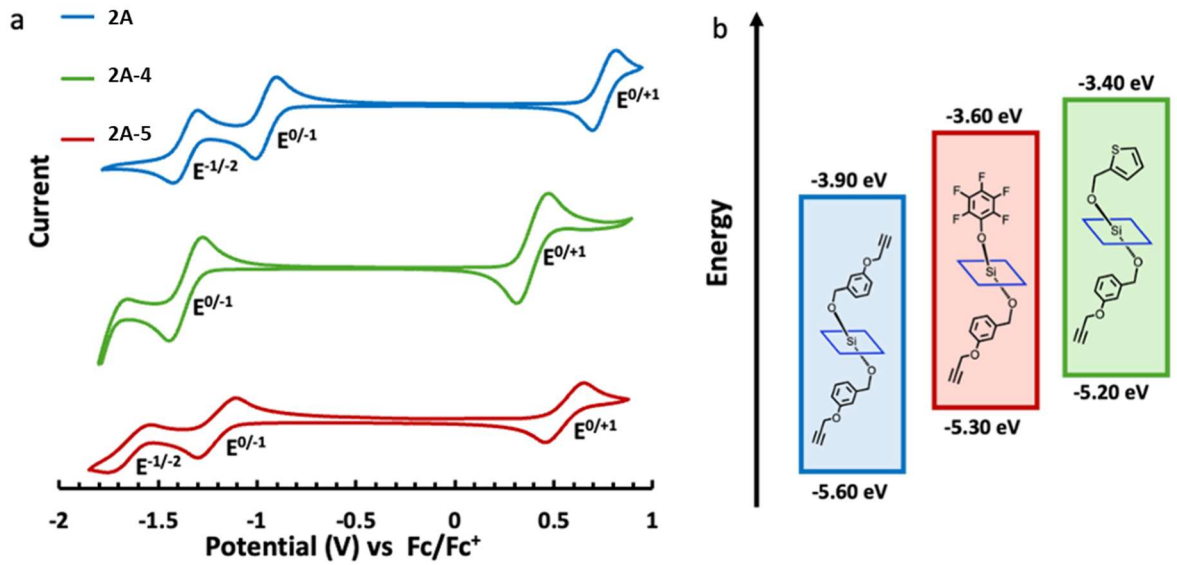

Figure 2.1: a). Cyclic voltammograms of **2A** (blue), **2A-4** (green) and **2A-5** (red) in DCM at 100 mV s^{-1} with 0.1 M $TBAPF_6$ as the supporting electrolyte. b). Energy level diagram determined from CV.

Table 2.1: Half potentials, HOMO and LUMO energy levels, and energy gap values determined from CV of **2A**, **2A-4** and **2A-5.**

SiPc Derivatives	$E^{0/+1}$ [a] (V)	$E^{0/-1}$ (V)	$E^{-1/-2}$ (V)	HOMO[b] (eV)	LUMO[b] (eV)	E_{gap}[c] (eV)
2A	0.77	-0.97	-1.40	-5.6	-3.9	1.70
2A-4	0.38	-1.34	-	-5.2	-3.4	1.80
2A-5	0.55	-1.20	-1.80*	-5.3	-3.6	1.70

[a]Half-potentials were calculated by using the cathodic and anodic peaks, $E^{0/+1} = (E^a - E^c)/2 + E^c$; *$E^{-1/-2}$ for **2A-5** E^c. [b]HOMO/LUMO levels were calculated using Fc/Fc^+ as a reference; HOMO = 4.8 + $E_{0/+1}$(vs.ferrocene) [eV], LUMO= 4.8 + $E_{0/-1}$(vs. Ferrocene) [eV].[52–54] [c]E_{gap} from the CV was determined by $E_{gap} = E_{LUMO} - E_{HOMO}$

2.2.4 Optical characteristics

Optical characterization for **2A**, **2A-4** and **2A-5** was conducted using UV-vis-NIR spectroscopy in solution with chlorobenzene. When compared to **2-0** (Cl_2-SiPc), all three materials undergo a hypsochromic shift with a λ_{max} of 678 nm for **2A** and **2A-4**, and 682 nm for **2A-5** (**Figure 2.2**). Previous studies using [3,5-bis(prop-2-ynyloxy)benzyloxy]$_2$SiPc, which has

similar axial connectivity to **2A**, also portrayed a similar absorption profile in its Q band, with a reported value of 675 nm in DMF solution.[55] Alternatively, a study using $(PDP)_2SiPc$, which possesses the same Si-O-aryl axial connectivity as **2A-5**, was reported to have a λ_{max} of 681 nm in solution with 1,2-dichlorobenzene.[30] The shift in the Q band seen between compounds **2A** and **2A-4** with that of compound **2A-5** may be accounted for by the break in conjugation at the CH_2 group. Additionally, the slight red shift for compound **2A-5** could also be impacted by the electron-withdrawing properties of the fluorine atoms located on the aryl ring. The λ_{max} overlap observed in compounds **2A** and **2A-4** suggests that the π-π interaction is not affected by the thienyl moiety and therefore the asymmetry has no inherent impact on the λ_{max} in solution. Compound **2A-5,** on the other hand, has a slightly red-shifted λ_{max} of 682nm in comparison to the two derivatives, which may be due to the extended conjugation realized through the introduction of the perfluoroaryl substituent. Previous reports suggest the symmetrical fluorinated derivative, $F_{10}SiPc$, has a similar property to **2-0** with reported λ_{max} of 686 and 685 nm in toluene, respectively.[30] Herein, the λ_{max} of **2A-5** and **2-0** are found to be 682 nm and 698 nm in chlorobenzene. Note that the difference between these values and those reported between $F_{10}SiPc$ and **2-0** may be attributed to solvation effects as well as the effect of the asymmetry introduced in this compound. When looking at **2A-5**, it has a λ_{max} that is between that of the symmetrical compounds **2A** and **2-0**, which suggests its optical properties are most likely a consequence of both the perfluorinated aryl and the 3-(prop-2-yn-1-yloxy)benzyloxy groups. A more significant difference for all the derivatives is observed between their onset of absorption. For example, **2-0** has an absorption onset at 714 nm, followed by **2A-5** at 703 nm, **2A** at 695 nm, and **2A-4** at 690 nm (**Table 2.2**). Another difference to point out is around the Soret region, where the three derivatives are slightly blue shifted in comparison to the Cl_2-SiPc. This may be

attributed to a break in the conjugation due to the change of the Si-halogen to the Si-oxygen bond. Note that direct overlap between all three compounds is seen around this region as well. Lastly, UV-vis-NIR spectra were collected in the solid-state from the thin-films of all three materials by spin coating a 10 mg/mL solution in chlorobenzene onto glass slides. The solid-state absorption profiles suggest a red shift for all three derivatives compared to their solution measurements, broadening of the peaks and an increase in intensity of the Soret region. Interestingly, **2A** and **2A-4** no longer have an overlapping λ_{max} (710 and 720 nm, respectively), while **2A-5** now exhibits an intermediate λ_{max} at 715 nm. The absorption onsets are also noteworthy as the reverse order is now observed in the solid-state, as seen in **Table 2.2**. Direct comparison of the solution to solid-state absorption profiles suggests that **2A** and **2A-4** are more bathochromically shifted than **2A-5** in the solid-state. Overall, looking at all three derivatives, it can be concluded that the symmetry of these complexes does play a role in the optical properties, more so due to the axial substituents' contribution to the π-π interactions.

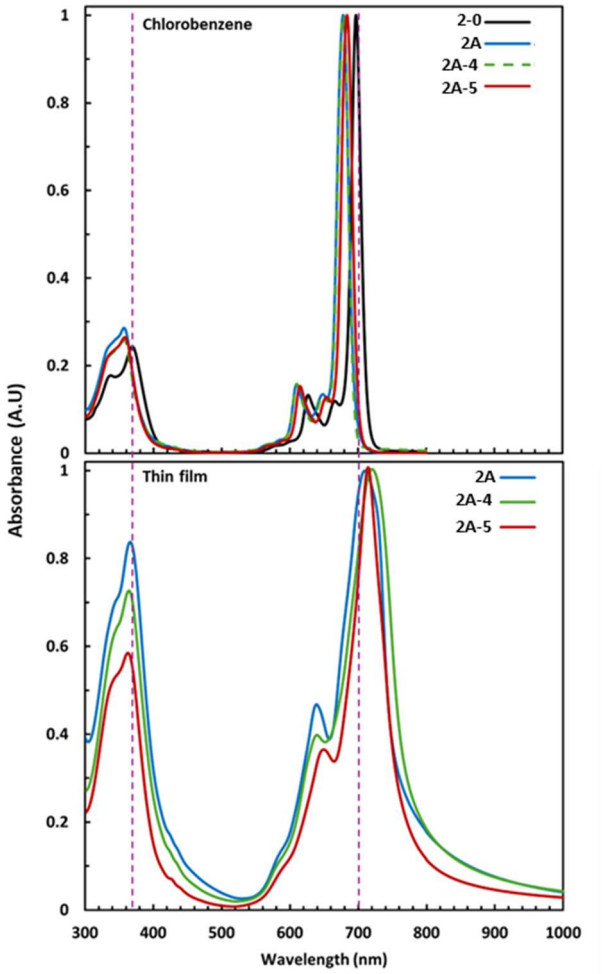

Figure 2.2*:* Normalized absorbance spectra of **2-0** (black), **2A** (blue), **2A-4** (green) and **2A-5** (red) in solution with chlorobenzene (top) and as thin-films on glass substrates (bottom).

Table 2.2: Photophysical properties of compounds **2-0**, **2A**, **2A-4** and **2A-5** obtained in solution with chlorobenzene and as thin-films on glass substrates.

	Solution			Solid State		
SiPc Derivatives	**λ_{max} (nm)**	**λ_{max} Onset (nm)**	**E_{gap} (eV)[a]**	**λ_{max} (nm)**	**λ_{max} Onset (nm)**	**E_{gap} (eV)[a]**
2-0	698	714	1.74	-	-	-
2A	678	695	1.78	710	850	1.46
2A-4	678	690	1.80	720	856	1.45
2A-5	682	703	1.76	715	820	1.51

[a]E_{gap} was determined by using E = 1240/ λ_{max} Onset

2.2.5 Organic Thin-Film Transistors

Solution-processed OTFTs were fabricated from the three SiPc derivatives to demonstrate their potential for integration in electronic devices. All films were spin-coated from chloroform solutions onto Si substrates with a thermally grown layer of SiO_2, which served as the dielectric and underwent either hexamethyldisilazane- (HMDS) and octyltrichlorosilane- (OTS) treatment. This reduces charge trapping and renders the surface hydrophobic to more closely match the surface energy of the SiPc derivatives, which alters the film structure. Ag with Mn (interlayer) source and drain electrodes were thermally evaporated over the films, yielding a bottom-gate top-contact (BGTC) architecture. The devices were characterized in a N_2 glovebox environment, and the derived performance metrics are listed in **Table 2.3**.

Table 2.3: Summary of device performance metrics obtained from *n* unique OTFTs.

SiPc derivative	Surface treatment	Polarity[a]	μ[b] [$\times 10^{-4}$ cm^2 V^{-1} s^{-1}]	V_T[c] [V]	$I_{on/off}$[d]	n[e]
2A[f]	HMDS	*n*	1.35 ± 0.43	26.8 ± 3.5	10^0	38
	OTS	-	-	-	-	-
2A-4	HMDS	*p*	1.92 ± 1.28	-32.4 ± 1.5	10^1	37
	OTS	*p*	1.89 ± 1.04	-33.5 ± 1.0	10^1	25
2A-5	HMDS	*p*	1.21 ± 0.55	-32.5 ± 2.2	10^1	38
	OTS	*p*	5.74 ± 1.92	-33.1 ± 0.85	10^2	8
		n	1.99 ± 0.73	27.8 ± 1.8	10^1	8

[a]Devices tested in *n*-type or *p*-type operation. [b]Average electron mobility, μ_e for n-type devices or hole mobility, μ_h for p-type devices. [c]Average threshold voltage, V_T. [d]On/off current ratio, $I_{on/off}$, with on-current defined as the maximum current and off-current defined as the median current in the off state. [e]Number of individual OTFTs. [f]No functional OTFTs were obtained on OTS-treated substrates for **2A**.

Compound **2A** behaved as an *n*-type semiconductor, aligning with observations from most other SiPc derivatives reported in literature,[27,39] and achieved an average electron mobility (μ_e) of 1.35 ± 0.43 × 10^{-4} cm^2 V^{-1} s^{-1} and an average threshold voltage (V_T) of 26.8 ± 3.5

V. These devices also benefitted from the good alignment of the LUMO energy level of **2A** with the work function of the Mn interlayer (-4.1 eV). Meanwhile, the shallower HOMO and LUMO energy levels of the asymmetric SiPc derivatives led to devices that were primarily functional in *p*-type operation with comparable performance metrics to one another when fabricated on HMDS-treated substrates. Although all studied derivatives afforded working devices on these surfaces, the greater hydrophobicity of the OTS-treated surfaces led to de-wetting of the solutions, particularly with the use of **2A**. Thus, no functional devices were obtained on OTS for **2A**, while a limited number of devices were obtained from the other derivatives. The performance of **2A-4** in OTFTs was not affected by the change in surface energy of the substrate, with average hole mobilities (μ_h) of $1.92 \pm 1.28 \times 10^{-4}$ cm^2 V^{-1} s^{-1} and $1.89 \pm 1.04 \times 10^{-4}$ cm^2 V^{-1} s^{-1} on HMDS and OTS, respectively, whereas for **2A-5**, OTFTs demonstrated a nearly five-fold increase in μ_h values on OTS as opposed to HMDS. The devices fabricated on OTS-treated surfaces also demonstrated fair ambipolarity, with *n*-type performance similar to that of **2A**. **Figure 2.3** displays representative output and transfer curves obtained from all devices. Though their OTFT performance is modest, these results suggest that the derivatives can be used to fabricate effective electronic devices in addition to enabling click reactions.

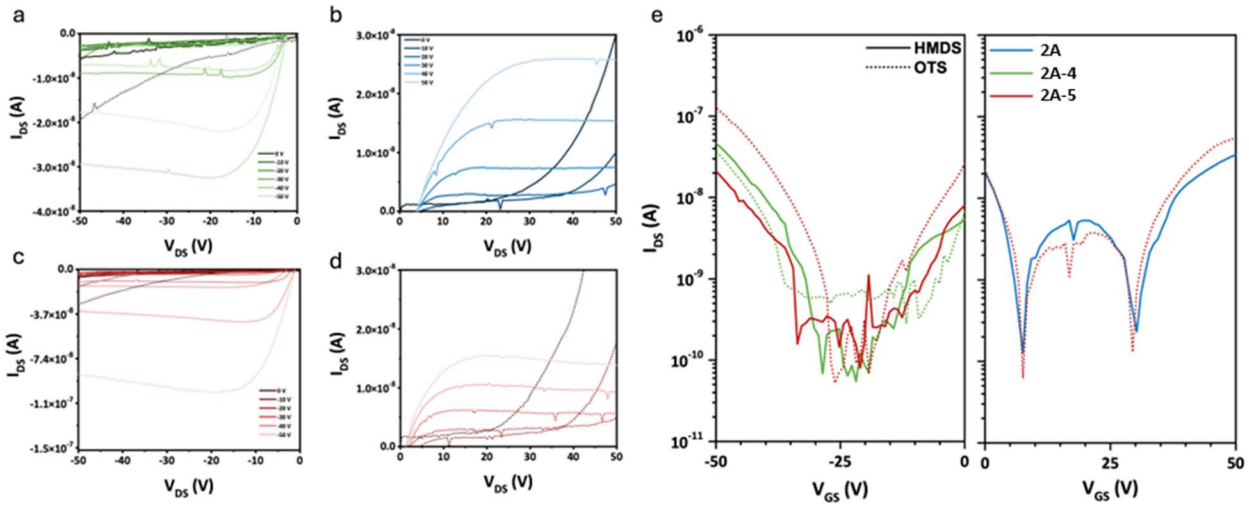

Figure 2.3*:* Representative *I-V* curves from fabricated OTFTs. Output characteristics of a). Compound **2A-4**, b). Compound **2A** and c) & d). Compound **2A-5** devices. e). Transfer characteristics of **2A** (blue), **2A-4** (green) and **2A-5** (red) devices. Solid lines indicate devices fabricated on HMDS-treated substrates, while dashed lines indicate devices fabricated on OTS-treated substrates.

2.2.6 Click Chemistry

To probe the potential use of alkyne-derived SiPcs in click chemistry applications, compound **2A** was subjected to click coupling with benzyl azide. Benzyl azide was synthesized *via* SN2 using benzyl bromide and sodium azide and was obtained in a 90% yield.[56] The product required no further purification after initial work up and was used as prepared. Prior to evaluating click chemistry on **2A**, benzyl azide was reacted with compound **2-1,** affording compound **2-6** (**Scheme 2.3a**) to demonstrate successful coupling. Subsequently, compound **2A** was then reacted with two equivalences of benzyl azide in DCM, which resulted in the click product **2A-6**. The reaction was conducted at room temperature overnight using 5% $CuBr(PPh_3)_3$ as a catalyst and the reaction progress was monitored by ^1H NMR. Upon loss of the alkyne proton peak (present at 2.21 ppm), suggesting completion of the triazole formation, the reaction mixture was poured onto hexanes thereby affording **2A-6** with a 53% yield as a blue powder.

Characterization such as ^{1}H NMR, HRMS, FTIR, HPLC, and CNMR were performed. UV-vis-NIR were also performed to compare the optical property with **2A** (**Section 2.5, Fig.S17**).

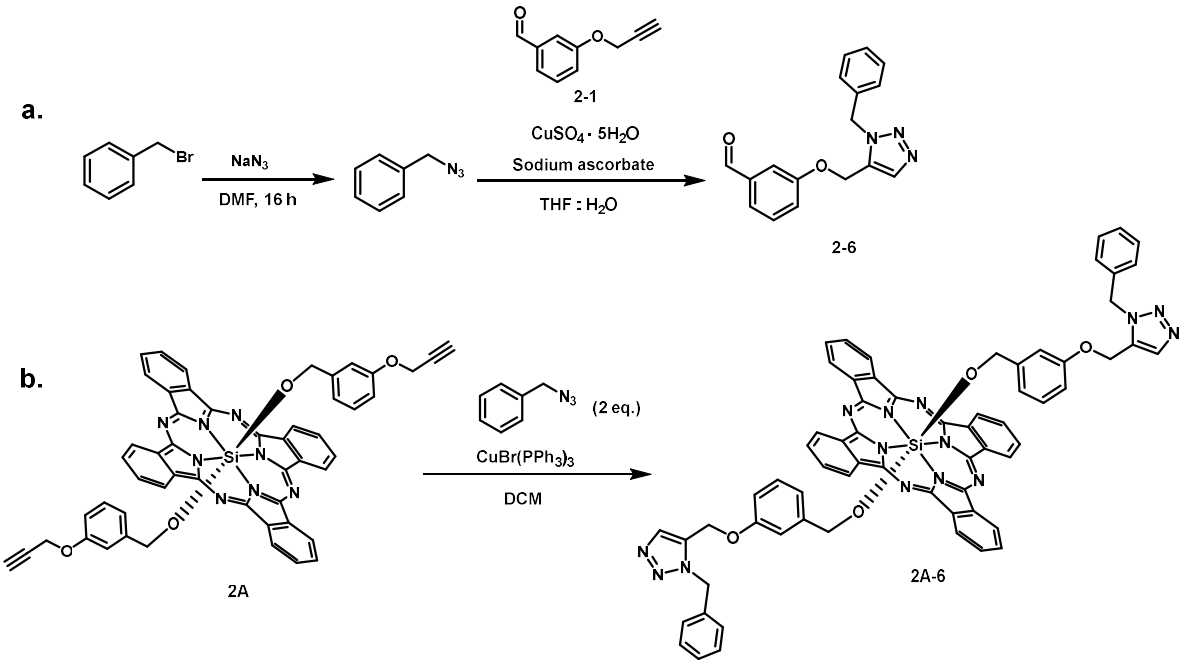

Scheme 2.3: a). General synthesis of the benzyl azide precursor and click reaction trial. b). Click reaction between the symmetrical SiPc **2A** and benzyl azide to afford **2A-6**.

Click chemistry serves as another avenue to tailor the properties of these axial substituted SiPcs. In doing so, applications of these derivatives could further be expanded. In this study, the alkyne site was used for the triazole formation in the symmetrical complex. UV-vis-NIR spectroscopy was conducted post-click (**Figure S2.17**), where it was observed that click product **2A-6** conserved the same absorption profile as its pre-click counterpart **2A**, which goes to highlight that the central components can be kept for an intended application, while also leaving possibilities for further functionalization.

2.3 CONCLUSION

Overall, this study demonstrates that SiPcs can be finetuned at the axial positions while maintaining their planar framework, thus modulating the electrochemical and photochemical properties. Symmetrically substituted SiPc **2A** acts not only as an alkyne-functionalized SiPc but also as a precursor to isolate the asymmetrical derivatives **2A-4** and **2A-5**. The optical properties of **2A-5** suggests that the asymmetry induces a red shift compared to its symmetrical analogue **2A**. Meanwhile, electrochemical characteristics of **2A-4** indicate the most destabilized HOMO/LUMO levels and the highest E_{gap}; whereas compound **2A-5** showed similar E_{gap} to its symmetrical counterpart **2A**, although its redox states are observed at lower potential. Successful proof of concept OTFTs were fabricated and characterized using these novel derivatives as semiconductor, exhibiting a modest performance. Lastly, through a strategic ligand design and axial SiPc synthesis, chemical tailoring/functionalization at the axial group is demonstrated through a click 1,2,3-cycloaddition. Axial ligation of SiPc ultimately provides two positions to initiate chemical changes and a deliberate architecture of the axial moiety, at which position said change happens, can be controlled through the introduction of asymmetry. The success of this study paves a way for future studies to selectively coordinate mono- or bis-functionalization at the axial positions, further advancing potential applications of SiPcs.

2.4 EXPERIMENTAL

2.4.1 Materials

All materials purchased were used as received. 3-hydroxybenzaldehyde (98%), pentafluorophenol (98%), and diiminoisoindoline (98%) were purchased from Ambeed Inc. Thiophene-2-methanol, silicon tetrachloride ($SiCl_4$) (99%), 2-propanol, 1,3-bis(dimethylamino)-

(97%), $NaBH_4$ (98%), and triethylamine(TEA) were purchased from Sigma-Aldrich Chemical Company. Benzyl bromine (98%) was purchased from TCI America; and sodium azide (99%) from AESER. Silicon phthalocyanine dichloride (**2-0**) was synthesized according to literature.[16]

2.4.2 Synthesis of 3-(prop-2-yn-1-yloxy) benzaldehyde (2-1)

1.0 g (8.19 mmol, 1.00 eq.) of 3-hydroxybenzaldehyde was dissolved in anhydrous DMF along with 1.70 g of K_2CO_3 (12.3 mmol, 1.50 eq.), followed by 0.75 mL (9.83 mmol, 1.20 eq.) of propargyl bromide (80% in toluene) per preceding literature.[57] The mixture was stirred at room temperature for 16 hours and monitored by TLC (9:1 hexanes: ethyl acetate (EtOAc)). After full consumption of the starting material, the crude mixture was extracted using EtOAc, then washed with water to remove any residual DMF. Organic layers are combined, dried using $MgSO_4$ and concentrated under reduced pressure to afford the crude product as a yellow oil. The crude oil was purified via flash column chromatography using a 3:7 EtOAc: Hexanes to afford the title product as a faint yellow oil (0.9 g, 90%). ^{1}H NMR (400 MHz, Chloroform) δ 9.97 (s, 1H), 7.52 – 7.42 (m, 3H), 7.25 – 7.23 (m, 1H), 4.75 (d, 2H), 2.53 (t, 1H). ^{13}C NMR (151 MHz, Chloroform) δ 191.90, 158.09, 137.82, 130.18, 124.14, 122.16, 113.57, 77.88, 77.24, 77.03, 76.82, 76.12, 56.00. HMRS (DART+) m/z: [M]+ calcd. for mass $C_{10}H_9O_2$: 161.05971; found: 161.05846.

2.4.3 Synthesis of 3-(prop-2-yn-1-yloxy)phenyl methanol (2-2)

To a flask cooled down to -5 °C, 24.8 mg (0.655 mmol) of **2-1** was dissolved in 10 mL of EtOH. Small portions of $NaBH_4$ were slowly added under N_2 until a total of 100 mg was reached, adapting a previously reported procedure[58] The reaction mixture was stirred for 1 hr and slowly brought up to room temperature. The pH of the mixture was brought down to 3 by adding 2 N HCl stepwise, which was then further mixed for an additional 10 min. Sat. $NaHCO_3$

was then added stepwise to neutralize the solution. The crude mixture was extracted using DCM, then washed with water three times. The organic phases were combined, dried over $MgSO_4$ and concentrated under reduced pressure to afford the product as a faint green oil (23.01 mg, 90%); final product was used without further purification. ^{1}H NMR (400 MHz, Chloroform) δ 7.30 – 7.25 (m, 1H), 7.00 – 6.96 (m, 2H), 6.91 – 6.87 (m, 1H), 4.69 (d, 2H), 4.67 (d, 2H), 2.50 (t, 1H). ^{13}C NMR (101 MHz, Chloroform) δ 157.83, 142.65, 129.67, 120.02, 114.14, 113.34, 78.56, 75.56, 65.16, 55.80. HMRS (DART+) m/z: $[M + NH_4]^+$ calcd. for mass $C_{10}H_{14}NO_2$: 180.1019; Found: 180.10120.

2.4.4 Synthesis of Bis (1,3-bis(dimethylamino)-2-propoxy) silicon phthalocyanine (2B)

1.0 g (1.65 mmol, 1.0 eq.) of **2-0** and 0.81 g (5.5 mmol, 3.3 eq.) of 1,3-bis(dimethylamino)-2-propanol were brought into solution using 20 ml toluene, following Lo *et al.*'s method[36]. The solution was refluxed overnight and cooled to room temperature. The blue solution was then precipitated out from toluene onto 250 mL of ^{i}PrOH. The crude product was recovered via vacuum filtration, washed with ^{i}PrOH and hexanes to afford a dark blue solid upon drying. ^{1}H NMR analysis suggested no presence impurities; thus, no further purification was performed. ^{1}H NMR (400 MHz, Chloroform) δ 9.66 – 9.56 (m, 8H), 8.30 – 8.24 (m, 8H), 0.50 – 0.41 (m, 24H), -0.77 – -0.86 (m, 4H), -1.58 (t, J = 6.3 Hz, 4H), -2.74 (d, J = 4.3 Hz, 2H).

2.4.5 Synthesis of Bis(3-(prop-2-yn-1-yloxy)benzyloxy) silicon phthalocyanine (2A)

The symmetrical axially substituted SiPc was synthesized by adapting Lessard *et al.*'s preceding report.[49] 139 mg (0.858 mmol, 4.33 eq.) of **2-2**, 117 mg (0.198 mmol, 1.00 eq.) of Cl_2-SiPc and 0.5 mL of triethylamine were dissolved in 10 mL of chlorobenzene. The mixture was refluxed over a period of 48 hrs. Upon cooling to room temperature, the mixture was diluted with 100 mL of isopropanol and set aside for 30 min to allow for crude to precipitate out. Crude

product was recovered via vacuum filtration to afford a blue powder. Crude was purified by recrystallization using DCM: hexanes mixture to afford the title product as a purple semicrystalline powder (128 mg, 75%). ^{1}H NMR (400 MHz, Chloroform) δ 9.62 – 9.51 (m, 8H), 8.32 (ddt, 8H), 7.24 (s, 7H), 6.06 – 5.93 (m, 4H), 4.15 (d, 2H), 3.72 (dd, 4H), 3.55 (s, 2H), 2.20 (td, 2H), -0.75 (s, 4H). HMRS (EI+) m/z: [M]+ calcd. for $C_{52}H_{34}N_8O_4Si$: 862.24668; found: 862.24646.

2.4.6 Synthesis of [Si, Si] Bis((3-(prop-2-yn-1-yloxy)benzyloxy), thienyl methoxy) silicon phthalocyanine (2A-4)

Asymmetrical SiPcs were synthesized by adapting the approach used by Lo *et al.*[36] 200 mg of **2A** (0.23 mmol, 100 eq.), 42 mg of thiophene-2-methanol (0.23 mmol, 1.00 eq.), and 1.0 mL of TEA were mixed in 50 mL of toluene under N_2. The mixture was refluxed for 22 hrs and monitored via ^{1}H NMR. The reaction mixture was then cooled to room temperature and diluted with methanol (200 mL) and let stand to precipitate. The crude product was recovered via vacuum filtration, washed with methanol and dried to afford a blue solid. The crude was purified by recrystallization using $CHCl_3$:hexanes mixture to afford the title product as a fine powder (145 mg, 75%). ^{1}H NMR (400 MHz, Chloroform) δ 9.59 (qd, 8H), 8.32 (dq, 8H), 6.11 (dd, 1H), 6.06 – 5.93 (m, 2H), 5.80 (dd, 1H), 4.48 (d, 1H), 4.16 (d, 1H), 3.72 (d, 2H), 3.55 (s, 1H), 2.24 – 2.18 (m, 1H), -0.62 (t, 2H), -0.75 (s, 2H). HMRS (DART+) m/z: [M]+ calcd. for $C_{47}H_{30}N_8O_3SSi$: 815.20036; Found: 815.20071.

2.4.7 Synthesis of [Si, Si] Bis((3-(prop-2-yn-1-yloxy)benzyloxy), pentafluorophenoxy) silicon phthalocyanine (2A-5)

Compound **2A-5** was synthesized and purified in a similar procedure to that of **2A-4** using pentafluorophenol (42 mg, 1.00 eq.). The title product was collected as a blue powder (132

mg, 65%). ^{1}H NMR (300 MHz, Chloroform) δ 9.62 (dd, 8H), 8.36 (dd3, 8H), 6.06 – 5.98 (m, 2H), 4.13 (d, 1H), 3.75 (d, 2H), 3.60 (s, 1H), 2.22 (t, 1H), -0.66 (s, 2H). ^{19}F NMR (283 MHz, Chloroform) δ -161.74 – -161.90 (m), -166.57 (dd), -168.96 – -169.20 (m). HMRS (DART+) m/z: [M]+ calcd. for $C_{48}H_{25}F_5N_8O_3Si$: 885.18118; Found: 885.18113.

2.4.8 Synthesis of benzyl azide

By adapting literature precedent,[56] a pre-dried flask, 0.35 ml (3 mmol, 1.00 eq.) of benzyl bromide was dissolved in 20 mL of DMF. 0.4 g (6 mmol, 3.00 eq.) of sodium azide was slowly added to the solution at room temperature, and the solution was left to stir overnight. The solution was then diluted with water, and extracted with diethyl ether, then washed with water three times. The organic layer was dried over $MgSO_4$ and concentrated under reduced pressure. The title product was recovered as an oil (0.31 ml, 83%); final product was used without further purification. ^{1}H NMR (400 MHz, Chloroform) δ 7.42 – 7.27 (m, 5H), 4.32 (s, 2H). ^{13}C NMR (101 MHz, Chloroform) δ 135.38, 128.86, 128.33, 128.24, 54.84.

2.4.9 Synthesis of 3-[(1-benzyl)1,2,3-triazole-5-methoxy] benzaldehyde (2-6)

3-[(1-benzyl)1,2,3-triazole-5-methoxy] benzaldehyde (**2-6**) was synthesized by modifying preceding literature.[59] To a pre-dried flask, 150 mg (0.93 mmol, 1.2 eq.) of **2-1** and 147 mg (1.12 mmol, 1.0 eq.) of benzyl azide were dissolved in 20 mL of a 1:1 THF: H_2O solution. 10% mmol of $CuSO_4$•$5H_2O$ and 20% mmol of sodium ascorbate were added to the solution, which was subsequently left to stir at room temperature. After 4 hrs, the solution was diluted with water and extracted using EtOAc and washed with water three times. The organic layer was dried over $MgSO_4$ and concentrated under reduced pressure. The crude was purified via flash column chromatography (9:1 hexanes: EtOAc) to obtain the title product as a colorless

oil (213 mg, 65%). ^{1}H NMR (400 MHz, Chloroform) δ 9.95 (s, 1H), 7.52 (s, 1H), 7.46 – 7.35 (m, 6H), 7.29 – 7.24 (m, 2H), 7.23 – 7.21 (m, 1H), 5.53 (s, 2H), 5.22 (s, 2H)

2.4.10 Synthesis of Bis(3-[(1-benzyl)1,2,3-triazole-5-methoxy] benzyloxy) silicon phthalocyanine (2A-6)

To a pre-dried flask, 250 mg of compound **2A** (0.29 mmol, 1 eq.) and 80 mg of benzyl azide (0.58 mmol, 2.0 eq.) were dissolved in 15 mL of DCM. 5% mmol of $CuBr(P(Ph_3)_3)$ was added to the solution and left to stir overnight at 50 °C, adapting a previously reported procedure.[60] The crude product was precipitated out into isopropanol, filtered, washed with diethyl ether, and dried under vacuum filtration. The crude was purified via flash column chromatography (9:1 methanol: DCM) on alumina gel, yielding the title product as a blue powder (118 mg, 53%). ^{1}H NMR (600 MHz, Chloroform) δ 9.63 – 9.52 (m, 8H), 8.38 – 8.20 (m, 8H), 7.44 – 7.37 (m, 5H), 7.28 (dd, J = 6.1, 3.4 Hz, 4H), 7.14 (s, 2H), 6.06 – 5.88 (m, 4H), 5.49 (d, J = 2.4 Hz, 5H), 4.18 (d, J = 1.8 Hz, 2H), 4.13 (d, J = 7.6 Hz, 2H), 3.58 (s, 2H), -0.78 (s, 4H). HMRS (ESI+) m/z: $[M + Na]^+$ calcd. for $C_{66}H_{48}N_{14}NaO_4Si$: 1151.3636; Target m/z:1151.3644.

2.4.11 Optical characterization

UV-vis-NIR spectra were collected using an Agilent Technologies Cary 6000*i* UV-Vis-NIR spectrophotometer. The samples were dissolved with chlorobenzene and filtered through a 0.45 μm pore PTFE syringe filter prior to the collection of the spectra. UV-vis-NIR measurements were collected at room temperature within the range of 250-800 nm. Solid state UV-vis-NIR measurements were conducted in a similar manner from 250-1000 nm on an evenly coated glass substrate.

2.4.12 Electrochemical characterization

Cyclic voltammetry was performed using a Bioanalytical Systems Inc. (BASi) Epsilon potentiostat with C3 cell stand, a glass cell and recorded using BASi Epsilon EC software (V 2.13.77 (c) 2013BASi). Platinum wires were used for the working, counter and reference electrodes. The measurements were performed at a 1 mg/mL solution in anhydrous DCM under argon, using 0.1 M tetrabutylammonium hexafluorophosphate (Aldrich) as the supporting electrolyte, with a scan rate of 100 mV s^{-1}. The solutions were filtered through a 0.45 μm pore PTFE syringe filter prior to measurements. All measurements were referenced to the Fc/Fc^{+} redox couple (+0.48 V *vs.* SCE) as an internal standard. Oxidation and reduction half potentials were determined using the anodic and cathodic peak potentials, respectively.

2.4.13 High performance liquid chromatography analysis

HPLC analysis was conducted on Waters e2695 Separations Module using a Symmetry C18 column as a stationary phase with a 2998 PDA Detector. The samples were dissolved in DMF and filtered through a 0.45 μm pore PTFE syringe filter prior to transferring the solutions into the autosampler vials. The instrument method was set to a flow rate of 1 mL/min at 25 °C, and sample set method was set to 20 μL injection volume for run times ranging between 3 – 5 minutes at a wavelength of 680 nm in the Empower® 3 software. Lastly, the Empower® 3 software was employed to integrate peaks and process data.

2.4.14 Organic thin-film transistor fabrication and characterization

OTFTs were fabricated on 15 mm × 20 mm substrates composed of *n*-doped Si wafers with a 230 nm thermally grown layer of SiO_2. They were first cleaned by sequentially sonicating for 5 minutes in soapy water, deionized water, acetone and methanol, dried under N_2 flow and treated with air plasma for 15 minutes. Surface treatment with either HMDS or OTS was then

carried out. For HMDS treatment, 50 µL of HMDS was statically spin-coated onto the substrates at 3,000 rpm for 30 seconds in a N_2 glovebox environment, followed by an annealing step at 150°C under vacuum. For OTS treatment, the substrates were rinsed with water and isopropanol, dried with N_2 flow and immersed in a 1 % v/v solution of OTS in anhydrous toluene for one hour. They were then rinsed with toluene and dried at 70°C under vacuum.

Solutions of **2A**, **2A-4** and **2A-5** were prepared by dissolving the compounds in chloroform at a concentration of 10 mg/mL, heating them to 50°C for one hour and filtering through a 0.22 µm pore PTFE filter. Films were cast by statically spin-coating 60 µL of the solutions onto the substrates at 1,500 rpm for 90 seconds in air and annealed under vacuum at 100°C for one hour. The substrates were then transported to a physical vapour deposition chamber (*Angstrom Engineering EvoVac*) without exposing them to oxygen, where 100 Å of Mn and 500 Å of Ag were deposited through high-density source and drain electrode masks (*Ossila Source−Drain Deposition Mask E321*) at a rate of 0.5 Å s^{-1} and 1.0 Å s^{-1}, respectively, resulting in 20 devices per substrate.

The devices were tested in a N_2 glovebox environment using a custom autotester with push pins to contact all device sites[61] and a Keithley 2614B sourcemeter interfaced with custom LabVIEW software to collect I-V characteristics. Output curves were obtained by sweeping V_{DS} from 0 to ±50 V with fixed V_{GS} values of 0, ±10 V, ±20 V, ±30 V, ±40 V and ±50 V, while transfer curves were obtained in the saturation regime by setting V_{DS} to ±50 V and sweeping V_{GS} from 0 to ±50 V bidirectionally. Each transfer curve was collected four times. The linear portion of the $\sqrt{I_{DS}}$ vs V_{GS} curve was fitted to determine V_T and μ, with the former being expressed as the x-intercept of the fitting and the latter being determined from the slope, as described by the MOSFET model shown below.

$$I_{DS} = \frac{\mu_e C_i W}{2L}(V_{GS} - V_T)^2$$

where W and L represent the channel dimensions – width and length – respectively, and C_i represents the capacitance density of the SiO_2 dielectric.

2.5 SUPPORTING INFORMATION

Characterization of Bis(3-(prop-2-yn-1-yloxy)benzyloxy) silicon phthalocyanine (2A)

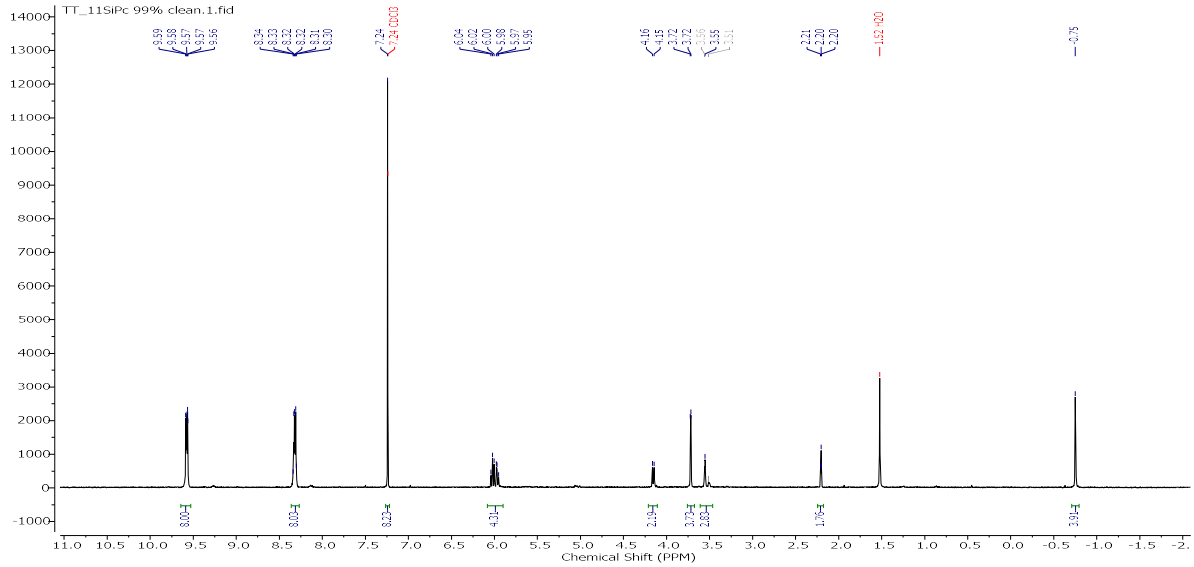

Figure S2.1: ^{1}H NMR spectrum of compound **2A** in Chloroform.

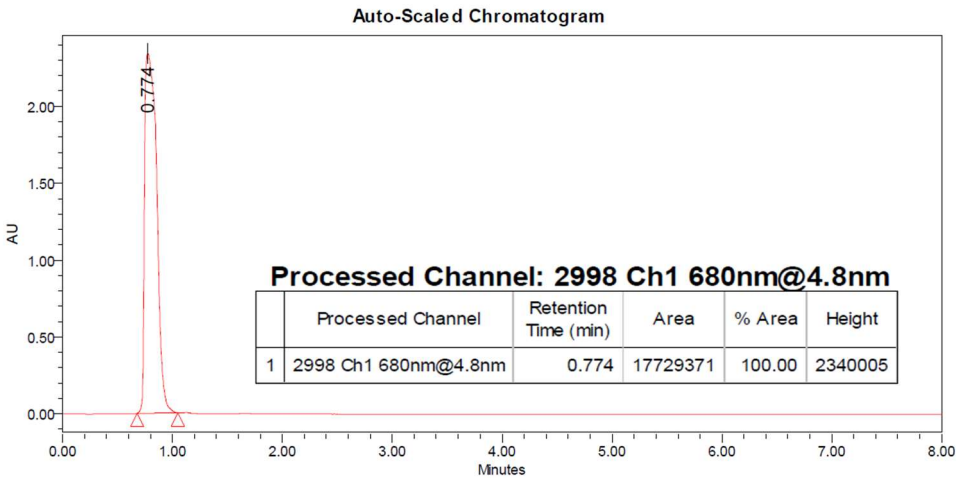

Figure S2.2: High-Performance Liquid Chromatography (HPLC) of compound **2A** in ran in 100% DMF, with a purity of 100%.

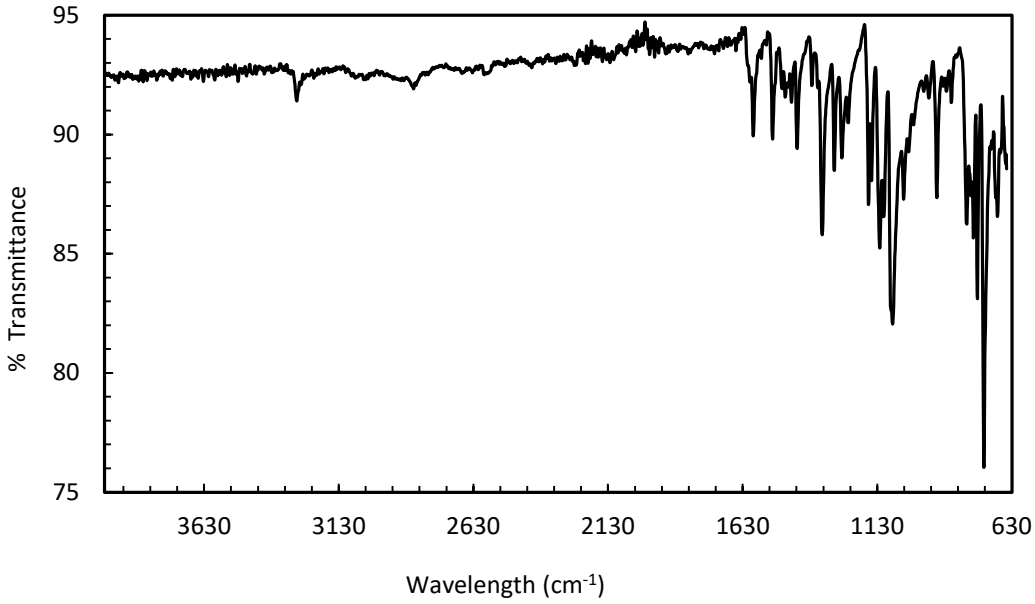

Figure S2.3: Fourier Transform Infrared (FTIR) spectra of compound **2A**; corresponding C-H stretch at 3287 cm^{-1} and Si-O-CH_2 peaks 1170-1090 m^{-1}.

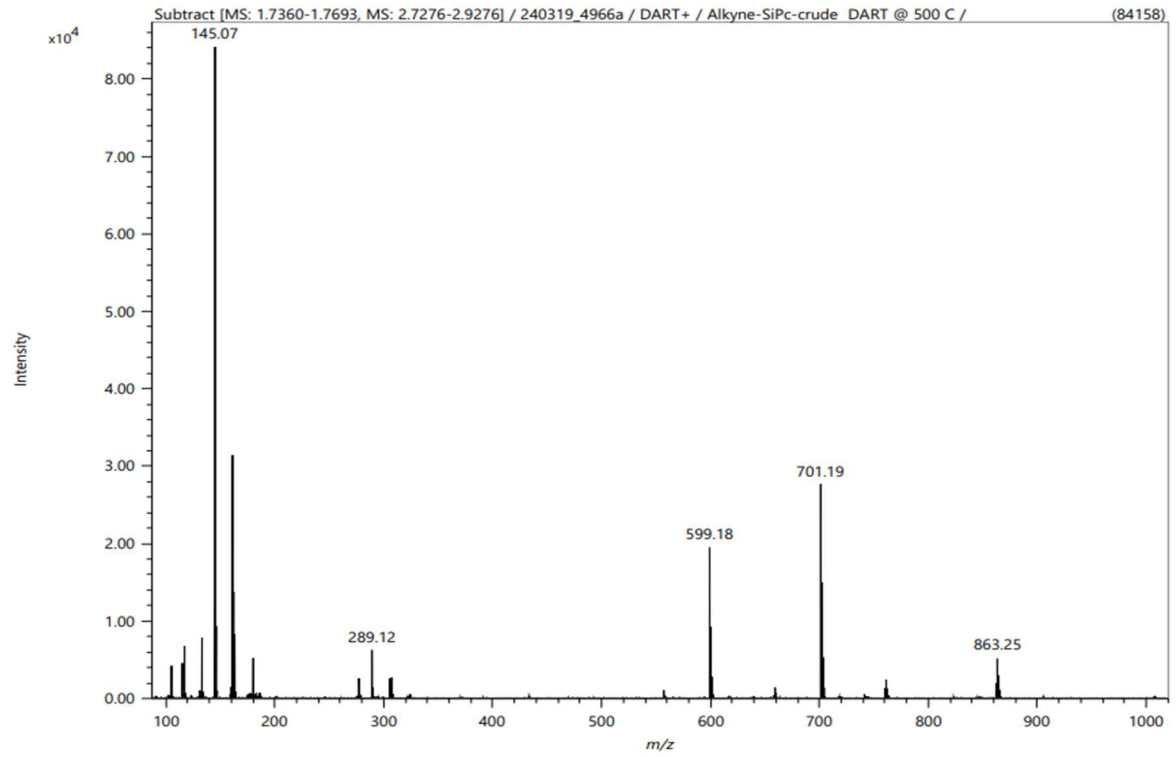

Figure S2.4: High-resolution mass spectrum (HRMS) of compound **2A**; m/z: [M]+ calcd. for $C_{52}H_{34}N_8O_4Si$: 862.24668; found: 862.24646.

Characterization of [Si, Si] ((3-(prop-2-yn-1-yloxy)benzyloxy), thienyl methoxy) silicon phthalocyanine (2A-4)

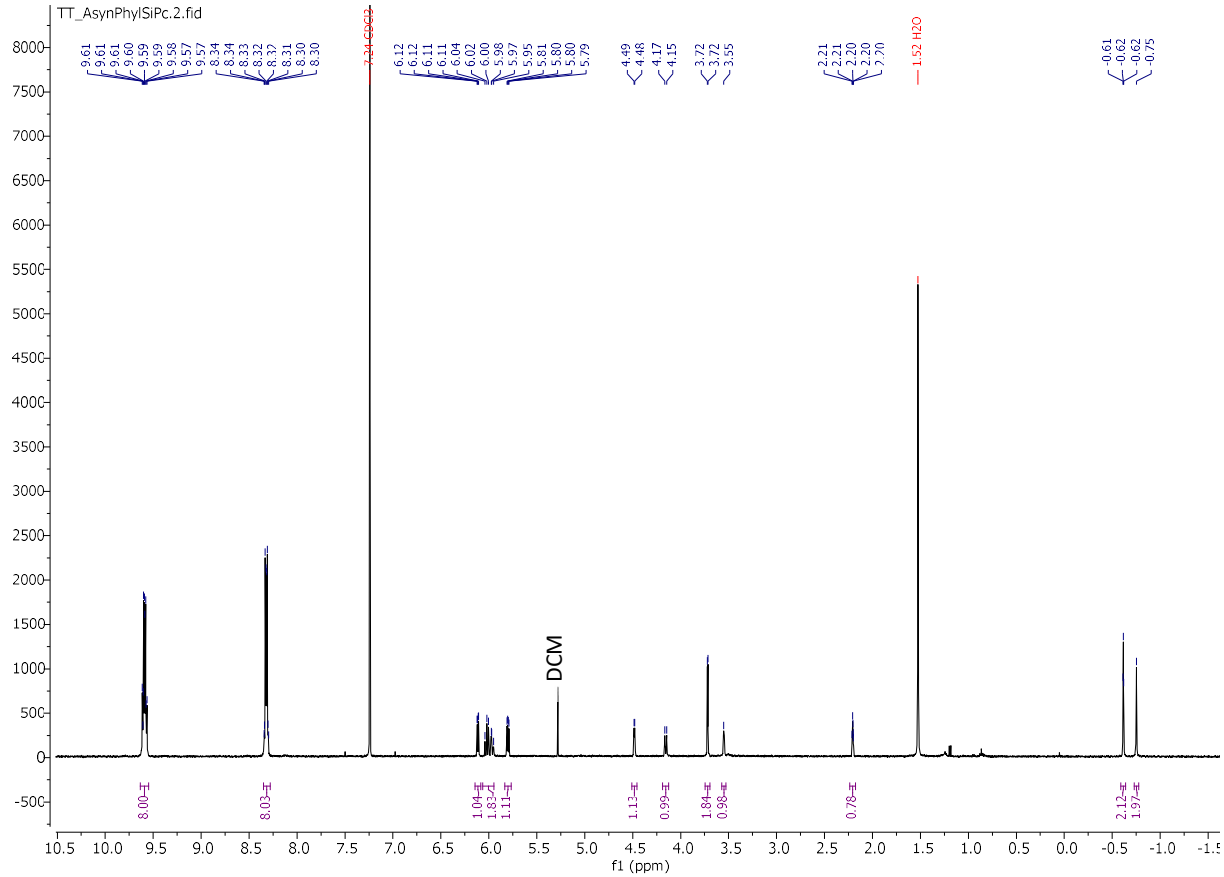

Figure S2.5: ^{1}H NMR spectrum of compound **2A-4** in Chloroform.

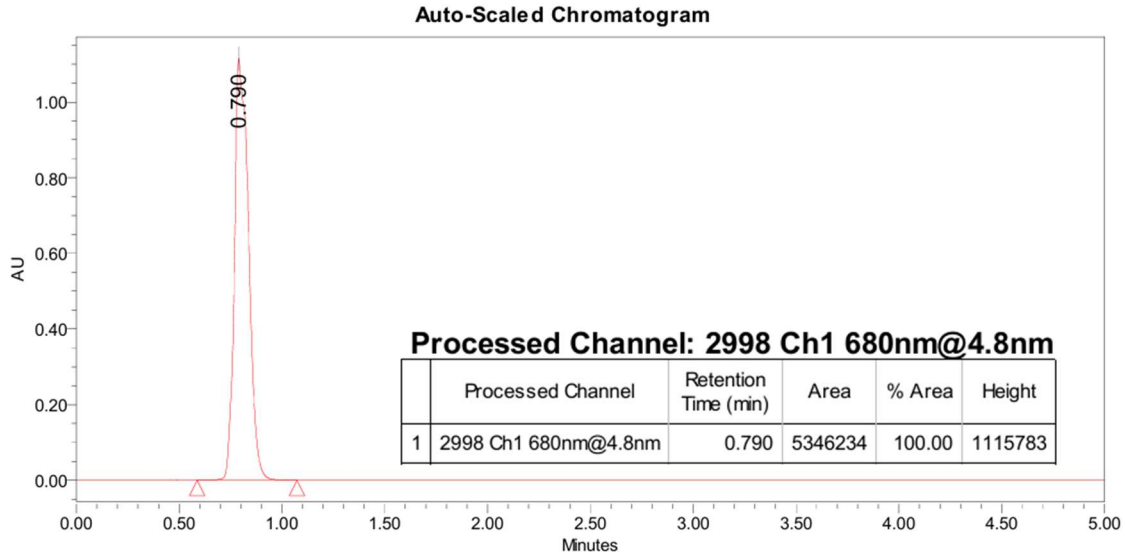

Figure S2.6: HPLC of compound **2A-4** in ran in 100% DMF, with a purity of 100%.

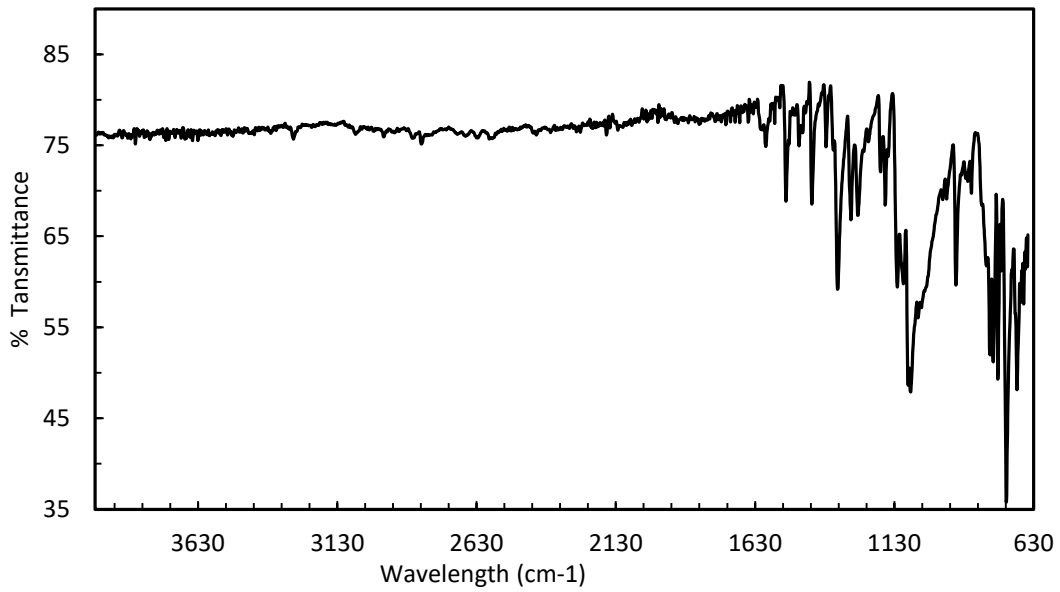

Figure S2.7: FTIR spectra of compound **2A-4**; C-H stretches at 3287 cm^{-1}, Si-O-CH_2 peaks 1170-1090 cm^{-1}, and thiophene stretches between 785-715 cm^{-1}.

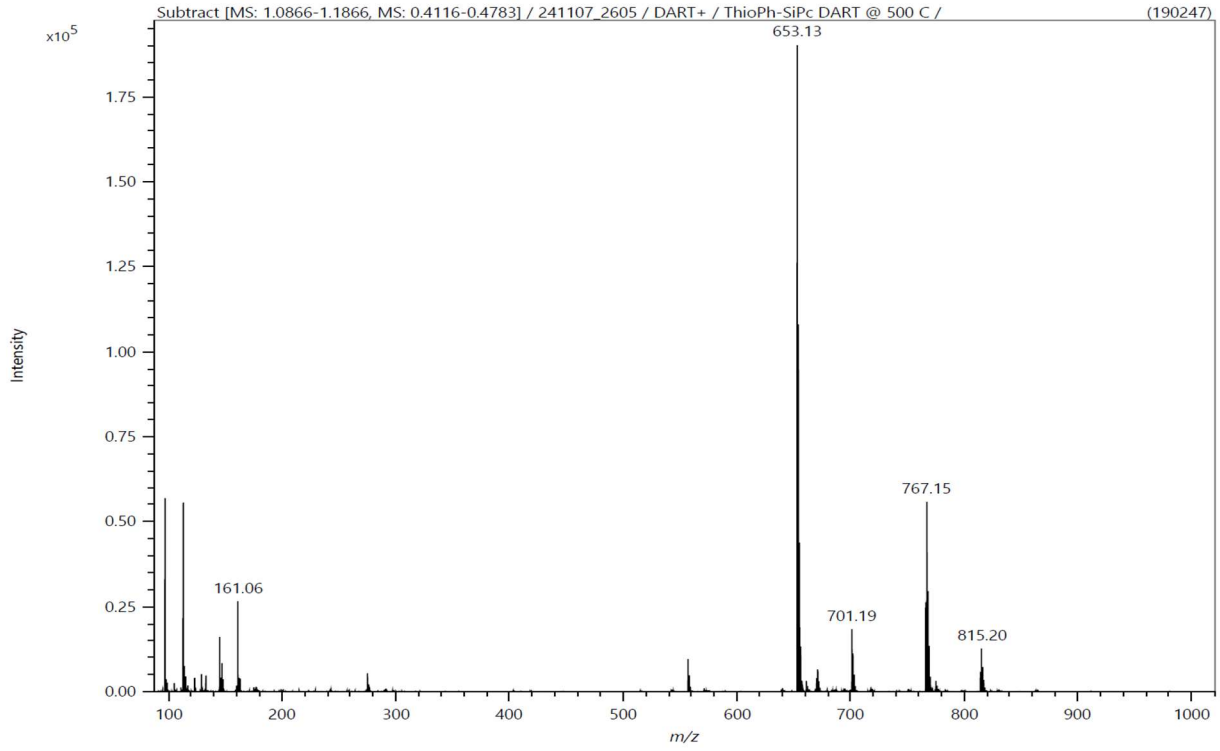

Figure S2.8: HRMS of compound **2A-4**; m/z: [M]+ calcd. for $C_{47}H_{30}N_8O_3SSi$: 815.20036; Found: 815.20071.

Characterization of [Si, Si] ((3-(prop-2-yn-1-yloxy)benzyloxy),(pentafluorophenoxy) silicon phthalocyanine (2A-5)

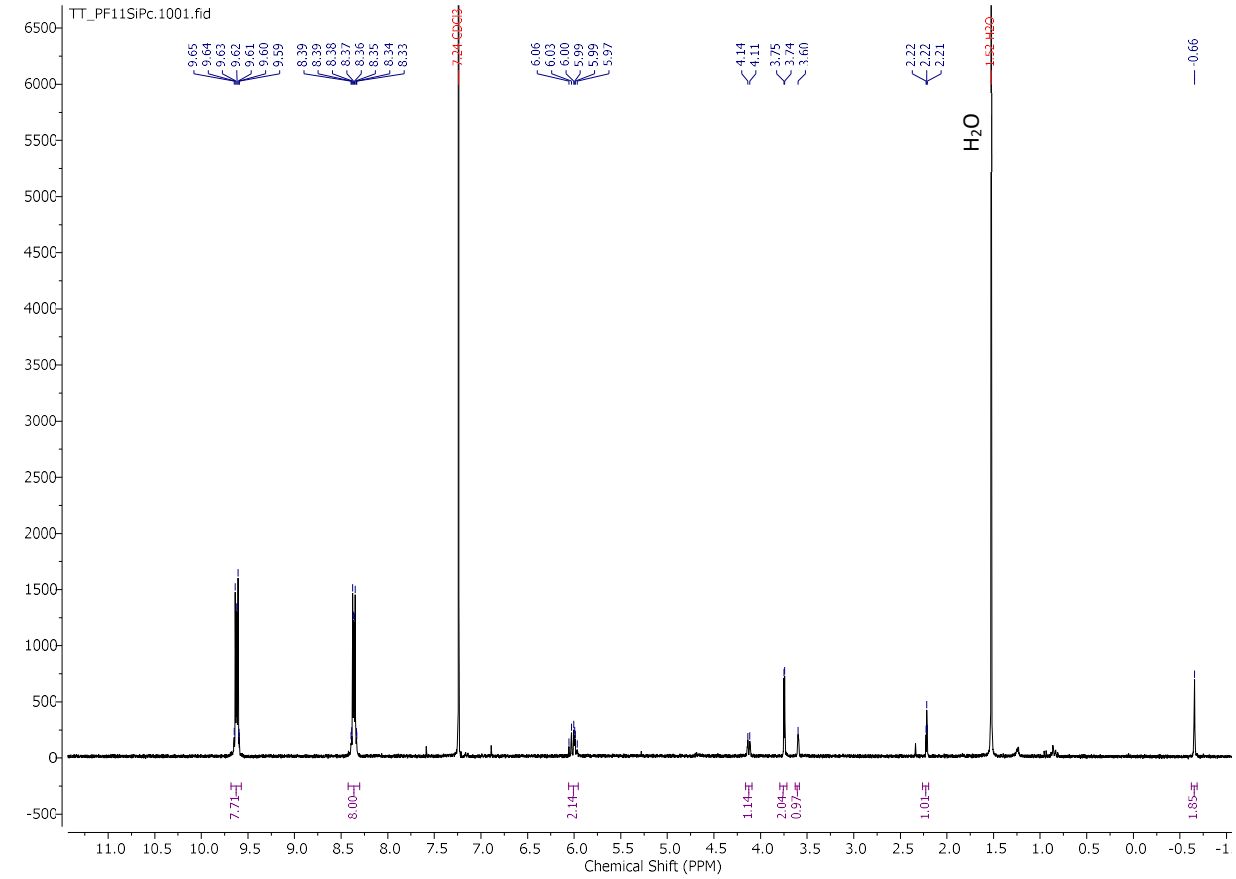

Figure S2.9: ^{1}H NMR spectrum of compound **2A-5** in Chloroform.

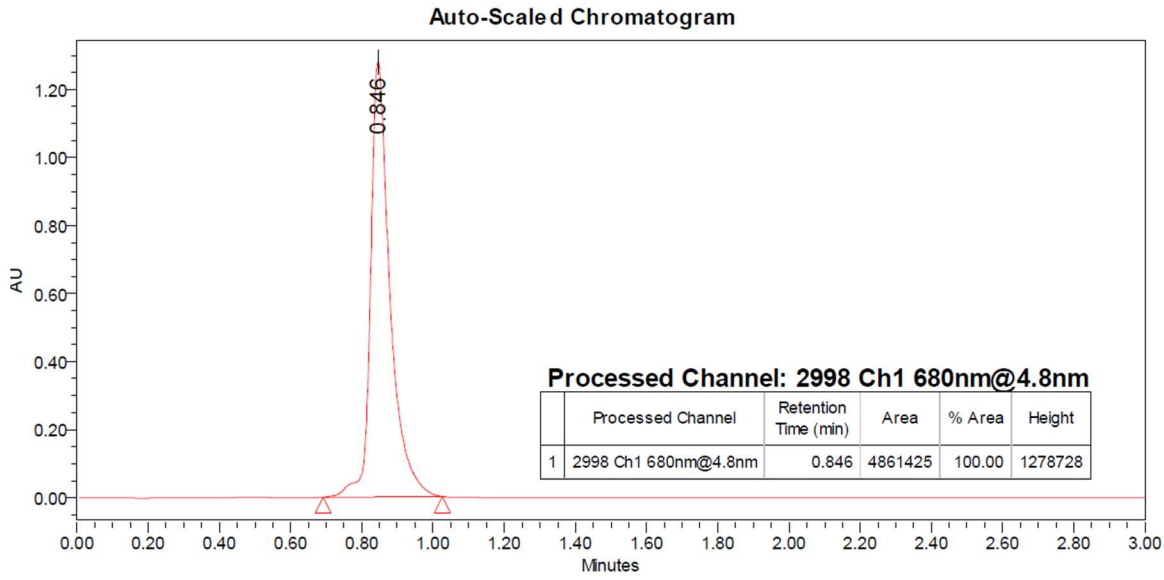

Figure S2.10: HPLC of compound **2A-5** in ran in 100% DMF, with a purity of 100%.

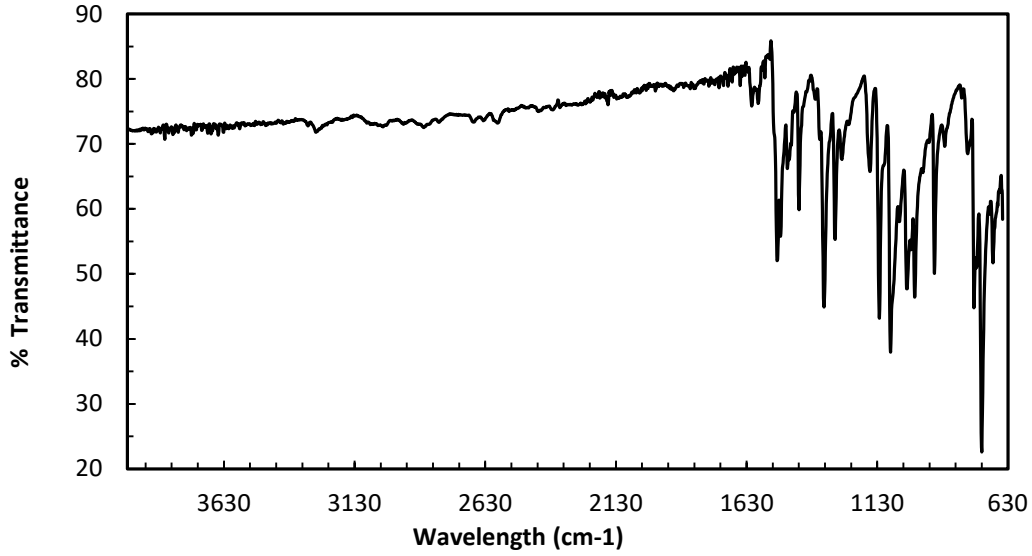

Figure S2.11: FTIR spectra of compound **2A-5**; corresponding C-H stretch at 3270 cm^{-1} and Si-O-CH_2 and Si-O-C peaks 1165-1090 cm^{-1}, C-F stretches at 1333 and 1080 cm^{-1}.

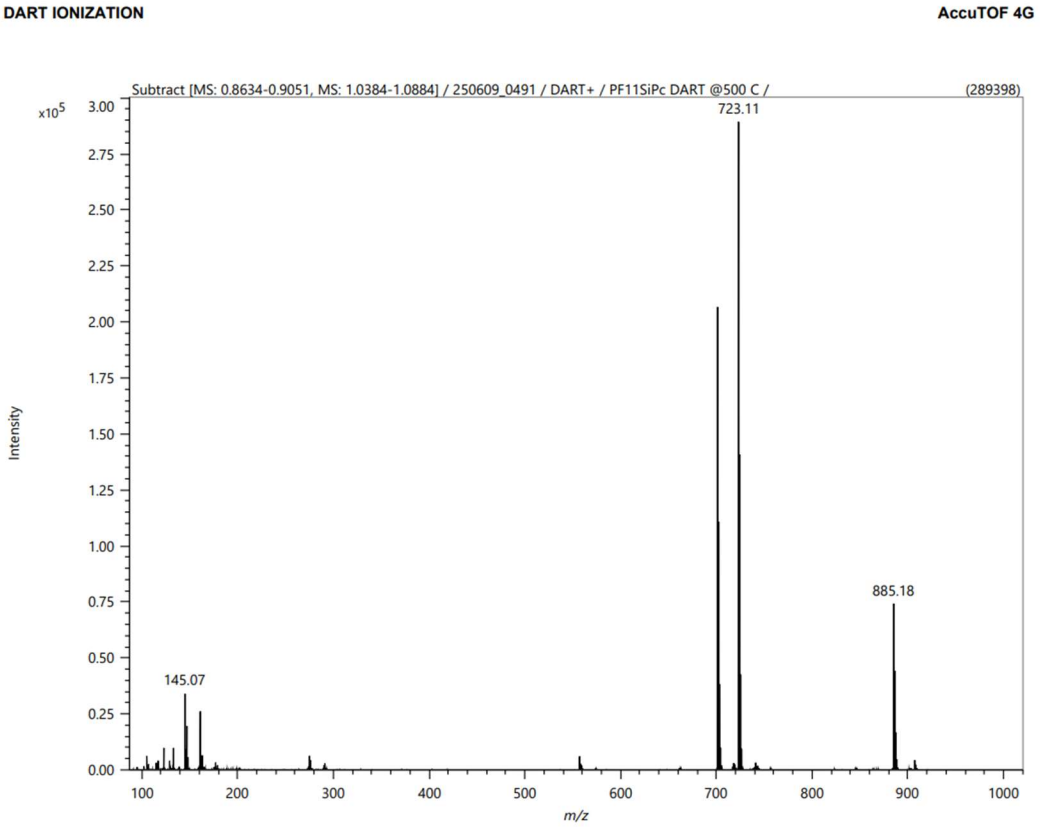

Figure S2.12: HRMS of compound **2A-5**; m/z: [M]+ calcd. for $C_{48}H_{25}F_5N_8O_3Si$: 885.18118; Found: 885.18113.

Characterization of Bis(3-[(1-benzyl)1,2,3-triazole-5-methoxy] benzyloxy) silicon phthalocyanine (2A-6)

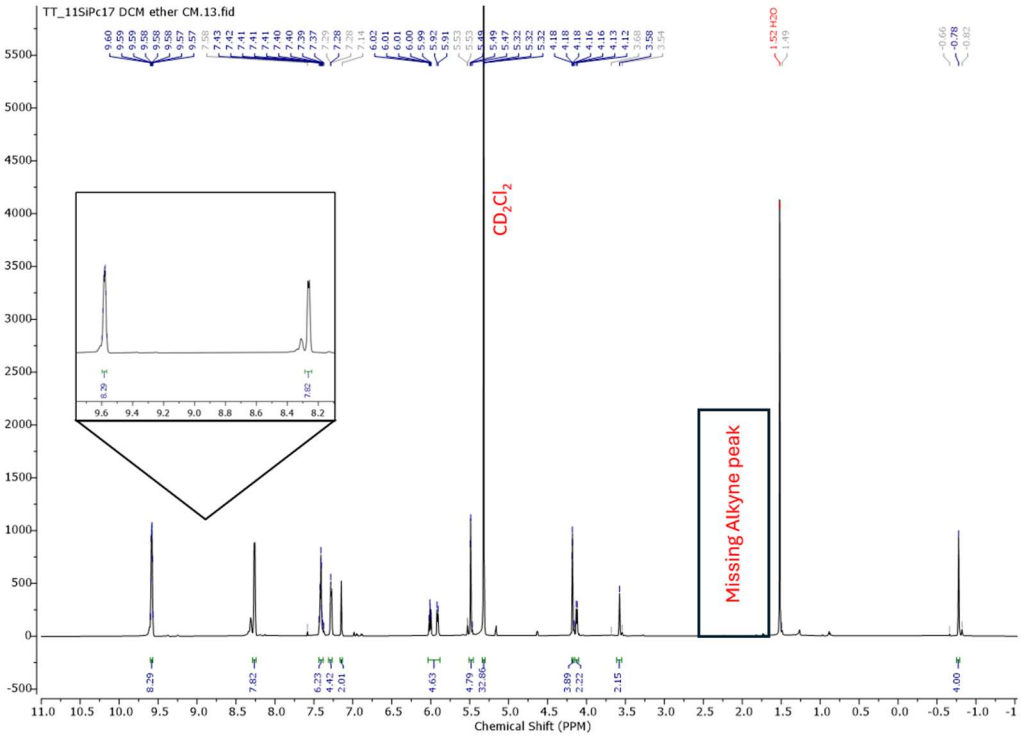

Figure S2.13: ^{1}H NMR spectrum of compound **2A-6** in Chloroform . The ^{1}H NMR shows that the alkyne proton previously present at 2.22 ppm is no longer present, it additionally indicates the presence of small impurities around 8.25 ppm as well.

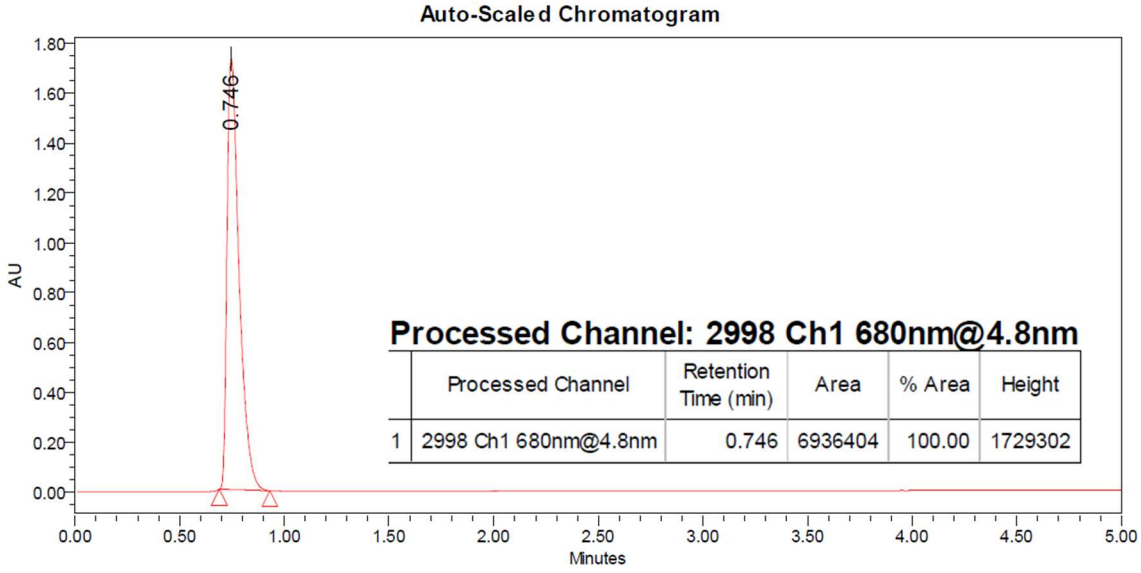

Figure S2.14: HPLC of compound **2A-6** in ran in 100% DMF, with a purity of 100%.

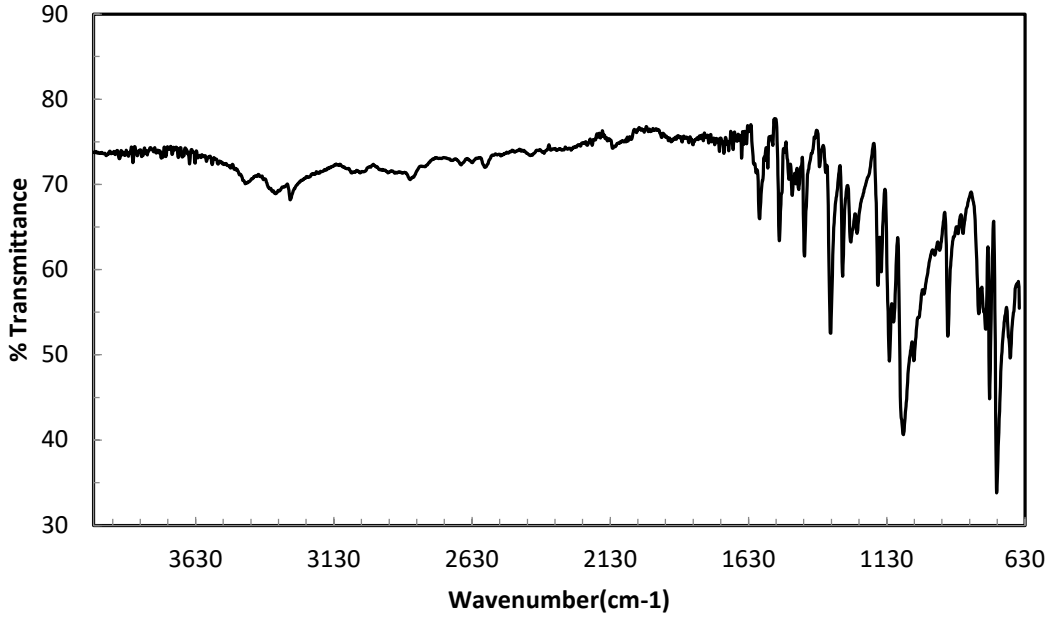

Figure S2.15: FTIR spectra of compound **2A-6**; triazole ring C-H stretch appearing around 3300 cm^{-1}.

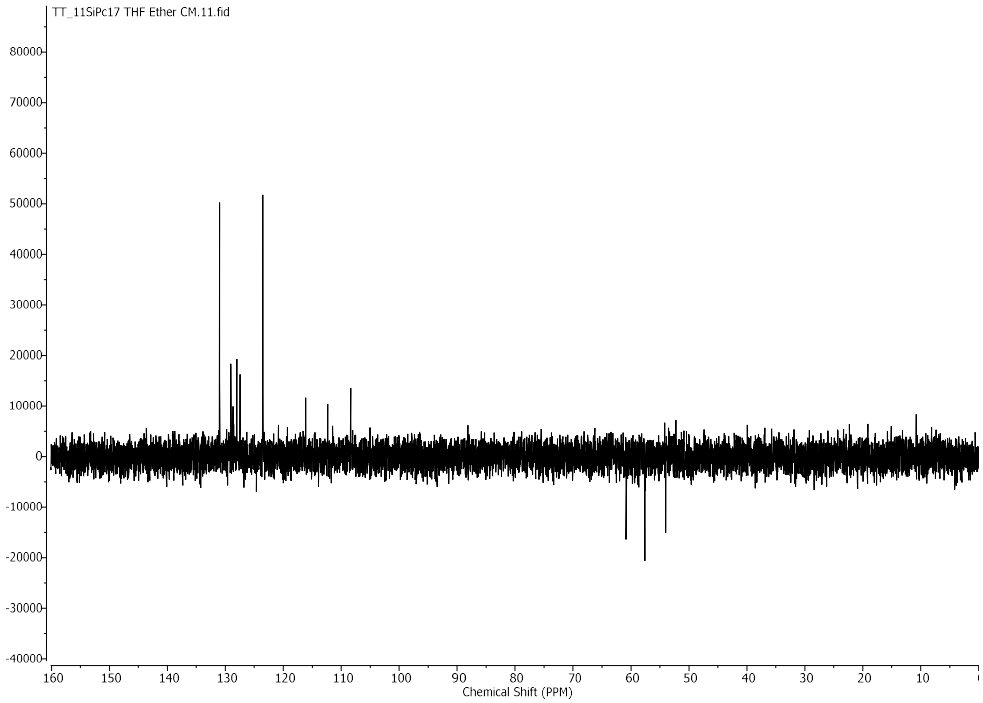

Figure S2.16: ^{13}C NMR spectrum of compound **2A-6** in Chloroform . The DEPT 135 analysis indicates the presence of 3 CH_2 groups, indicated the attachment of the benzyl group forming the triazole ring.

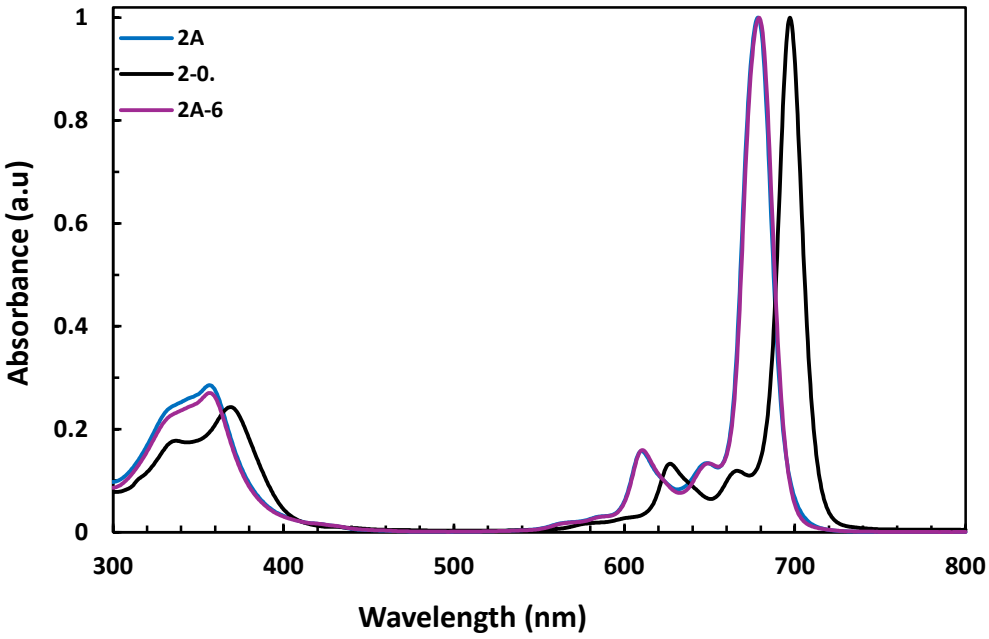

Figure S2.17: Normalized absorbance spectra of compounds **2-0** (black), **2A** (blue) and **2A-6** (purple) in solution with chlorobenzene.

Characterization of 3-(prop-2-yn-1-yloxy) benzaldehyde (2-1)

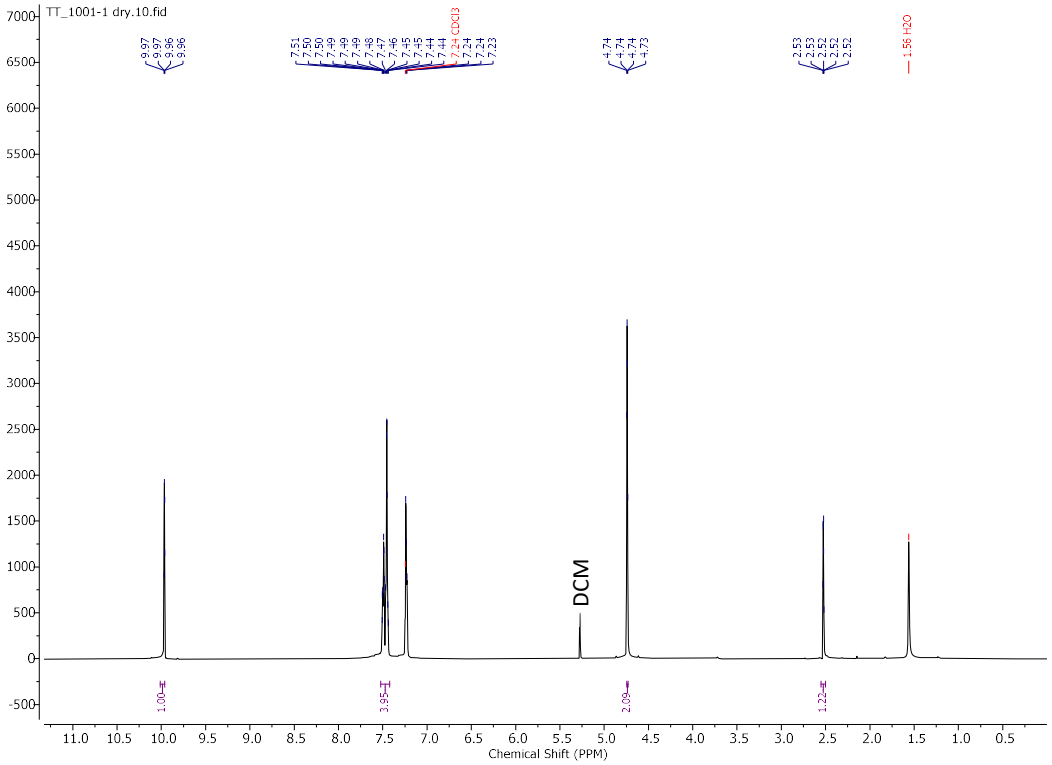

Figure S2.18: ^{1}H NMR spectrum of compound **2-1** in Chloroform.

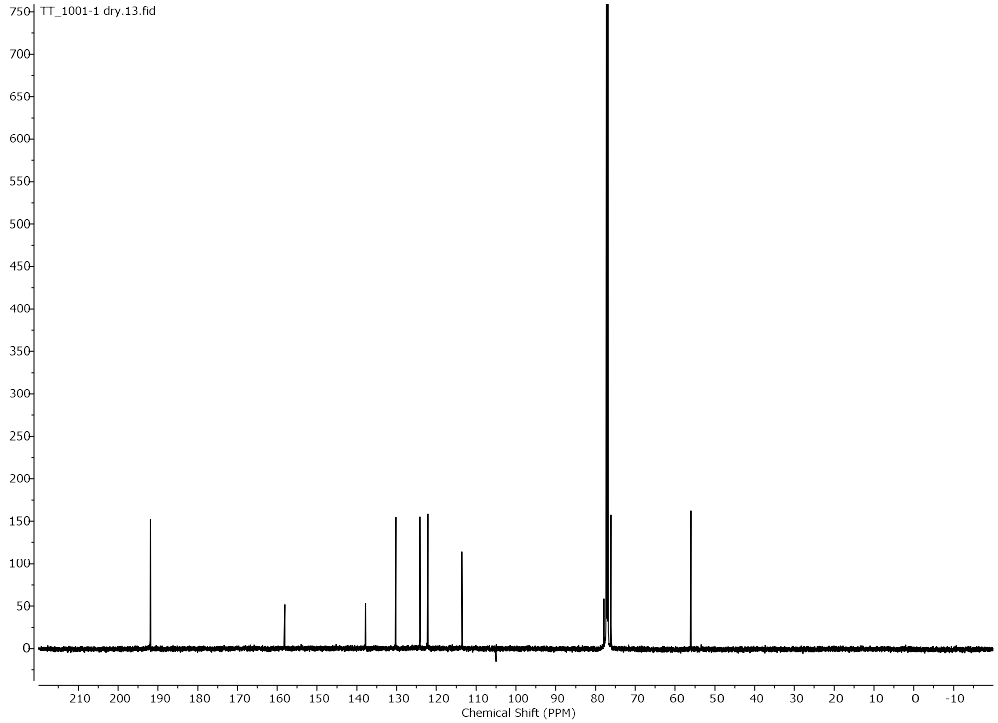

Figure S2.19: ^{13}C NMR spectrum of compound **2-1** in Chloroform.

Characterization of 3-(prop-2-yn-1-yloxy)phenyl methanol (2-2)

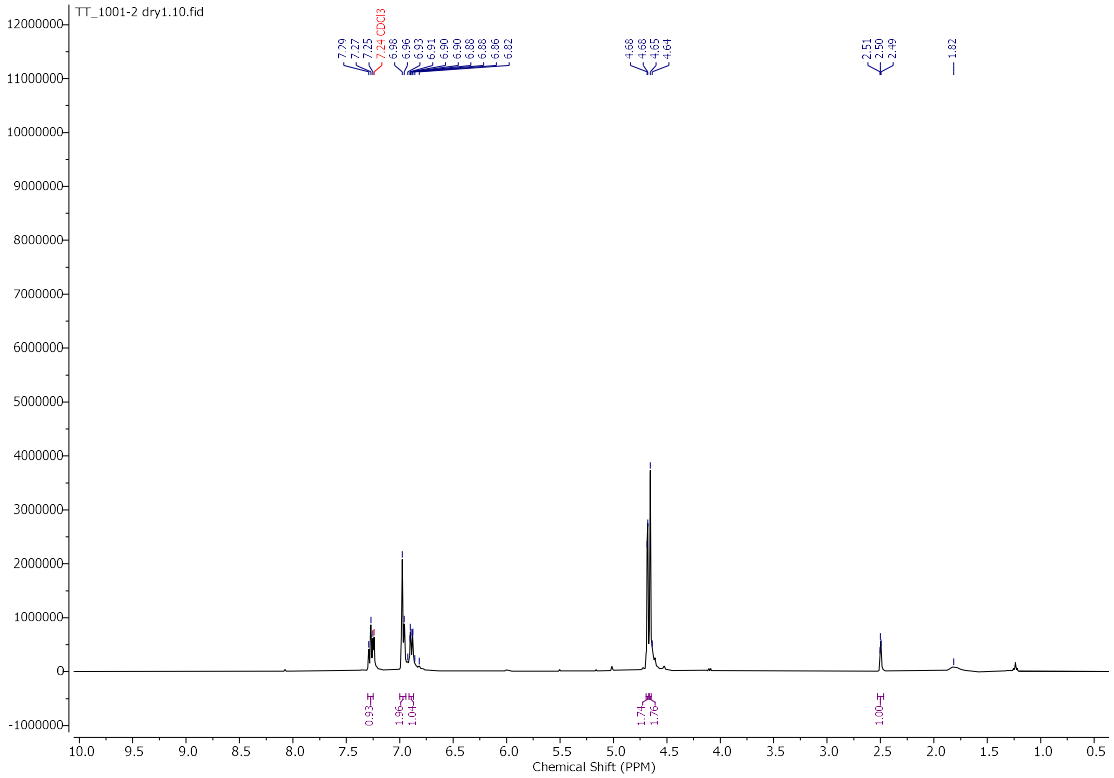

Figure S2.20: ^{1}H NMR spectrum of compound **2-2** in Chloroform.

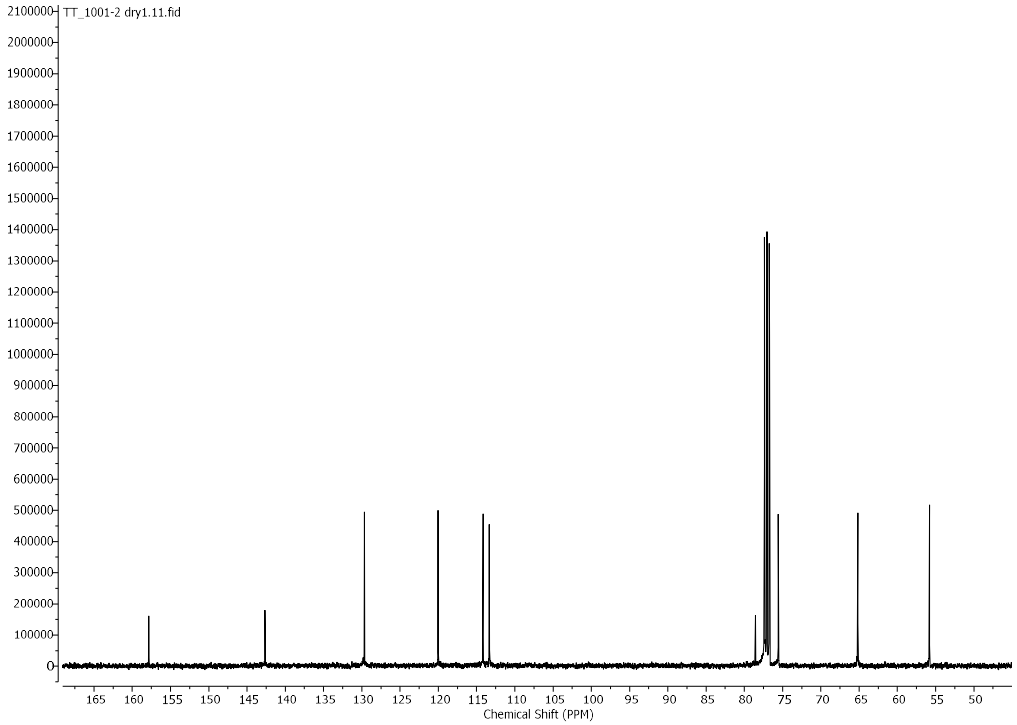

Figure S2.21: ^{13}C NMR spectrum of compound **2-2** in Chloroform.

Characterization of benzyl azide

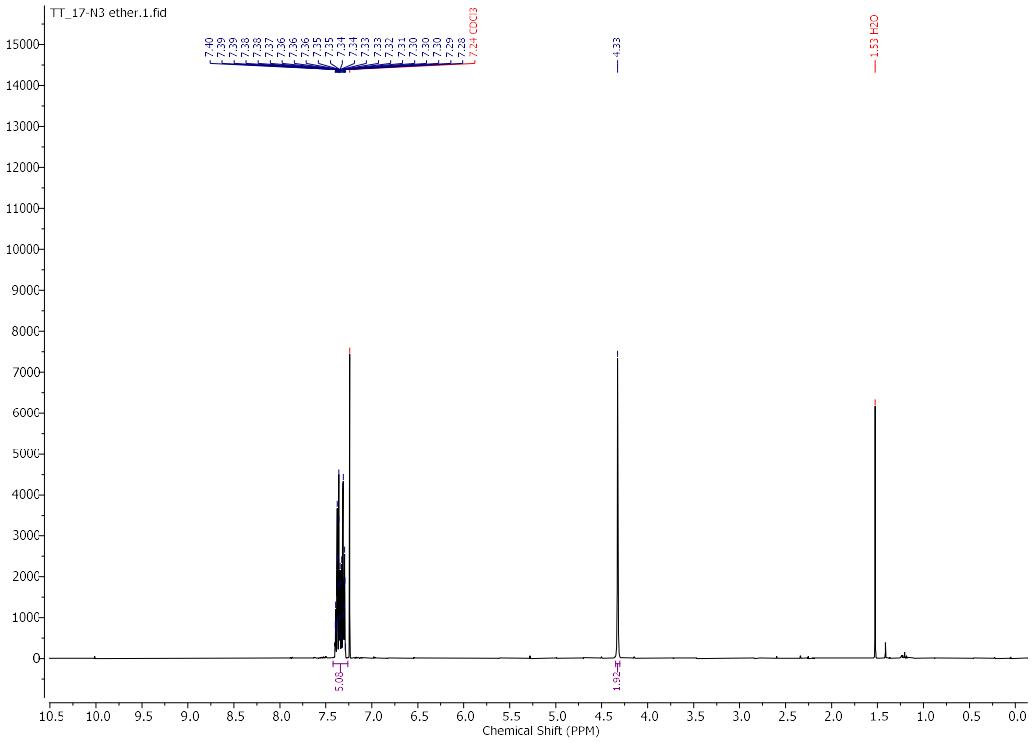

Figure S2.22: ^{1}H NMR spectrum of benzyl azide in Chloroform.

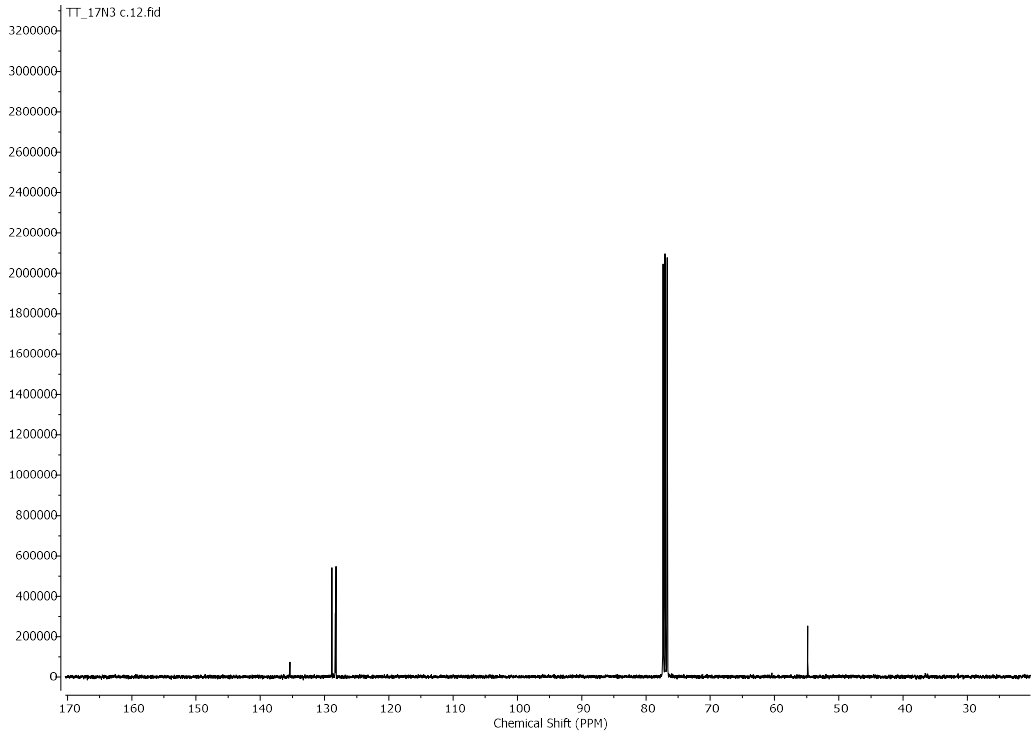

Figure S2.23: ^{13}C NMR spectrum of benzyl azide in Chloroform.

2.6 REFERENCES

1. Boileau NT, Melville OA, Mirka B, Cranston R and Lessard BH. *RSC Adv.* 2019; **9**: 2133-2142.

2. Gil-Martínez A, Hernández A, Galiana-Roselló C, López-Molina S, Ortiz J, Sastre-Santos Á, García-España E and González-García J. *J Biol Inorg Chem* 2023; **28**: 495-507.

3. Wang T, Zhang W, Li T, Xia Q, Yang S, Weng J, Chen K, Chen W, Liu M, Du S, Zhang X and Song Y. *Inorg Chem* 2024; **63**: 3181-3190.

4. Feng Y-C, Wang X and Wang D. *Mater. Chem. Front.* 2023; **8**: 228-247.

5. Cao R, Thapa R, Kim H, Xu X, Gyu Kim M, Li Q, Park N, Liu M and Cho J. *Nat Commun* 2013; **4**: 2076.

6. Urdaniz C, Taherpour S, Yu J, Reina-Galvez J and Wolf C. *J. Phys. Chem. A* 2025; **129**: 2173-2181.

7. Wong EWY, Walsby CJ, Storr T and Leznoff DB. *Inorg. Chem.* 2010; **49**: 3343-3350.

8. GÜNSEL A, USLUOĞLU A, BİLGİÇLİ AT, Büşra T, ARABACI G and YARAŞIR MN. *Turk J Chem* 2020; **44**: 923-931.

9. Cranston RR and Lessard BH. *RSC Adv.* 2021; **11**: 21716-21737.

10. Zhou W, Yutronkie NJ, Lessard BH and Brusso JL. *Mater. Adv.* 2021; **2**: 165-185.

11. Mitra K and Hartman MCT. *Org. Biomol. Chem.* 2021; **19**: 1168-1190.

12. Wang C, Shao J, Chen F and Sheng X. *RSC Adv.* 2020; **10**: 28066-28074.

13. Santos KLM, Barros RM, da Silva Lima DP, Nunes AMA, Sato MR, Faccio R, de Lima Damasceno BPG and Oshiro-Junior JA. *Photodiagnosis and Photodynamic Therapy* 2020; **32**: 102032.

14. Yutronkie NJ, Grant TM, Melville OA, Lessard BH and Brusso JL. *Materials* 2019; **12**: 1334.

15. El-Khouly ME, Kim JH, Kay K-Y, Choi CS, Ito O and Fukuzumi S. *Chemistry* 2009; **15**: 5301-5310.

16. Lowery MK, Starshak AJ, Esposito JN, Krueger PC and Kenney ME. *Inorg. Chem.* 1965; **4**: 128-128.

17. Dang M-T, Grant TM, Yan H, Seferos DS, Lessard BH and Bender TP. *J. Mater. Chem. A* 2017; **5**: 12168-12182.

18. Sasa N, Okada K, Nakamura K and Okada S. *Journal of Molecular Structure* 1998; **446**: 163-178.

19. Pearson AJ, Plint T, Jones STE, Lessard BH, Credgington D, Bender TP and Greenham NC. *J. Mater. Chem. C* 2017; **5**: 12688-12698.

20. Zysman-Colman E, Ghosh SS, Xie G, Varghese S, Chowdhury M, Sharma N, Cordes DB, Slawin AMZ and Samuel IDW. *ACS Appl. Mater. Interfaces* 2016; **8**: 9247-9253.

21. Ourabi M, Vebber MC, Cyr M, Weintrager FS-D, Ledos N, Lamontagne HR, Nyayachavadi A, Brusso JL and Lessard BH. *J. Mater. Chem. C* July 2025.

22. Melville OA, Grant TM, Lochhead K, King B, Ambrose R, Rice NA, Boileau NT, Peltekoff AJ, Tousignant M, Hill IG and Lessard BH. *ACS Appl. Electron. Mater.* 2020; **2**: 1313-1322.

23. Melville OA, Grant TM, Mirka B, Boileau NT, Park J and Lessard BH. *Adv Elect Materials* 2019; **5**: 1900087.

24. Cranston RR, Vebber MC, Faleiro Berbigier J, Brusso J, Kelly TL and Lessard BH. *Advanced Electronic Materials* 2022; **8**: 2200696.

25. Vebber MC, Rice NA, Brusso JL and Lessard BH. *Scientific Reports* 2021; **11**: 15347.

26. Kim Y-H, Anthony JE and Park SK. *Organic Electronics* 2012; **13**: 1152-1157.

27. Melville OA, Grant TM and Lessard BH. *J. Mater. Chem. C* 2018; **6**: 5482-5488.

28. Park B, Jeon HG, Choi J, Kim YK, Lim J, Jung J, Cho SY and Lee C. *J. Mater. Chem.* 2012; **22**: 5641-5646.

29. Pal AK, Varghese S, Cordes DB, Slawin AMZ, Samuel IDW and Zysman-Colman E. *Sci Rep* 2017; **7**: 12282.

30. Lessard BH, White RT, AL-Amar M, Plint T, Castrucci JS, Josey DS, Lu Z-H and Bender TP. *ACS Appl. Mater. Interfaces* 2015; **7**: 5076-5088.

31. Uslan C, Oppelt KT, Reith LM, Sesalan BŞ and Knör G. *Chem. Commun.* 2013; **49**: 8108-8110.

32. Ţînţaş M-L, Peulon-Agasse V, Piparo M, Giusti P, Mallet J-M and Cardinael P. *Journal of Chromatography Open* 2025; **7**: 100221.

33. Biyiklioglu Z, Bas H and Alp H. *Dalton Trans.* 2015; **44**: 14054-14062.

34. Ağırtaş MS, Solğun DG, Savaş B and Öztürk T. *Polycyclic Aromatic Compounds* 2023; **43**: 3278-3290.

35. Grant TM, Gorisse T, Dautel O, Wantz G and Lessard BH. *J. Mater. Chem. A* 2017; **5**: 1581-1587.

36. Lo P-C, Huang J-D, Cheng DYY, Chan EYM, Fong W-P, Ko W-H and Ng DKP. *Chemistry – A European Journal* 2004; **10**: 4831-4838.

37. Li J, Yang Y, Zhang P, Sounik JR and Kenney ME. *Photochem Photobiol Sci* 2014; **13**: 1690-1698.

38. Gümrükçü Köse G, Karaoğlan GK, Erdağ Maden Y and Koca A. *Dyes and Pigments* 2022; **207**: 110686.

39. Cranston RR, Vebber MC, Berbigier JF, Rice NA, Tonnelé C, Comeau ZJ, Boileau NT, Brusso JL, Shuhendler AJ, Castet F, Muccioli L, Kelly TL and Lessard BH. *ACS Appl. Mater. Interfaces* 2021; **13**: 1008-1020.

40. Barker CA, Findlay KS, Bettington S, Batsanov AS, Perepichka IF, Bryce MR and Beeby A. *Tetrahedron* 2006; **62**: 9433-9439.

41. Lau JTF, Lo P-C, Tsang Y-M, Fong W-P and Ng DKP. *Chem. Commun.* 2011; **47**: 9657-9659.

42. Huang Y, Liu G, Zheng F, Chen J, Lin Y, Wang J, Huang Y and Peng Y. *Colloids and Surfaces B: Biointerfaces* 2024; **238**: 113890.

43. Zheng B-Y, Wang L, Hu Q-Y, Shi J, Ke M-R and Huang J-D. *Dyes and Pigments* 2020; **177**: 108286.

44. Li R, Zhou Y, Liu Y, Jiang X, Zeng W, Gong Z, Zheng G, Sun D and Dai Z. *Sig Transduct Target Ther* 2022; **7**: 64.

45. Gümüşgöz Çelik G, Gonca S, Şahin B, Özdemir S, Atilla D and Gürek AG. *Dalton Trans.* 2022; **51**: 7517-7529.

46. Martín-Gomis L, Peralta-Ruiz F, Thomas MB, Fernández-Lázaro F, D'Souza F and Sastre-Santos Á. *Chemistry – A European Journal* 2017; **23**: 3863-3874.

47. Cranston RR, Vebber MC, Faleiro Berbigier J, Brusso J, Kelly TL and Lessard BH. *Advanced Electronic Materials* 2022; **8**: 2200696.

48. Zheng B-Y, Wang L, Hu Q-Y, Shi J, Ke M-R and Huang J-D. *Dyes and Pigments* 2020; **177**: 108286.

49. Lessard BH, Dang JD, Grant TM, Gao D, Seferos DS and Bender TP. *ACS Appl. Mater. Interfaces* 2014; **6**: 15040-15051.

50. Pal AK, Varghese S, Cordes DB, Slawin AMZ, Samuel IDW and Zysman-Colman E. *Sci Rep* 2017; **7**: 12282.

51. King B, Melville OA, Rice NA, Kashani S, Tonnelé C, Raboui H, Swaraj S, Grant TM, McAfee T, Bender TP, Ade H, Castet F, Muccioli L and Lessard BH. *ACS Appl. Electron. Mater.* 2021; **3**: 325-336.

52. Ślęczkowski P. *Int J Mol Sci* 2023; **24**: 6924.

53. Lin S-H, Wu F-I and Liu R-S. *Chem. Commun.* 2009: 6961-6963.

54. Hauschild M, Borkowski M, Dral PO, Marszalek T, Hampel F, Xie G, Freudenberg J, Bunz UHF and Kivala M. *Organic Materials* 2020; **02**: 204-213.

55. Xiao S, Chen X, Ye Q, Chen K, Xiao W, Guan X, Huang B, Liu G, Wei H and Peng Y. *Journal of Coordination Chemistry* 2020; **73**: 1232-1244.

56. Todorova Z, Koseva N, Ugrinova I and Troev K. *Journal of Polymer Science Part A: Polymer Chemistry* 2017; **55**: 1730-1741.

57. Hans RH, Guantai EM, Lategan C, Smith PJ, Wan B, Franzblau SG, Gut J, Rosenthal PJ and Chibale K. *Bioorganic & Medicinal Chemistry Letters* 2010; **20**: 942-944.

58. Zhao J, Huang L, Cui X, Li S and Wu H. *J. Mater. Chem. B* 2015; **3**: 9194-9211.

59. Shaikh MH, Subhedar DD, Nawale L, Sarkar D, Khan FAK, Sangshetti JN and Shingate BB. *Med. Chem. Commun.* 2015; **6**: 1104-1116.

60. Lal S and Díez-González S. *J. Org. Chem.* 2011; **76**: 2367-2373.

61. Dallaire N, Boileau NT, Myers I, Brixi S, Ourabi M, Raluchukwu E, Cranston R, Lamontagne HR, King B, Ronnasi B, Melville OA, Manion JG and Lessard BH. *Advanced Materials* 2024; **36**: 2406105.

2.7 COPYRIGHT PERMISSION

CHAPTER 3: AXIAL SUBSTITUTION OF SILICON PHTHALOCYANINE WITH ETHYNL THIONOPHENE HANDLES

Context

Inspired by the work presented in **Chapter 2**, this chapter explores axial substitution of silicon phthalocyanines with thienyl moieties in place of the previously investigated benzyloxy ligands. As in **Chapter 2**, compounds exhibiting adequate purity and promising optoelectronic properties were intended for incorporation into organic thin-film electronic devices. Accordingly, the design of thienyl analogues to the benzyloxy ligands incorporated a terminal alkyne functionality to enable future post-synthetic modification via click chemistry. The synthetic strategy started from 5-bromothiophene-2-carboxaldehyde and involved the addition of a trimethylsilyl-protected acetylene for subsequent click reactivity. Throughout this sequence, challenges associated with the synthesis of thiophene-based ligands and the preservation of chemical purity were encountered and addressed.

The first SiPc derivative obtained via this approach, bis(5-ethynyl-2-thienylmethoxy) silicon phthalocyanine (**3B**), exhibited poor solubility and was unsuitable for purification by sublimation. As a result, no functional organic thin-film transistors (OTFTs) were fabricated. Subsequent modifications to both the ethynyl-thiophene handle were explored to improve processability and stability; however, due to time constraints, these materials were not evaluated in OTFT devices.

Contribution

The materials in this chapter were synthesized, purified, and characterized by me. Mélanie Cyr performed the TGA analysis. OTFT devices were fabricated by May Ourabi.

Abstract

Ethynyl thiophene moiety-based silicon phthalocyanines were synthesized to explore their optoelectronic properties. In doing so, the purification challenges imposed by axial ligand instability and solubility limitations were encountered through the investigations and were addressed. Two symmetrical derivatives (bis(5-[2-(Trimethylsilyl)ethynyl]-2-thienylmethoxy) silicon phthalocyanine (**3A)** and bis(5-ethynyl-2-thienylmethoxy) silicon phthalocyanine (**3B**) and one asymmetrical derivative (**3C-2**) were synthesized. Optical analyses revealed no substantial difference in the absorption profiles of all three compounds. Cyclic voltammetry (CV) analysis of **3A** showed SiPc core-based redox activity with minimal axial group, while the poor solubility nature of the other two samples barred the CV analysis. To that end, solubility tests revealed a strong dependence on axial ligand identity, with TMS-protected derivatives demonstrating significant enhancement in solubility compared to their unprotected counterparts. Notably, asymmetric substitution improved solubility and offered the potential for selective post-functionalization via click chemistry. These results demonstrate the importance of axial ligand stability, and solubility must be balanced when creating SiPc derivatives.

3.1 INTRODUCTION

Thiophene moieties represent ideal π-conjugated systems for organic electronic applications,[1–3] which may be attributed to their electron-rich nature coupled with their planar and rigid frameworks, regularly affording extensive π–π and sulfur–sulfur interactions in the solid state.[2,4–6] Due to these characteristics, thiophene-based compounds have been employed extensively in organic thin film transistors (OTFTs),[5] photovoltaics[4] and organic light-emitting diodes (OLEDs),[7] often leading to high-performing electronic devices.[5,8] In addition to π conjugation, thiophene units can also serve as a versatile site for chemical reactivity. Among their wide chemical functionalities, recent efforts have demonstrated their applicability in electropolymerization[9,10] and photopolymerization[11,12] to form functional polymers, as well as their implementation as chemosensors.[13,14] Given the potential for functionalization through the addition of substituents such as alkynes directly on the thiophene, may be leveraged in homo-coupling or click reactions, further offering chemical tunability.

Metallophthalocyanines, which consist of a highly conjugated system made up of four isoindole units connected by nitrogen atoms with a central atom, are another family of aromatic materials that have been employed in applications such as organic electronics.[15] In particular, silicon phthalocyanines (SiPcs) are of significant relevance to this thesis due to their pronounced absorption profile, relatively stable chemical properties, and ease of synthesis. These attributes have made SiPcs key materials of interest for organic electronic applications in recent years.[16,17] Beyond these characteristics, SiPcs offer further chemical and physical modulation via peripheral or axial substitutions. The tetravalency of the silicon atom is often credited with improving solubility and limiting aggregation, among other chemical fine-tuning achieved through the substitution of different moieties at the axial position.[13] Thus far, axial moieties

ranging from simple alkyl chains to more complex ring systems have been reported for various applications.[15,17–19] Similarly, there have been reports of axial substitution with heteroaryl substituents like thienyl and benzothienyl.[11,20–23] Despite this precedent, thienyl axial substituents in SiPc-based materials remain relatively uncommon compared to phenoxy or alkyl/aryl siloxy derivatives.

The combination of SiPcs with thiophene moieties at the axial position represents a promising platform for accessing new chemical functionality and tuning electronic behavior. For example, Chen e*t al*. reported a series of axially substituted SiPcs bearing thienyl, benzothienyl, and dibenzothienyl ligands, demonstrating that increased steric bulk from thienyl-based substituents can suppress aggregation and influence photophysical properties.[20] Such findings suggest the potential of integrating thiophene-based units with SiPc cores to generate advanced materials for optoelectronic devices. Building on this precedent, the present chapter explores synthetic strategies for incorporating ethynyl-functionalized thiophene units as axial substituents on SiPc derivatives. The ethynyl thiophene moiety was selected both for its potential impact on optoelectronic properties and for providing a reactive handle to enable post-synthetic modification via click chemistry. Through these studies, the stability of the terminal alkyne functional group proved challenging; thus, the addition of a TMS protecting group was required to reduce instability and improve solubility. Initial findings indicate that the electrochemical properties of the resulting SiPc derivative bis(5-[2-(Trimethylsilyl)ethynyl]-2-thienylmethoxy) SiPc (**3A**) was not influenced by the thienyl handle. In addition, enhanced solubility of bis(5-ethynylthienylmethoxy) silicon phthalocyanine (**3B**) was achieved through axial ligand exchange, yielding the mixed-ligand derivative [Si, Si] bis(5-ethynylthienylmethoxy, butoxy) silicon phthalocyanine (**3C-2**).

3.2 RESULTS AND DISCUSSION

3.2.1 Synthesis and characterization of the thienyl axial substituent group

The synthetic approach to producing bis(5-[2-(Trimethylsilyl)ethynyl]-2-thienylmethoxy) silicon phthalocyanine (**3A)** was initially found to be challenging due to the stability of the thiophene starting material 5-[2-(trimethylsilyl)ethynyl]-2-thiophenemethanol (**Scheme 3.1**). This reagent was initially sought after to facilitate i) nucleophilic substitution on the SiPc and ii) obtain a terminal alkyne moiety on the thiophene. To that end, a three-step reaction was carried out starting from 5-bromothiophene-2-carboxaldehyde to afford the desired reagent 5-(trimethylsilyl)ethynyl thiophene-2-carbaldehyde (**3-1**). Unfortunately, the first step in the synthetic procedure presented challenges during the Sonogashira reaction between 5-bromothiophene-2-carboxaldehyde and trimethylsilane acetylene to produce 5-(trimethylsilyl)ethynyl thiophene-2-carbaldehyde (**3-1; Scheme 3.1a),** where a possible homocoupling was observed under the reported conditions**.**[24] Using 1% copper iodide (CuI) and 1% bis(triphenylphosphine)palladium(II) dichloride, $[[(C_6H_5)_3P]_2PdCl_2]$, with 1.0 to 1.1 eq. of the 5-bromothiophene-2-carboxaldehyde and trimethylsilane acetylene reagents , respectively, a black, glue-like substance was formed. However, by adapting the procedure so that trimethylsilane acetylene was the last reagent added to the reaction mixture and by replacing the catalyst with tetrakis(triphenylphosphine) palladium(0), ($[Pd(C_6H_5)_3)_4]$, the desired product **3-1** could be isolated with minimal byproducts in a shorter amount of time (as shown in **Scheme 3.1b**). Compound **3-1** was further purified using a 9:1 hexanes: dichloromethane elution system on silica gel, yielding a white solid in 90% yield and characterized in accordance with literature precedence.[25] Upon successful preparation of **3-1**, it was subsequently reduced with sodium borohydride ($NaBH_4$) to yield 5-[2-(trimethylsilyl)ethynyl]-2-thiophenemethanol (**3-2**), which

was recovered as a dark yellow oil (83% yield). It should be noted that during the workup stages the TMS group may be lost, which was revealed upon inspection of the NMR spectra. To that end, the TMS group appeared to be unstable and easily cleaved off the thiophene unit, as evidenced by additional TMS signals observed via ^{1}H NMR spectroscopy. Furthermore, peaks corresponding to 5-ethynyl-2-thiophenemethanol (total TMS elimination) were followed over time and there were clear batch-to-batch variances. Finally, 5-ethynyl-2-thiophenemethanol (**3-3**) was produced by deprotecting the TMS groups of **3-2** overnight with K_2CO_3, yielding a dark brown oil in 88% yield. Note that **3-3** appeared to become more viscous and darker over time, which put into question its long-term stability.

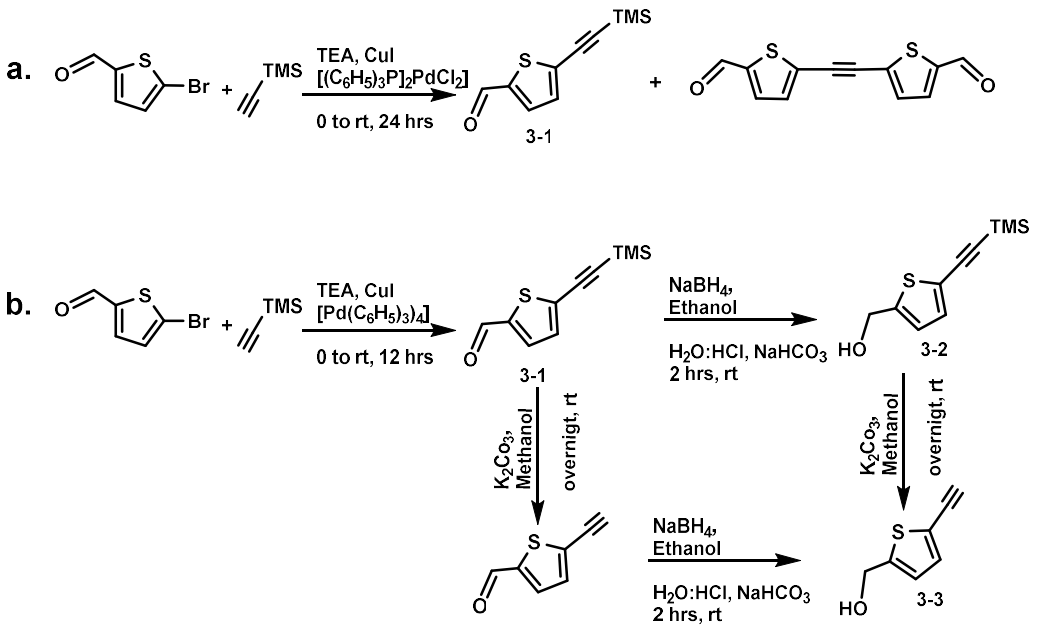

Scheme 3.1: Synthesis of thiophene moieties with a terminal alkyne unit. a). initial synthesis conditions following literature precedent,[24] leading to a highly impure product; b). modified conditions, using an alternative catalysis and reduced reaction time to synthesize **3-1**, followed by its further modulations to obtain **3-2** and **3-3**.

3.2.2 Synthesis and characterization of bis(5-[2-(Trimethylsilyl)ethynyl]-2-thienylmethoxy) SiPc (3A)

As shown in **Scheme 3.2,** bis(5-[2-(Trimethylsilyl)ethynyl]-2-thienylmethoxy) SiPc (**3A)** was synthesized by adapting the procedure reported by Lessard *et al.*[26] The synthesis used 1 to

4 equivalents of dichloro silicon phthalocyanine (Cl_2-SiPc) and 5-[2-(trimethylsilyl)ethynyl]-2-thiophenemethanol (**3-2)**, respectively, which were refluxed in toluene with triethylamine (TEA) for 48 hours. Unfortunately, the desired axially substituted derivative (**3A**) was isolated with contaminants that varied across batches by 10-15%, likely due to the associated impurities and instability of **3-2,** suggesting that the TMS-alkyne bond may not be stable once coupled to the SiPc.

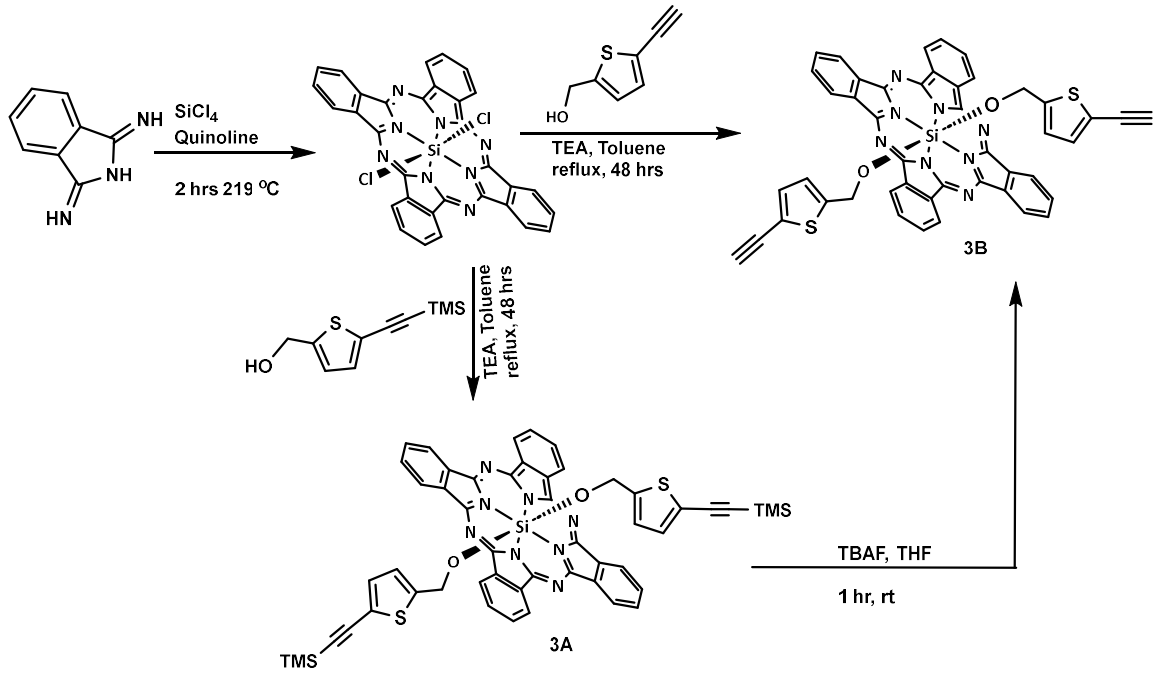

Scheme 3.2: General synthetic scheme for preparation of symmetrical derivative **3A** from Cl_2-SiPc as well as two routes outlining the preparation of **3B**, either from direct synthesis from Cl_2-SiPc or starting from **3A.**

Contaminants observed in the ^{1}H NMR and HPLC investigations correlate to cleaving of the TMS groups, leaving the derivative with either a singular TMS unit on one side or the total loss of both units. Although **3A** has poor solubility after the removal of the TMS groups, the ^{1}H NMR shows a new peak at 2.30 ppm, which may correspond to the alkyne proton, as well as new peaks on the shoulders of 5.96 and 4.26 ppm, which may correspond to the two protons on the thienyl ring based on integration. Given the observed impurity peaks in the ^{1}H NMR, it is

proposed that the contaminant may be the desilylated thienyl-substituted SiPc analogue. This compound has minimal solubility; however, its solubility might be enhanced in the highly soluble media of compound **3A**, potentially explaining the presence of these peaks in the ^{1}H NMR spectrum of **3A**.

Unfortunately, purification through sublimation was not feasible, as signs of the material decomposition was seen at around 240 °C during initial sublimation attempts. Reports by Biyikliogluare *et al.* indicate that the decomposition of axially disubstituted SiPcs is influenced by their bond patterns.[27,28] For example, they noted that axially disubstituted SiPcs tend to decompose around 264 °C.[27,28] Specifically, their SiPcs with Si-O-methylene bond patterns decompose between 250 °C and 280 °C.[27,28] In contrast, SiPcs with bond patterns such as Si-O-aryl, Si-O-(Si), and Si-F have been reported to decompose above 340 °C.[29–31] Thermogravimetric analysis (TGA) of compound **3A** showed that decomposition begins around 240 °C (see **Figure 3.1**). This suggests that the axial moiety may be decomposing or cleaving off, which aligns with the findings of Biyikliogluare *et al.* regarding the Si-O-methylene bond pattern. Typically, silicon phthalocyanines axially substituted with rigid phenolic ligands, short or branched alkylsiloxy groups, and phenolic acid derivatives can be purified by sublimation; however, analogues with longer alkylsiloxy or extended alkyl-chain substituents are generally better suited for purification by distillation.[15] This indicates that in the case of **3A**, the methylene spacer present between the macrocycle and the thienyl unit, along with the trimethylsilyl (TMS) group, may increase **3A**'s susceptibility to decomposition, making it unsuitable for sublimation.

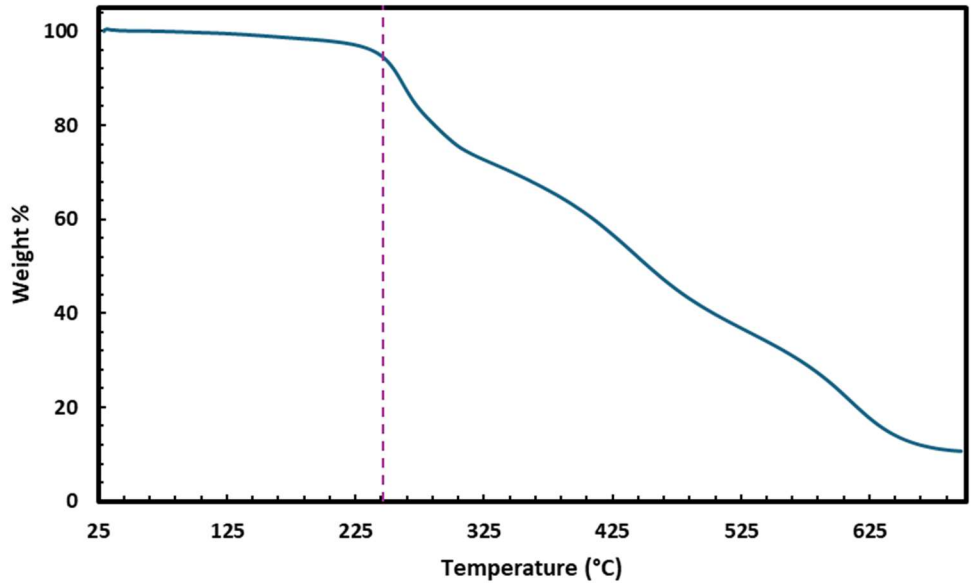

Figure 3.1: TGA plot for **3A**, ramping at 20.00 °C/min to 700.00 °C, collected under nitrogen.

Alternative purification attempts using silica gel also suggested the removal of axial groups, which was evident in the ^{1}H NMR spectra, where the peaks of the thiophene starting materials (**3-2** or **3-3)** were visible. As such, purification was achieved solely through multiple washes and precipitation, which yielded a blue powder in 78%. The final compound was characterized using Fourier-transform infrared spectroscopy (FT-IR), cyclic voltammetry (CV), high-performance liquid chromatography (HPLC), and ultraviolet-visible spectroscopy (UV-vis), high-resolution mass spectrometry(HRMS), in addition to ^{1}H NMR, all of which suggested the synthesizes of **3A.**

3.2.3 Synthesis and characterization of bis(5-ethynylthienyl-methoxy) silicon phthalocyanine (3B)

Bis(5-ethynyl-2-thienylmethoxy) silicon phthalocyanine (**3B**) can be synthesized using two different methods, as shown in **Scheme 3.2**. The first method utilizes reagents Cl_2-SiPc and 5-ethynyl-2-thiophenemethanol (**3-3**) in refluxing toluene in the presence of TEA for 48 hours.

This approach was initially considered, which produced insoluble material, hindering further purification and characterization of **3B**. Additionally, the instability of the alkyne functional group and the associated impurities from **3-3** were present in the reaction, contributing to the overall impurity of the compound. Thus, this route to produce **3B** was deemed ineffective.

The second method involves the initial synthesis of **3A**, followed by the deprotection of the TMS groups. This route allows for some initial characterization to confirm coupling of the thienyl functional groups to the SiPc framework. Attempts to deprotect using K_2CO_3 showed only minimal removal of the TMS protecting groups after reacting for 48 hours at room temperature in DMF. While the deprotection using K_2CO_3 calls for the use of a protic solvent, **3A** is only soluble in chlorinated or high-boiling solvents, thus may explain the ineffectiveness of this reaction. To overcome this challenge, tert-butylammonium fluoride (TBAF) was used to deprotect the thienyl substituents, which proved effective in removing the TMS groups within 1 to 2 hours. This deprotection process was rapid and visually apparent, as the reaction changed color from a light blue to a dark, deep blue solution, with precipitates forming. However, the precipitate exhibited limited solubility prohibiting characterization.

While TBAF proved to be the most effective reagent for the deprotection, it is important to note that it can also lead to the formation of a Si-F bond, which may lead to potential byproducts in the poorly soluble material isolated. Prior studies have demonstrated that the use of a perfluorinated reagent for axial substitution of SiPc resulted in the formation of Si-F bonds.[32] Furthermore, the π–π, CH–π and H-bonding interactions in phthalocyanine are known to enhance aggregation, resulting in reduced solubility and consequently limiting purification and characterization.[33] As well, the rigidity of the thienyl moiety, limited rotation, and possible CH–π interactions between the alkyne group with either the phthalocyanine or a thienyl

ligand,[34] might enhance the solid-state aggregation of **3B,** further contributing to the limited solubility observed. In **3A**, the TMS group has methyl substituents that can disrupt aggregation, and removal of TMS restores planarity and symmetry, which is in alignment with what is observed in converting **3A** to **3B**. The isolated compound was characterized using FT-IR, HPLC, and UV-vis. Note that for HPLC and UV-vis, the bulk material of **3B** was not soluble, only minimal amount of **3B** went into solution. As shown in **Table 3.1**, the material was only soluble at elevated temperatures in certain solvents. After cooling, the material precipitated out of all solvents tested.

Table 3.1: Solubility test for **3B** at different temperatures.

Solvents	Room temperature	Heat
Chlorobenzene	Minimal	Yes
Toluene	No	Yes
NMP	No	Yes
DMF	Minimal	Yes
1,2-Dichlorobenzene	No	Yes
DMSO	No	Yes
DCM	No	No
Chloroform	No	No
Acetone	No	No

3.2.4 Electrochemical analysis of 3A

Cyclic voltammetry (CV) was conducted to evaluate the electrochemical properties of **3A**. The CV analysis showed three redox processes, which are typical for some SiPc derivatives

(see **Figure 3.2)**. The oxidation half potential was determined to be 0.5 V, while the two reduction processes exhibit half potentials of -1.2 and -1.6 V, which indicates HOMO/LUMO energy levels of -5.3 eV and -3.6 eV, respectively, as determined from the redox processes. The redox process observed here has a similar electronic profile as other SiPc derivatives, suggesting that the oxidation is due to electron delocalization on the macrocycle, rather than the thienyl axial substituents. Previous reports have suggested that the oxidation half-potential of thiophene moieties lies above +1.0 V.[35] Incorporation of these groups onto SiPc might result in potential shifts, but comparing the redox process seen here to SiPcs reported in the literature reveals that what is distinguished here is unlikely to be a result of a significant contribution made from the thienyl substitution. Despite having a conjugated system, the thienyl-TMS group does not directly extend to the macrocycle. In other words, the thienyl moiety is separated from the SiPc framework, thus does not contribute to the π-conjugation in the plane of the macrocycle. It is probable that oxidation processes at higher potential could be limited due to the solvent window. Since thiophene and its moieties often have higher redox potentials[36], and due to the electron-donating nature of thienyl substituents, a higher potential beyond the current window shown here might be required to observe any other oxidation process. Functionalization of thiophene units is known to modulate their oxidation potentials; for example, substitution with alkynyl or silyl groups can lower the oxidation potential of thiophene relative to its unsubstituted analogue.[37] However, even with such functionalization, oxidation of thiophene-based substituents typically occurs anodically relative to the oxidation potential in SiPc; consistent with a recent study on bis(3,4-ethylenedioxythiophene)-substituted SiPcs, which reports two electronically distinct oxidation processes, where macrocycle oxidation occurred at +1.16 V, while oxidation of the thienyl-based substituent was observed at +1.73 V.[23] This value is substantially more

anodically shifted than the oxidation potential measured for **3A**, reinforcing the conclusion that the observed oxidation in **3A** is dominated by the SiPc macrocycle rather than the thienyl-TMS axial group; as axial substituents that are non-conjugated or weakly conjugated typically do not introduce new redox processes.[38]

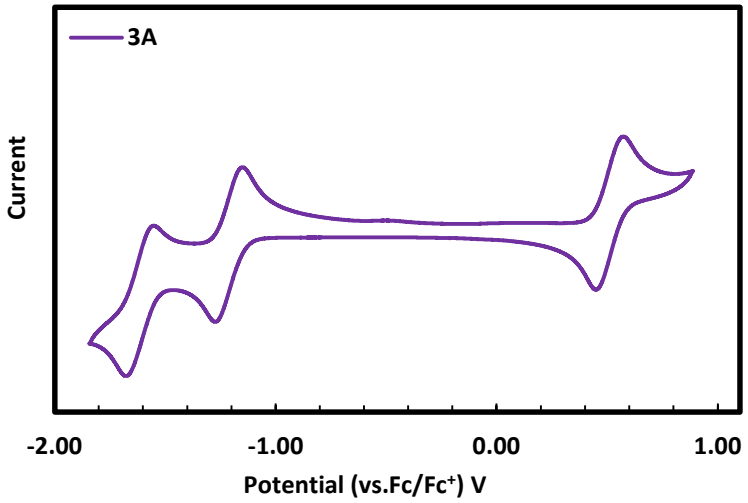

Figure 3.2: Cyclic voltammograms of **3A** in DCM at 100 mV s^{-1} with 0.1 M $TBAPF_6$ as the supporting electrolyte.

3.2.5 Optical Characterization

UV-vis-NIR spectroscopy was employed to investigate the optical properties of compounds **3A** and **3B**, both of which exhibit absorption profiles characteristic of axially substituted silicon phthalocyanines (**Figure 3.3**). Relative to the parent compound, Cl_2-SiPc, both **3A** and **3B** display a blue-shifted Q-band, with λ_{max} at 680 nm in chlorobenzene solution, compared to 698 nm for Cl_2-SiPc. This hypsochromic shift indicates that the axial thienyl substituent does not extend the conjugation or significantly contribute to the phthalocyanine π-system. This behavior might be due to the methylene group adjacent to the axial oxygen

intervening and disrupting the effective π-conjugation between the SiPc core and the thienyl moiety.

A comparison of the absorption spectra of **3A** and **3B** reveals nearly identical photophysical characteristics, indicating minimal electronic differentiation between the two axial substituents. Although compound **3B** possesses a reduced electronic density at the axial position due to the removal of the TMS group, this modification does not measurably influence the Q-band position, further supporting the conclusion that these axial groups do not directly affect λ_{max}. Importantly, this observation does not imply that axial ligation is universally inconsequential to the optical properties of SiPcs. As discussed in **Chapter 2**, Si-O-aryl axial bonding motifs induce more pronounced perturbations in the electronic structure, often resulting in red-shifted absorption relative to Si-O-CH_2-linked analogues.

Overall, substitution of the axial chlorides in Cl_2-SiPc with oxygen-linked substituents to form the symmetrical compounds **3A** and **3B** leads to apparent changes in photophysical behavior, underscoring the role of axial bond identity in modulating the optical properties of silicon phthalocyanines.

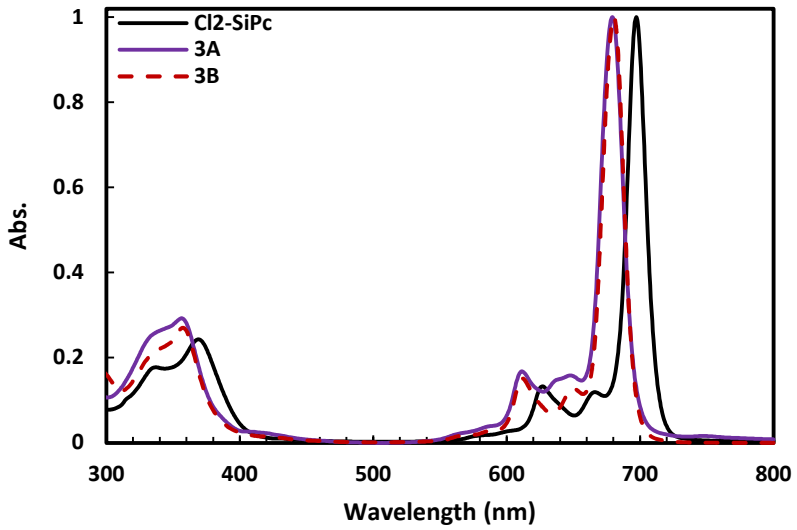

Figure 3.3: Normalized absorption spectrum for **3A** and **3B** in chlorobenzene solutions.

3.2.6 Attempts toward selective mono-axial click functionalization of SiPc

To successfully synthesize SiPc derivatives featuring a single clickable functionality or a distinctive thienyl-alkyne moiety on the axial position, various synthetic strategies were evaluated. One approach involved initiating the reaction with one equivalent of Cl_2-SiPc and systematically introducing differing equivalents or concentrations of the targeted thiophene reagent to explore the conversion to the mono-thienyl-substituted SiPc (Thienyl-SiPc-Cl) effectively. Different batches were prepared either by varying the reactant concentrations or by the addition of a base.

During these experiments, three different concentrations were chosen to promote the conversion, as shown in **Table 3.2**. By monitoring the conversion rates through ^{1}H NMR, it became evident that the formation of disubstituted compounds was markedly more favourable. At a reagent concentration of 12.5 mg/mL, conversion to the mono-substituted product remained below 5%, whereas a lower concentration of 8.38 mg/mL resulted in a modest increase in mono-substitution (25%). Under the most concentrated conditions (25 mg/mL), mono-substitution

increased to approximately 20%; however, no clear or reproducible trend correlating dilution with selectivity could be established. These observations suggest that concentration effects alone are insufficient to reliably control mono- versus di-substitution and that the reaction outcome is dominated by an inherent preference for double axial substitution.

To further bias selectivity, a series of bases (namely, 1,8-diazabicyclo[5.4.0]undec-7-ene (DBU), pyridine, and triethylamine (TEA)) were evaluated under otherwise identical conditions. In all cases, di-substitution remained the dominant pathway. The reactions with DBU and pyridine revealed a 15% conversation, while TEA afforded a slightly higher mono-substitution ratio of 25% based on ^{1}H NMR. The total crude yield (di + mono-substituted) also favoured the use of triethylamine (62%), when comparing to the other reaction conditions performed with the varying concentrations or the two other bases (32-60%). In contrast, a noticeable decline in total crude yield was recorded when the reaction mixture became more diluted or when no base was employed at all.

Overall, variation of concentration and base identity did not provide a reliable or reproducible route to selectively attach a single thienyl moiety at the axial position of SiPc. Under all conditions examined, di-substitution was favored according to ^{1}H NMR analyses. The lack of consistent selectivity, coupled with challenges in reproducibility and product isolation, ultimately motivated the exploration of alternative synthetic strategies for the controlled synthesis of asymmetrically substituted silicon phthalocyanines.

Table 3.2: Conditions to synthesize mono and di-substituted SiPc; different concentrations of 5-[2-(Trimethylsilyl)ethynyl]-2-thiophenemethanol (**3-2**) were introduced to Cl_2-SiPc under nitrogen. Although separation was not possible, the ^{1}H NMR ratio indicates that the bis-substituted SiPc is favored. *1:1 eq., ** new impurities present.

Starting materials	**Equivalency**	**Solvent mL** (Chlorobenzene)	**Base**	**Conc. of 3-2**	**Crude yield (%)**	**^{1}H NMR ratio** (Di : Mono)
Cl_2-SiPc + 3-2	1: 2.5	50	-	25 mg/mL	60	80: 20
Cl_2-SiPc + 3-2	1: 2.5	100	-	12.5 mg/mL	58	92: < 5
Cl_2-SiPc + 3-2	1: 1	127	-	8.38 mg/mL*	48	75: 25
Cl_2-SiPc + 3-2	1: 2.5	50	DBU (0.1 mmol)**	25 mg/mL	45	85: 15
Cl_2-SiPc + 3-2	1: 2.5	50	Pyridine (1 mL)	25 mg/mL	32	85: 15
Cl_2-SiPc + 3-2	1: 2.5	50	TEA (1 mL)	25 mg/mL	62	75: 25

3.2.7 Synthesis of asymmetrical 3C-1 and 3C-2

Since the routes described thus far were not very effective in reproducibly isolating monosubstituted SiPcs, other means of obtaining the mono-functionalized thienyl-alkyne derivatives were considered. It was previously reported that a simple ligand exchange with methanol takes place on a symmetrical SiPc when placed in a methanol solution at room temperature. In the same study, longer alkoxides were also used to produce asymmetrical SiPcs after refluxing.[39] Inspired by this, starting from **3A** and adding an excess amount of butanol, a modest amount of asymmetrical SiPc **(3C-1)** was produced after refluxing (see **Scheme 3.3a**). This ligand exchange reaction was first refluxed in toluene with 2.0 equivalents of butanol for 48 hours. However, conversion to the asymmetrical analogue was unsuccessful. To facilitate the

exchange, an excess amount of sodium hydride (NaH) was added to the reaction mixture. With the addition of the strong base, the starting material (**3A**) appeared to decompose, and a grey insoluble powder was collected after 24 hours at reflux. However, when using less than 2 mg (0.08 mmol) of NaH, complete replacement of both thienyl axial groups with butanol was observed, suggesting that the butanol was highly reactive towards the silicon center.

Upon replacing NaH with triethylamine (TEA) and allowing the reaction to proceed for three days at reflux, [Si, Si] bis(5-trimethylsilylethynylthiophene-2-methoxy, butoxy) SiPc (**3C-1**) was obtained (see **Scheme 3.3a**). Here, a minimal amount of complete replacement of the thienyl axial moieties of **3A** with the butanol reagent was noticed even when using an excess amount of butanol. ^{1}H NMR analysis indicated that the impurities observed in the symmetrical SiPc (**3A**) remained, which are believed to be the derivative **3B**, suggesting instability of the TMS units.

To reduce the impurities transferred from the **3A** starting material, the asymmetric derivative **3C-1** was synthesized by reacting bis(butoxy) SiPc (**3D**) with 5-[2-(trimethylsilyl)ethynyl]-2-thiophenemethanol (**3-2**) as shown in **Scheme 3.3b**. Fortunately, starting from **3D** resulted in a slight reduction in impurities. However, purification via column chromatography appeared to increase the number of impurities, and ^{1}H NMR analysis indicated the complete removal of the thienyl unit from the silicon core. Other purification methods, such as solvent washes and recrystallization, were also found to be unsuccessful.

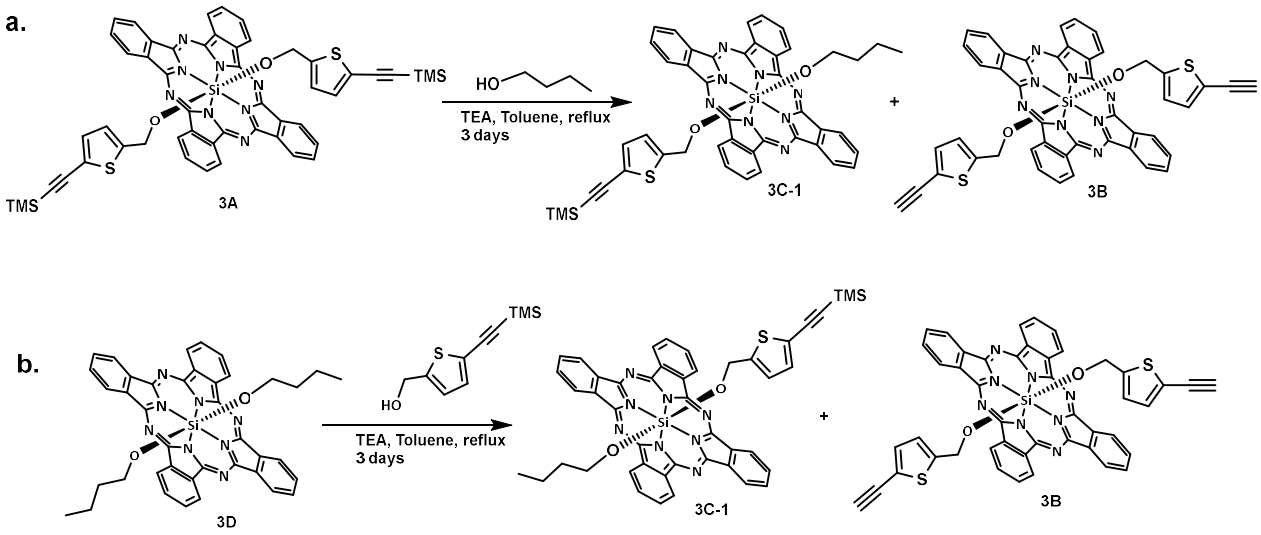

Scheme 3.3: Asymmetric SiPc synthesis using thienyl-alkyne and butanol moieties.

To alleviate this problem, direct deprotection of the TMS unit from **3C-1** was attempted using TBAF. The deprotection seemed successful, yielding [Si, Si] (5-ethynyl-2-thienylmethoxy, butoxy) SiPc **(3C-2)**. The deprotection was rapid and visually evident, as the reaction changed color from light blue to a dark, deep blue solution, with precipitates forming like those observed when deprotecting the symmetric derivative **3B**. Unexpectedly, the deprotected derivative was found to have minimal solubility, and the alkyl chain did not impart any difference. Mass spectrometry suggested the presence of **3C-2** and**3B** (see **Figure 3.4)**. Additionally, according to mass spectrometry, the initially suspected fluorination of the silicon core by the TBAF reagent was not detected. This suggested the rigidity of the thienyl unit to have a larger impact than the butoxyl in the overall solubility of the material.

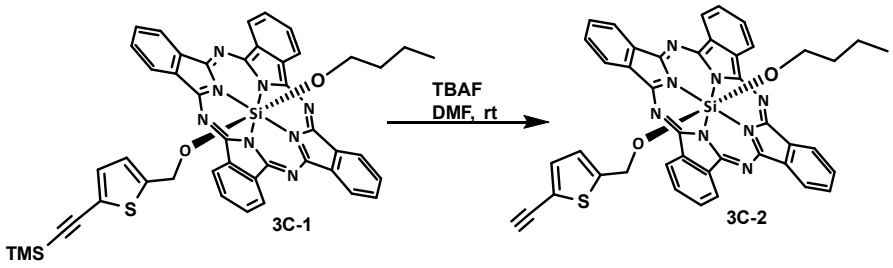

Scheme 3.4: Deprotection of **3C-1** with TBAF to yield **3C-2**.

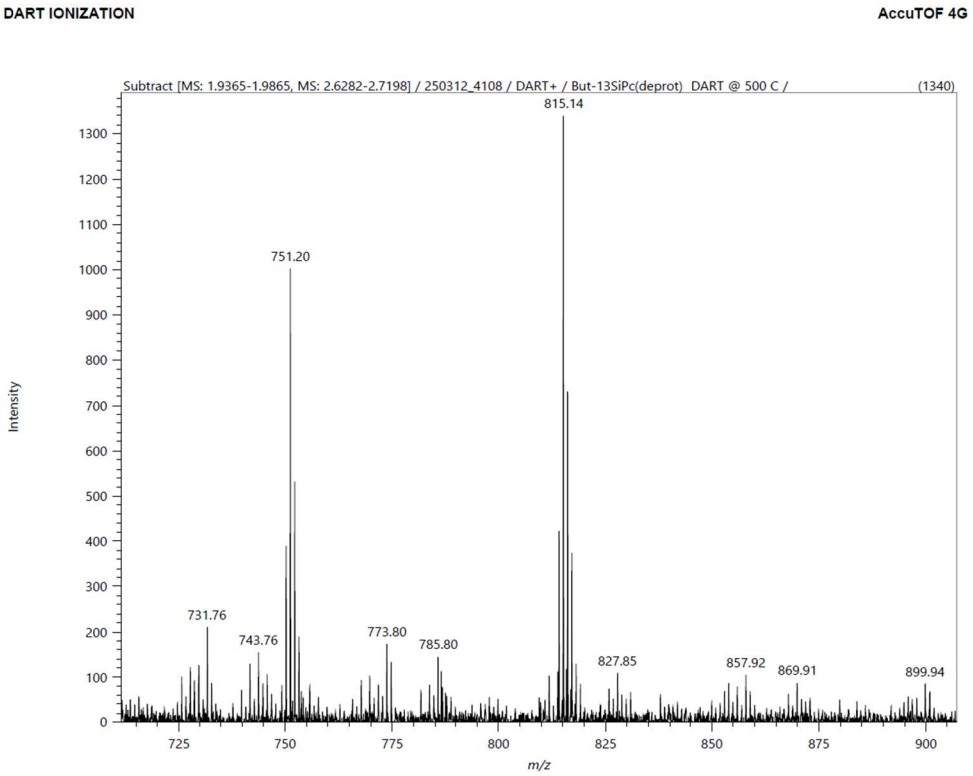

Figure 3.4: Asymmetrical **3C-2** HRMS with DART ionization (m/z = 751.20), along with peaks corresponding to the symmetrical **3B** derivative (m/z = 815.14).

The idea of using butanol to create an asymmetric derivative was not only to facilitate a lone thienyl-alkyne ligation but also to enhance solubility through the alkyl chain, which was unfortunately not the case as described above. Incorporating alkyl or alkylsilane substituents has been shown to improve the solubility and processability of SiPc in its symmetrical

form.[15,40,41] Based on initial results for the asymmetric **3C-2**, the addition of the singular alkyl unit appears not to introduce enough disruption of stacking to produce a soluble product.

A different route to produce **3C-2** was attempted that alleviates the need to deprotect post-asymmetry synthesis. Interestingly, when reacting **3B (**No TMS**)** and butanol with TEA, the conversion to **3C-2** remained elusive, as shown in **Scheme 3.5a**. Although **3B** has limited solubility, it can be dissolved under reflux in toluene to facilitate the ligand exchange. Whereas starting with **3D** (bis(butoxy) SiPc) and adding **3-3** under the same conditions mentioned above, a slightly soluble **3C-2** with fewer impurities was obtained (see **Scheme 3.5b**). Hexanes, isopropanol, and acetone were used to wash the isolated compound under vacuum filtration before it was dried and collected as a blue powder in a 32% yield. This route allowed for obtaining a material (**3C-2)** that had enhanced solubility. The development of a new soluble substance suggests that the deprotection method was producing other insoluble byproducts in the previous route. Two distinct contaminants were revealed by HPLC examination, despite the ^{1}H NMR suggesting a cleaner product of **3C-2** (see **Figure 3.5**)**.** Additional characterizations using FTIR, HRMS, CV and UV-vis were carried out, all suggesting that **3C-2** was successfully prepared.

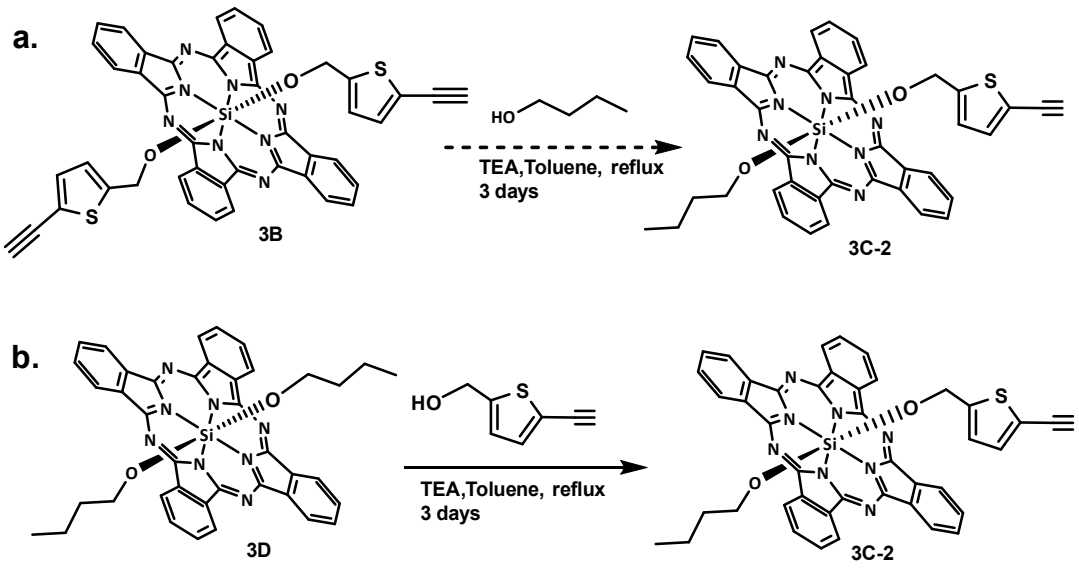

Scheme 3.5: Synthesis of **3C-2** from two different symmetrical SiPcs; a). unsuccessful route using **3B** as a precursor to produce **3C-2**; b). Successful **3C-2** synthesis process after swapping the symmetrical **3B** with **3D**, as a precursor.

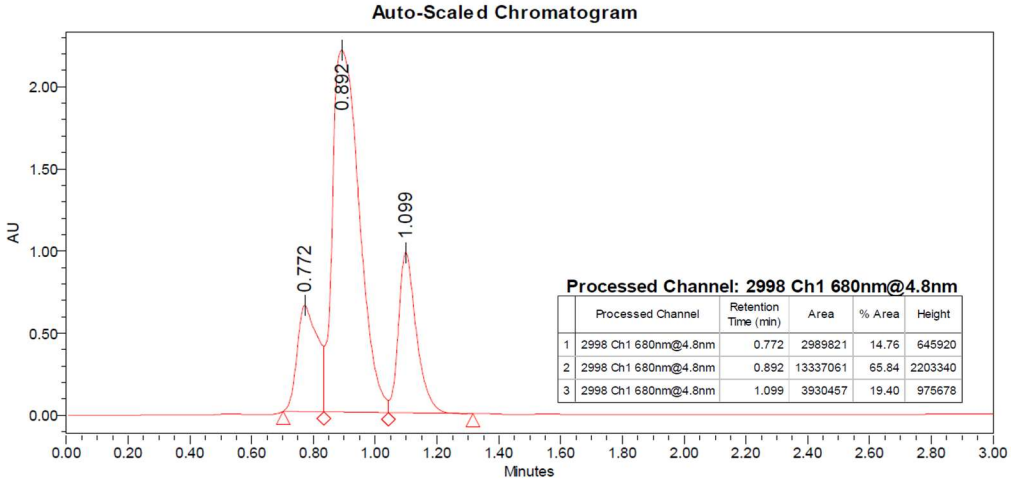

Figure 3.5: Asymmetrical **3C-2** purity analysis on HPLC with DMF as eluent, when t = 0.892 mins (81%), following the elution of an impurity at t = 0.772 and followed by another when t = 1.099 mins. The impurities correspond to the symmetrical groups associated with.

The limited solubility going from **3C-1** to **3C-2** obtained through in-situ deprotection could be attributed to formation of byproducts or increased aggregation resulting from the rapid

deprotection process. The rapid fluoride assisted cleavage with TBAF might lead to the formation of insoluble byproducts, including Si–F species or cause a mixture of partially deprotected derivatives and their precipitation out. Aggregation is suggested to be dependent on the concentration, solvent, and temperature;[42] based on this, the limited solubility observed for **3C-2** could be explained due to the fast conversion from **3C-1** to **3C-2**, ultimately increasing the concentration of **3C-2**. In contrast, the ligand-exchange route (stating with **3D** and **3-3**) operates under milder, slower reaction rate, and elevated temperature to produce **3C-2**, producing a product with fewer contaminants, and reduced aggregation, ultimately leading to a more soluble material (**3C-2**).

3.2.8 Optical Characteristics

The optical characteristics of **3C-2** indicate that the removal of the secondary thiophene group does not alter the photochemical properties of the SiPcs; the photophysical features of the initial symmetrical starting material were still preserved upon substitution with the alkyl chain (see **Figure 3.6**).The butoxy group does not participate in the SiPc's π system, whereas the thiophene has a conjugated system that has minimal influence on it. In contrast, the asymmetrical group (**3C-2**) is far more soluble than the symmetrical derivative (**3B**), which was only slightly soluble. Even while the simple chain in this instance does not contribute to the optical properties, it does demonstrate that alternative alkyl chains or more electronically active groups could be introduced and potentially impact the optical properties.

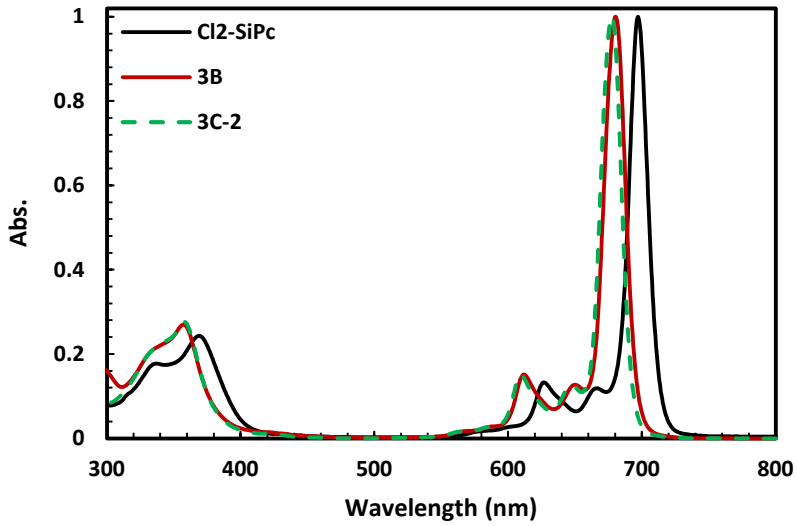

Figure 3.6: Normalized absorbance spectra of **3B**(red), **3C-2** (green), and **Cl_2-SiPc** (black) in chlorobenzene solutions.

3.3 APPLICATIONS

The silicon phthalocyanine-thiophene derivatives were synthesized to be integrated as organic semiconductors in organic thin-film transistors (OTFTs). Additionally, an alkyne group was incorporated to provide a reactive site for an alkyne-azide click reaction with a polymer containing azide functional groups. The objective was to produce a readily accessible terminal alkyne chain, which was achieved through the synthesis of compound **3B**. However, **3B** demonstrated poor solubility and could not be sublimed, limiting its application in OTFTs and hindering the click reaction in solution. Initial device fabrication using **3B** was unsuccessful due to its limited solubility in the chloroform and chlorobenzene solvents intended for spin coating.

Although the goal was to obtain a readily available terminal alkyne, the inclusion of a TMS group on the alkyne enhanced its solubility, as seen for compound **3A**, which can facilitate the spin coating process. It is important to note that the addition of the TMS group could lead to variations in device performance compared to the unmodified alkyne. Nevertheless, the click

reaction after sample deposition remains feasible, either through steric hindrance-influenced triazole formation or by removing the TMS group after deposition and followed by performing the click reaction via thermal or photo-activated methods.[43–49] The synthesis of **3A** effectively addressed the solubility issue, making the thienyl-SiPc suitable for OTFT applications and paving the way for future device fabrication.

To achieve a click reaction with a polymer, having a symmetric structure can hinder functionality by causing the polymer to fold over and react with both alkyne sites. This could lead to cross-linking, which may impair device performance. Since both compounds **3A** and **3B** are symmetric, this concern is a possibility. However, introducing asymmetry on the axial position should reduce potential cross-linking and improve solubility.

Compound **3C-2** includes a butoxy group and thienylmethoxy axial substitution on either side of the SiPc plane. The addition of the butoxy chain increased the solubility of the deprotected alkyne derivative. The solubilities of the three compounds are ranked as follows: **3A** > **3C-2** > **3B**. The intermediate solubility of **3C-2** allows for further characterization, potential for spin-coat processing, and provides a method to control the intentional polymer-semiconductor attachment for future device fabrication.

3.4 CONCLUSION

The synthesis of symmetric SiPc derivatives **3A** and **3B** underscores the crucial role of solubility introduced through axial substitution. Although the TMS group was initially employed to enhance the stability and protect the terminal alkyne, its attachment ultimately served as a valuable strategy for managing solubility and enabling further characterization. Optoelectronic

analysis of **3A** revealed that the thienyl moieties have minimal contribution to the overall optoelectronic behaviour of the compounds.

Initial attempts to synthesize a mono-thienyl substituted SiPc were met with challenges, as ^{1}H NMR analysis suggested a preference for di-substitution. Nonetheless, by utilizing an excess of **3-3**, TEA, and extending the reaction time, the asymmetrical derivative **3C-2** was successfully synthesized from the symmetrical **3D**. The introduction of asymmetry into the structure allows for the manipulation of solubility, as demonstrated by the properties of **3C-2**. Additionally, the asymmetry synthesis demonstrated that the axial position could serve as a chemical handle without disrupting the electrochemical and photochemical performance.

Overall, this study demonstrated (i) TMS protection of terminal alkynes is essential not only for synthetic stability but also for achieving usable solubility; (ii) asymmetric axial substitution is an effective strategy for improving solubility; (iii) axial thiophene ligands remain electronically decoupled from the SiPc macrocycle, acting as functional handles rather than active electronic contributors. These findings establish a practical pathway for incorporating reactive axial ligands into SiPcs while preserving optoelectronic properties, enabling future development of click-functionalized phthalocyanine based materials for organic electronic applications. Thus, based on the concluding findings of these derivatives, future work should be applying **3A** and **3C-2** in devices, as well as utilizing both symmetrical and asymmetrical groups in click reactions.

3.5 EXPERIMENTAL

3.5.1 Material

All materials purchased were used as received. 5-bromothiophene-2-carboxaldehyde, trimethylsilane acetylene were purchased from Ambeed. Silicon tetrachloride ($SiCl_4$) (99%), 1-butanol, reagentplus, 99.9%, $NaBH_4$ (98%), and triethylamine(TEA) were purchased from Sigma-Aldrich Chemical Company. Cl_2-SiPc was synthesized according to **Chapter 2**

3.5.2 Synthesis of 5-Trimethylsilylethynylthiophene-2-carbaldehyde (3-1)

Adapted from literature precedent,[24] to a dry flask, 30 mg (1%) [$Pd(P(C_6H_5)_3)_4$] and 10 mg (1%) copper iodide (CuI) were dissolved in 10 ml of THF, followed by the addition of 0.30 ml of 5-bromothiophene-2-carboxaldehyde (2.61 mmol, 1.0eq.) and 10 ml triethylamine. The reaction was left to mix for 10 minutes under atmospheric conditions before adding 0.4 ml trimethylsilane acetylene (2.80 mmol, 1.1eq.). The mixture was left to stir for 12 hours at room temperature in the dark. Reaction completion was confirmed via TLC and ^{1}H NMR, then the solution was filtered through Celite and concentrated. The organic layer was extracted using dichloromethane and dried over magnesium sulphate. Further purification was achieved using silica gel chromatography with 5 % ethyl acetate in hexanes. An off-white solid was collected with 85% yield. ^{1}H NMR (400 MHz, $CDCl_3$) δ 9.83 (s, 1H), 7.60 (d, J = 4.0 Hz, 1H), 7.24-7.23 (d, J = 4.0 Hz,1H), 0.23 (s, 9H). ^{13}C NMR (101 MHz, $CDCl_3$) δ 182.44, 143.84, 135.74, 133.13, 132.59, 104.67, 96.40.

3.5.3 Synthesis of 5-[2-(Trimethylsilyl)ethynyl]-2-thiophenemethanol (3-2)

To a dry flask in an ice bath, 0.160 g of **3-1** (1.0 mmol, 1.0 eq) was added to 10 ml of ethanol, followed by 0.024 g $NaBH_3$ (6.5 mmol, 6.5 eq) under nitrogen adapting precedent

literature[50]. The reaction was monitored for completion for over an hour using TLC. Upon completion, 2N HCl was added to the solution until a pH of ~3 was reached. After 10 minutes, saturated $NaHCO_3$ was added to the mixture until a pH of ~7 was reached. The mixture was extracted using 100 mL of ethyl acetate, followed by three washes with water and dried using $MgSO_4$. Upon concentration, 5-[2-(Trimethylsilyl)ethynyl]-2-thiophenemethanol (**3-2**) was collected as a yellow oil with a 77% yield. ^{1}H NMR (600 MHz, $CDCl_3$) δ 7.07 (d, J = 3.7 Hz, 1H), 6.82 (d, J = 3.7 Hz, 1H), 4.76 (dd, J = 6.2, 0.8 Hz, 2H), 0.22 (d, J = 0.6 Hz, 9H).

3.5.4 Synthesis of 5-ethnyl-2-thiophenemethanol (3-3)

Adapted from literature precedent,[25] 0.368 g of 5-trimethylsilylethynylthiophene-2-carbaldehyde (2.0 mmol, 1.0 eq.) was reacted overnight with 0.024 g of K_2CO_3 (0.174 mmol) in methanol. Upon consumption of the starting material, the organic layer was extracted with ethyl acetate and concentrated under vacuum, yielding 0.107 g of 5-ethnylthiophene-2-carbaldehyde (73%) as a dark oil. 5-ethnylthiophene-2-carbaldehyde was then reduced analogously to **3-2** to yield **3-3**. The concentrated extract yielded a dark brown oil (92%, 0.094 g). ^{1}H NMR (600 MHz, $CDCl_3$) δ 7.13 (d, J = 3.6 Hz, 1H), 6.84 (dd, J = 3.6, 0.9 Hz, 1H), 4.78 (d, J = 6.0 Hz, 2H), 3.32 (s, 1H).

3.5.5 Synthesis of Bis(5-[2-(trimethylsilyl)ethynyl]-2-thienylmethoxy) silicon phthalocyanine (3A)

3A was synthesized by mixing 790 mg (3.76 mmol, 4.0 eq.) of **3-2** and 574 mg (0.94 mmol, 1.0 eq.) of Cl_2-SiPc in 95 ml of toluene and 3ml of triethylamine. The mixture was refluxed over a period of 48 hrs. A successive addition of **3-2** after the 12, 24, and 36 hours was done to push the di-substitution. Upon cooling to RT, the mixture was diluted with 300 ml of hexanes and set aside for 30 minutes to precipitate out. The hexanes mixture was vacuum

filtered, followed by successive washes with methanol, ether, and acetone. Finally, the solid was dissolved in dichloromethane and gravity filtered to remove any unreacted Cl_2-SiPc and other insoluble impurities. The DCM solution was rotovap dried, and a blue/teal powder was collected (682 mg, 76%). ^{1}H NMR (400 MHz, $CDCl_3$) δ 9.62 (dd, J = 5.6, 3.0 Hz, 8H), 8.34 (dd, J = 5.8, 2.9 Hz, 8H), 5.97 (d, J = 3.7 Hz, 2H), 4.27 (d, J = 3.7 Hz, 2H), 0.06 (s, 18H), -0.68 (s, 4H). FTIR: C-H (3043-2850 cm^{-1}) and C-C (2158 cm^{-1}). HRMS:[C_{52} H_{42} $N_8O_2Si_3S_2$], mass: 958.21773, calculated: 958.21745.

3.5.6 Synthesis of Bis(5-ethynyl-2-thienylmethoxy) silicon phthalocyanine (3B)

3B was synthesized in two ways. **Route 1:** followed a similar synthetic procedure to **3A**, but using **3-3** (0.190g, 1.38 mmol, 5.4 eq.) and 0.165 g of Cl_2-SiPc (0.26 mmol, 1.0 eq). The final product was vacuum-dried and washed with methanol and acetone to collect a blue powder (0.110 g, 52 %). **Route 2**: **3A** was reacted with 2 equivalents of TBAF to remove the TMS groups in DMF at room temperature. After one hour, reaction completion was suggested by the precipitation of the title compound. The mixture was vacuum filtered; the collected solid was treated to two successive washes with methanol and acetone, then left to dry under vacuum. The dry material was collected as a blue powder with 84% yield. λ_{max}: 680 nm. FTIR: C-H (3243 cm^{-1}) and C-C (2158 cm^{-1}).

3.5.7 Synthesis of Bis(butoxy) silicon phthalocyanine (3D)

3D was synthesized similarly to **3A** with 0.20 g (0.38 mmol, 0.20 eq.) of Cl_2-SiPc and an excess amount of butanol (2.0 ml). The resulting mixture was poured into 300 mL of isopropanol and left to precipitate out. A shiny purple powder was collected after vacuum filtration and drying in 61% yield (0.137 g). ^{1}H NMR (400 MHz, $CDCl_3$) δ 9.62 (dd, J = 5.7, 3.0 Hz, 8H), 8.31 (dd, J = 5.7, 2.9 Hz, 8H), -0.69 (t, J = 7.4 Hz, 6H), -1.37 (h, J = 7.4 Hz, 4H), -1.68 – -1.82 (m,

4H), -2.14 (t, J = 6.3 Hz, 4H). ^{13}C NMR (101 MHz, $CDCl_3$) δ 149.24, 136.12, 130.68, 123.61, 54.51, 31.39, 16.76, 12.27.

3.5.8 Synthesis of [Si, Si] Bis(butoxy, 5-ethynyl-2-thienylmethoxy) silicon phthalocyanine (3C-2)

3C-2 was synthesized by using 200 mg of **3A** (0.209 mmol, 1.0 eq) and 3 mL of 1-butanol in toluene and refluxed for 72 hours with the addition of TEA as a base. The solution is then precipitated out using hexanes. Further purification was done using silica gel chromatography by using DCM as an eluent, with a final yield of 33%. ^{1}H NMR (400 MHz, $CDCl_3$) δ 9.62 (dd, J = 5.6, 3.0 Hz, 8H), 8.33 (dd, J = 5.8, 2.9 Hz, 8H), 5.99 (d, J = 3.7 Hz, 1H), 4.32 (d, J = 3.8 Hz, 1H), 2.89 (s, 1H), -0.70 (dd, J = 14.0, 6.6 Hz, 5H), -1.36 (q, J = 7.4 Hz, 2H), -1.72 (t, J = 7.4 Hz, 2H), -2.10 (t, J = 6.4 Hz, 2H). FTIR: C-H (3243 cm^{-1}), C-H (3043-2850 cm^{-1}) and C-C (2158 cm^{-1}). HRMS:[$C_{43}H_{31}N_8O_2SiS$], mass: 751.20453, calculated: 751.20545.

3.5.9 Optical characterization

UV-vis-NIR spectra were collected using an Agilent Technologies Cary 6000*i* UV-Vis-NIR spectrophotometer. The samples were dissolved with chlorobenzene and filtered through a 0.45 μm pore PTFE syringe filter prior to the collection of the spectra. UV-vis-NIR measurements were collected at room temperature within the range of 250-800 nm.

3.5.10 Electrochemical characterization

Cyclic voltammetry was performed using a Bioanalytical Systems Inc. (BASi) Epsilon potentiostat with C3 cell stand, a glass cell and recorded using BASi Epsilon EC software (V 2.13.77 (c) 2013BASi). Platinum wires were used for the working, counter and reference electrodes. The measurements were performed at a 1 mg/mL solution in anhydrous DCM under argon, using 0.1 M tetrabutylammonium hexafluorophosphate (Aldrich) as the supporting

electrolyte, with a scan rate of 100 mV s^{-1}. The solutions were filtered through a 0.45 μm pore PTFE syringe filter prior to measurements. All measurements were referenced to the Fc/Fc^{+} redox couple (+0.48 V *vs.* SCE) as an internal standard. Oxidation and reduction of half potentials were determined using the anodic and cathodic peak potentials, respectively.

3.5.11 Thermogravimetric analysis

TGA analyses were performed in a 100 mL DTGA/Q5000 IR Platinum Pan using a discovery 5500 equipment from TA Instruments under nitrogen atmosphere, at a 20 °C/ min heating rate. Samples were heated up to 700 °C and the decomposition temperature (Td) was determined at 5 % weight loss.

3.5.12 High performance liquid chromatography analysis

HPLC analysis was conducted on Waters e2695 Separations Module using a Symmetry C18 column as a stationary phase with a 2998 PDA Detector. The samples were dissolved in DMF and filtered through a 0.45 μm pore PTFE syringe filter prior to transferring the solutions into the autosampler vials. The instrument method was set to a flow rate of 1 mL/min at 25 °C, and sample set method was set to 20 μL injection volume for run times ranging between 3 – 5 minutes at a wavelength of 680 nm in the Empower® 3 software. Lastly, the Empower® 3 software was employed to integrate peaks and process data.

3.6 SUPPORTING INFORMATION

Characterization of 3A

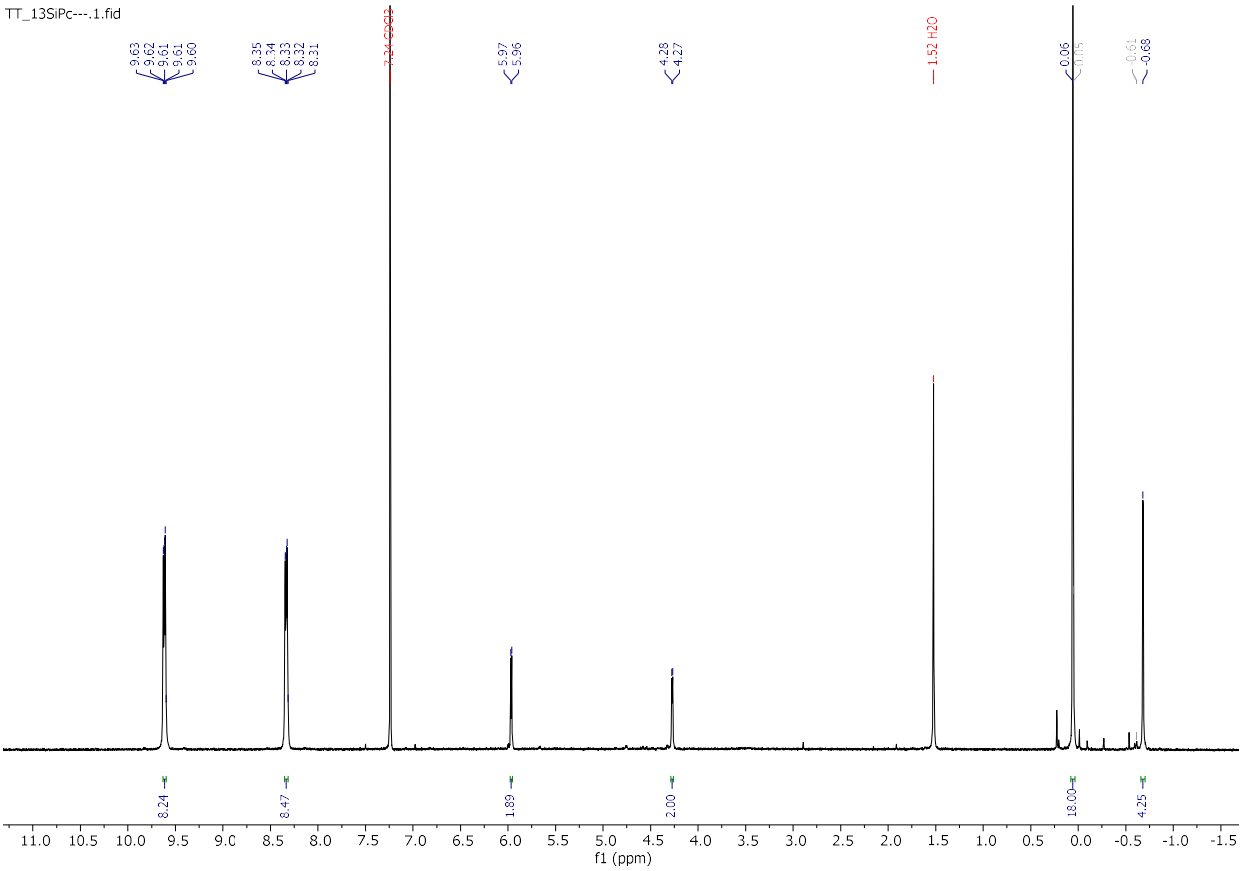

Figure S3.1: ^{1}H NMR of **3A** in chloroform.

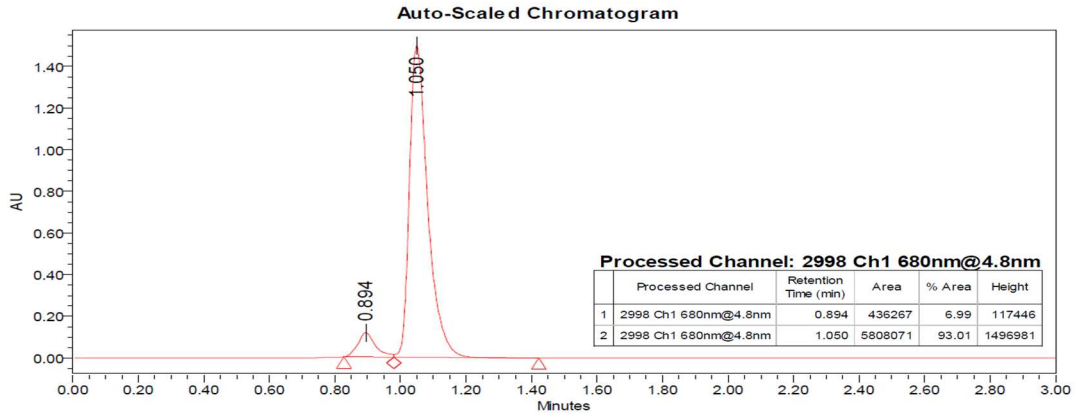

Figure S3.2: Symmetrical 3A purity analysis on HPLC in DMF solvent (93.01%) eluted when t = 1.050 mins, after the elution, 7% impurity at t= 0.894

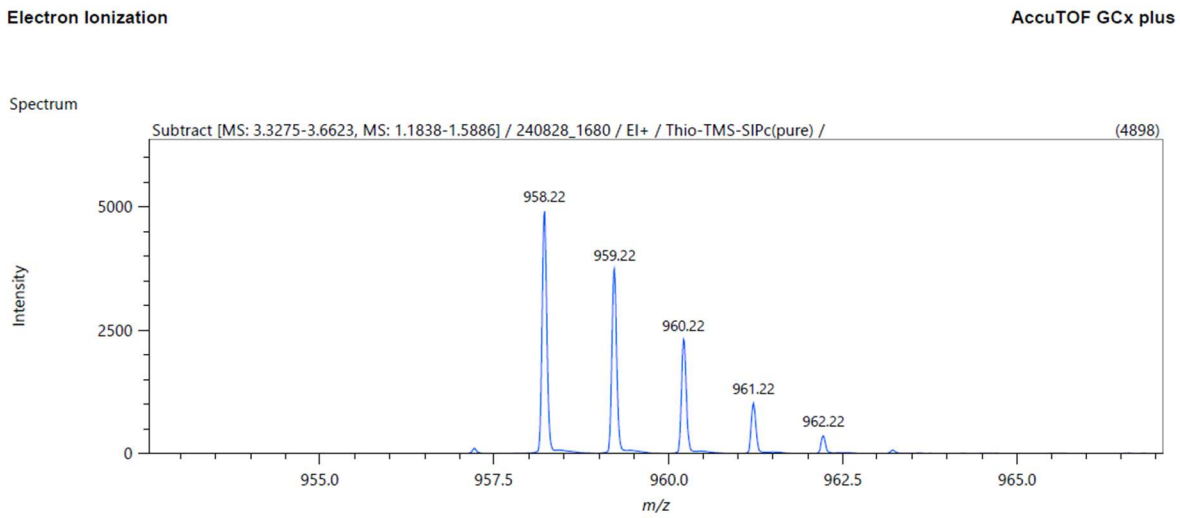

Figure S3.3: Symmetrical **3A** HRMS with electron ionization (m/z=959.22)

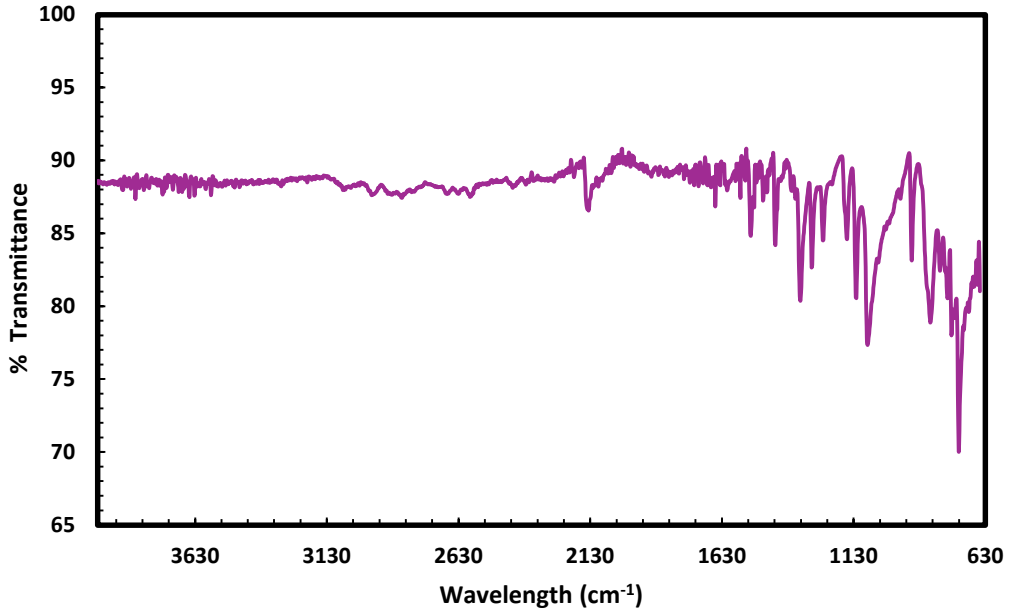

Figure S3.4: FTIR of **3A,** C-C peaks at 2158 cm^{-1}.

Characterization of 3D

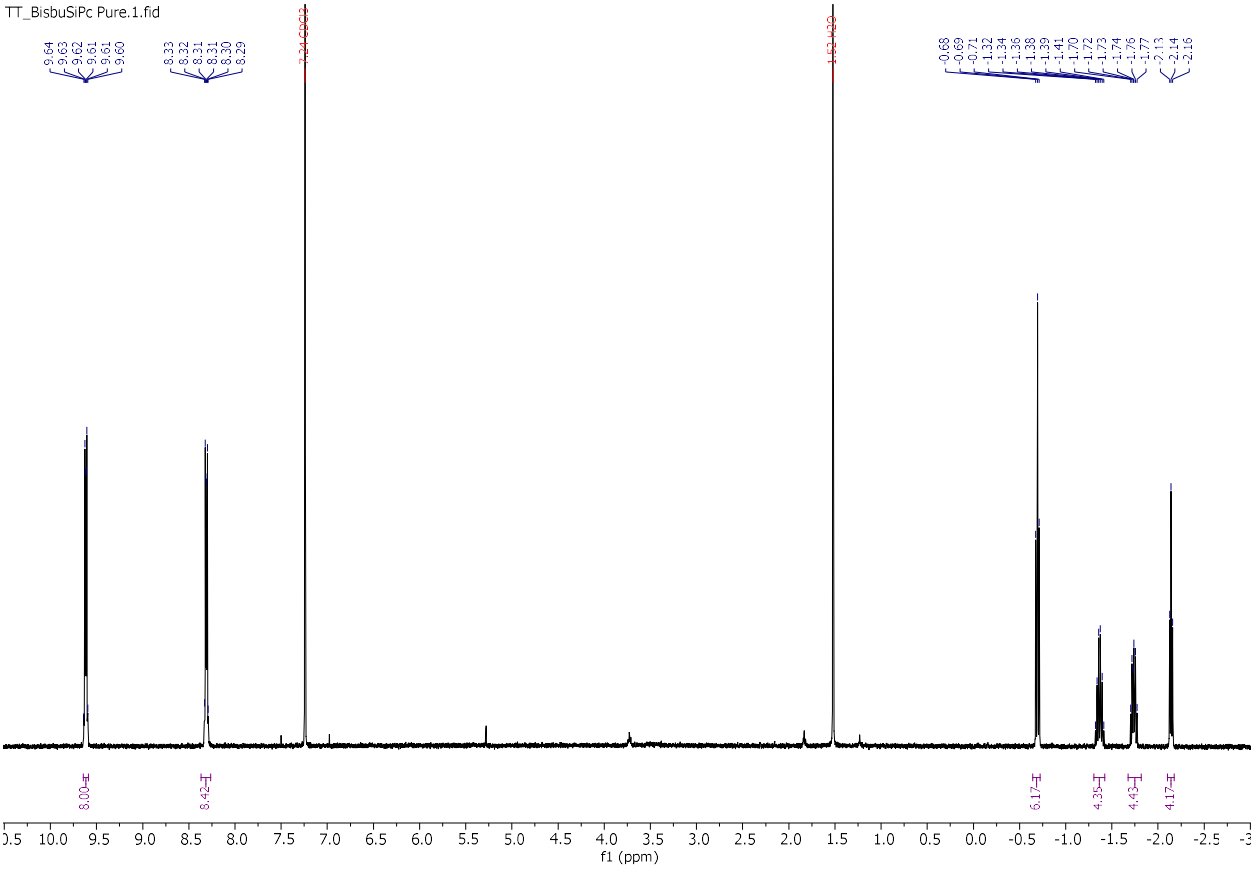

Figure S3.5: ^{1}H NMR of 3D in chloroform.

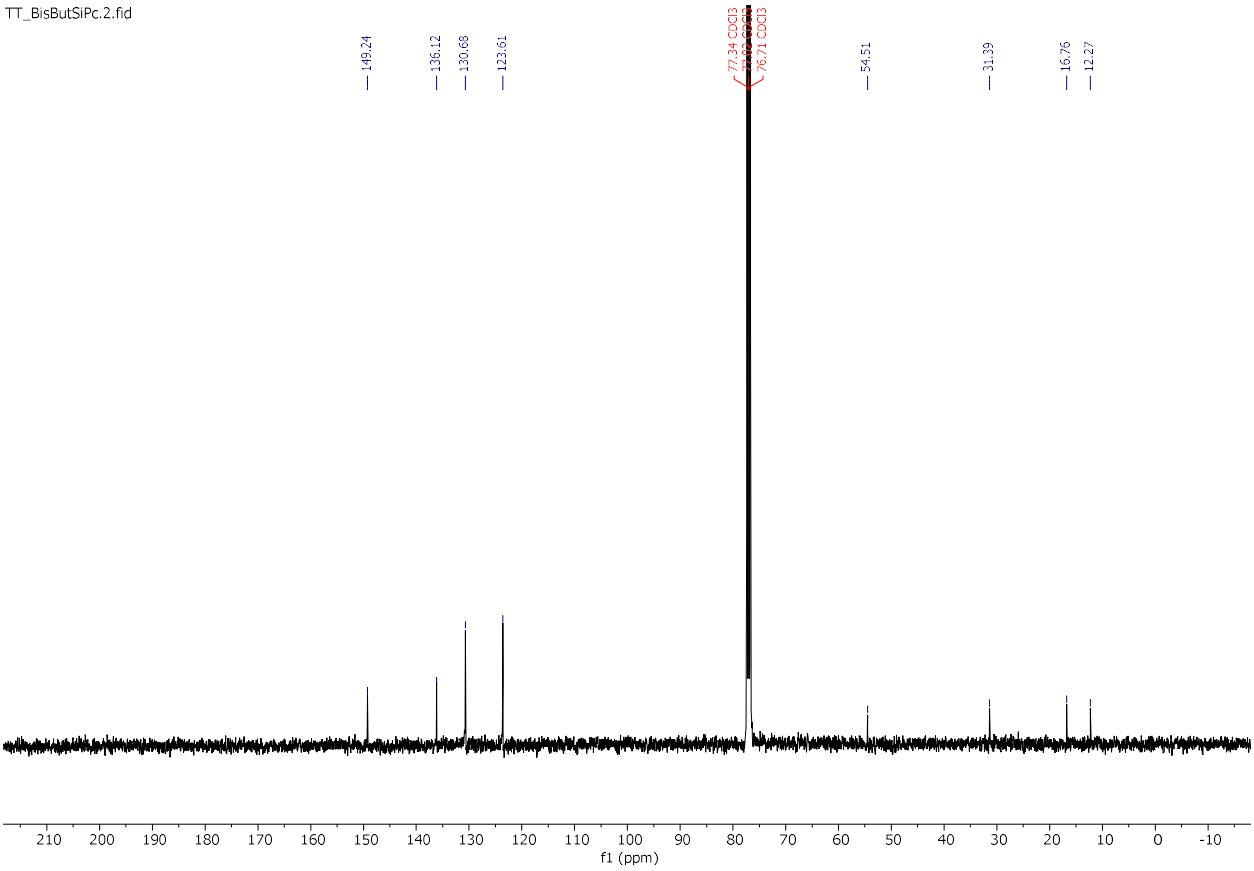

Figure S3.6: ^{13}C NMR of **3D** in chloroform.

Characterization of 3B

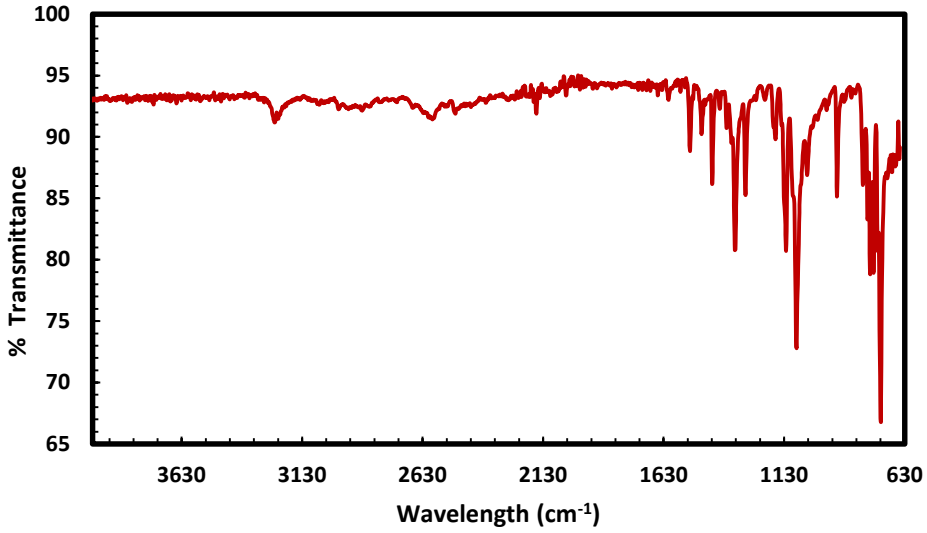

Figure S3.7: FTIR of **3B**, C-H stretches at 3243 cm^{-1} and C-C peaks at 2158 cm^{-1}.

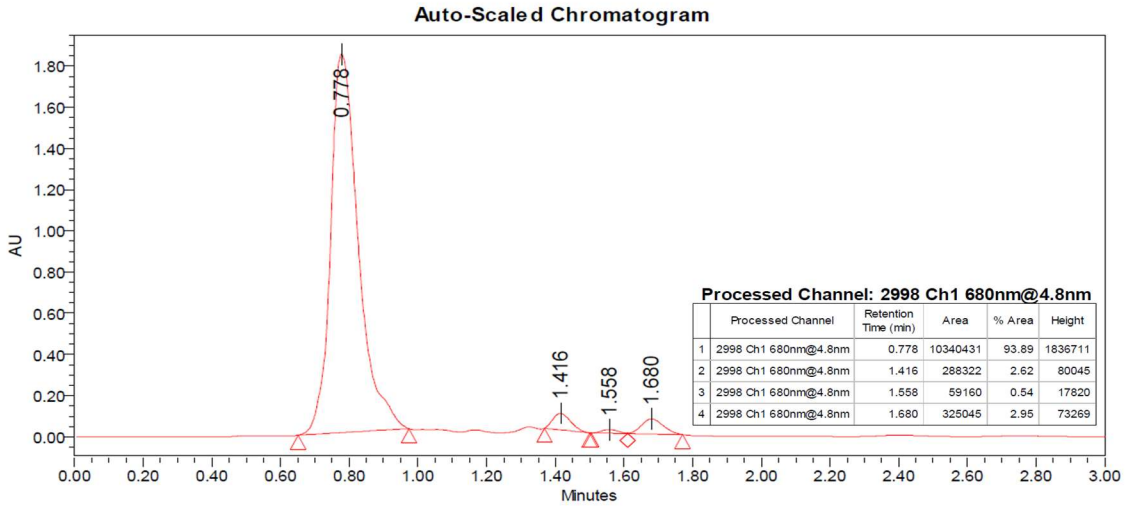

Figure S3.8: Symmetrical **3B** purity analysis on HPLC in DMF solvent: first peak appearing at 0.778 mins (94%), followed by minor impurities at minutes 1.416, 1558, 1.680.

Characterization of 3C-2

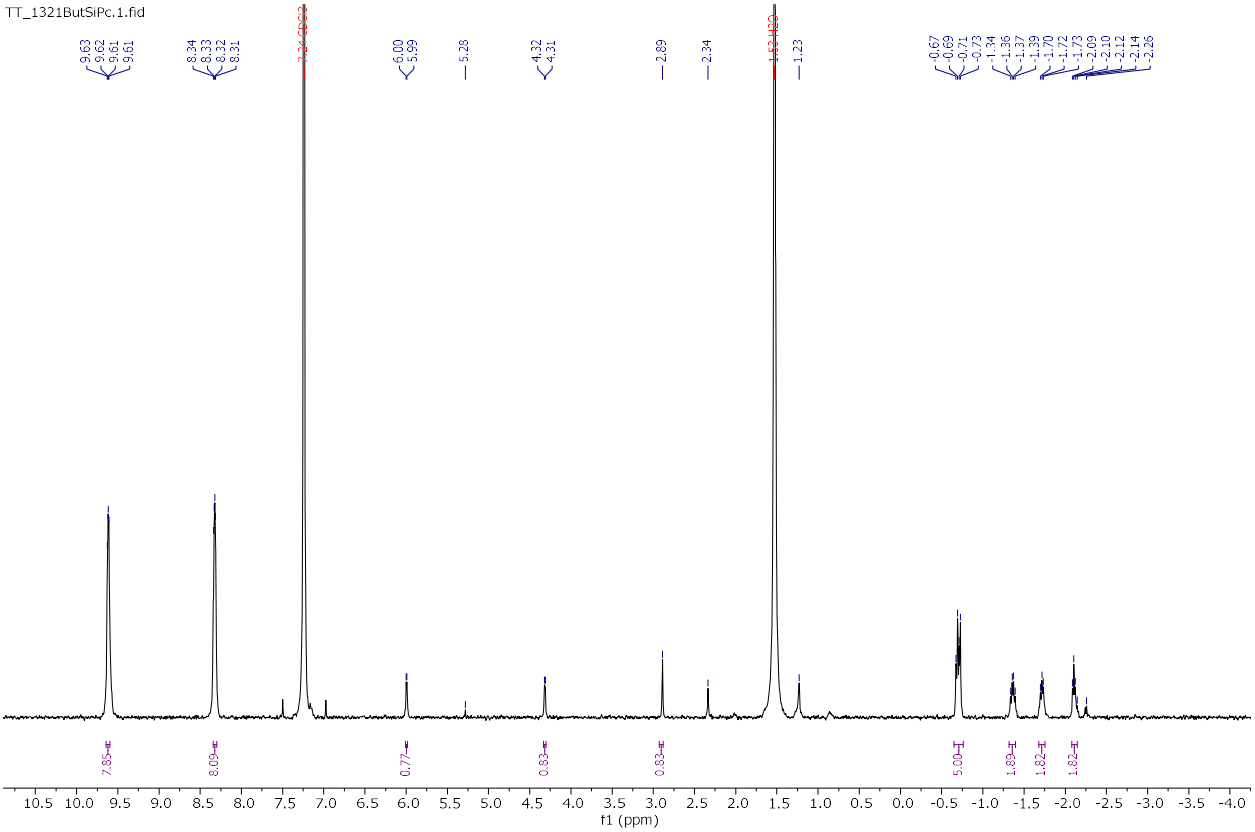

Figure S3.9: ^{1}H NMR of **3C-2** in chloroform.

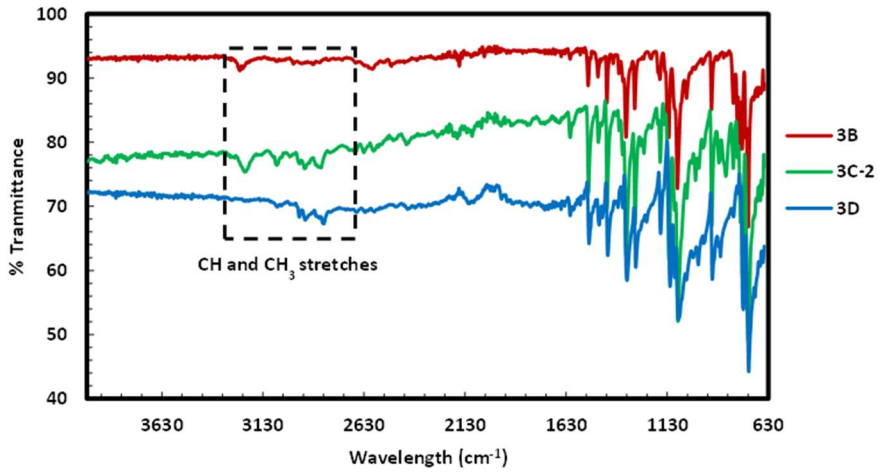

Figure S3.10: Asymmetrical **3C-2** FTIR, with symmetrical analogs **3D** and **3B**. The black box shows the combined features of **3B** and **3D** on **3C-2.**

3.7 REFERENCES

1. Turkoglu G, Cinar ME and Ozturk T. *Top Curr Chem (Z)* 2017; **375**: 84.
2. Ali R and Siddiqui R. *RSC Advances* 2022; **12**: 36073-36102.
3. Elizabeth George S. *IJSR* 2024; **13**: 1293-1295.
4. Zhang F, Wu D, Xu Y and Feng X. *J. Mater. Chem.* 2011; **21**: 17590-17600.
5. Zhang C and Zhu X. *Acc. Chem. Res.* 2017; **50**: 1342-1350.
6. Altınışık S, Özdemir M, Kortun A, Zorlu Y, Yalçın B, Köksoy B and Koyuncu S. *ACS Omega* December 2023: acsomega.3c05602.
7. Li L, Li J, Guo L, Xu Y, Bi Y, Pu Y, Zheng P, Chen X-K, Wang Y and Li C. *Chem. Sci.* 2024; **15**: 11435-11443.
8. Kumagai S, Ishida T, Kakiuchi S, Yamagishi M, Sato H, Ishii H, Nishihara Y and Okamoto T. *Chem. Commun.* 2024; **60**: 11152-11155.
9. Zhang Y, Li R, Chang L, Ma Y, Hou Y and Niu H. *Macromolecular Chemistry and Physics* 2022; **223**: 2100341.
10. Tanaka K, Shichiri T, Wang S and Yamabe T. *Synthetic Metals* 1988; **24**: 203-215.
11. Esen C, Antonietti M and Kumru B. *ChemPhotoChem* 2021; **5**: 857-862.
12. Woods EF, Berl AJ and Kalow JA. *ChemPhotoChem* 2021; **5**: 4-11.
13. Fernandes RS, Shetty NS, Mahesha P and Gaonkar SL. *J Fluoresc* 2022; **32**: 19-56.
14. Thakur N, Kandwal P and Pandey R. *Ind. Eng. Chem. Res.* 2023; **62**: 12864-12879.
15. Lessard BH. *ACS Appl. Mater. Interfaces* 2021; **13**: 31321-31330.
16. Melville OA, Grant TM and Lessard BH. *J. Mater. Chem. C* 2018; **6**: 5482-5488.
17. Mitra K and Hartman MCT. *Org. Biomol. Chem.* 2021; **19**: 1168-1190.
18. Lau JTF, Lo P-C, Tsang Y-M, Fong W-P and Ng DKP. *Chem. Commun.* 2011; **47**: 9657-9659.
19. Li J, Yang Y, Zhang P, Sounik JR and Kenney ME. *Photochem Photobiol Sci* 2014; **13**: 1690-1698.
20. Chen K, Li X, Huang B, Ye Q, Xiao W, Guan X, Chen L and Peng Y. *New J. Chem.* 2021; **45**: 457-462.

21. Barker CA, Findlay KS, Bettington S, Batsanov AS, Perepichka IF, Bryce MR and Beeby A. *Tetrahedron* 2006; **62**: 9433-9439.

22. Farren C, FitzGerald S, R. Bryce M, Beeby A and S. Batsanov A. *Journal of the Chemical Society, Perkin Transactions 2* 2002; **0**: 59-66.

23. Yıldız B, Budak Ö, Koca A and Şener MK. *Dyes and Pigments* 2024; **223**: 111958.

24. Teng C, Yang X, Yang C, Li S, Cheng M, Hagfeldt A and Sun L. ACS Publications.

25. Lu J, Xu X, Cao K, Cui J, Zhang Y, Shen Y, Shi X, Liao L, Cheng Y and Wang M. *J. Mater. Chem. A* 2013; **1**: 10008-10015.

26. Lessard BH, Dang JD, Grant TM, Gao D, Seferos DS and Bender TP. *ACS Appl. Mater. Interfaces* 2014; **6**: 15040-15051.

27. Bıyıklıoğlu Z and Çakır D. *Spectrochimica Acta Part A: Molecular and Biomolecular Spectroscopy* 2012; **98**: 178-182.

28. Biyiklioglu Z, Bas H and Alp H. *Dalton Trans.* 2015; **44**: 14054-14062.

29. Lessard BH, White RT, AL-Amar M, Plint T, Castrucci JS, Josey DS, Lu Z-H and Bender TP. *ACS Appl. Mater. Interfaces* 2015; **7**: 5076-5088.

30. Grant TM, Dindault C, Rice NA, Swaraj S and Lessard BH. *Mater. Adv.* 2021; **2**: 2594-2599.

31. Lessard BH, Grant TM, White R, Thibau E, Lu Z-H and Bender TP. *J. Mater. Chem. A* 2015; **3**: 24512-24524.

32. Lessard BH, White RT, AL-Amar M, Plint T, Castrucci JS, Josey DS, Lu Z-H and Bender TP. *ACS Appl. Mater. Interfaces* 2015; **7**: 5076-5088.

33. Kobak RZU, Arı MU, Tekin A and Gül A. *Chemical Physics* 2015; **448**: 91-97.

34. Pal AK, Varghese S, Cordes DB, Slawin AMZ, Samuel IDW and Zysman-Colman E. *Sci Rep* 2017; **7**: 12282.

35. Palma-Cando A, Brunklaus G and Scherf U. *Macromolecules* 2015; **48**: 6816-6824.

36. Kanibolotsky AL, Findlay NJ and Skabara PJ. *Beilstein J. Org. Chem.* 2015; **11**: 1749-1766.

37. Pohjakallio M, Sundholm G and Talonen P. *Journal of Electroanalytical Chemistry* 1996; **401**: 191-200.

38. Cheng G, Peng X, Hao G, Kennedy VO, Ivanov IN, Knappenberger K, Hill TJ, Rodgers MAJ and Kenney ME. *J. Phys. Chem. A* 2003; **107**: 3503-3514.

39. Lo P-C, Huang J-D, Cheng DYY, Chan EYM, Fong W-P, Ko W-H and Ng DKP. *Chemistry – A European Journal* 2004; **10**: 4831-4838.

40. Solgun DG, Tanriverdi AA, Yildiko U and Ağirtaş MS. *J Incl Phenom Macrocycl Chem* 2022; **102**: 851-860.

41. Vebber MC, Grant TM, Brusso JL and Lessard BH. *Langmuir* 2020; **36**: 2612-2621.

42. Tekin S, Yaglioglu HG, Elmali A, Kürüm U, Yanık H, Tekdaş DA, Durmuş M and Ahsen V. *Materials Chemistry and Physics* 2013; **138**: 270-276.

43. Li H, Wang J, Zhi Sun J, Hu R, Qin A and Zhong Tang B. *Polymer Chemistry* 2012; **3**: 1075-1083.

44. Cetin M, Esen C, Daglar O, Luleburgaz S, Hizal G, Durmaz H and Tunca U. *Polym. Chem.* 2016; **7**: 7094-7100.

45. Chen RT, Marchesan S, Evans RA, Styan KE, Such GK, Postma A, McLean KM, Muir BW and Caruso F. *Biomacromolecules* 2012; **13**: 889-895.

46. Li H, Li L, Wu H, Lam JWY, Sun JZ, Qin A and Tang BZ. *Polym. Chem.* 2013; **4**: 5537-5541.

47. Li S-X, Feng L-R, Guo X-J and Zhang Q. *J. Mater. Chem. C* 2014; **2**: 3517-3520.

48. Canalle LA, van Berkel SS, de Haan LT and van Hest JCM. *Advanced Functional Materials* 2009; **19**: 3464-3470.

49. Gonzaga F, Yu G and Brook MA. *Macromolecules* 2009; **42**: 9220-9224.

50. Zhao J, Huang L, Cui X, Li S and Wu H. *J. Mater. Chem. B* 2015; **3**: 9194-9211.

CHAPTER 4: EXPLORING THE SYNTHESIS OF ASYMMETRIC SILICON PHTHALOCYANINE USING A SERIES OF AXIAL MOIETIES

Context

Like the objectives outlined in the previous chapters, this work focused on the synthesis of silicon phthalocyanines (SiPc) with axial chemical diversity suitable for click reactions. The incorporation of asymmetrical units bearing clickable functionalities proved challenging, prompting a deeper investigation into the reaction pathways leading to these derivatives. To address these challenges, reactions that were unsuccessful in **Chapters 2** and **3** were reassessed, and new chemical moieties were introduced to identify trends in reactivity. To facilitate successful RR′–SiPc synthesis, this project assessed the reactivity of different axial ligands as efficient precursors. To support the findings of newly synthesized compounds, asymmetric SiPc derivatives that were previously isolated are revisited in this chapter, as well as other RR′–SiPcs that have been reported in literature.

Contribution

All content in the chapter was carried out and interpreted by me.

Abstract

Asymmetrically functionalized silicon phthalocyanines (RR′-SiPcs) can be tailored to adjust solubility, axial reactivity, and electrical properties of the resulting material, yet their synthesis is often non-trivial. Using electronically different alcohols, silanes, phenols, and polyfluorinated phenoxy reagents, how steric hindrance, acidity, and solubility affect substitution was examined. Most reactions with bulky or weakly acidic substituents simply recovered the

starting materials, with no sign of reactivity. Polyfluorinated phenols, on the other hand, yielded products in up to 78% and consistently provided the desired RR'-SiPc species across various SiPc starting platforms, including thienyl, siloxy, and alkoxy substituted systems. Upon electrochemical evaluation, anodically shifted reduction potentials and the appearance of new redox processes were linked to RR′-SiPcs synthesis. Additionally, UV-vis-NIR spectroscopy revealed slight bathochromic shifts in absorption profiles when compared to the parent R_2-SiPcs. Overall, these findings suggest the size and acidity of the axial moieties are key factors influencing selective mono-displacement reactivity and offer a useful foundation for creating asymmetrical SiPcs with adjustable solubility and electrical properties.

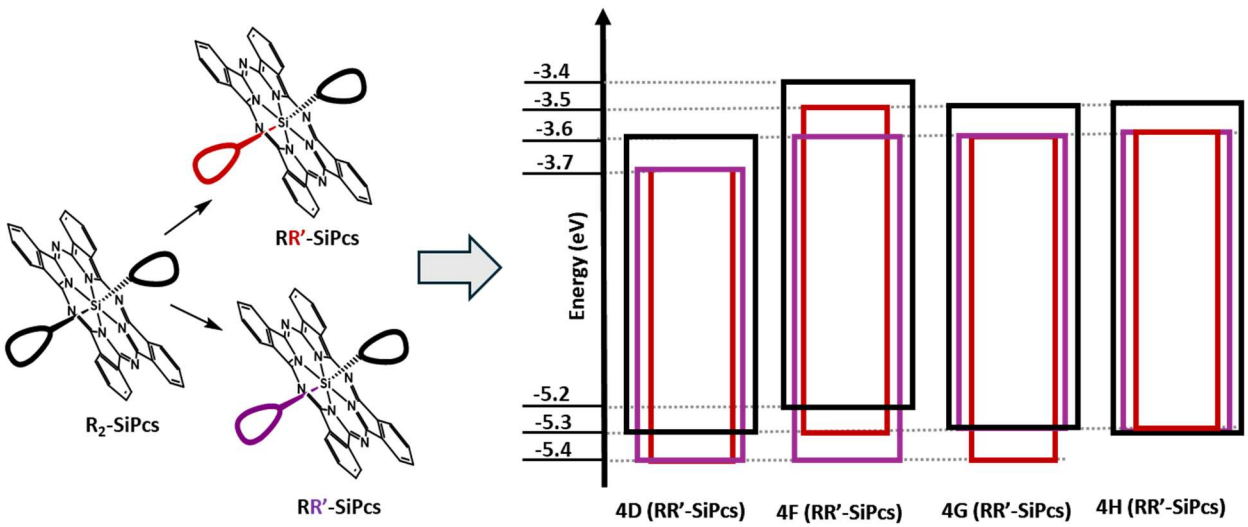

4.1 INTRODUCTION

Axially substituted silicon phthalocyanines (SiPcs) have been used in various applications, such as organic electronics[1–4] and photodynamic therapies.[5,6] In many cases, substitution occurs via nucleophilic displacement of either a chlorine (Cl_2-SiPc) or a hydroxy ($(OH)_2$-SiPc)

moiety. Note that both the Cl_2-SiPc and $(OH)_2$-SiPc starting materials typically exhibit poor solubility[7–9] and thus have limited applications. Substitution at the axial position tends to improve solubility and limit aggregation without significantly affecting electro and photochemical properties, extending the possible applications of these compounds.[7,10–12] Substituents such as silanes, alkyls, or bulky polar groups are reported to increase solubility by disrupting the planarity of the SiPc,[8,12–14] although this effect is not universal. Conversely, direct substitution of phenolic acids (such as pentafluorophenoxy or 2,3,5,6-tetrafluorophenoxy) or benzylic acids are suggested to have limited solubilities,[15,16] and as a result, SiPc of these derivatives are often thermally evaporated to fabricate thin films used for electronic devices. However, inclusion of alkyl chains in these groups, like that of 3-pentadecylphenoxy, can improve the solubility;[16,17] consequently, permitting solution-based processibility.[14,18]

Beyond solubility, these substitutions have been credited with improving solid-state packing and interactions with functional groups. The axial units are typically two identical moieties on either side of the SiPc plane (R_2-SiPc), giving each side of the plane a uniform chemical characteristic. Chemical diversification can occur as a result of modifying the chemical properties of axial units.[19,20] Li *et al*. recently refined a specific axial unit of their photodynamic therapy agent, p-hydroxyphenyl propionic acid-substituted SiPc, by using amide condensation to add a target-specific active functional group. They carefully applied the condensation reaction to only one axial unit, allowing each side of the SiPc plane to exhibit different chemical characteristics.[21] Chemical diversification through axial substituent asymmetry (RR′-SiPc) synthesis has been utilized to create functional transistors, where the silicon core is substituted with a fluorine atom on one side and a tri-alkyl silane on the other. In addition to introducing asymmetry within the molecule, the fluorine atom played a significant

role in the self-assembly of the molecules within the thin film during device fabrication.[18] Likewise, Xu *et al*. fabricated ternary blends using RR'-SiPc (where R = tri-n-hexylsilyl oxide, R' = tri-benzylsilyl oxide) ($SiPcBz_6$). In doing so, one substituent was compatible with a donor polymer and the other compatible with an acceptor, which effectively improved the photocurrent generation by 30%.[22] Likewise, in **Chapter 2,** chemical tailoring via click chemistry on the axial substituents of SiPcs and the asymmetry effect on device performance were explored.

Due to the wide-range chemical tunability afforded by asymmetrical silicon phthalocyanines (RR′-SiPc), recent efforts have focused on the synthesis of asymmetrical silicon phthalocyanines (RR′-SiPc), in which each axial position of the SiPc core is substituted with a different group, thereby expanding the scope of chemical functionalization as seen in **Figure 4.1**.[7,21,23–25] Although these asymmetrical derivatives hold promise for tuning the electronic and chemical properties of SiPc, their preparation remains challenging or requires multiple steps. For instance, in a two-part substitution of dichlorosilicon phthalocyanine (Cl_2-SiPc) with bulky alcohols (R) under excess sodium hydride (NaH) conditions, the first substitution produces RO–SiPc–Cl and the second affords RO–SiPc–OR′ (RR′-SiPc) in poor yields (10–14%).[5] Another route is by first preparing the R_2-SiPc, and subjecting it to a lone ligand exchange reaction to obtain the asymmetrical RO–SiPc–OR'.[19] To bypass the inefficiency of double substitution, alternative strategies have employed pre-functionalized asymmetrical precursors such as OH/Cl–SiPc-alkyl, enabling direct access to RR′-SiPcs.[18,25] Despite these synthetic advances, RR′-SiPc remain relatively unexplored in the context of organic electronics. To the best of the author's knowledge, Lessard *et al*. and Xu *et al*. are two groups that have reported having incorporated RR'-SiPc in organic electronics.[18,22]

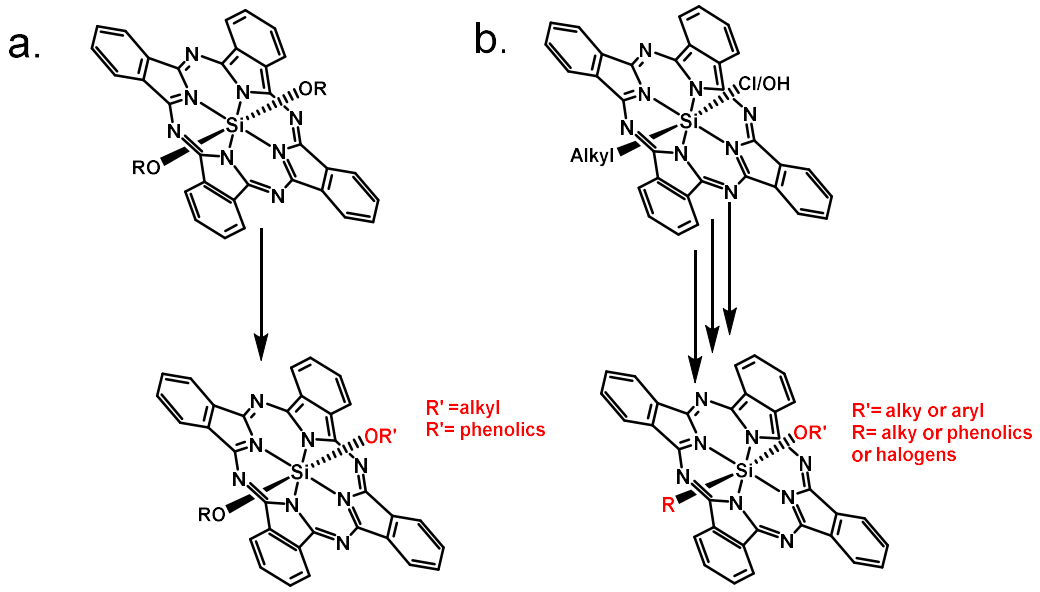

Figure 4.1*:* A representative figure to produce RR'-SiPc from literature. a). a common approach to initiate RR'-SiPc production from phenolics and alkoxy ligands starting from symmetrical R_2-SiPc, whereas b) demonstrates a multistep synthesis process for alkyl and aryl functionalized RR'-SiPcs starting from chloro alkyl SiPcs.

This study explores various synthetic processes for producing functional RR'-SiPc derivatives using R_2-SiPc and chloro methyl SiPc (Cl-SiPcMe) precursors, along with axial moieties previously utilized in the fabrication of organic electronic devices. The research examines the effects of acidity, steric hindrance, and solubility on the success of mono-displacement reactions. Notably, the RR′-SiPc derivatives were successfully synthesized only when the incoming moiety had greater acidity or a smaller molecular size compared to the existing axial ligand. These findings underscore important considerations for the targeted preparation of asymmetrical SiPcs and highlight the roles of axial-group acidity and structural size in guiding selective mono-substitution.

4.2 RESULTS & DISCUSSION

4.2.1 Synthesis of asymmetrical SiPcs (RR'-SiPc) from R_2-SiPc starting materials.

Previous reports have indicated that asymmetrical SiPc (RR′-SiPc) have been employed for various biological applications;[19,20,23,26] however, its use in organic electronics is relatively unexplored. Most RR′-SiPc synthetic routes start from a known symmetrical piece (R_2-SiPc), and another functional group is introduced to obtain the asymmetric analogue RR′-SiPc (R = original unit, R' = new unit). One report suggested obtaining an asymmetrical SiPc derivative from a simple overlayering of a solution of the symmetric bis(1,3-bis(dimethylamino)-2-propoxy) SiPc (**4A**) with methanol to substitute a singular axial moiety with a methoxy group at room temperature; whereas for longer alkyls, the reaction was refluxed to produce RR′-SiPcs.[19] Inspired by this, the incorporation of various chemical moieties to produce RR′-SiPc from R_2-SiPcs as potential organic semiconductors are demonstrated below. As seen in **Scheme 4.1**, **4A** was reacted with an incoming alcohol ligand (R = ((5-[2-(trimethylsilyl) ethynyl]-2-thiophenemethanol or 3-(prop-2-yn-1-yloxy) phenyl methanol, respectively), to lead to products **4A-1** and **4A-2**, which were explored under the reported conditions, where they were refluxed in chloroform for up to 48 hours,[19] followed by solvent and temperature changes (refluxed in toluene); unfortunately, this did not lead to the desired outcomes.

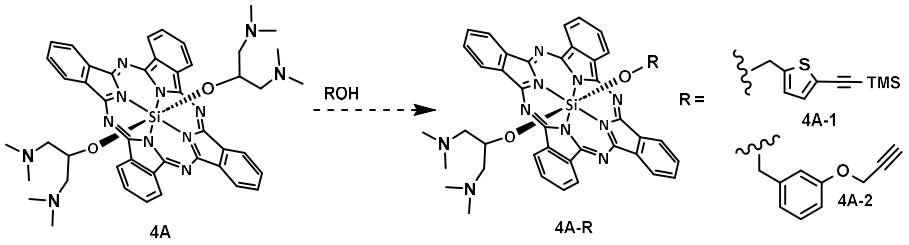

Scheme 4.1*:* Initial approach to synthesize RR′-SiPcs using symmetrical **4A** as a precursor, following literature precedent[19], as well as with increased reaction time, equivalency, temperature, and solvent modification. No RR'-SiPc was produced as indicated by the dashed arrow.

Focus was then shifted to bis(thienylmethoxy) SiPc (**4B**) as a precursor instead, to explore if other chemical properties would lead to the synthesis of RR'-SiPc using the above reagents. Compound **4B** was prepared under an adapted procedure, reacting Cl_2-SiPc with 2-thiophenemethanol.[27] It was found that **4B** has poor solubility in common solvents such as chloroform and dichloromethane (DCM), but is soluble in high-boiling-point solvents such as toluene and chlorobenzene under heat. When **4B** was reacted with 2 to 2.5 equivalents of ROH (where R = (5-[2-(trimethylsilyl)ethynyl]-2-thiophenemethanol or 3-(prop-2-yn-1-yloxy)phenyl methanol), it did not yield the desired RR'-SiPc (**4B-1** or **4B-2**) under reaction conditions (i) and (ii) detailed in **Scheme 4.2**. It is worth noting that while compound **4A** exhibits good solubility, the poor solubility of **4B** is taken into consideration as a possible reason for the shortcomings of these reactions. **Scheme 4.2** explores four different reaction conditions, the forward reaction showing conditions (i) and (ii), where singular axial ligand exchange was induced on **4B**, and reaction conditions (iii) and (iv) explore using soluble R_2-SiPcs, **4C (**where R = 3-(prop-2-yn-1-yloxy)benzyloxy) and **4D (**where R = (5-[2-(trimethylsilyl)ethynyl]-2-thienylmethoxy) with 2-thiophenemethanol as the incoming reagent for the singular displacement. Only when **4C** was reacted under condition (iv) with 2-thiophenemethanol in the presence of a base (i.e., triethylamine; TEA), it produced **4C-2** (R = 3-(prop-2-yn-1-yloxy)benzyloxy and R' = 2-thiophenemethoxy) as detailed in **Chapter 2, Scheme 2.2**. Under similar conditions to **4C-2**, when the asymmetry was pushed using 2-thiophenemethanol and a base on **4D**, no replacement was observed. It is notable that the incoming 2-thiophenemethanol and the axial thienyl unit on **4D** exhibit similar chemical properties.

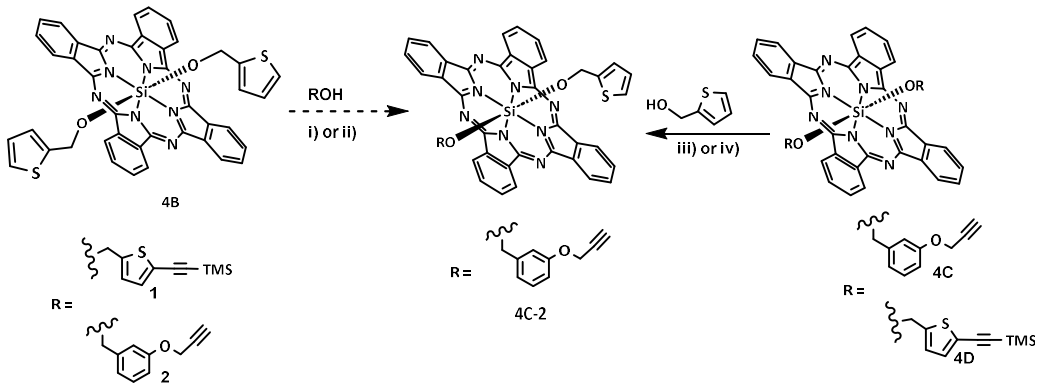

Scheme 4.2: Attempts to synthesize RR′-SiPc from **4B**, **4C** and **4D**. Reaction conditions: i) ROH (where R = 3-(prop-2-yn-1-yloxy)benzyloxy or R = 5-[2-(trimethylsilyl)ethynyl]-2-thienylmethoxy) in 1-2.0 eq. in toluene, reflux for 12-48 hours; ii) ROH (where R = 3-(prop-2-yn-1-yloxy)benzyloxy or R = 5-[2-(trimethylsilyl)ethynyl]-2-thienyl- methoxy) in 2.5 eq. in toluene, reflux for 72 hour; iii) 1-2.0 eq. of 2-thiophenemethanol in toluene, reflux for 12-48 hours; iv) 1-2.0 eq of 2-thiophenemethanol and TEA in toluene, refluxed for 24 hours. Reactions i, ii, and iii did not produce the RR'-SiPcs. Reaction iv produced the RR'-SiPc only when using **4C** as a precursor; the reaction with **4D** remained elusive.

Considering the impact of solubility on the reaction, silanol-substituted SiPcs (**4F** and **4E**), which exhibit excellent solubility in common organic solvents such as chloroform, DCM, and acetone, were chosen as starting reagents to produce RR′-SiPc using the same incoming axial reagents as the above reactions (see **Scheme 4.3**). When employing **4E,** conversion to the RR′-SiPcs was not observed, as both R_2-SiPc precursor and ROH reagents were recovered after reacting them for an extended reaction time, with or without the use of base, as outlined below in **Scheme 4.3**. This may be attributed to the acidity and molecular size of the pentamethyldisiloxanol axial substituent, which is similar to the incoming ROH. To investigate whether the size of pentamethyldisilanol was hindering the nucleophilic substitution, bis(trimethylsiloxy) SiPc (**4F**) was reacted with the same incoming reagents. However, mono-displacement of the axial substituent was not observed once again, despite the trimethylsiloxy being smaller in molecular size and more acidic (see **Scheme 4.3b)**

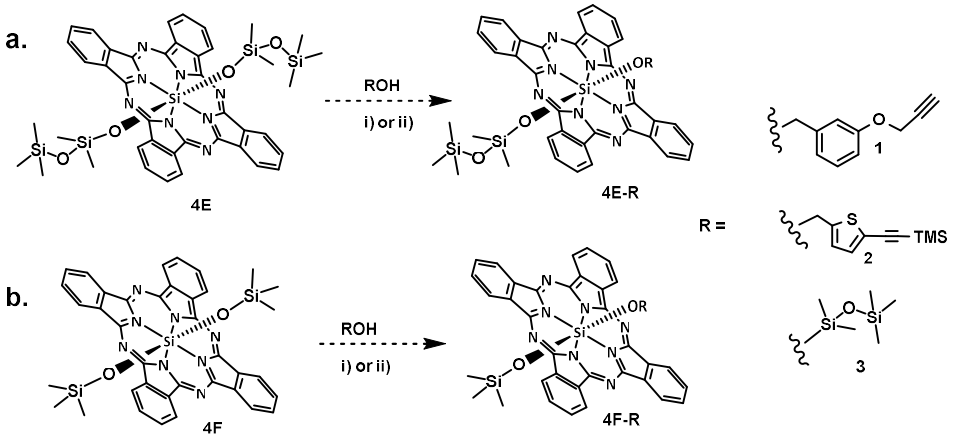

Scheme 4.3: Attempts to synthesize RR'-SiPc from symmetrical siloxy functionalized SiPcs. The reaction conditions for a) & b) include i) toluene reflux for 24-48 hours, or ii) Toluene reflux, TEA for 24 hours. No RR'-SiPcs were produced in both reactions.

It was reported that producing asymmetric SiPcs becomes more challenging upon extension of the alkyl chain length,[7,19] suggesting that electronic or steric hindrance may play a crucial role in the mono-displacement, which provides a probable reason for the limitations of **Scheme 4.1**. The result seen for **Schemes 4.2** and **4.3** might also be explained by this, as well, since the ROH groups and the pre-existing axial moiety are bulky. Although solubility might play a factor in the lone axial substitution, the trend seen so far for these reactions suggests other key factors might also contribute, thus suggesting investigation beyond solubility as a factor for the RR′-SiPc synthesis producibility.

Under one specific condition, starting with bis(5-[2-(trimethylsilyl)ethynyl]-2-thienylmethoxy) silicon phthalocyanine (**4D**, as prepared in **Chapter 3**) and introducing an excess amount of butanol, a small conversion to **4D-4** (RR'-SiPc, where R = 5-[2-(trimethylsilyl)ethynyl]-2-thienylmethoxy, R' = butoxy, **Scheme 4.4a**) was observed after refluxing in toluene for three days. Excess amount of butanol, extended reaction time, and the addition of a base are credited for the conversion; however, the reaction yield remained low

(28%). Without a base, no displacement occurred, suggesting that the reaction required an external force to proceed. It is important to note that adding more base or a stronger base, such as sodium hydride (NaH), resulted in double replacement of the axial units with butoxy groups, as discussed in **Chapter 3**. Similarly, compound **4C-2** (**Scheme 4.2**), the conversion was only observed with the addition of a base and an extended reaction time, suggesting that 2-thiophenemethanol might not be as reactive. Both the butanol and 2-thiophenemethanol reagents exhibit similar acidic properties. Although the addition of the base and the extended reaction times did result in the isolation of RR'-SiPcs, this was not always the case, as was observed when **4D** was reacted in a basic medium (as seen in **Scheme 4.2**), and there was a potential risk of double replacing the axial units. This prompted the exploration of reactions without added bases and a shortened reaction time. Attempts to produce the respective RR′-SiPc starting with compound **4C** and adding an incoming butanol moiety remained unsuccessful (**Scheme 4.4b**), showcasing that without a base to push the conversion, the reaction will remain elusive. As the alkyl chain extends, difficulties in producing the RR′-SiPc have been reported previously,[7] in alignment with what was observed when swapping butanol for hexanol in this study's case (see **Scheme S4.2a**).

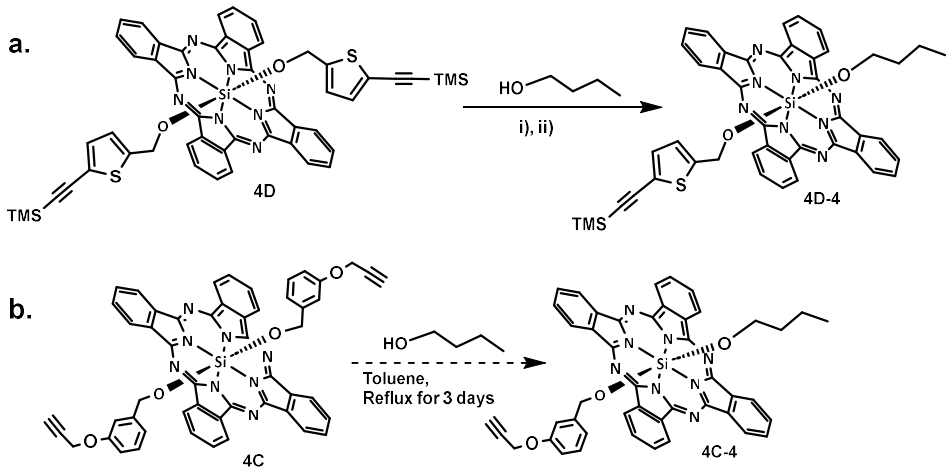

Scheme 4.4*:* Benzyloxy and thienylmethoxy functionalized R_2-SiPc precursors for RR′-SiPc synthesis. a) Thienylmethoxy initiated RR′-SiPc synthesis with the incoming butanol group. Reaction conditions: i). Reflux in toluene 2-3 days, no RR′-SiPc formation, ii). Reflux in toluene with TEA for 3 days, producing **4D-4**. b) Reflux in toluene for 3 days without a base to displace the benzyloxy moiety, similar to the thienyl, no RR'-SiPc formation.

To better understand the trends in synthesizing RR′-SiPcs from R_2-SiPcs, the use of other electronically active reagents, such as pentafluorophenol (PF), 2,3,5,6-tetrafluorophenoxy (TF), and phenol, were investigated. These groups have been previously used to synthesize their symmetrical SiPc equivalents and employed as OSC in OTFTs through vapour deposition due to their minimal solubility.[16] When inducing the singular ligand exchange on **4D** using polyfluorinated phenols, conversion to the RR'-SiPc products (**4D-6** and **4D-7**, where R = 5-[2-(trimethylsilyl)ethynyl]-2-thienylmethoxy and R' = PF or TF) were observed. Compounds **4D-6** and **4D-7** were refluxed in toluene for 12 hours and monitored using ^{19}F NMR. The resulting title compounds were collected as blue powders with yields ranging from 72% to 78%; full characterization details are provided in **Section 4.5**. Similarly, conversion to RR'-SiPc is observed for **4C** when reacted with PF, as discussed in **Chapter 2**. However, despite extending the reaction time to 52 hours, unlike the polyfluorinated moieties, the incoming bare phenol

reagent was unable to mono-displace the thienyl unit on **4D** (see **Scheme 4.5b**). This shortcoming was also noticed when **4C** was reacted with the phenol (see **Section 4.5).**

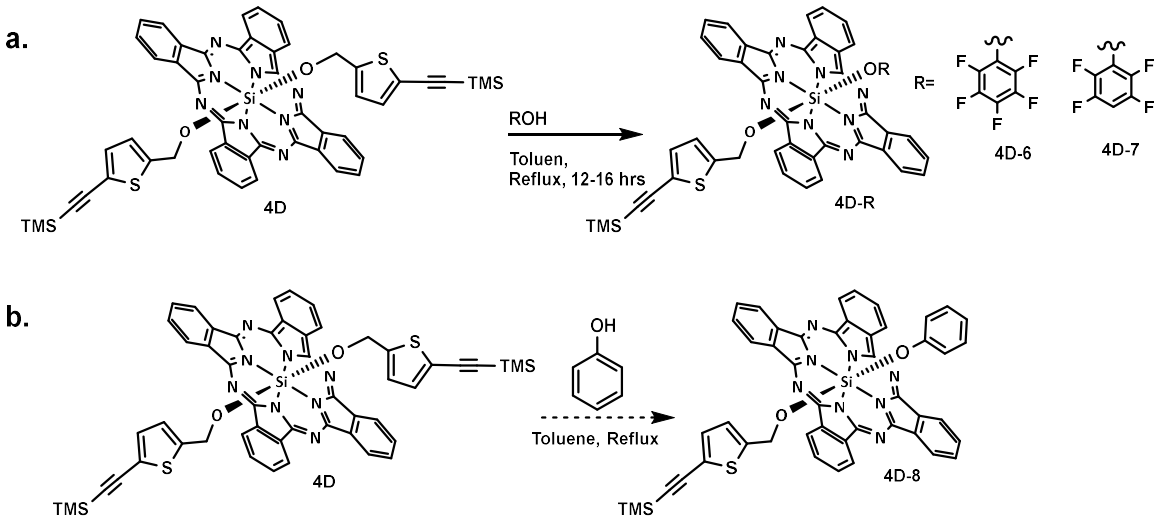

Scheme 4.5: Thienylmethoxy based RR′-SiPc synthesis process with incoming phenols. a). Effective RR′-SiPc synthesis using polyfluorinated reagents: pentafluorophenoxy and 2,3,5,6-tetrafluorophenoxy, without the addition of a base or extended reaction time b). Failed RR′-SiPc synthesis process with incoming phenol reagent, refluxed in toluene for up to 52 hours.

The polyfluorinated moieties, unlike the benzyloxy and thienylmethoxy groups (ROH groups of **Scheme 4.1)**, consist of a strong electron-withdrawing group. The previously synthesized asymmetric SiPc, **4C-2** (where R = 3-(prop-2-yn-1-yloxy)benzyloxy, R' = 2-thienylmethoxy), exhibits increased reactivity of the new group toward lone displacement upon addition of a base, which might be due to the thermodynamic push from the new acid-base difference. The trend among the reagents that led to the successful isolation of asymmetric RR′-SiPc derivatives appears to be an increased acidity of the incoming moiety compared to that of the existing axial substituent, as well as thermodynamic push from the acid-base differences. This suggests that the acidity of the incoming group may play a crucial role in the straightforward mono-displacement process. Huang *et al*. successfully synthesized Chol-SiPc-

TPP (asymmetrical SiPc) in a two-part reaction where they reacted Cl_2-SiPc with cholesterol(R) in a 1:1 equivalent in a basic medium, followed by the addition of two equivalents of 6-triphenylphosphinohexanoic acid(R') (12% yield).[28] Although the article does not mention if the first part produced a mono or di-substitution, it's noteworthy that the second reagent added has more of an acidic nature than the cholesterol. The extra base added in the second might suggest an increased thermodynamic push due to the acid-base. In another study, where Cl_2-SiPc is reacted with two reagents, meloxicam (pKa:1.1 & 4.08)[29] and triethyleneglycolmonomethylether (alcohol), in a one-part reaction (equal equivalency), yielded 9% of the RR′-SiPc.[23] In this case, both structural and acidity differences exist between the axial units; however, since equal amounts of both reagents are reacted simultaneously with Cl_2-SiPc, the reasons for the low yield and reaction push remain less clear. It is uncertain whether the reaction's effectiveness is influenced by the differences in acidity or related solely to thermodynamic factors.

Since polyfluorinated phenols appear to yield RR′-SiPc derivatives by displacing a single axial unit, they were further explored with siloxy derivatives (**4E** and **4F**) to produce the corresponding RR′-SiPcs. Initially, compound **4E** and PF, in similar conditions to **Scheme 4.5a**, were refluxed for 12 hours in toluene, followed by extending the reaction time to 48 hours. The progress of the reaction was monitored using ^{19}F NMR, but ligand exchange was not observed. Nevertheless, unintentional formation of a RR′-SiPc species with R = pentamethyldisiloxy and R' = fluoro was observed according to the NMR assessments, suggesting that a single fluorine atom might displace one of the axial moieties instead (see **Scheme 4.6a,** and **Section 4.5**, **Fig. S4.20**). It's worth noting that the axial siloxy unit and PF have comparable molecular sizes but significant differences in acidity due to the electron-withdrawing groups on the phenol. This

shortcoming suggests acidity might not be the only determining factor for RR′-SiPc production; instead, the lone fluorine bonded to the silicon core suggests molecule size might be a factor as well. When employing a simple phenol (pKa ~10) instead of PF (pKa ~ 5.5) on **4E**, the reaction remained elusive, despite the phenol being somewhat smaller in size in comparison to the polyfluorinated phenol (PF), but still more acidic than the pentamethyldisiloxy axial unit (see **Scheme 4.6b)**. The phenol reagent was previously used in **Scheme 4.5b** and **Scheme S4.2f**, which did not produce the asymmetric material, suggesting the phenol is not as reactive, or the acidity difference is not large enough for the mono-displacement. Whereas in **Scheme 4.6a**, a large difference in acidity is present; however, the bulkiness of the siloxy axial units might hinder PF's direct access to the central silicon atom; nonetheless, a sacrificial F from the PF group could maneuver around to make the substitution due to its smaller size and reactivity towards the Si atom. Additionally, when reacting with hexafluoroisopropanol, a reagent with a similar pKa as phenol, a singular fluorine atom replacing the siloxy unit was observed again on **4E** (see **Section 4.5, Scheme S4.2c**).

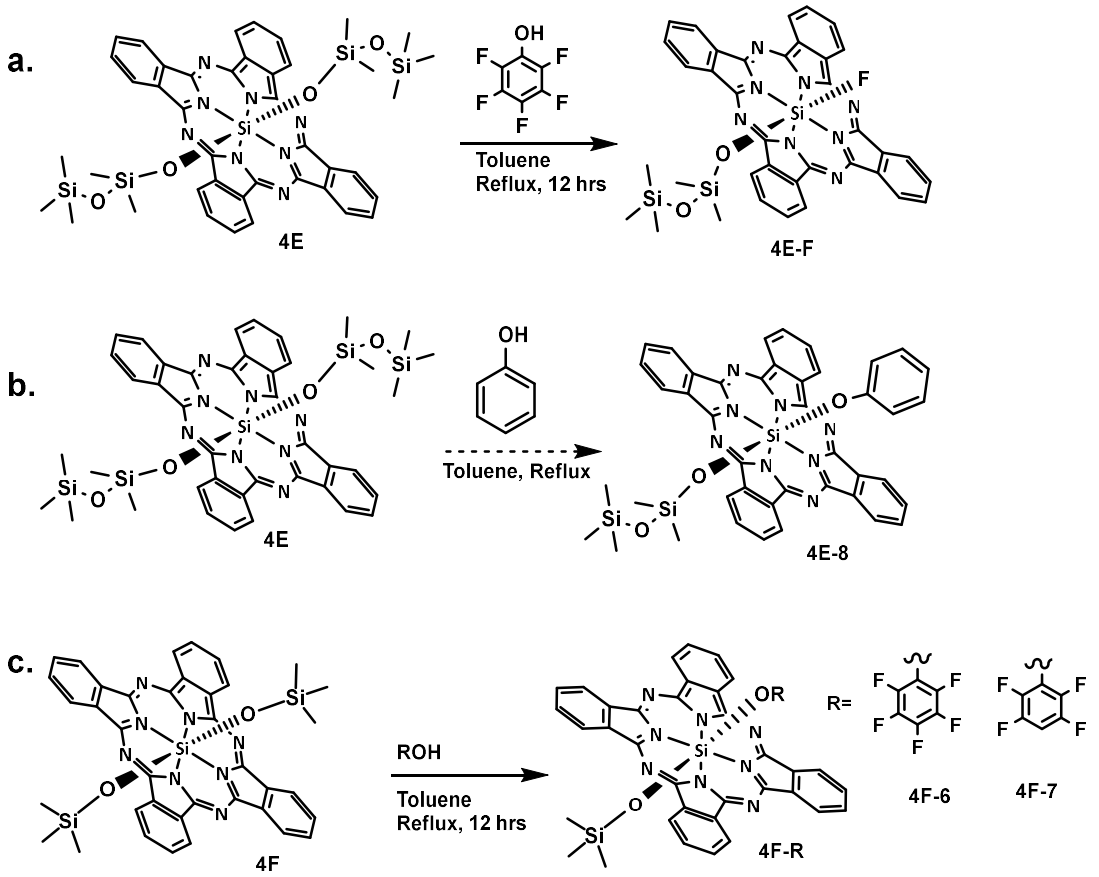

Scheme 4.6: Synthetic pathway to obtain RR'-SiPcs from Siloxy functionalized R_2-SiPc. a). Pentamethyldisiloxy functionalized R_2-SiPc producing unintentional Si-F RR'-SiPs when reacted with pentafluorophenoxy; b). Pentamethyldisiloxy functionalized R_2-SiPc producing no RR'-SiPc when reacted with phenol; c). Effective RR′-SiPc synthesis using polyfluorinated phenols on trimethylsiloxy functionalized R_2-SiPc.

Scheme 4.6c demonstrates that PF and TF can be effective in mono-displacing a smaller siloxy group, to produce the intended RR′-SiPcs **4F-6** (where R = trimethylsiloxy, R' = pentafluorophenoxy) and **4F-7** (where R = trimethylsiloxy, R' = 2,3,5,6-tetrfluorophenoxy). Here, the Si-F (R' = F) substitution taking place was not observed via ^{19}F NMR, in contrast to what was observed for **Scheme 4.6a**. The trimethylsiloxy groups on compound **4F** successfully produce the RR′-SiPcs, suggesting that structural size and acidity are factors in the synthesis

process. The reactions in **Scheme 4.6c** were conducted in a 1:1 equivalence for 12 hours and yielded purple powders in 65% (**4F-6**) and 73% (**4F-7**) yields.

Ng and co. credited the singular displacement axial unit of their R_2-SiPc (R = 1,3-bis(dimethylamino)-2-propoxy) with a methoxy to the vulnerability of ligand-exchange reactions resulting from the large 1,3-bis(dimethylamino)-2-propoxy group,[19] which is in alignment with the Si-F substitution observed for **Scheme 4.6a**. Previous reports have also suggested Si-F substitution taking place when bis(pentafluorophenoxy) SiPc was subjected to thermal treatment.[30] To further distinguish what is driving the production of RR′-SiPc derivatives, compound **4F** was employed to yield the respective RR′-SiPcs as shown in **Scheme 4.3b**. This reaction proved unsuccessful, aligning with what's deduced thus far, that the acidity and molecular size are key factors in the singular ligand exchange. In **Scheme 4.3b**, the newly added reagents (ROH: R = 3-(prop-2-yn-1-yloxy)phenyl methanol or R = (5-[2-(trimethylsilyl)ethynyl]-2-thiophenemethanol or R = pentamethyldisilanol) have a lower acidity than the trimethylsiloxy axial units, in addition to their large molecular sizes, which is a probable limitation for the reactions. In **Schema 4.3a**, compound **4E**, with pentamethyldisiloxy as axial substituent, has a similar acidity nature and size to the mono-displacer reagents, and the reactions remained ineffective. These observations suggest that to successfully replace a lone ligand on the axial position, the pKa of the incoming substituent must be lower than that of the leaving group, and/or/and smaller in size. Similarly, Anderson *et al*. effectively used compound **4A** (R = 1,3-bis(dimethylamino)-2-propoxy) to realize three different RR′-SiPc derivatives in 78 - 81% yields by introducing 4-methylumbelliferone (pKa ~7.7)[31] and other acidic phenolic reagents.[32]

Lastly, to demonstrate the polyfluorinated phenols as an effective reagent to yield RR′-SiPc, symmetrical SiPcs possessing linear alkyl chain axial substituents were reacted with PF

and TF reagents. As outlined in **Scheme 4.7**, the reactions yielded the desired asymmetric products under similar conditions to the successful reactions in **Schemes 4.5a** and **4.6c**. Here, a large difference in acidity is still present, as well as the linearity of the pre-existing axial units, all of which contribute to the success of the substitution reactions. Reactions **a** and **b** both yielded purple powders in 57% (**4G-1**) and 64-73% (**4H-6** & **4H-7**), respectively. All the RR'-SiPcs synthesized here were purified and subjected to characterization techniques such as NMR, FTIR, UV-vis-NIR, and CV. The analyses, which can be found in **Section 4.5**, suggested successful RR'-SiPc products.

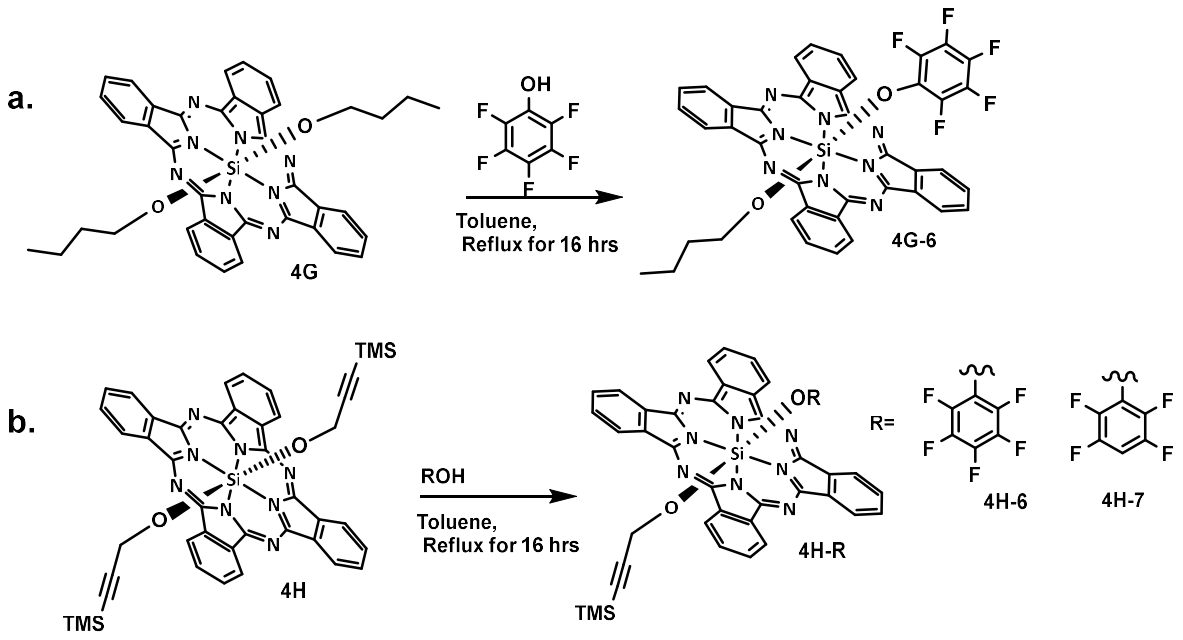

Scheme 4.7: Synthetic pathway to obtain RR'-SiPcs from alkyl functionalized R_2-SiPc precursors by using polyfluorinated incoming reagents. a). singular axial ligand exchange on **4G** by pentafluorophenol; b). singular axial ligand exchange on **4F** by polyfluorinated phenols.

To summarize, starting from R_2-SiPc and introducing various functional moieties for a lone displacement, RR′-SiPc with diverse chemical properties can be obtained. The synthetic routes described in this chapter for the isolation of asymmetric SiPc highlight that the acidity and structural size of the axial substituent matter. More specifically, this work facilitates a potential

pathway to control the solubility of SiPc by combining soluble and insoluble axial moieties. For a better illustration of acidity and structural size playing a role in the mono-displacement of the axial units of SiPcs, other reaction conditions that were employed yet did not yield the desired results can be found in **Section 4.5.**

4.2.2 Optical and Electrochemical analysis.

Electrochemical analyses of the R_2-precursors and asymmetric RR′ SiPc derivatives were conducted to probe how a combination of two different axial ligands would impact the redox properties. Cyclic voltammetry for each compound was carried out in anhydrous DCM with 0.1 M NBu_4PF_6 as the supporting electrolyte and Pt wires as the working, counter, and reference electrodes, along with ferrocene as an internal reference. In general, direct comparison of the R_2-SiPc to the RR'-SiPc compounds suggests some differences in electrochemical properties upon variation in axial functionalization. Most importantly, for the siloxy derivatives (**4F-6**, where R = trimethylsiloxy and R' = pentafluorophenoxy, and **4F-7**, where R = trimethylsiloxy and R' = 2,3,5,6-tetrafluorophenoxy), inclusion of the polyfluorinated phenoxy unit appears to afford a secondary redox process, along with an overall anodic shift in potential compared to the parent compound **4F** (where R = trimethylsiloxy), as seen in **Figure 4.2b**. A similar shift is also observed for the RR′-SiPc derived from **4H** (**Figure 4.2d**). Although similar numbers of reduction and oxidation processes are seen for the **4D** derivatives (**Figure 4.2a)**, the polyfluorinated axial moieties appear to shift the redox processes to higher potentials, likely due to their electron-withdrawing nature. The CV analysis of the **4G** derivatives directs no clear correlation between the axial moieties. When R = butoxy, R' = pentafluorophenoxy or 5-[2-(Trimethylsilyl)ethynyl]-2-thienylmethoxy, a comparison with the parent R2-SiPc (where R = butoxy) reveals that the polyfluorinated derivative surprisingly exhibits a lower redox potential

(see **Figure 4.2c**). CV analysis suggests that new electrochemical characteristics can be achieved through asymmetrical di-substitution within a specific solvent window. This approach is beneficial for various applications that require slight modifications of electrochemical properties or enhanced solubility without compromising electronic characteristics. The onsets of the redox processes and the energy gaps for each CV analysis are summarized in **Table 4.1** below.

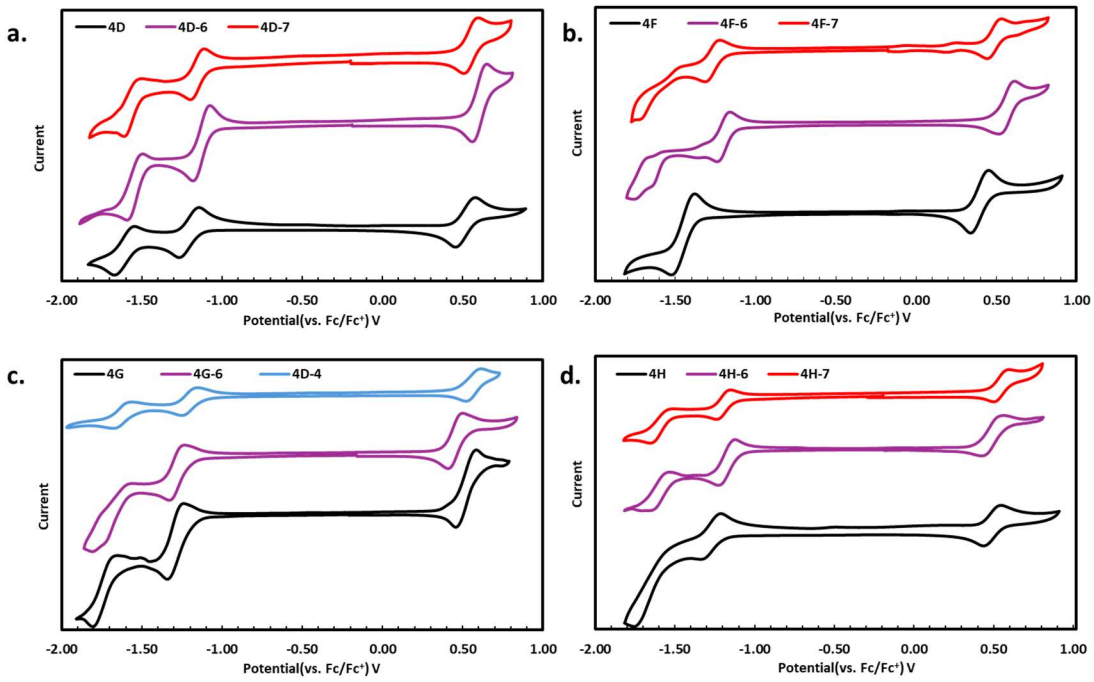

Figure 4.2: Cyclic voltammograms of asymmetrical SiPcs (Red: R'= pentafluorophenoxy containing derivatives, Purple: R'= 2,3,5,6-tetrafluorophenoxy containing derivatives, Blue: R'= 5-[2-(Trimethylsilyl)ethynyl]-2-thienylmethoxy) and parent symmetrical SiPcs (Black). a). **4D, 4D-6, and 4D-7** b). **4F**, **4H-6** and **4A-2**, c) **4G**, **4D-4**, and **4G-6**, d). **4H**, **4H-6**, and **4H-7** in DCM at 100 mV s^{-1} with 0.1 M $TBAPF_6$ as the supporting electrolyte.

Table 4.1: Half potentials, HOMO and LUMO energy levels, and energy gap values determined from the CV of R_2-SiPcs and RR′-SiPcs.

SiPc Derivatives	$E^{0/+1a}$ (V)	$E^{0/-1}$ (V)	$E^{-1/-2}$ (V)	HOMO[b] (eV)	LUMO[b] (eV)	E_{gap}[c] (eV)
4D	0.51	-1.20	-1.61	-5.3	-3.6	1.70
4D-6	0.62	-1.14	-1.55	-5.4	-3.7	1.70
4D-7	0.55	-1.15	-1.55	-5.4	-3.7	1.70
4F	0.41	-1.42	-	-5.2	-3.4	1.80

4F-6	0.55	-1.20	-1.77*	-5.4	-3.6	1.80
4F-7	0.49	-1.29	-1.70*	-5.3	-3.5	1.80
4G	0.53	-1.30	-1.73	-5.3	-3.5	1.80
4G-6	0.46	-1.28	-1.80*	-5.3	-3.6	1.70
4D-4	0.59	-1.22	-1.73	-5.4	-3.6	1.80
4H	0.53	-1.27	-1.76*	-5.3	-3.5	1.77
4H-6	0.50	-1.19	-1.60	-5.3	-3.6	1.70
4H-7	0.53	-1.21	-1.67	-5.3	-3.6	1.70

Half-potentials were calculated by using the cathodic and anodic peak potential, $E^{0/+1} = (E^a - E^c)/2 + E^c$; *$E^c$ used as $E^{0/-1}$ or $E^{-1/-2}$. [b]HOMO/LUMO levels were calculated using Fc/Fc^+ as a reference; HOMO = 4.8 + $E_{0/+1}$(vs.ferrocene) [eV];[33–35] LUMO= 4.8 + $E_{0/-1}$(vs. Ferrocene) [eV]. [c]E_{gap} from the CV was determined by $E_{gap} = E_{LUMO} - E_{HOMO}$

A similar comparison of the optical properties via UV-vis-NIR was conducted (see **Figure 4.3**). The UV-vis-NIR analysis suggested that the λ_{max} of the compound is shifted to a higher wavelength when the asymmetrical moieties both have conjugated axial units. This is most obvious in the butoxy derivatives, where the bis(butoxy) SiPc (**4G**) has a similar absorption profile to **4D-4** (where R= 5-[2-(trimethylsilyl)ethynyl]-2-thienylmethoxy and R'= butoxy**)** in comparison to **4G-6** (where R= butoxy and R'= pentafluorophenoxy), which is red-shifted. Likewise, a red shift is observed for the **4H-6** & **4H-7** compared to the parent symmetrical **4H** compound. A much more noticeable difference in absorption profile in the λ_{max} is seen for the siloxy derivatives **4F** vs. **4F-6** & **4F-7** (670 vs. 680 nm), where the polyfluorinated materials are red-shifted. The symmetrical pentafluorophenoxy and 2,3,5,6-tetrafluorophenoxy SiPcs are reported to have a $\boldsymbol{\lambda_{max}}$ of 686 nm in toluene.[15,36] The in-between $\boldsymbol{\lambda_{max}}$ seen in **4F-6** and **4F-7** can be characterized as a combined absorption profile due to the asymmetrical substitutions. All the polyfluorinated derivatives herein have a $\boldsymbol{\lambda_{max}}$ of 680-685 nm, at least 5 nm greater than the parent symmetrical SiPcs, a shift that can be credited to the polyfluorinated moieties. Overall, the optical analysis suggests that the SiPc absorption profile can be slightly manipulated through the

introduction of axial unit asymmetry. The energy gap and λ_{max} onsets are determined based on the absorption, as seen in **Table 4.2**.

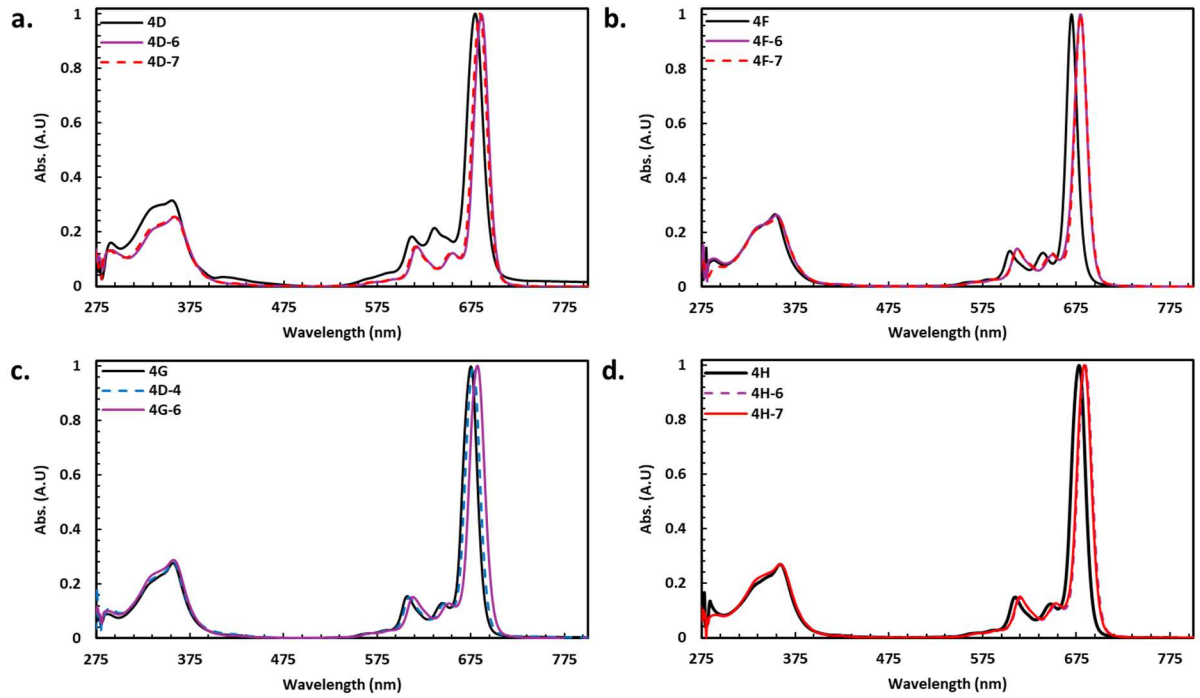

Figure 4.3: Absorption profiles for the parent compound R_2-SiPcs (black) and their RR'-SiPc analogues in solution with chlorobenzene. a). RR'-SiPcs, R= trimethylsiloxy, R' = PF(**4F-6**) or TF(**4F-7**)). b). RR'-SiPcs, R = 5-[2-(trimethylsilyl)ethynyl]-2-thienylmethoxy, R' = PT (**4D-6**) or TF (**4D-7**). C). RR'-SiPcs, R= butoxy, R' = 5-[2-(trimethylsilyl)ethynyl]-2-thienylmethoxy (**4D-4**) or PF (**4G-1**). d). RR'-SiPcs, R= trimethylsilyl propargyloxy, R' = PF (**4H-6**) or TF (**4H-7**).

Table 4.2: Energy gap and λ_{max} onsets determined based on the absorption profiles of the parent R_2-SiPcs and their RR'-SiPc analogues.

SiPc Derivatives	λ_{max} (nm)	λ_{max} Onset (nm)	E_{gap} (eV)[a]
4D	680	710	1.75
4D-6	685	717	1.73
4D-7	685	717	1.73
4F	670	699	1.77
4F-6	680	709	1.75
4F-7	680	709	1.75
4G	675	708	1.75
4G-6	682	718	1.73

4D-4	677	714	1.74
4H	678	705	1.76
4H-6	684	716	1.73
4H-7	684	716	1.73

[a]E_{gap} was determined by using E = 1240/ λ_{max} Onset.

4.2.3 Alternative synthetic approaches to RR'-SiPc starting from ClSiPcMe

Below is a brief discussion of alternative synthetic approaches that were explored for the isolation of asymmetric RR'-SiPc derivatives; however, in contrast to the preceding sections, many of these methods proved elusive. As such, extensive characterization or analyses of the resulting compounds was not feasible. Nonetheless, this section is included to highlight the efforts taken to prepare a variety of RR'-SiPc derivatives.

One approach to prepare asymmetrical SiPcs is by using chloro methyl silicon phthalocyanine (ClSiPcMe; **4(Me)** in **Scheme 4.8a**) as a starting material, where a singular nucleophilic substitution can result in **4(Me)-R.** The asymmetric **4(Me)** and excess amount of ROH (where ROH = 3-(prop-2-yn-1-yloxy)phenyl methanol or 5-trimethylsilylethynylthienphenemethanol or trimethylsilanol) were refluxed in toluene for 24 hours to obtain **4(Me)-1, 4(Me)-2,** and **4(Me)-3**(see **Scheme 4.8a**). ^{1}H NMR analysis suggested the formation of the asymmetrical **4(Me)-R** SiPc**,** where ^{1}H NMR revealed the CH_3 peak around -6 ppm for all three materials, which is in the range expected due to the strong electron current of the SiPc ring.[19] The initial step of this synthesis yields a soluble crude material; however, due to the light-sensitive nature of the Si-Methyl bond, over time, an insoluble impurity was observed, and the proton integration no longer corresponded to the initial analyses. With the new insoluble impurities forming, purification at this stage was not ideal, and the compounds were carried over to the next step without purification.

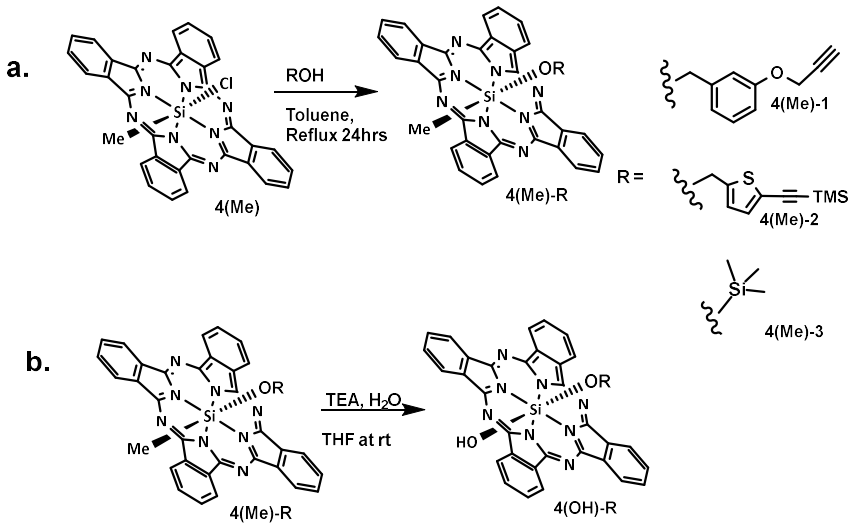

Scheme 4.8: Alternative RR'-SiPc synthesis method from ClSiPcMe (**4(Me)**). a). synthesis of **4(Me)-R** by refluxing ROH reagents with **4(Me)** in toluene for 24 hours; b). attempts to hydroxylate the **4(Me)-R** materials to form **4(OH)-R,** at room temperature, until a color change from green to blue was observed.

To mitigate this issue and form a more stable derivative, a photo reaction was induced to replace the Si-Me bond with a Si-OH, affording **4(OH)-R**. The light reaction was performed by adapting precedent literature.[18,22] Briefly, the **4(Me)-R** derivatives were dissolved in THF along with six equivalents of water and TEA at room temperature. A white LED spotlight lamp (10 W) was passed through the solution until a color change (green to blue) was observed. In doing so, ^{1}H NMR analysis suggested the removal of the methyl moiety, which is no longer present at -6 ppm; however, new unidentified impurities were observed in the downfield of the ^{1}H NMR. Additionally, FT-IR analysis did not reveal the presence of an OH moiety for the reaction of **4(Me)-1** and **4(Me)-2** to afford the **4(OH)-1** and **4(OH)-2** pieces. It should be noted that in most solvents, when the Si-Me bond is still present, the solution has a deep green appearance; however, upon removal of the Me substituent, a typical SiPc blue colour is observed in solution. The aforementioned color change was previously used as an indication for the completion of the reaction, which initially was followed in this case. The color change was seen

within around the four-hour mark; however, despite the color change, there was no observation of OH peaks in the FT-IR spectra, even after further reacting for 3 to 5 days. To overcome these challenges, changing the solvent from THF to DCM, reacting with and without base, were also attempted; yet the OH substitution remained elusive as per the FT-IR characterization.

Attempts to hydroxylate RR′-SiPc to isolate a more stable derivative, which may permit the substitution of a secondary axial moiety, highlighted the challenges associated with isolating asymmetric RR′-SiPc derivatives. Instead of replacing the methyl, a direct etherification with a pentafluorphenanol (PF) via photo reaction was attempted on **4(Me)-3** to afford **4(PF)-3 (**see **Scheme 4.10)**. Here, **4(Me)-3** was reacted under similar conditions as described above, using PF instead of H_2O. Although no appreciable clean product was collected, ^{19}F NMR and ^{1}H NMR suggested some success. Comparisons of the NMR spectra of the new product to that of **4F-6** (synthesized from the R_2-SiPc, as outlined in **Scheme 4.6**) showed similar characteristics (see **Figure 4.4)**. Unfortunately, due to time constraints, no further characterizations were conducted, and this attempt was not further pursued. Nonetheless, this may represent a promising pathway for the use of RO-SiPc-alkyl as a starting material to prepare asymmetric RR′-SiPc derivatives.

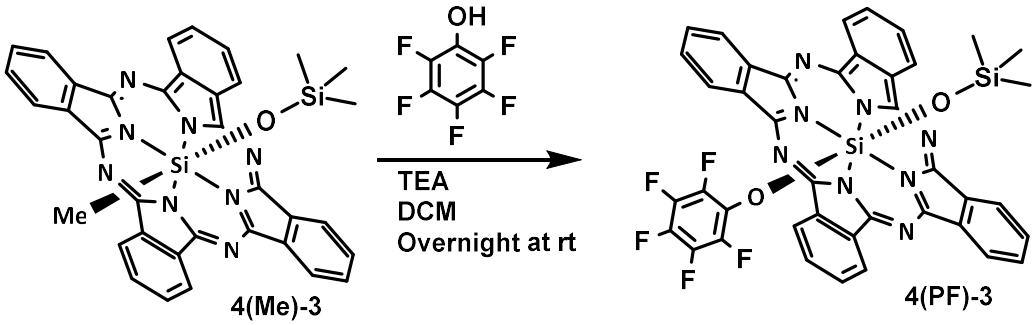

Scheme 4.9: Proposed synthetic pathways for RR'-SiPcs based on initial observations made for the synthesis of **4(PF)-3.**

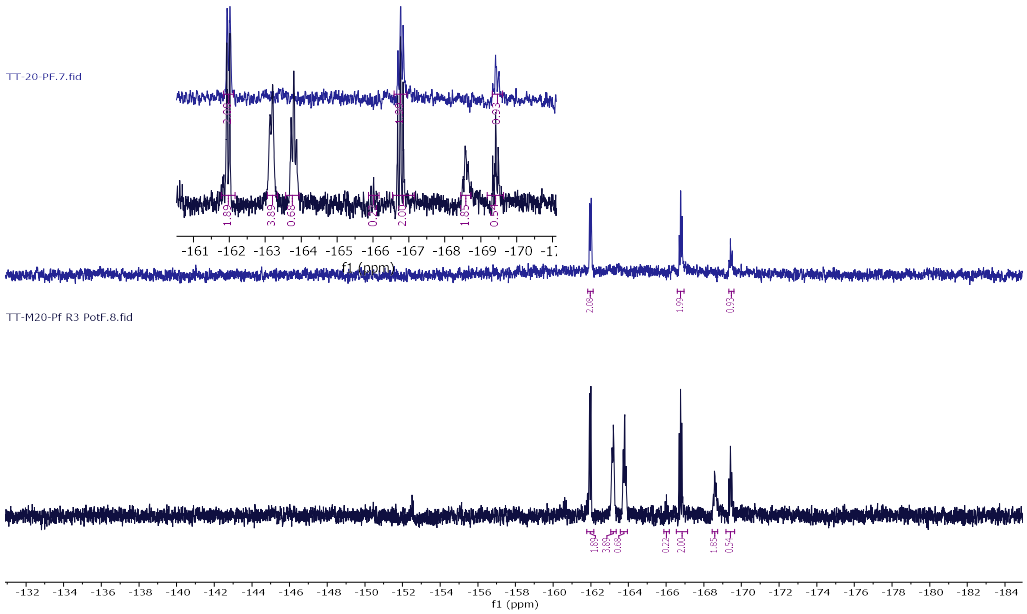

Figure 4.4: Stacked ^{19}F NMR of **4(PF)-3 (**Bottom) and **4F-6** (Top) exhibiting similar integration and peaks.

4.3 CONCLUSION

Based on the findings of this work, it is reasonable to suggest that acidity and the size of the axial substituent play a role in successful mono-displacement at the silicon core of R_2-SiPcs. Regardless of solubility or reaction length, weakly acidic or sterically demanding reagents, including linear alcohols, bulky silanols, and phenol, failed to produce significant asymmetrical products in all reactions studied. Polyfluorinated phenols, on the other hand, were effective in affording asymmetric derivatives RR′-SiPcs′-SiPcs (**4D-6, 4D-7, 4F-6, 4F-7, 4G-6, 4H-6,** and **4H-7).** Due to the electron-withdrawing nature of the polyfluorinated axial groups, the resulting asymmetrical SiPcs exhibit slightly altered electrochemical and optical properties, most notably anodically shifted reduction potentials and mild redshifts in the Q-band absorption in comparison to the parent starting symmetric SiPc material. Together, these results demonstrate the usefulness of acidic nucleophiles for producing functional RR′-SiPcs appropriate for applications requiring

controlled solubility and tunable electronic properties. Overall, this work offers clear design guidelines for the selective synthesis of asymmetrical SiPc derivatives.

4.4 EXPERIMENTAL

4.4.1 Materials and general procedures

All materials purchased were used as received. Diiminoisoindoline (98%) were purchased from Ambeed Inc. Pentafluorophenol (98%) and 2,3,5,6-tetrafluorophenol were purchased from Oakwood chemicals. America. Silicon tetrachloride ($SiCl_4$) (99%), 2-propanol, 1,3-bis(dimethylamino)-(97%), $NaBH_4$ (98%), and triethylamine(TEA) were purchased from Sigma-Aldrich Chemical Company. Cl_2-SiPc,[37] **4(Me),**[18] **4A**[19], 1,1,3,3,3-pentamethyldisiloxanol,[38] **4G**[12], 5-[2-(Trimethylsilyl)ethynyl]-2-thiophenemethanol[39,40] were prepared according to precedent literature.

4.4.2 Synthesis of Bis(5-[2-(Trimethylsilyl)ethynyl]-2-thienylmethoxy) silicon phthalocyanine (4D)

In a procedure adapted from literature,[27] **4D** was synthesized by mixing 660mg of 5-[2-(Trimethylsilyl)ethynyl]-2-thiophenemethanol (3.14 mmol, 3.33 mmol) and 574 mg of Cl_2-SiPc (0.94 mmol, 1.00 mmol) in 47 mL of toluene and 2mL of triethylamine. The mixture was refluxed over a period of 48 hrs. A successive addition of 5-[2-(Trimethylsilyl)ethynyl]-2-thiophenemethanol after 12, 24, and 36 hours was followed. Upon cooling to room temperature, the mixture was diluted with 300 mL of hexanes and set aside for 30 minutes to precipitate out. The precipitate was vacuum filtered, followed by successive washes with methanol, ether, and acetone. Finally, the solid was dissolved in dichloromethane and gravity filtered to remove any unreacted Cl_2-SiPc and other insoluble impurities. The DCM solution was vacuum filtered to dry, and a blue/teal powder was collected (685 mg, 76%). ^{1}H NMR (400 MHz, $CDCl_3$) δ 9.62 (dd, J

= 5.6, 3.0 Hz, 8H), 8.34 (dd, J = 5.8, 2.9 Hz, 8H), 5.97 (d, J = 3.7 Hz, 2H), 4.27 (d, J = 3.7 Hz, 2H), 0.06 (s, 18H), -0.68 (s, 4H). ^{1}H NMR (400 MHz, $CDCl_3$) δ 9.62 (dd, J = 5.6, 3.0 Hz, 8H), 8.34 (dd, J = 5.8, 2.9 Hz, 8H), 5.97 (d, J = 3.7 Hz, 2H), 4.27 (d, J = 3.7 Hz, 2H), 0.06 (s, 18H), -0.68 (s, 4H).

4.4.3 Synthesis of [Si, Si] Bis(5-trimethylsilylethynylthieny-lmethoxy, pentafluorophenoxy) silicon phthalocyanine (4D-6)

To a dry flask, 200 mg of **4D** (0.21 mmol, 1.0 eq.) and 38.0 mg of pentafluorophenol (0.21 mmol, 1.0 eq.) were mixed in 50 mL of toluene and refluxed for 12 hours. The reaction was cooled and poured onto 200 mL of isopropanol and set aside for 30 minutes. The solution was then vacuum filtered, followed by three rounds of washing with isopropanol, hexanes, and ether. The solid was left to dry under vacuum for one hour and collected as a blue powder (141 mg, 72%). ^{1}H NMR (600 MHz, $CDCl_3$) δ 9.64 (tt, *J* = 5.0, 2.7 Hz, 8H), 8.37 (dt, *J* = 4.9, 1.8 Hz, 8H), 5.97 (dd, *J* = 3.9, 1.4 Hz, 1H), 4.27 (dd, *J* = 3.8, 1.6 Hz, 1H), 0.10 – 0.06 (m, 9H), -0.57 (d, *J* = 1.7 Hz, 2H). ^{19}F NMR (283 MHz, $CDCl_3$) δ -161.68 – -161.94 (m), -166.38 – -166.64 (m), -168.93 (dt, *J* = 22.3, 4.8 Hz).

4.4.4 Synthesis of [Si, Si] Bis(5-[2-(Trimethylsilyl)ethynyl]-2-thienylmethoxy, 2,3,5,6-tetrafluorophenoxy) silicon phthalocyanine (4D-7)

4D-7 was synthesized following a similar procedure to that of **4D-6,** using 38.0 mg of 2,3,5,6-tetrafluorophenol (0.21 mmol, 1.1 eq.) instead of pentafluorophenol. Upon drying, a blue powder was collected (154 mg, 80%). ^{1}H NMR (300 MHz, $CDCl_3$) δ 9.69 (dd, *J* = 5.7, 3.0 Hz, 8H), 8.41 (dd, *J* = 5.7, 2.9 Hz, 8H), 6.03 (d, *J* = 3.6 Hz, 1H), 4.33 (d, *J* = 3.6 Hz, 1H), 0.13 (d, *J* = 0.8 Hz, 9H), -0.52 (s, 2H). ^{19}F NMR (283 MHz, $CDCl_3$) δ -142.65 – -143.18 (m), -161.48 – -161.79 (m).

4.4.5 Synthesis of Bis(2-thienylmethoxy) silicon phthalocyanine (4B)

4B was synthesized like **4D**, using 200 mg of 2-thiophenemethanol instead. The final product was collected as a blue powder with a 75% crude yield. FT-IR: C-S stretch 720-650 cm^{-1}, UV-vis: λ_{max} 680 nm.

4.4.6 Synthesis of Bis(1,1,3,3,3-pentamethyldisiloxy) silicon phthalocyanine (4E)

To a dry two-necked flask, 200 mg (0.33 mmol, 1.0 eq) of Cl_2-SiPc and 211 mg (1.33 mmol, 4.0 eq.) of 1,1,3,3,3-pentamethyldisilanol were charged and brought to a solution using 50 mL of toluene. After mixing for a few minutes, 5 mL of triethylamine was added to the mixture. The mixture was brought to reflux at 130 °C under a nitrogen atmosphere for 22 hours. Upon cooling to room temperature, 300 mL of hexanes was used to precipitate out the purple powder. The powder was washed with DCM, and the filtrate was concentrated under reduced pressure. Further purification was done on a silica gel using a 7:3 hexanes: DCM, or by boiling the powder with toluene and precipitating it out again with hexanes to afford 32% yield. And characterized as precedent literature.[41]

4.4.7 Synthesis of Bis(trimethylsiloxy) silicon phthalocyanine (4F)

4F was synthesized and purified in the same manner as **4E**, using 500 mg of trimethylsilanol in excess, yielding a purple semi-crystalline powder upon drying (146 mg, 62%). ^{1}H NMR (400 MHz, $CDCl_3$) δ 9.63 (dd, J = 5.6, 3.0 Hz, 1H), 8.32 (dd, J = 5.8, 2.9 Hz, 1H), -2.83 (d, J = 1.1 Hz, 2H).

4.4.8 Synthesis of [Si, Si] Bis(trimethylsiloxy, pentafluorophenoxy) silicon phthalocyanine (4F-6)

A dry flask was charged with 150 mg of **4F** (0.21 mmol, 1.0 eq.) and 38.4 mg of pentafluorophenol (0.21 mmol, 1.0 eq.), along with 45 mL of toluene and refluxed for 12 hours.

Upon cooling to room temperature, the mixture was rotovap followed by ether, and hexanes washes under vacuum filtration. The filtrate was dissolved in DCM, passed through silica gel and concentrated, giving **4F-6** as a purple powder with a 65% yield (111 mg). ^{1}H NMR (300 MHz, $CDCl_3$) δ 9.67 – 9.62 (m, 8H), 8.36 (dd, *J* = 5.8, 3.0 Hz, 8H), -2.78 (s, 9H). ^{19}F NMR (377 MHz, $CDCl_3$) δ -161.86 – -162.03 (m), -166.56 – -166.85 (m), -169.39 (ddd, *J* = 22.2, 17.5, 5.0 Hz).

4.4.9 Synthesis of [Si, Si] Bis(trimethylsilyoxy), 2,3,5,6-tetrafluorophenoxy) silicon phthalocyanine (4F-7)

4F-7 was synthesized and purified like **4F-6**, using 34.9 mg of 2,3,5,6-tetrafluorophenol (0.21 mmol, 1.0 eq.). 122 mg of **4F-7** was collected as a purple powder (73%). ^{1}H NMR (300 MHz, $CDCl_3$) δ 9.70 (dd, *J* = 5.7, 3.0 Hz, 8H), 8.41 (dt, *J* = 5.8, 3.4 Hz, 8H), 5.41 (t, *J* = 7.0 Hz, 1H), -2.72 (s, 9H). ^{19}F NMR (283 MHz, $CDCl_3$) δ -143.10 – -143.44 (m), -161.68 – -161.85 (m).

4.4.10 Synthesis of [Si, Si] Bis(butoxy, pentafluorophenoxy) silicon phthalocyanine

4G-6 was synthesized by charging a dry flask with 150 mg of **4G** (0.22 mmol, 1.0 eq.) and 20.0 mg of pentafluorophenol (0.27 mmol, 1.2 eq.), along with 45 mL of toluene and refluxing for 12 hours. The reaction mixture was then cooled to room temperature and diluted with isopropanol (200 mL) and allowed to stand to precipitate. The crude product was recovered via vacuum filtration, washed with ether & hexanes and dried to afford a blue solid. The filtrate was dissolved in DCM, passed through silica gel and concentrated, giving **4F-6** as a purple powder with a 65% yield (114 mg).

4.4.11 Synthesis of [Si, Si] Bis(butoxy, 5-[2-(Trimethylsilyl)ethynyl]-2-thienylmethoxy) silicon phthalocyanine (4D-4)

4D-4 was synthesized by mixing 200 mg of **4D** (0.21 mmol, 1.0 eq), 3 mL of 1-butanol and 3 mL of TEA in 50 mL of toluene. The solution was then refluxed for 72 hours, while

monitoring for the ligand exchange by ^{1}H NMR. Upon completion, the solution was cooled down to room temperature and poured into 200 mL of hexanes. The precipitate was then vacuum filtered to give a blue powder. Further purification was done on silica gel chromatography by using DCM as an eluent, with a final yield of 33%. ^{1}H NMR (400 MHz, $CDCl_3$) δ 9.62 (dd, J = 5.6, 3.0 Hz, 8H), 8.33 (dd, J = 5.8, 2.9 Hz, 8H), 5.99 (d, J = 3.7 Hz, 1H), 4.32 (d, J = 3.8 Hz, 1H), 2.89 (s, 1H), -0.70 (dd, J = 14.0, 6.6 Hz, 5H), -1.36 (q, J = 7.4 Hz, 2H), -1.72 (t, J = 7.4 Hz, 2H), -2.10 (t, J = 6.4 Hz, 2H).

4.4.12 Synthesis of Bis(trimethylsilyl propargyloxy) silicon phthalocyanine (4H)

250 mg of Cl_2-SiPc (0.41 mmol, 1.0 eq.) and 1.00 mL (6.76 mmol, 16 eq.) of trimethyl silane propargyl alcohol were refluxed in 50 mL toluene with 1.00 mL of TEA for 24 hours. Reaction was monitored via ^{1}H NMR. Upon cooling to room temperature, the mixture was diluted with 100 mL of isopropanol and set aside for 30 min to allow the crude to precipitate out. Crude product was recovered via vacuum filtration to afford a blue powder. The solid was washed with ether and hexanes under vacuum filtration, followed by redissolving the filtrate with DCM and passing it on silica gel. The final product was collected as a blue powder, yielding 176 mg (54%). ^{1}H NMR (400 MHz, $CDCl_3$) δ 9.63 (s, 8H), 8.33 (s, 8H), -0.41 (s, 18H), -1.07 (s, 4H).

4.4.13 Synthesis of [Si, Si] Bis(trimethylsilyl propargyloxy, pentafluorophenoxy) silicon phthalocyanine (4H-6)

4H-6 was synthesized similarly to **4D-6,** using 250 mg (0.31 mmol, 1.0 eq.) of **4H** and 58.0 mg (0.31 mmol, 1.0 eq.) of pentafluorophenol. A purple powder was collected with a 64% yield (169 mg). ^{1}H NMR (400 MHz, $CDCl_3$) δ 9.65 (dt, J = 6.0, 3.7 Hz, 8H), 8.36 (dd, J = 5.8, 2.9 Hz, 8H), -0.41 (s, 9H), -0.94 (s, 2H). ^{19}F NMR (377 MHz, $CDCl_3$) δ -161.82 (d, J = 22.1 Hz), -166.69 (t, J = 21.6 Hz), -169.18 (t, J = 22.4 Hz).

4.4.14 Synthesis of [Si, Si] Bis(trimethylsilyl propargyloxy, 2,3,5,6-tetrafluorophenoxy) silicon phthalocyanine (4H-7)

4H-7 was synthesized like **4D-6,** using 250 mg (0.31 mmol, 1.0 eq.) of **4H** and 52.0 mg of 2,3,5,6-tetrafluorophenol **(**0.31 mmol, 1.0 eq.). A purple powder was collected with 72% yield (186 mg). ^{1}H NMR (400 MHz, $CDCl_3$) δ 9.69 – 9.61 (m, 8H), 8.38 – 8.32 (m, 8H), 5.40 – 5.30 (m, 1H), -0.41 (s, 9H), -0.94 (s, 2H). ^{19}F NMR (377 MHz, $CDCl_3$) δ -142.98 – -143.51 (m), -161.60 (d, *J* = 21.0 Hz).

4.4.15 Synthesis of [Si, Si] Bis(3-(prop-2-yn-1-yloxy)benzyloxy, methyl)) silicon phthalocyanine (4(Me)-1).

4(Me)-1 was synthesized by refluxing 350 mg (0.59 mmol, 1.20 eq.) of ClSiPcMe and 80 mg (0.49 mmol, 1.0 eq.) of 3-(prop-2-yn-1-yloxy)phenyl methanol in 100 ml of toluene for 24 hours. Upon cooling to room temperature, the mixture was diluted with 300 mL of isopropanol and set aside for 30 min to allow the crude to precipitate out. The precipitate was subsequently washed with isopropanol under vacuum filtration until the solution passing had a faint green color. The green solid was left to dry under vacuum to yield **4(Me)-1 (**crude yield 78%). ^{1}H NMR (400 MHz, $CDCl_3$) δ 9.64 – 9.57 (m, 8H), 8.35 – 8.28 (m, 8H), 6.04 – 5.91 (m, 2H), 4.15 (dd, *J* = 17.7, 7.3 Hz, 1H), 3.67 (s, 2H), 3.45 (s, 1H), 2.21 (s, 1H), -0.90 (s, 2H), -6.29 (s, 3H).

4.4.16 Synthesis of [Si, Si] Bis(5-[2-(Trimethylsilyl)ethynyl]-2-thienylmethoxy, methyl)) silicon phthalocyanine (4(Me)-2).

4(Me)-2 was synthesized similarly to **4(Me)-1**, using 95 mg (0.45 mmol, 1.0 eq.) of 5-trimethylsilylethynylthiophenemethanol, yielding a green powder with a crude yield of 62%. ^{1}H NMR (400 MHz, $CDCl_3$) δ 9.62 (d, *J* = 5.4 Hz, 8H), 8.35 – 8.30 (m, 9H), 5.93 (s, 1H), 4.23 (s, 1H), 0.05 (s, 18H), -0.85 (s, 2H), -6.31 (s, 3H).

4.4.17 Synthesis of [Si, Si] Bis(trimethylsilyl, methyl) silicon phthalocyanine (4(Me)-3).

4(Me)-3 was synthesized similarly to **4(Me)-1**, using 65 mg of trimethylsilanol, yielding a green powder with a crude yield of 86%. ^{1}H NMR (400 MHz, $CDCl_3$) δ 9.63 – 9.61 (m, 8H), 8.33 – 8.30 (m, 8H), -2.83 (s, 9H), -6.37 (d, *J* = 2.6 Hz, 3H).

4.4.18 Synthesis of [Si, Si] Bis(trimethylsiloxy, pentafluorophenoxy) silicon phthalocyanine (4(PF)-3).

Adapting the procedure from previous literature, [13,18] In a 250 mL flask, 350 mg (0.54 mmol, 1.0 eq.) of **4(Me)-3**, 200 mg of pentafluorophenoxy (1.08 mmol, 2 eq.), and 2 mL of triethylamine (TEA) were added and stirred at room temperature overnight in DCM. A 10 W white LED spotlight lamp was used to assist in the photolysis, positioned to ensure that most of the light passed through the solution. After the reaction, the mixture was concentrated and washed with ether and hexanes using vacuum filtration. The crude product, **4(PF)-3,** was collected with a 57% yield as a dark blue powder. ^{1}H NMR (300 MHz, $CDCl_3$) δ 9.68 – 9.55 (m, 8H), 9.49 (dd, *J* = 5.6, 3.0 Hz, 6H), 8.31 (dt, *J* = 5.3, 2.6 Hz, 11H), 3.10 (q, *J* = 7.3 Hz, 9H), 2.16 (s, 9H), -2.83 (s, 9H), -2.86 (s, 5H).

4.4.19 Optical characterization

UV-vis-NIR spectra were collected using an Agilent Technologies Cary 6000*i* UV-Vis-NIR spectrophotometer. The samples were dissolved with chlorobenzene and filtered through a 0.45 μm pore PTFE syringe filter before the collection of the spectra. UV-vis-NIR measurements were collected at room temperature within the range of 250-800 nm.

4.4.20 Electrochemical characterization

Cyclic voltammetry was performed using a Bioanalytical Systems Inc. (BASi) Epsilon potentiostat with C3 cell stand, a glass cell and recorded using BASi Epsilon EC software (V

2.13.77 (c) 2013BASi). Platinum wires were used for the working, counter and reference electrodes. The measurements were performed at a 1 mg/mL solution in anhydrous DCM under argon, using 0.1 M tetrabutylammonium hexafluorophosphate (Aldrich) as the supporting electrolyte, with a scan rate of 100 mV s^{-1}. The solutions were filtered through a 0.45 μm pore PTFE syringe filter prior to measurements. All measurements were referenced to the Fc/Fc^{+} redox couple (+0.48 V *vs.* SCE) as an internal standard. Oxidation and reduction half potentials were determined using the anodic and cathodic peak potentials, respectively.

4.5 SUPPORTING INFORMATION

4.5.1 Characterization of asymmetrical SiPcs (RR'-SiPc) synthesised from R_2-SiPc starting materials.

Characterization of compound 4D based RR'-SiPcs

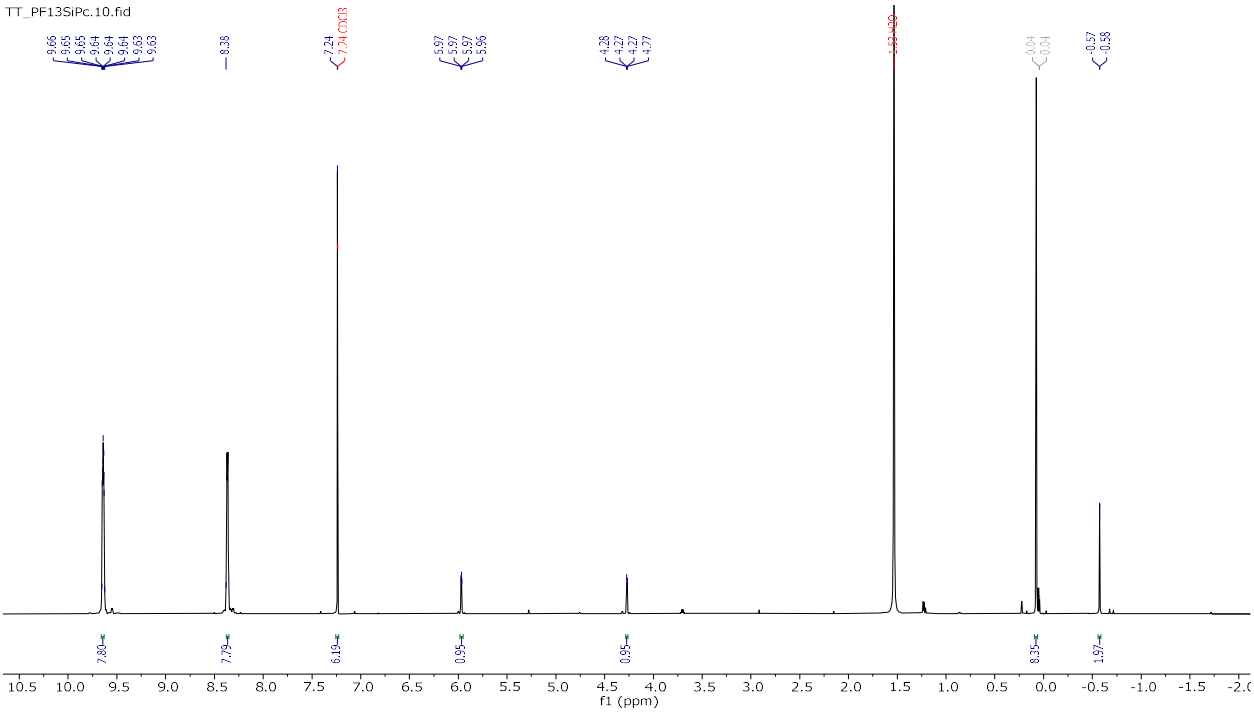

Figure S4.1: ^{1}H NMR of **4D-6** in chloroform.

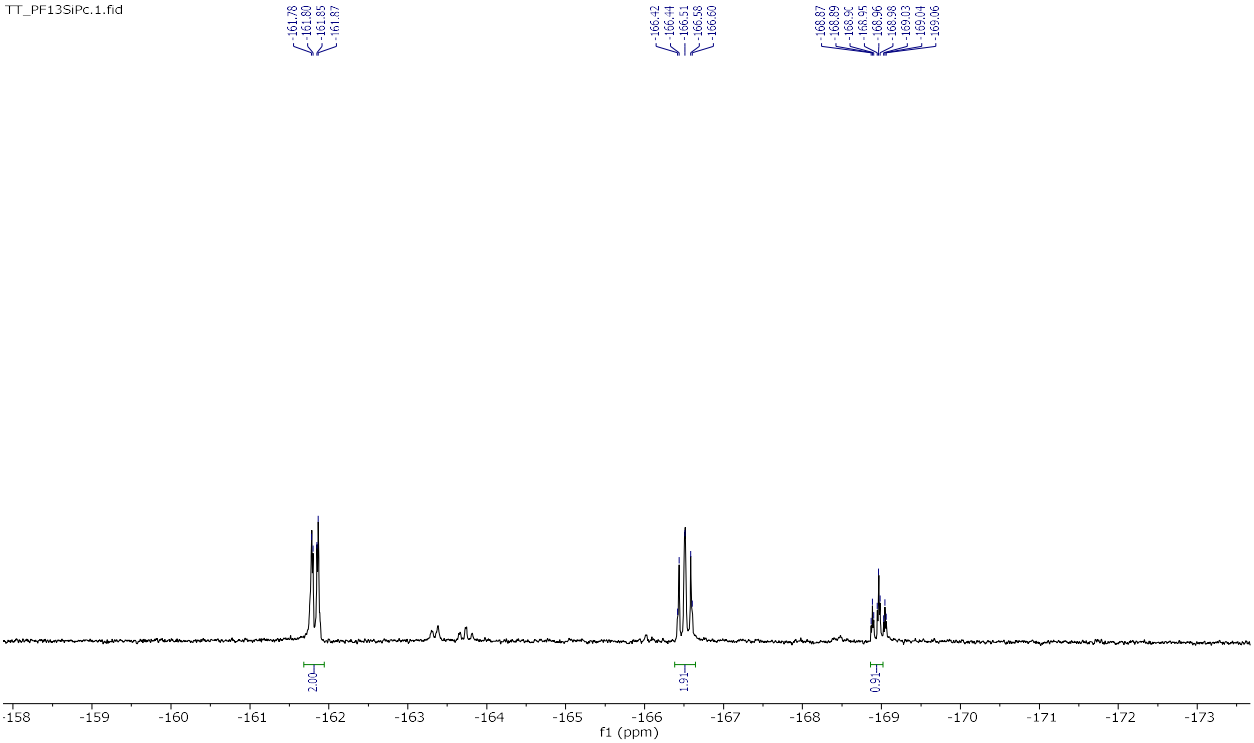

Figure S4.2 : ^{19}F NMR of **4D-6** in chloroform.

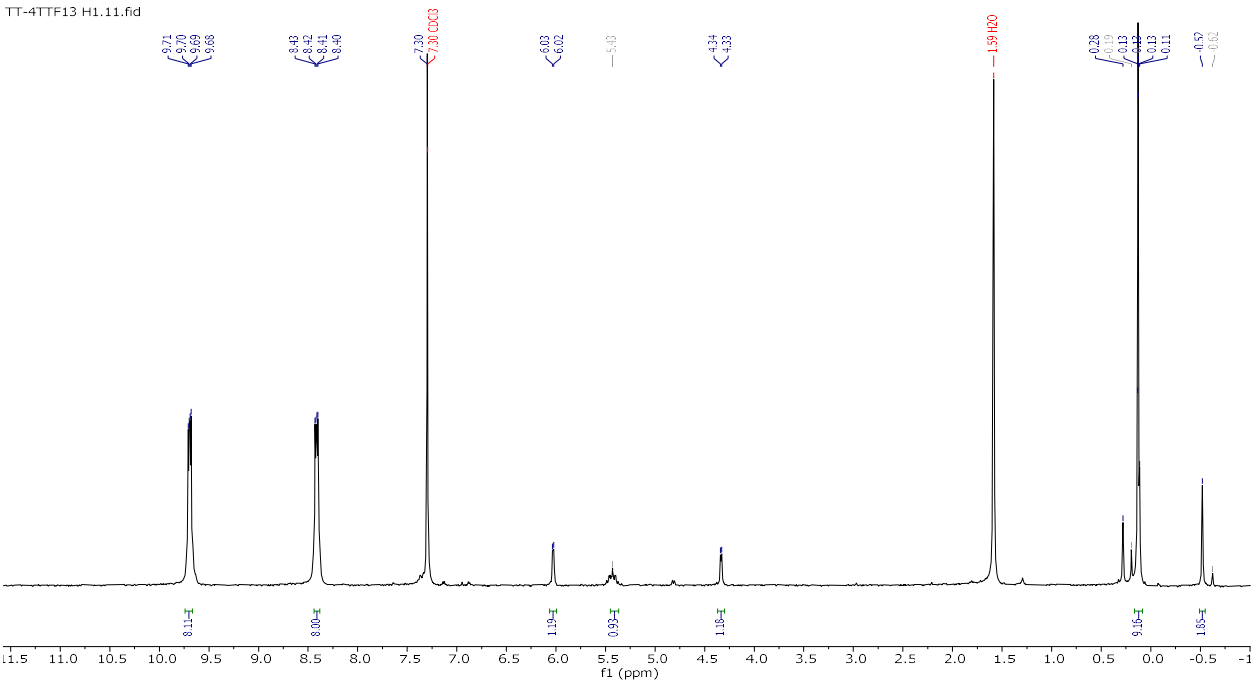

Figure S4.3: : ^{1}H NMR of **4D-7** in chloroform.

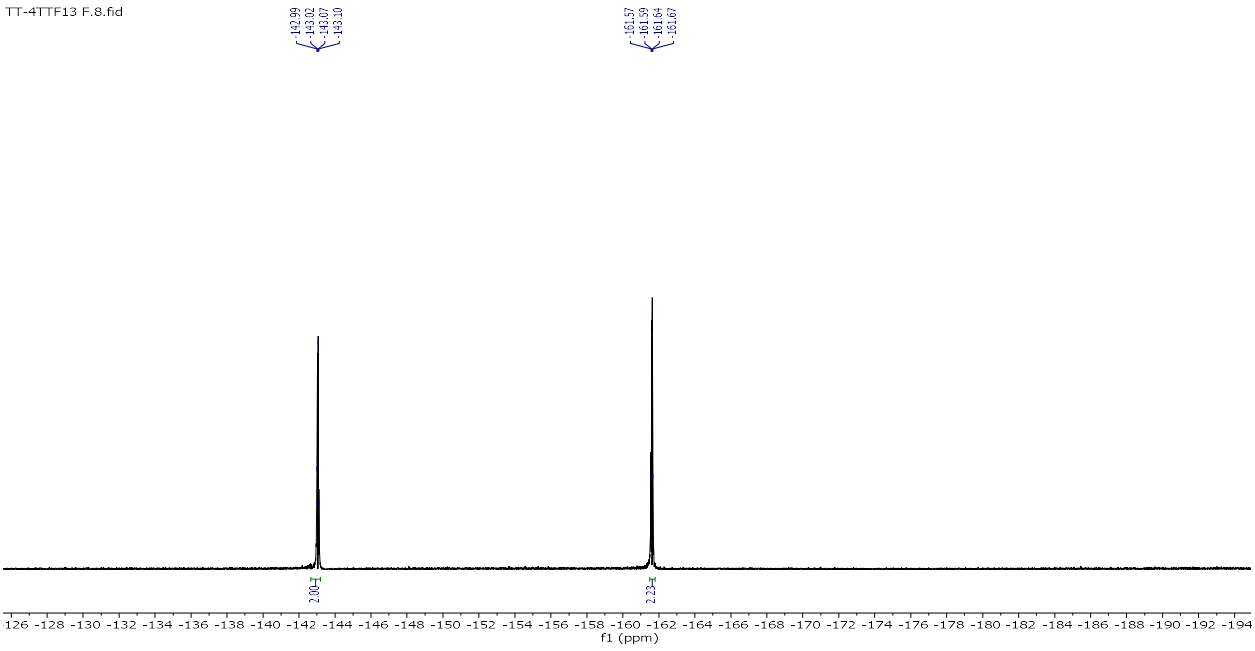

Figure S4.4: ^{19}F NMR of **4D-7** in chloroform.

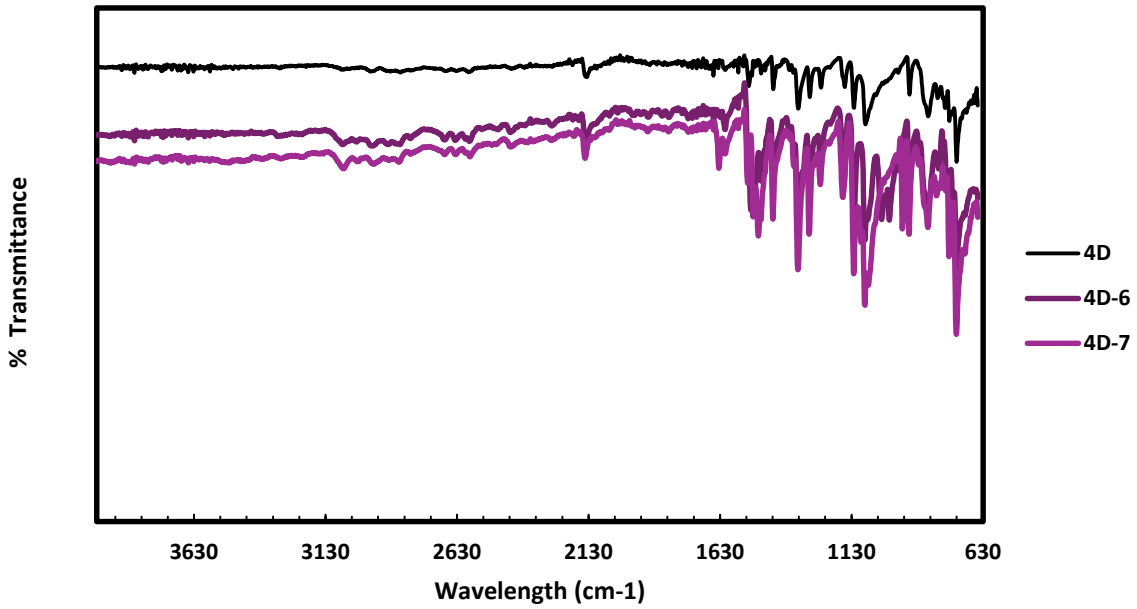

Figure S4.5: FT-IR spectra **4D**, **4D-6** and **4D-7**. Weak C-H stretches between 2850–2960 cm^{-1} and weak C≡C stretching vibrations ~ 2100–2150 cm^{-1} are noticed across all three samples. **4D-6** and **4D-7** exhibit additional strong absorptions in the 1100–1260 cm^{-1} range, consistent with aryl C–F stretching.

Characterization of compound 4F based RR'-SiPc

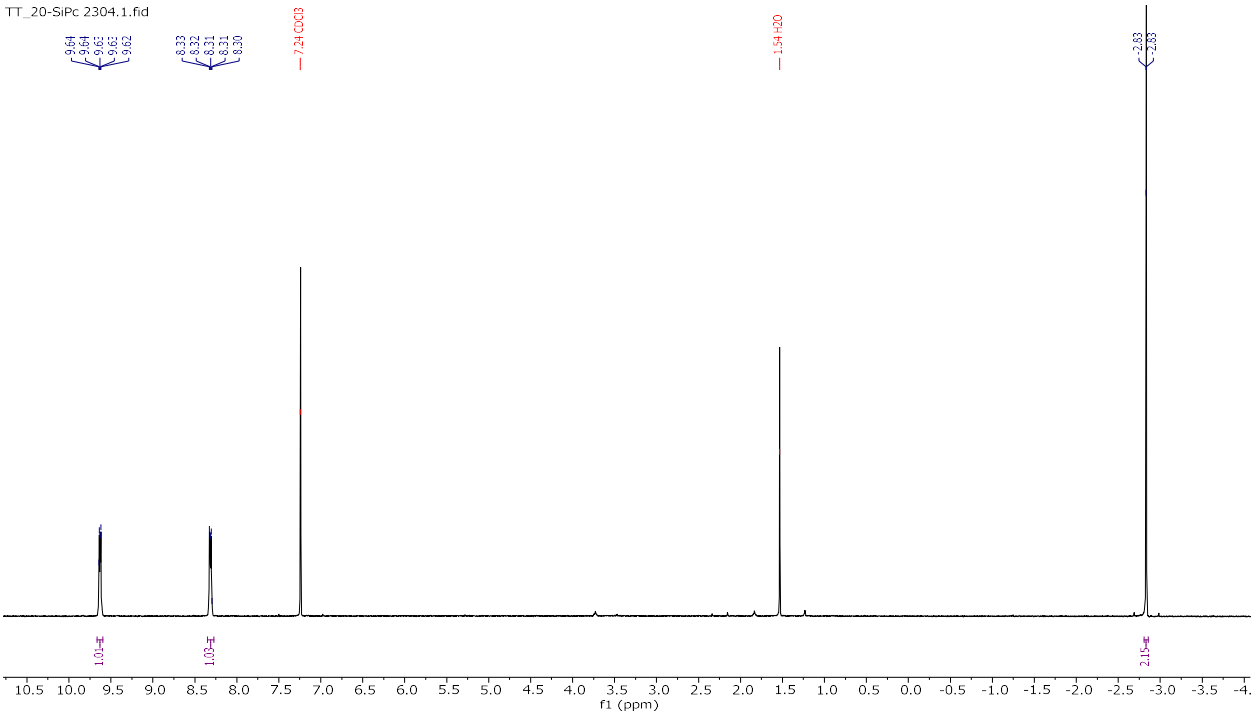

Figure S4.6: ^{1}H NMR of **4F** in chloroform.

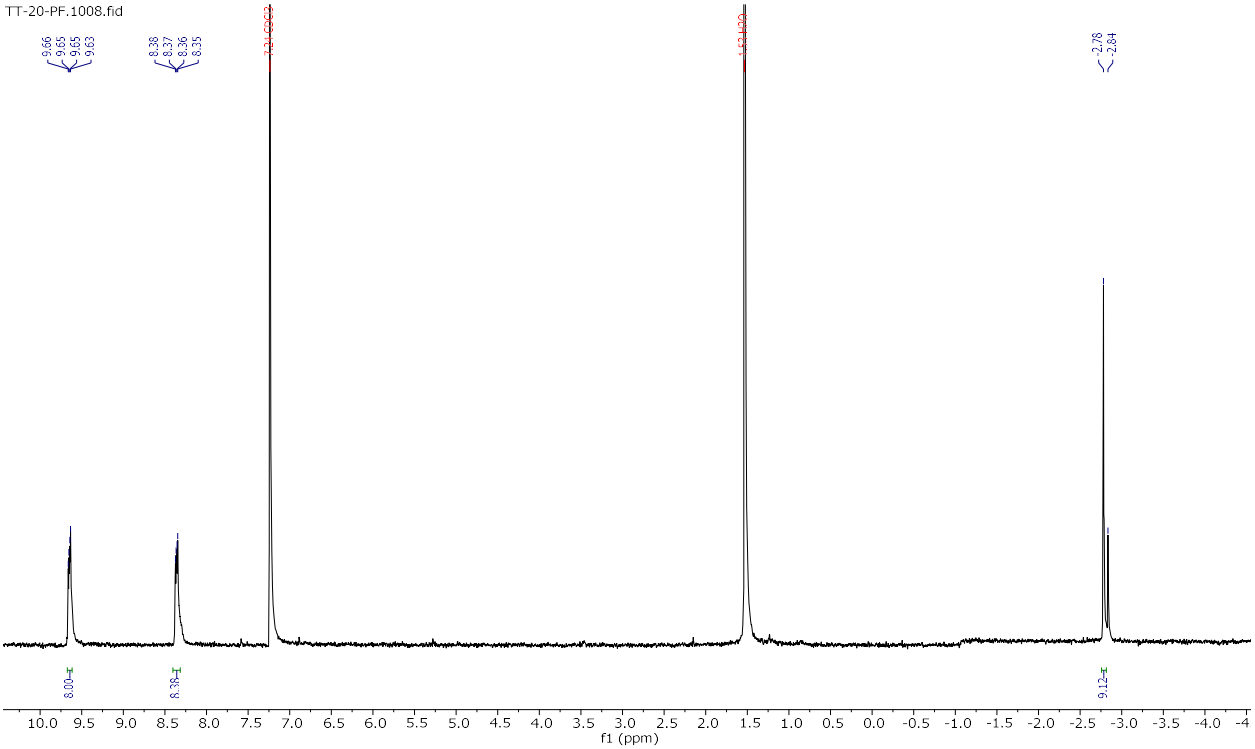

Figure S4.7: ^{1}H NMR of **4F-6** in chloroform.

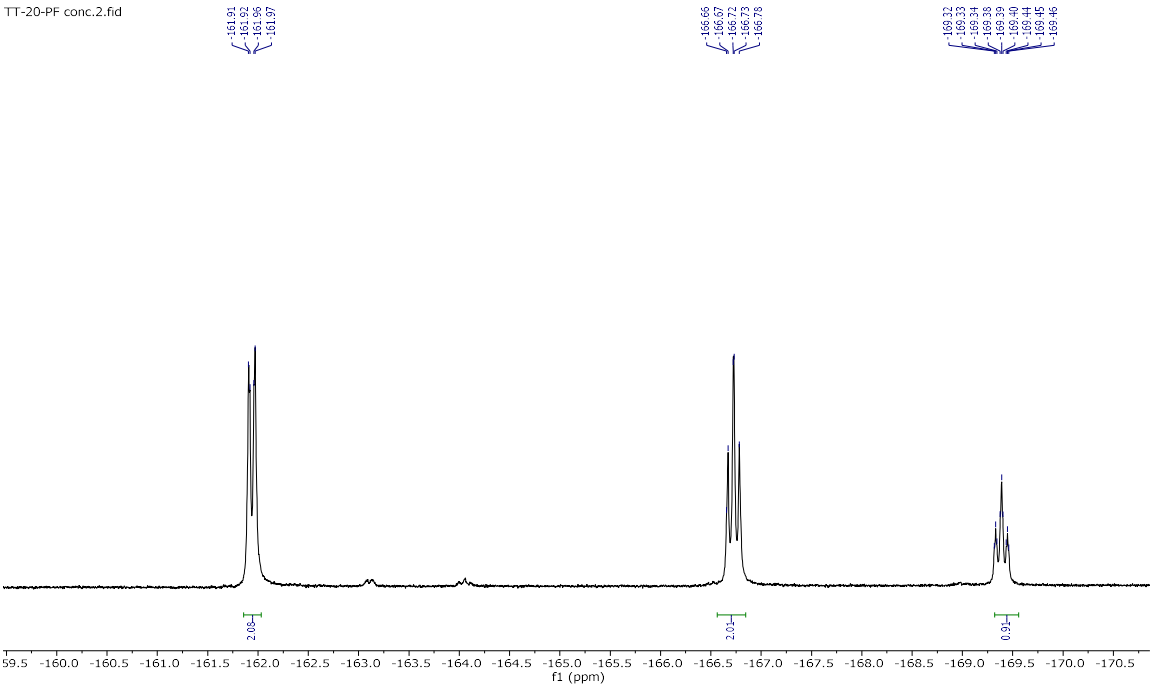

Figure S4.8: ^{19}F NMR of **4F-6** in chloroform**.**

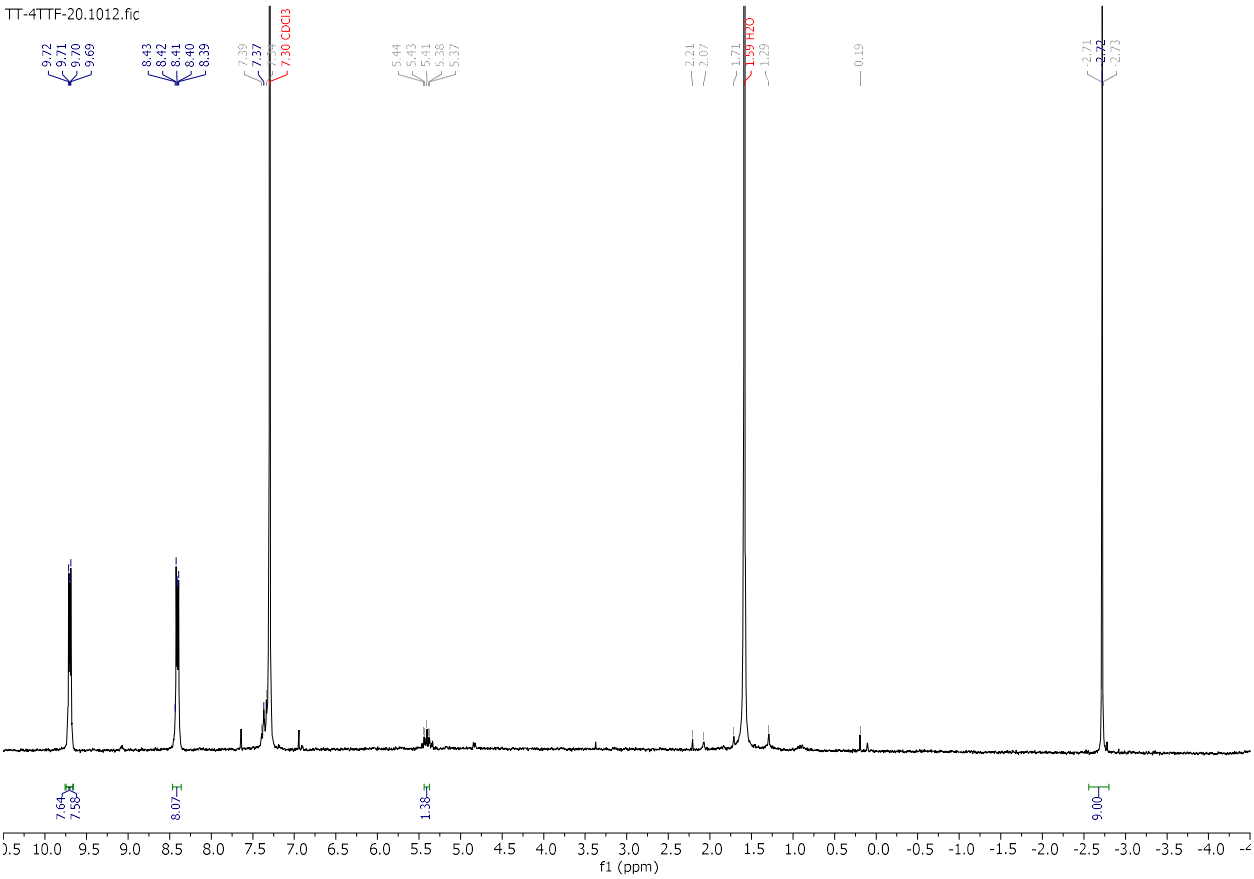

Figure S4.9: ^{1}H NMR of **4F-7** in chloroform.

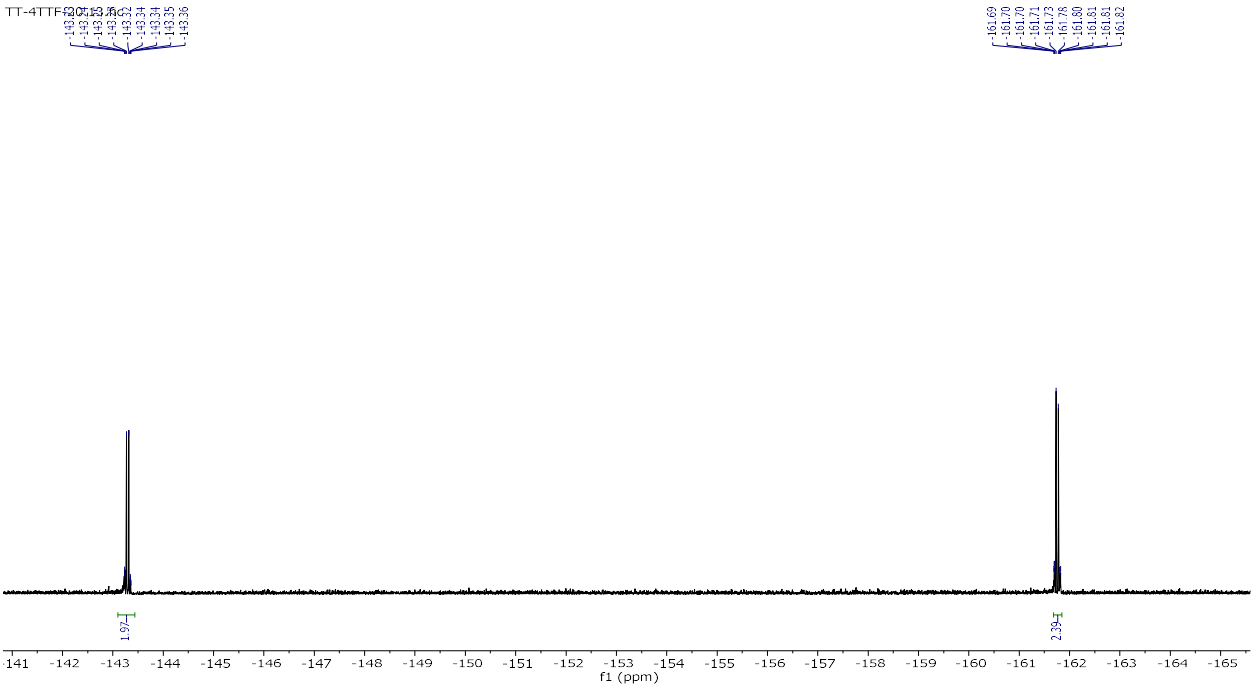

Figure S4.10: ^{19}F NMR of **4F-7** in chloroform.

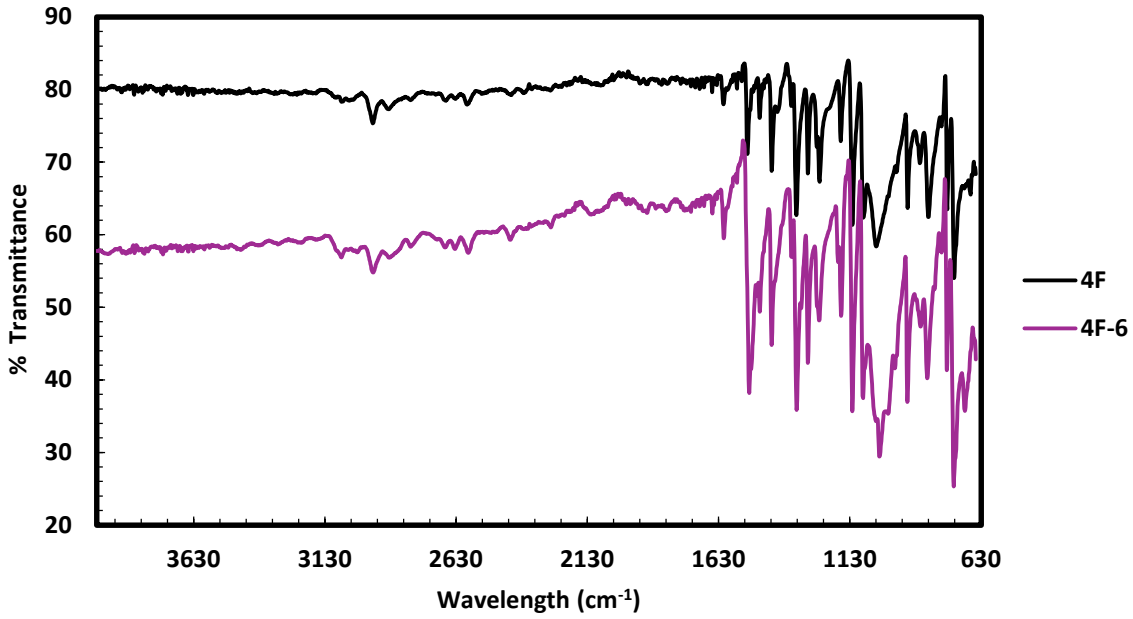

Figure S4.11: The spectrum of **4F-6** shows additional intense bands in the fingerprint region (1350–700 cm⁻¹), attributed to C–F stretching and bending modes of the pentafluorophenyl group, which are absent in 4F. C–H stretching modes of the trimethylsilyl groups observed near 2950–2850 cm⁻¹ for both **4F** and **4F-6**.

Characterization of compound 4G based RR'-SiPc

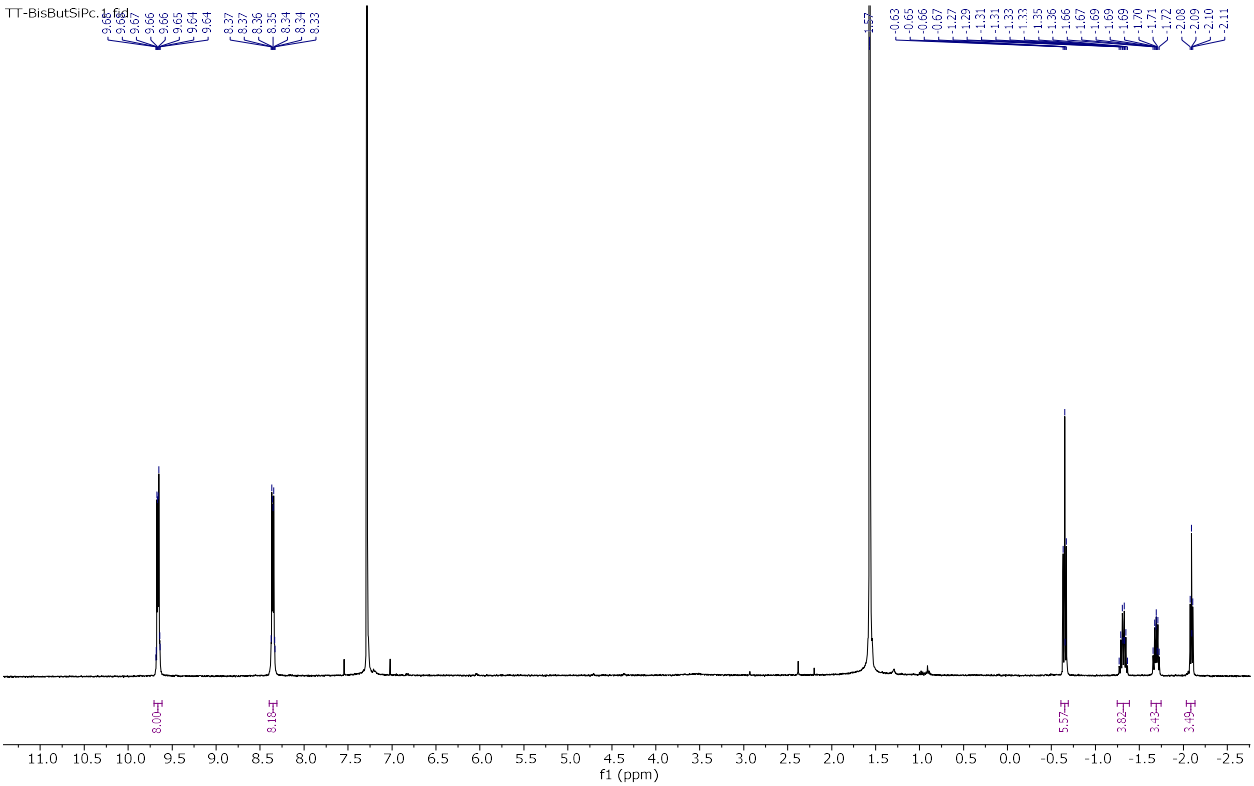

Figure S4.12: ^{1}H NMR of **4G** in chloroform.

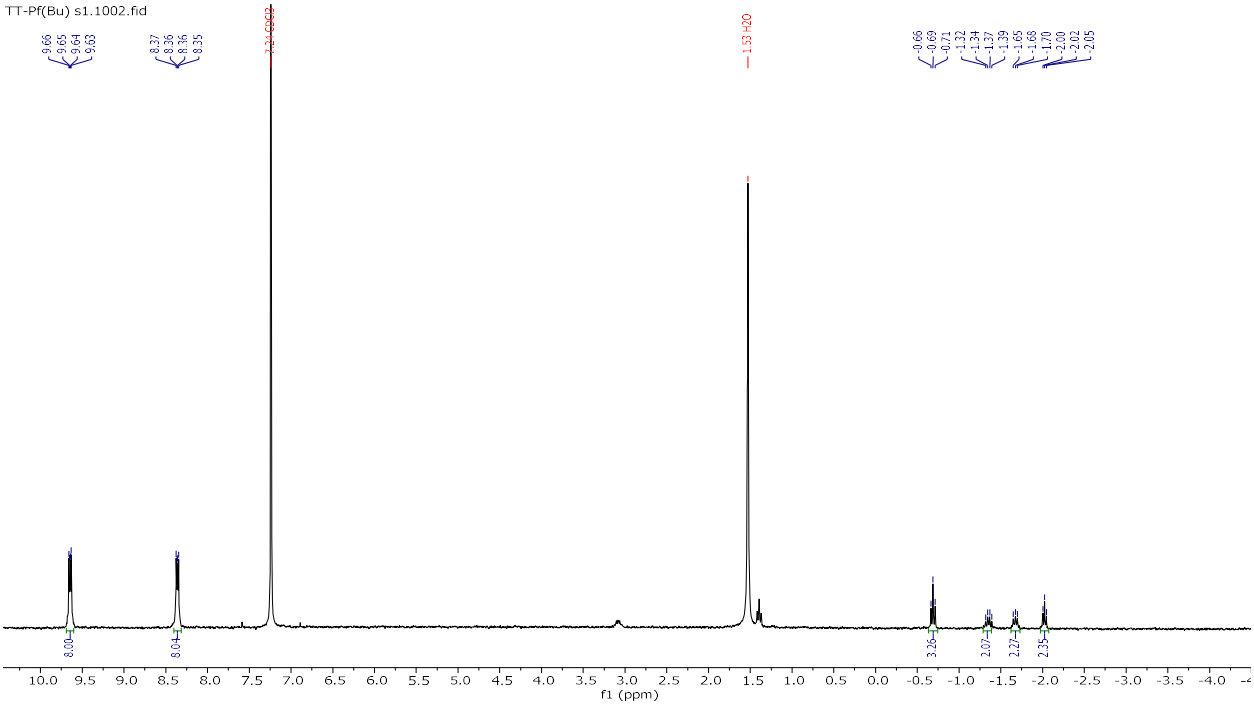

Figure S4.13: ^{1}H NMR of **4G-6** in chloroform.

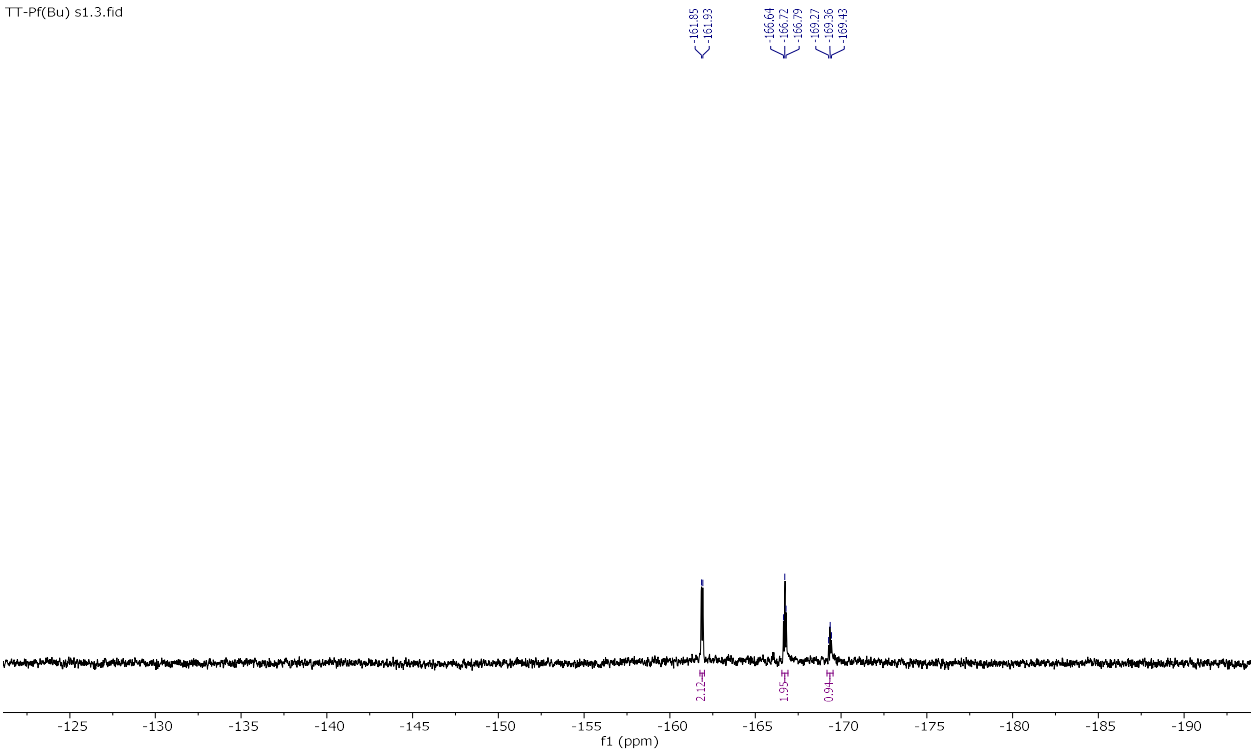

Figure S4.14: ^{19}F NMR of **4G-6** in chloroform.

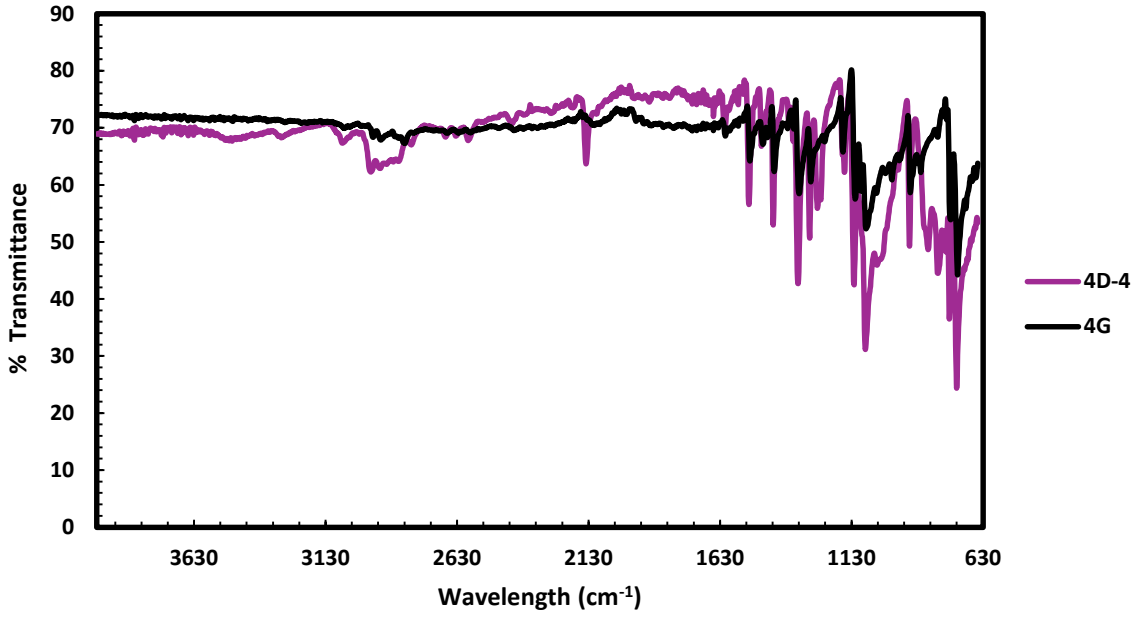

Figure S4.15: 4G based RR'-SiPc FT-IR, C-H_2 stretching and bending modes ~2850-3000 cm^{-1} and C≡C stretching vibrations ~ 2100–2150 cm^{-1}.

Characterization of compound 4H based RR'-SiPcs

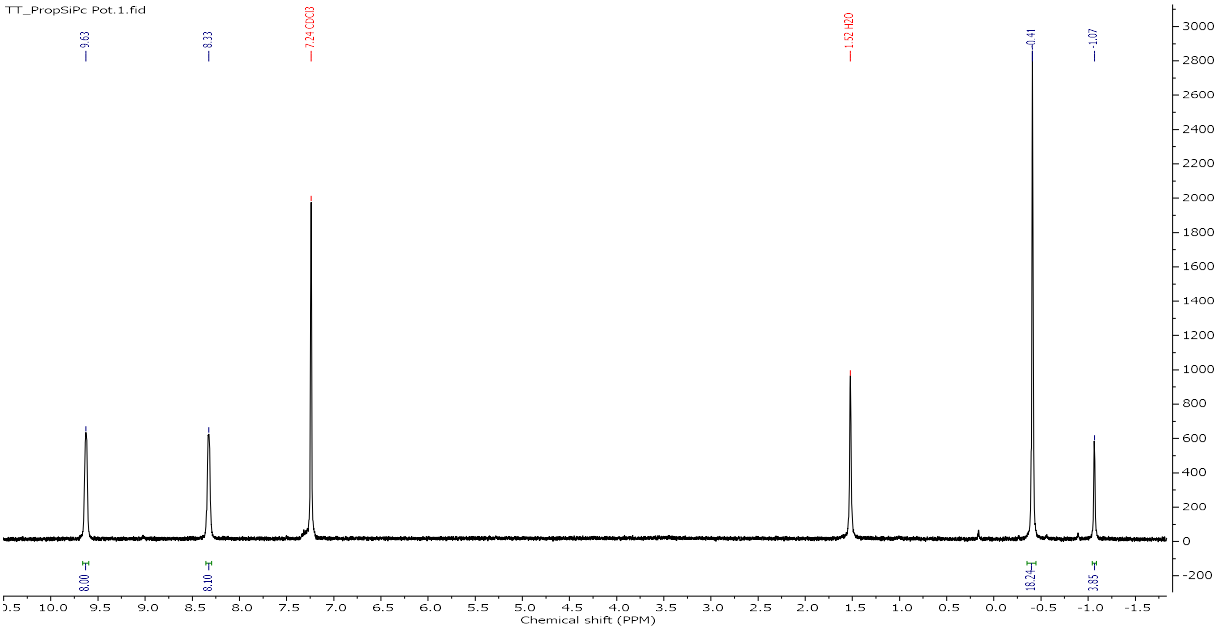

Figure S4.16: ^{1}H NMR **4H** in chloroform.

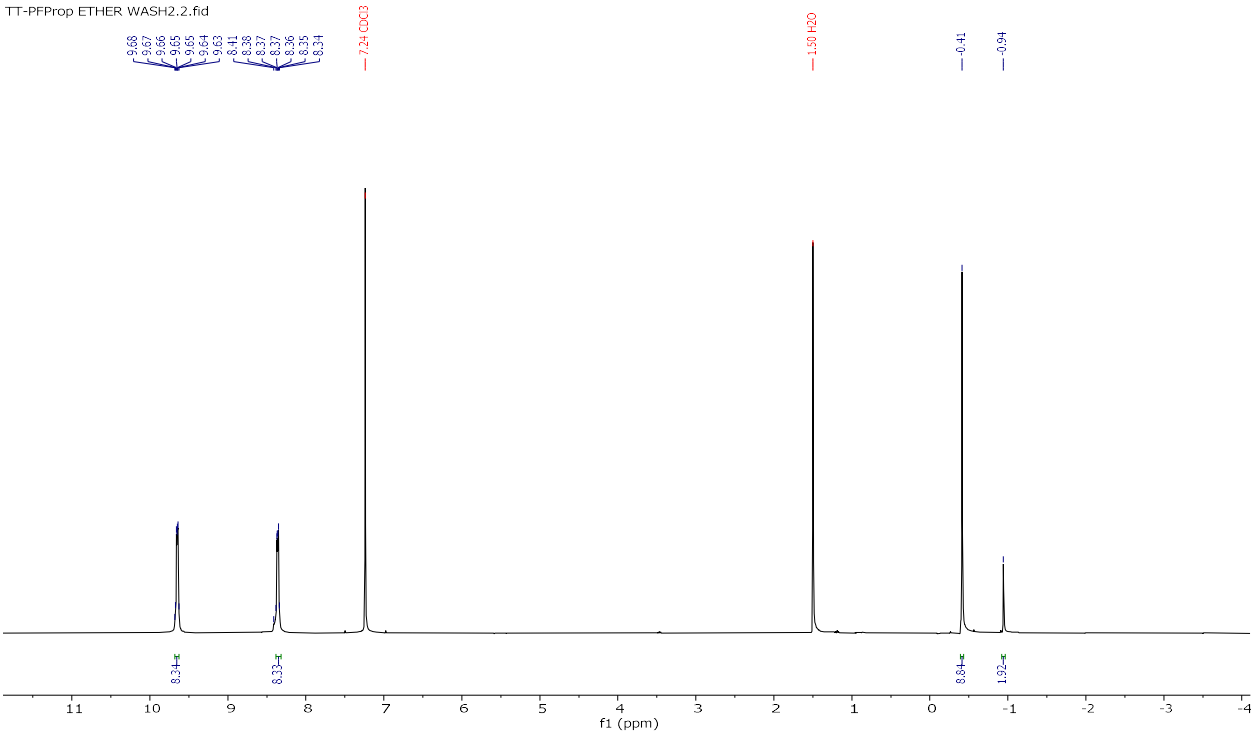

Figure S4.17: ^{1}H NMR of **4H-6** in chloroform.

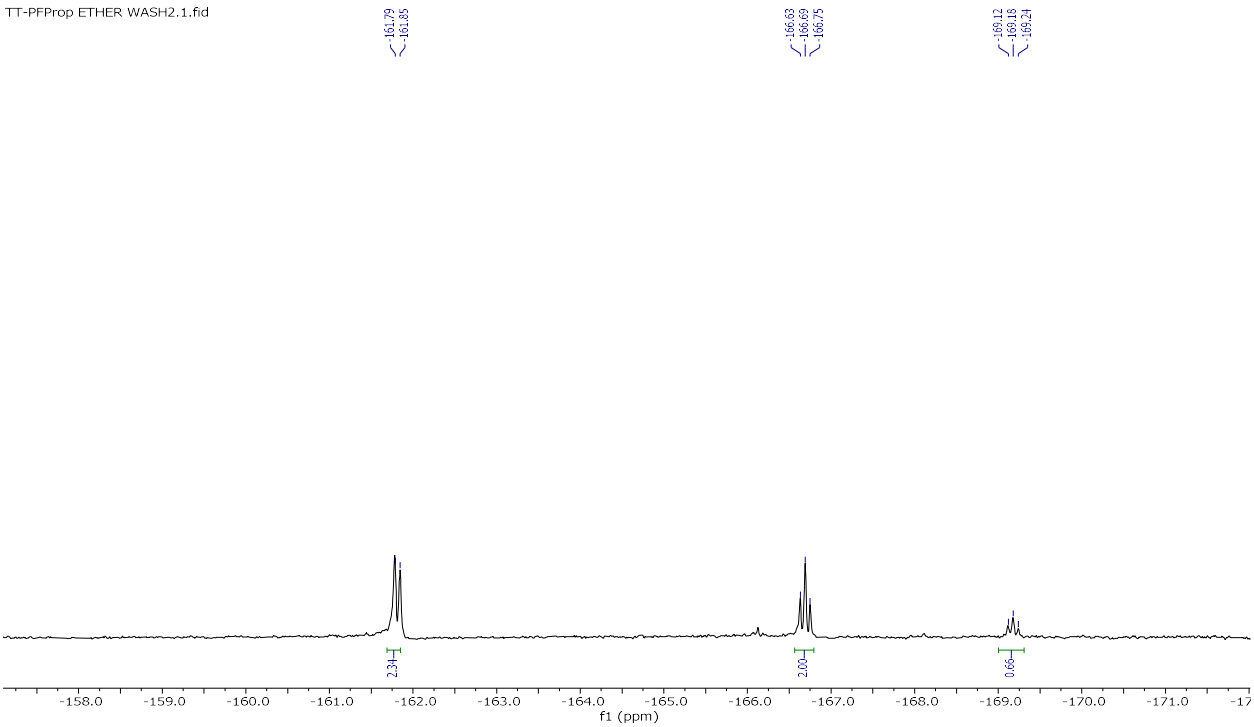

Figure S4.18: ^{19}F NMR of **4H-6** in chloroform.

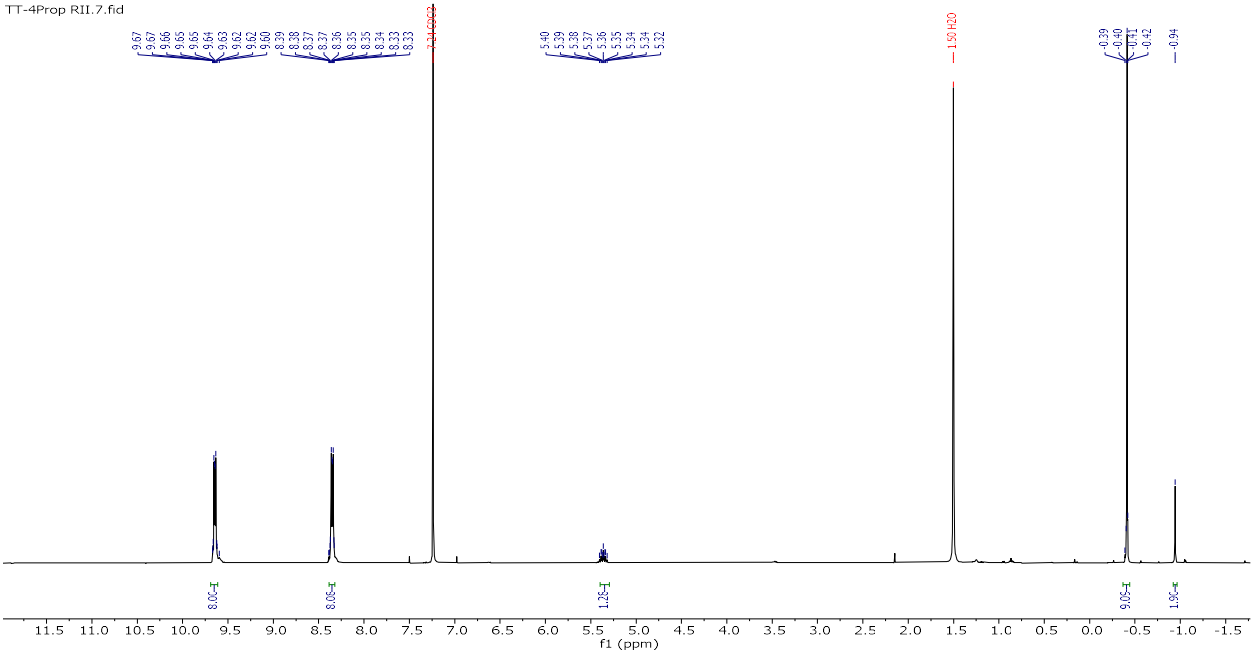

Figure S4.19: ^{1}H NMR of **4H-7** in chloroform.

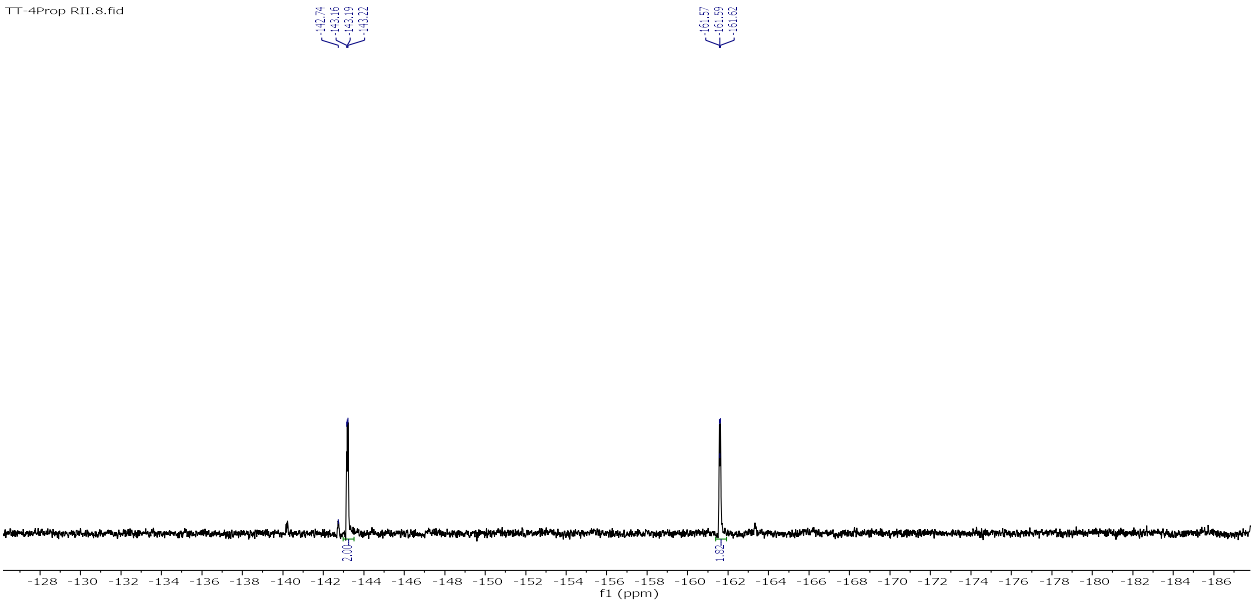

Figure S4.20: ^{19}F NMR of **4H-7** in chloroform.

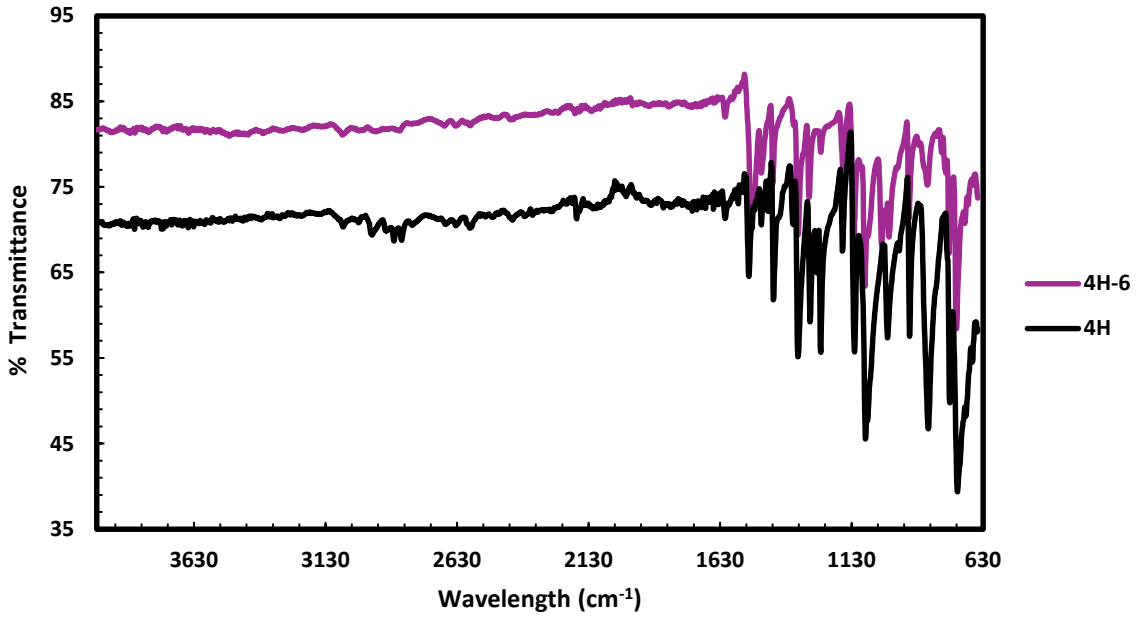

Figure S4.21: weak C≡C stretching vibrations ~ 2100–2150 cm⁻¹, The spectrum of **4H-6** shows additional intense bands in the fingerprint region (1350–700 cm⁻¹), attributed to C–F stretching and bending modes of the pentafluorophenyl group, which are absent in **4H**. C–H stretching modes of the trimethylsilyl groups observed near 2950–2850 cm⁻¹ for both **4H** and **4H-6**.

Characterization of Si-F coupling on 4E

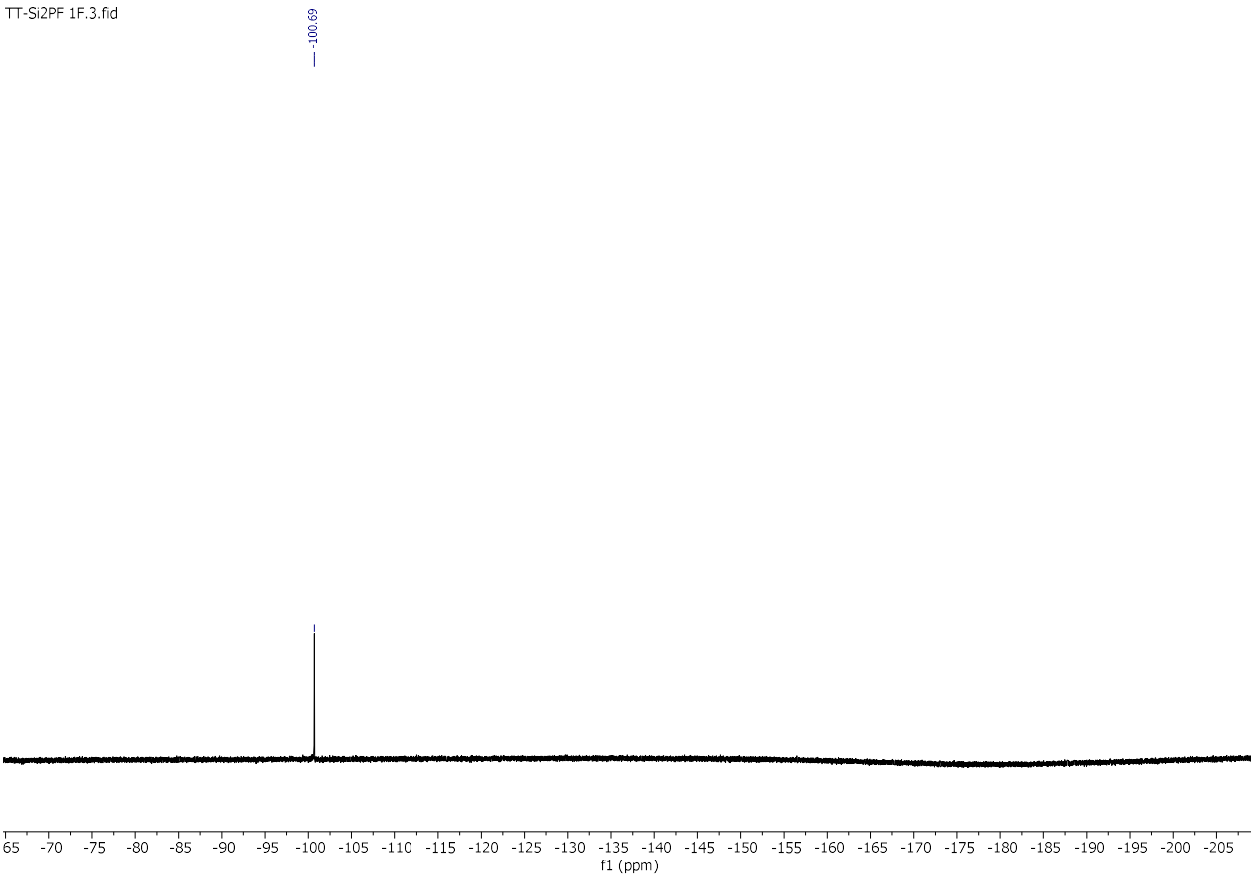

Figure S4.22: ^{19}F NMR in chloroform for the unintentionally synthesized asymmetrical Si-F coupling on **4E**.

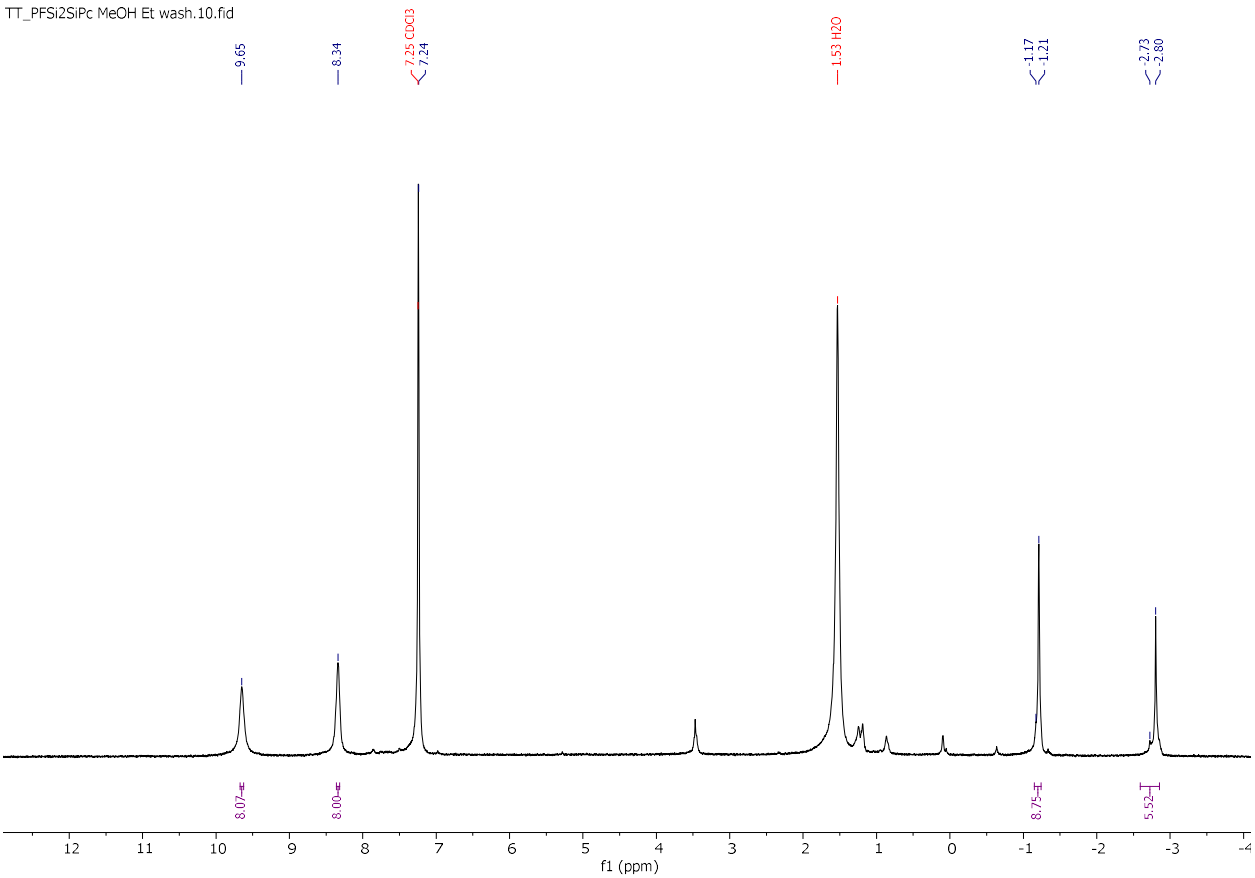

Figure S4.23: ^{1}H NMR in chloroform of the unintentionally synthesized asymmetrical Si-F coupling on **4E**.

4.5.2 *Alternative synthetic approaches for RR'-SiPc starting from ClSiPcMe characterization*

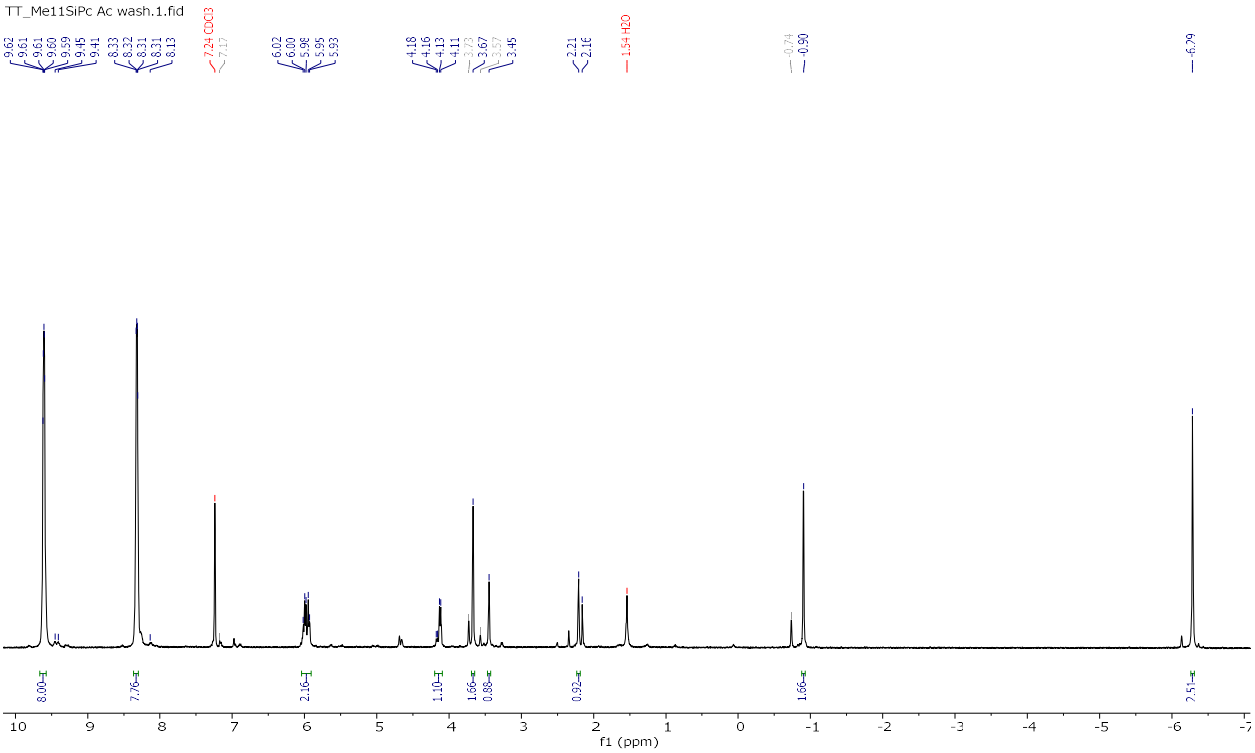

Figure S4.24: ^{1}H NMR of **4(Me)-1** in chloroform.

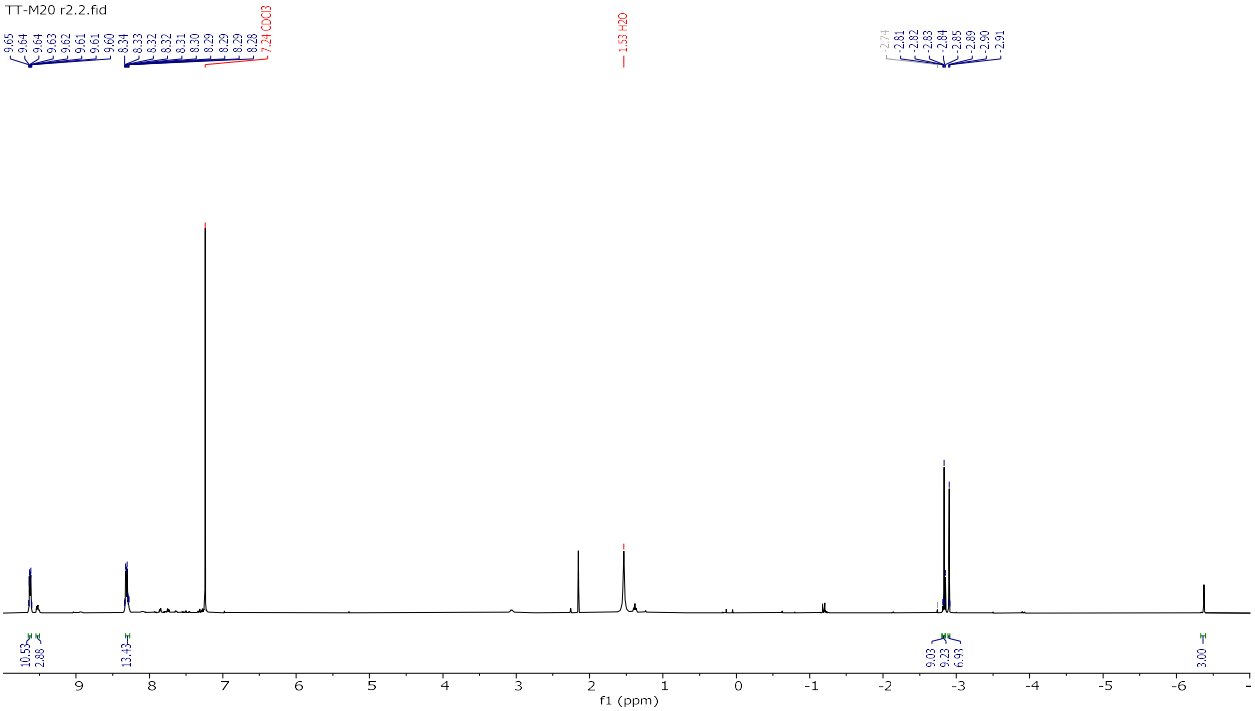

Figure S4.25: ^{1}H NMR of **4(Me)-3** in chloroform.

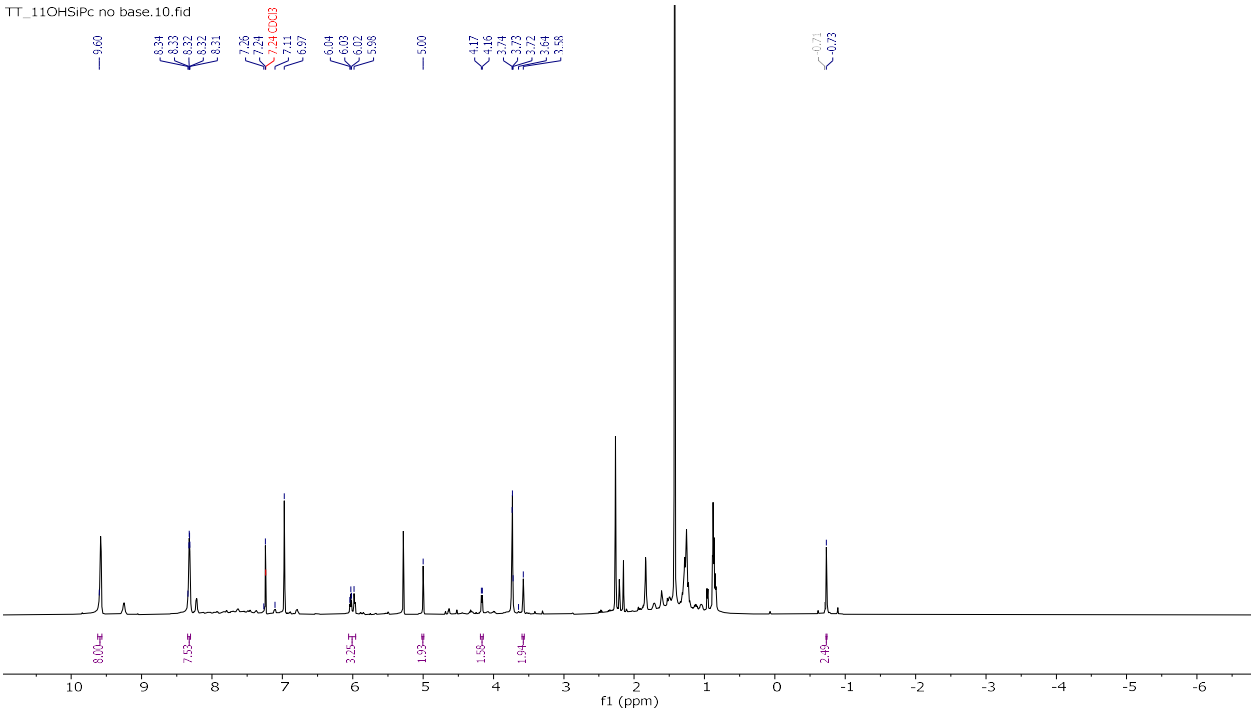

Figure S4.26: ^{1}H NMR of **4(OH)-1** in chloroform.

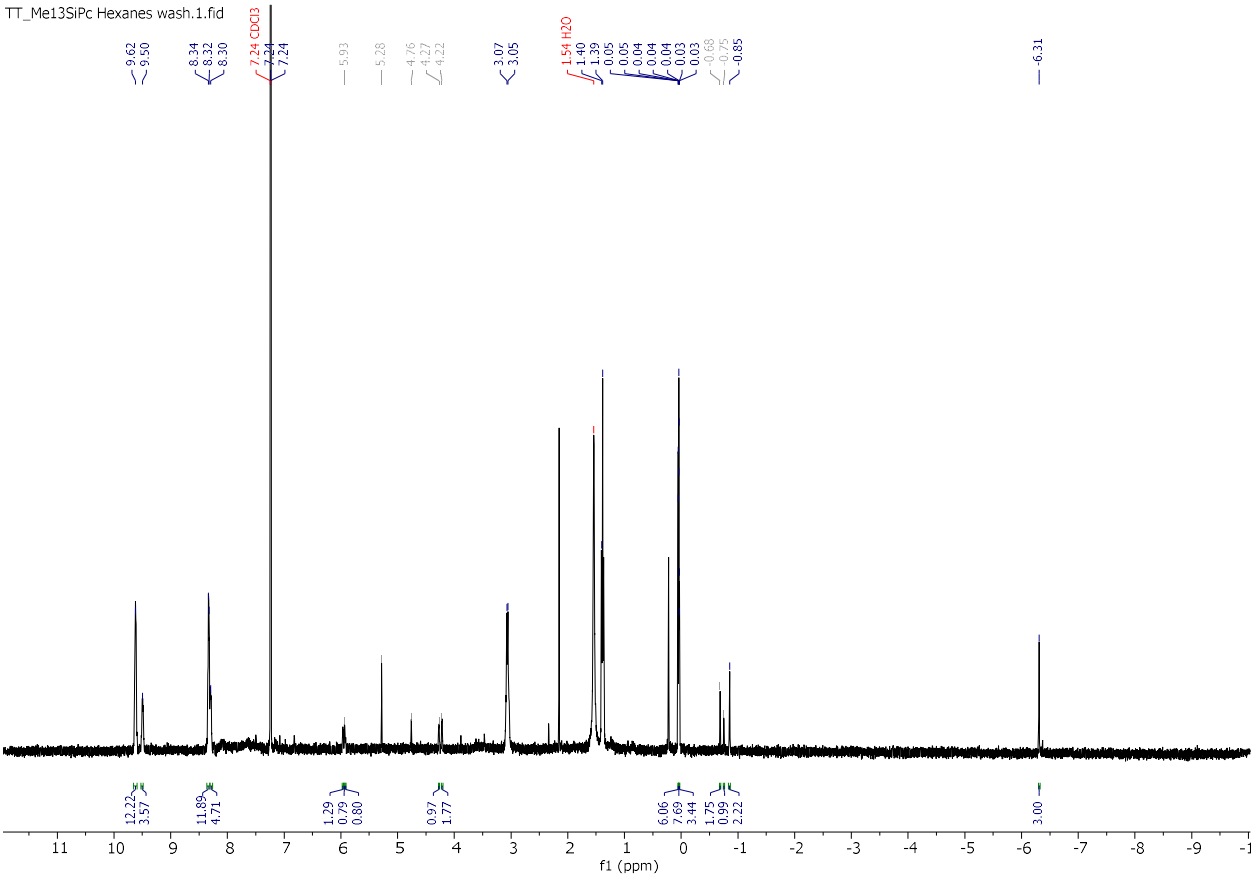

Figure S4.27: ^{1}H NMR of **4(Me)-2** in chloroform.

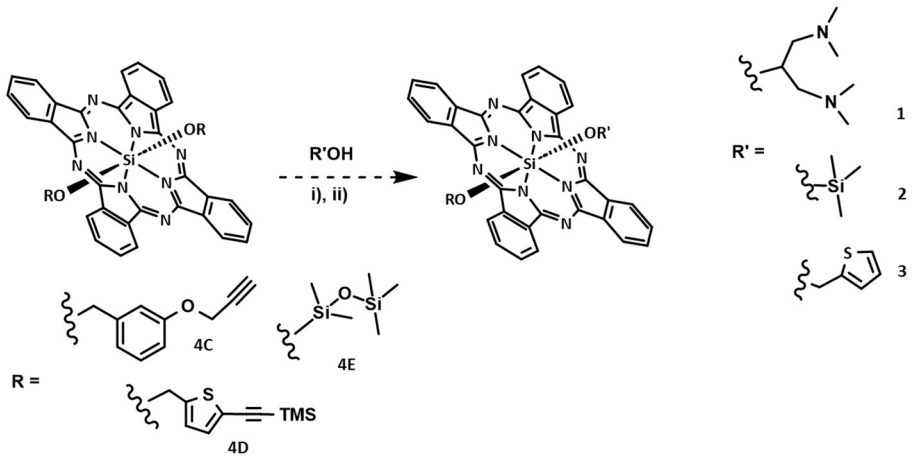

Scheme S4.1: Attempt to synthesize RR'-SiPcs from highly soluble symmetrical SiPcs.

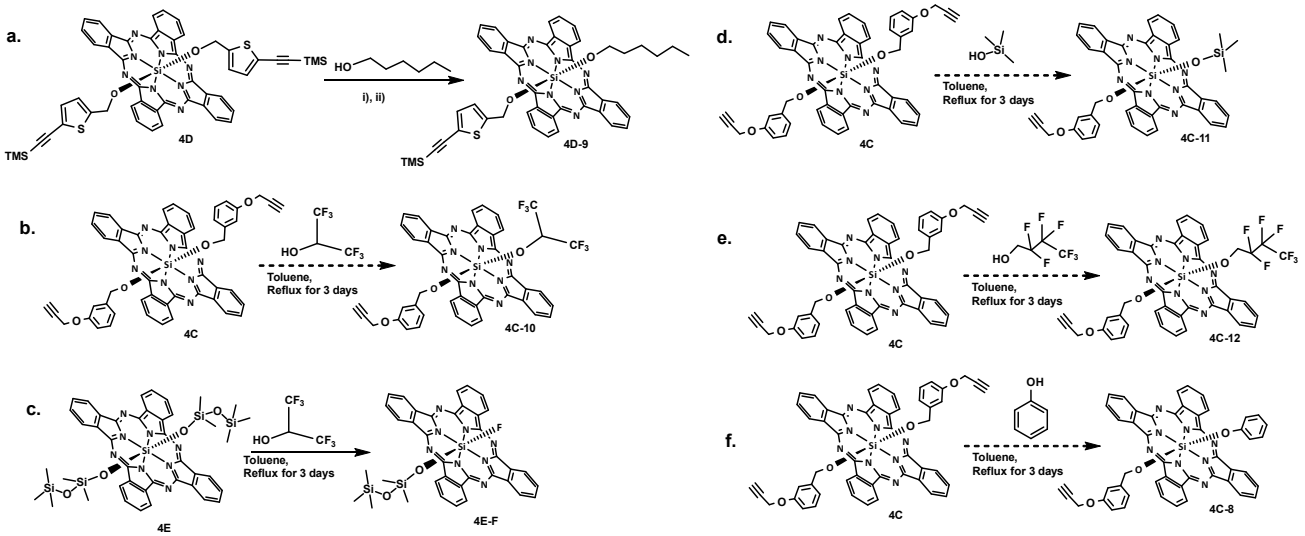

Scheme S4.2: RR'-SiPc synthesis attempts from varying chemical moieties; a). successful singular hexoxide substitution (**4D-9**) on **4D** in an adjacent conditions to **4D-4**; b and e). ineffective attempts to produce RR'-SiPc analogues using polyfluorinated alkyl unit; c). unintentional RR'-SiPc synthesis from hexafluoro isopropanol; d). ineffective attempts to produce RR'-SiPc analogues using trimethylsilane on **4C**; f). ineffective attempts to produce RR'-SiPc analogues using phenol on a symmetrical **4C**.

4.6 REFERENCES

1. Ourabi M, Vebber MC, Cyr M, Weintrager FS-D, Ledos N, Lamontagne HR, Nyayachavadi A, Brusso JL and Lessard BH. *J. Mater. Chem. C* 2025; **13**: 18167-18175.

2. Pal AK, Varghese S, Cordes DB, Slawin AMZ, Samuel IDW and Zysman-Colman E. *Sci Rep* 2017; **7**: 12282.

3. Yutronkie NJ, Grant TM, Melville OA, Lessard BH and Brusso JL. *Materials* 2019; **12**: 1334.

4. Chen H, Martín-Gomis L, Xu Z, C Fischer J, A Howard I, Herrero D, Sobrino-Bastán V, Sastre-Santos Á, Haldar R and Wöll C. July 2023.

5. Lau JTF, Lo P-C, Tsang Y-M, Fong W-P and Ng DKP. *Chem. Commun.* 2011; **47**: 9657-9659.

6. Jiang X-J, Yeung S-L, Lo P-C, Fong W-P and Ng DKP. *J. Med. Chem.* 2011; **54**: 320-330.

7. Mitra K and T. Hartman MC. *Organic & Biomolecular Chemistry* 2021; **19**: 1168-1190.

8. Chen K, Li X, Huang B, Ye Q, Xiao W, Guan X, Chen L and Peng Y. *New Journal of Chemistry* 2021; **45**: 457-462.

9. Salih Ağırtaş M. *Dyes and Pigments* 2008; **79**: 247-251.

10. Ağırtaş MS. *Heterocyclic Communications* 2020; **26**: 130-136.

11. Wysocki M, Ziental D, Biyiklioglu Z, Jozkowiak M, Dlugaszewska J, Piotrowska-Kempisty H, Güzel E and Sobotta L. *Int J Mol Sci* 2025; **26**: 7447.

12. Harada W, Hirahara M, Togashi T, Ishizaki M, Kurihara M, Haga M and Kanaizuka K. *Langmuir* 2018; **34**: 1321-1326.

13. Lim B, Bloking JT, Ponec A, McGehee MD and Sellinger A. *ACS Appl. Mater. Interfaces* 2014; **6**: 6905-6913.

14. Zysman-Colman E, Ghosh SS, Xie G, Varghese S, Chowdhury M, Sharma N, Cordes DB, Slawin AMZ and Samuel IDW. *ACS Appl Mater Interfaces* 2016; **8**: 9247-9253.

15. Lessard BH, Grant TM, White R, Thibau E, Lu Z-H and Bender TP. *J. Mater. Chem. A* 2015; **3**: 24512-24524.

16. Lessard BH. *ACS Appl. Mater. Interfaces* 2021; **13**: 31321-31330.

17. Ke L, Min J, Adam M, Gasparini N, Hou Y, Perea JD, Chen W, Zhang H, Fladischer S, Sale A-C, Spiecker E, Tykwinski RR, Brabec CJ and Ameri T. *Advanced Energy Materials* 2016; **6**: 1502355.

18. Cranston RR, Vebber MC, Faleiro Berbigier J, Brusso J, Kelly TL and Lessard BH. *Advanced Electronic Materials* 2022; **8**: 2200696.

19. Lo P-C, Huang J-D, Cheng DYY, Chan EYM, Fong W-P, Ko W-H and Ng DKP. *Chemistry – A European Journal* 2004; **10**: 4831-4838.

20. Zhao X, Huang Y, Yuan G, Zuo K, Huang Y, Chen J, Li J and Xue J. *Chem. Commun.* 2019; **55**: 866-869.

21. Li R, Zhou Y, Liu Y, Jiang X, Zeng W, Gong Z, Zheng G, Sun D and Dai Z. *Signal Transduct Target Ther* 2022; **7**: 64.

22. Xu H, Ohkita H, Tamai Y, Benten H and Ito S. *Advanced Materials* 2015; **27**: 5868-5874.

23. Çelik GG, Gonca S, Şahin B, Özdemir S, Atilla D and Gürek AG. *Dalton Trans.* 2022; **51**: 7517-7529.

24. Li Z and Lieberman M. *Inorg. Chem.* 2001; **40**: 932-939.

25. Li J, Yang Y, Zhang P, Sounik JR and Kenney ME. *Photochem Photobiol Sci* 2014; **13**: 1690-1698.

26. Zheng B-Y, Wang L, Hu Q-Y, Shi J, Ke M-R and Huang J-D. *Dyes and Pigments* 2020; **177**: 108286.

27. Lessard BH, Dang JD, Grant TM, Gao D, Seferos DS and Bender TP. *ACS Appl. Mater. Interfaces* 2014; **6**: 15040-15051.

28. Huang Y, Liu G, Zheng F, Chen J, Lin Y, Wang J, Huang Y and Peng Y. *Colloids and Surfaces B: Biointerfaces* 2024; **238**: 113890.

29. Oliveira É de FS, Azevedo R de CP, Bonfilio R, Oliveira DB de, Ribeiro GP and Araújo MB de. *Braz. J. Pharm. Sci.* 2009; **45**: 67-73.

30. Lessard BH, White RT, AL-Amar M, Plint T, Castrucci JS, Josey DS, Lu Z-H and Bender TP. *ACS Appl. Mater. Interfaces* 2015; **7**: 5076-5088.

31. Nagy N, Kuipers HF, Frymoyer AR, Ishak HD, Bollyky JB, Wight TN and Bollyky PL. *Front Immunol* 2015; **6**: 123.

32. Anderson ED, Gorka AP and Schnermann MJ. *Nat Commun* 2016; **7**: 13378.

33. Ślęczkowski P. *Int J Mol Sci* 2023; **24**: 6924.

34. Lin S-H, Wu F-I and Liu R-S. *Chem. Commun.* 2009: 6961-6963.

35. Hauschild M, Borkowski M, Dral PO, Marszalek T, Hampel F, Xie G, Freudenberg J, Bunz UHF and Kivala M. *Organic Materials* 2020; **02**: 204-213.

36. Lessard BH, White RT, AL-Amar M, Plint T, Castrucci JS, Josey DS, Lu Z-H and Bender TP. *ACS Appl. Mater. Interfaces* 2015; **7**: 5076-5088.

37. Lowery MK, Starshak AJ, Esposito JN, Krueger PC and Kenney ME. *Inorg. Chem.* 1965; **4**: 128-128.

38. Sarai NS, Fulton TJ, O'Meara RL, Johnston KE, Brinkmann-Chen S, Maar RR, Tecklenburg RE, Roberts JM, Reddel JCT, Katsoulis DE and Arnold FH. *Science* 2024; **383**: 438-443.

39. Zhao J, Huang L, Cui X, Li S and Wu H. *J. Mater. Chem. B* 2015; **3**: 9194-9211.

40. Teng C, Yang X, Yang C, Li S, Cheng M, Hagfeldt A and Sun L. ACS Publications.

41. Ledos N, Lamontagne HR, Manion JG, Brusso JL and Lessard BH. *Mater. Chem. Front.* 2025: 10.1039.D5QM00722D.

CHAPTER 5: CONCLUSIONS AND FUTURE WORK

Silicon phthalocyanines (SiPcs) are a multipurpose, adaptable material whose properties can be varied through axial substitution. This thesis has established new synthetic processes for symmetrical and asymmetrical alkyne-functionalized SiPcs to facilitate post-synthetic modification and demonstrate how structural alterations directly affect semiconductor behaviour. By carefully examining the implications of symmetry, substituent identity, and ligand stability, this research demonstrates the structure-property relationships that regulate solubility, aggregation, energy level stabilization, and optoelectronic performance. These findings suggest that SiPcs are adaptable platforms for creating organic electronics, and by linking molecular design to device performance, this study contributes to the broader effort of developing solution-processable, tunable semiconductors for next-generation flexible electronics.

In **Chapter 2**, the synthesis and characterization of new symmetric and asymmetric alkyne-functionalized SiPcs are described, which enable post-synthetic modification and tunable semiconductor behaviour. The symmetric derivative provided a stable platform with distinct HOMO/LUMO levels and served as a precursor for the isolation of asymmetric analogues with thienyl or fluorinated substituents. Electrochemical and optical studies reveal that symmetry and axial substituents have a major impact on energy level stabilization, band gaps, and absorption patterns. The fluorinated asymmetrical derivative shows ambipolar transistor performance and red-shifted absorption. Organic thin-film transistors with low mobilities were made using these substances. Compound **2A-5** exhibited both *p*-type and *n*-type mobility, depending on the substrate treatment. The alkyne groups enabled successful click reactions catalyzed by copper without compromising optical characteristics, demonstrating the potential of these derivatives as

adaptable, chemically flexible platforms for incorporation into improved functional materials and organic electronics.

The work in **Chapter 3** examined the axial integration of ethynyl-thiophene substituents onto SiPcs and found that ligand solubility and instability control the synthesis and properties of the resulting derivatives. The TMS-protected thienyl terminal alkyne significantly improved solubility and enabled various characterizations of the SiPc, whereas deprotected alkynes produced poorly soluble and impurity-prone compounds. Optical and electrochemical studies revealed that the macrocycle dominated the absorbance and redox profiles, with thiophene axial groups contributing relatively little to the SiPc electronic structure. In attempts to create monosubstituted SiPcs, di-substitution was often favoured; nevertheless, in the end, an asymmetric derivative with butoxy and thienyl alkyne ligands was created, which offered better solubility compared to the symmetrical TMS free-alkyne analogue. Overall, the work presented in chapter 3 highlights the challenges of stabilizing terminal alkyne, the critical role of axial ligand identity in solubility control, and the potential of asymmetrical substitution for enabling click chemistry and solution processing of SiPcs in future device applications.

Chapter 4 demonstrates that the successful synthesis of asymmetrical silicon phthalocyanines (RR′-SiPcs) depends strongly on the interplay between axial substituent acidity and steric size. While bulky or weakly acidic ligands failed to produce mono-displacement, perfluorinated phenols consistently afforded RR′-SiPc derivatives in moderate to high yields, establishing them as reliable reagents for asymmetry. Electrochemical and optical analyses confirmed that RR′-SiPcs introduce new redox features, anodic shifts, and slight bathochromic absorption changes compared to their symmetrical counterparts. Overall, these results highlight

acidity and molecular size as key determinants of reactivity and provide a foundation for tailoring RR′-SiPcs with tunable solubility and electronic properties for future applications.

The work summarized here provides a foundation for preparing axially substituted silicon phthalocyanines with adjustable properties. The SiPcs developed in this study exhibited minimal effects on their electrochemical and photochemical characteristics. However, new electrochemical properties were observed in **Chapter 4** due to the introduction of asymmetry. It is recommended that future SiPc derivatives take advantage of the asymmetry synthesis process to create more chemically diverse SiPcs to further evaluate or optimize the optoelectronic properties. Most importantly, future research should focus on incorporating these or similar SiPc derivatives into polymers as pendants, using the method demonstrated in **Chapter 2**. This approach could lead to the synthesis of covalently linked polymer-SiPc organic semiconductors, potentially advancing the development of mechanically stable and flexible OTFTs.